

# Lecture Notes in Physics

## Editorial Board

R. Beig, Wien, Austria  
B.-G. Englert, Ismaning, Germany  
U. Frisch, Nice, France  
P. Hänggi, Augsburg, Germany  
K. Hepp, Zürich, Switzerland  
W. Hillebrandt, Garching, Germany  
D. Imboden, Zürich, Switzerland  
R. L. Jaffe, Cambridge, MA, USA  
R. Lipowsky, Golm, Germany  
H. v. Löhneysen, Karlsruhe, Germany  
I. Ojima, Kyoto, Japan  
D. Sornette, Nice, France, and Los Angeles, CA, USA  
S. Theisen, Golm, Germany  
W. Weise, Trento, Italy, and Garching, Germany  
J. Wess, München, Germany  
J. Zittartz, Köln, Germany

**Springer**

*Berlin*  
*Heidelberg*  
*New York*  
*Hong Kong*  
*London*  
*Milan*  
*Paris*  
*Tokyo*

**Physics and Astronomy**



<http://www.springer.de/phys/>

## Editorial Policy

The series *Lecture Notes in Physics* (LNP), founded in 1969, reports new developments in physics research and teaching – quickly, informally but with a high quality. Manuscripts to be considered for publication are topical volumes consisting of a limited number of contributions, carefully edited and closely related to each other. Each contribution should contain at least partly original and previously unpublished material, be written in a clear, pedagogical style and aimed at a broader readership, especially graduate students and nonspecialist researchers wishing to familiarize themselves with the topic concerned. For this reason, traditional proceedings cannot be considered for this series though volumes to appear in this series are often based on material presented at conferences, workshops and schools (in exceptional cases the original papers and/or those not included in the printed book may be added on an accompanying CD ROM, together with the abstracts of posters and other material suitable for publication, e.g. large tables, colour pictures, program codes, etc.).

## Acceptance

A project can only be accepted tentatively for publication, by both the editorial board and the publisher, following thorough examination of the material submitted. The book proposal sent to the publisher should consist at least of a preliminary table of contents outlining the structure of the book together with abstracts of all contributions to be included. Final acceptance is issued by the series editor in charge, in consultation with the publisher, only after receiving the complete manuscript. Final acceptance, possibly requiring minor corrections, usually follows the tentative acceptance unless the final manuscript differs significantly from expectations (project outline). In particular, the series editors are entitled to reject individual contributions if they do not meet the high quality standards of this series. The final manuscript must be camera-ready, and should include both an informative introduction and a sufficiently detailed subject index.

## Contractual Aspects

Publication in LNP is free of charge. There is no formal contract, no royalties are paid, and no bulk orders are required, although special discounts are offered in this case. The volume editors receive jointly 30 free copies for their personal use and are entitled, as are the contributing authors, to purchase Springer books at a reduced rate. The publisher secures the copyright for each volume. As a rule, no reprints of individual contributions can be supplied.

## Manuscript Submission

The manuscript in its final and approved version must be submitted in camera-ready form. The corresponding electronic source files are also required for the production process, in particular the online version. Technical assistance in compiling the final manuscript can be provided by the publisher's production editor(s), especially with regard to the publisher's own Latex macro package which has been specially designed for this series.

## Online Version/ LNP Homepage

LNP homepage (list of available titles, aims and scope, editorial contacts etc.):

<http://www.springer.de/phys/books/lnp/>

LNP online (abstracts, full-texts, subscriptions etc.):

<http://link.springer.de/series/lnp/>

J. Trampetić J. Wess (Eds.)

# Particle Physics in the New Millennium

Proceedings of the 8th Adriatic Meeting



RUDJER BOŠKOVIĆ INSTITUTE

Max-Planck-Gesellschaft  
zur Förderung der Wissenschaften e.V.



Springer

## Editors

Josip Trampetić  
Rudjer Boskovic Institute  
Theoretical Physics Division  
P.O.Box 180  
10 002 Zagreb  
Croatia

Julius Wess  
Sektion Physik der Ludwig-Maximilians-  
Universität  
Theresienstr. 37  
80333 München  
and  
Max-Planck-Institut für Physik  
(Werner-Heisenberg-Institut)  
Föhringer Ring 6  
80805 München  
Germany

---

*Cover Picture:* (see Fig.1 contribution by D. Denegri in this volume)

---

Library of Congress Cataloging-in-Publication Data.

ISSN 0075-8450

ISBN 3-540-00711-3 Springer-Verlag Berlin Heidelberg New York

This work is subject to copyright. All rights are reserved, whether the whole or part of the material is concerned, specifically the rights of translation, reprinting, reuse of illustrations, recitation, broadcasting, reproduction on microfilm or in any other way, and storage in data banks. Duplication of this publication or parts thereof is permitted only under the provisions of the German Copyright Law of September 9, 1965, in its current version, and permission for use must always be obtained from Springer-Verlag. Violations are liable for prosecution under the German Copyright Law.

Springer-Verlag Berlin Heidelberg New York  
a member of BertelsmannSpringer Science+Business Media GmbH

<http://www.springer.de>

© Springer-Verlag Berlin Heidelberg 2003  
Printed in Germany

The use of general descriptive names, registered names, trademarks, etc. in this publication does not imply, even in the absence of a specific statement, that such names are exempt from the relevant protective laws and regulations and therefore free for general use.

Typesetting: Camera-ready by the authors/editor  
Cover design: *design & production*, Heidelberg

Printed on acid-free paper  
54/3141/du - 5 4 3 2 1 0

# Table of Contents

<b>Some Recent Results of Electromagnetic Nucleon Form Factors Measurements Using Transfer of Polarization</b> <i>Damir Bosnar (for the A1 collaboration at MAMI)</i> . . . . .	1
<b>Dyons in Nonabelian Born–Infeld Theory</b> <i>Antun Balaž, Maja Burić, Voja Radovanović</i> . . . . .	7
<b>One-Loop Finite Relations in the Standard Model</b> <i>Martin Buysse</i> . . . . .	11
<b>Gravitational Waves from Brane World <math>\nu</math> Oscillations During Supernova Core-Collapse</b> <i>Herman J. Mosquera Cuesta, Amol S. Dighe, André C. de Gouvêa</i> . . . . .	17
<b>Towards Adelic Noncommutative Quantum Mechanics</b> <i>Goran S. Djordjević, Ljubiša Nešić</i> . . . . .	25
<b>Three Loop Leading Top Mass Contributions to the <math>\rho</math> Parameter</b> <i>Michael Faisst</i> . . . . .	33
<b><math>\Delta S = 2</math> Decays of <math>B^-</math> Meson</b> <i>Svetlana Fajfer, Paul Singer</i> . . . . .	37
<b>Charmonium Hadro–Production at HERA-B</b> <i>Olga Igonkina (for the HERA-B collaboration)</i> . . . . .	45
<b>Finite Chern-Simons Matrix Model – Algebraic Approach</b> <i>Larisa Jonke and Stjepan Meljanac</i> . . . . .	53
<b>Expectations for Charged Higgs in CMS</b> <i>Ritva Kinnunen</i> . . . . .	61
<b>Heavy Ion Physics in CMS</b> <i>Olga Kodolova (for CMS collaboration)</i> . . . . .	69
<b>Tracking in a High Rate Environment</b> <i>Gordana Medin (for the HERA-B Collaboration)</i> . . . . .	77

<b>Resonances from Strongly-Interacting Electroweak Symmetry Breaking Sector at Future <math>e^+e^-</math> Colliders</b> <i>Mikuláš Gintner, Ivan Melo</i> .....	83
<b>Predictions for Deeply Virtual Compton Scattering on a Spin-One Target</b> <i>Axel Kirchner, Dieter Müller</i> .....	91
<b><math>H \rightarrow \tau\tau</math> Studies in CMS</b> <i>Alexander Nikitenko</i> .....	99
<b>Self-gravitating Bosons at Finite Temperature</b> <i>Hrvoje Nikolić</i> .....	107
<b>BLM Scale for the Pion Transition form Factor</b> <i>Blaženka Melić, Bene Nižić, Kornelija Passek</i> .....	114
<b>Selected Conversions of Massive Neutrinos</b> <i>Krešimir Kumerički, Ivica Picek</i> .....	123
<b>Pion and Vacuum Properties in the Nonlocal NJL Model</b> <i>Michał Praszalowicz, Andrzej Rostworowski</i> .....	130
<b>Black Hole Entropy from Horizon CFT in Gauss-Bonnet Gravity</b> <i>Maro Cvitan, Silvio Pallua, Predrag Prester</i> .....	139
<b>An Overview of the Sources for Electroweak Baryogenesis</b> <i>Tomislav Prokopec</i> .....	147
<b>Quantum Corrections for BTZ Black Hole via 2D Reduced Model</b> <i>Maja Burić, Marija Dimitrijević, Voja Radovanović</i> .....	157
<b>Squarks and Gluino Searches with CMS at LHC</b> <i>Gabriele Segneri</i> .....	161
<b>Target Mass Effects and the Jost-Lehmann-Dyson Representation for Structure Functions</b> <i>Igor L. Solovtsov</i> .....	169
<b>Family Replicated Calculation of Baryogenesis</b> <i>Holger B. Nielsen, Yasutaka Takanishi</i> .....	178
<b>Measurement of <math>\sin 2(\beta)</math> with BaBar</b> <i>Gloria Vuagnin (for the BaBar Collaboration)</i> .....	186
<b>Rare Decay <math>D^0 \rightarrow \gamma\gamma</math></b> <i>Svetlana Fajfer, Paul Singer, Jure Zupan</i> .....	193

## List of Contributors

**Damir BOSNAR**  
University of Zagreb

**Maja BURIĆ**  
University of Belgrade

**Martin BUYSSE**  
Universite Catholique de Louvain

**Herman J. M. CUESTA**  
Centro Brasileiro de Pesquisas Fisicas,  
Rio de Janeiro

**Goran DJORDJEVIĆ**  
University of Niš

**Michael FAISST**  
University of Karlsruhe

**Svjetlana FAJFER**  
University of Ljubljana

**Olga IGONKINA**  
ITEP, Moscow

**Larisa JONKE**  
Rudjer Bošković Institute, Zagreb

**Ritva KINNUNEN**  
Helsinki Institute of Physics

**Olga L. KODOLOVA**  
Skobeltcyn Institute of Nuclear  
Physics, Moscow

**Krešimir KUMERIČKI**  
University of Zagreb

**Matt LILLEY**  
Heidelberg University

**Gordana MEDIN**  
University of Montenegro, Podgorica

**Ivan MELO**  
University of Zilina

**Dieter MUELLER**  
University of Wuppertal

**Alexander NIKITENKO**  
ITEP, Moscow

**Hrvoje NIKOLIĆ**  
Rudjer Bošković Institute, Zagreb

**Kornelija PASSEK**  
Rudjer Bošković Institute, Zagreb

**Ivica PICEK**  
University of Zagreb

**Michael PRASZALOWICZ**  
Jagellonian University, Krakow

**Predrag PRESTER**  
University of Zagreb

**Tomislav PROKOPEC**  
Heidelberg University

**Voja RADOVANOVIĆ**  
University of Belgrade

VIII List of Contributors

**Gabriele SEGNERI**

INFN, Pisa

**Paul SINGER**

Technion, Haifa

**Yu. A. SITENKO**

Bogolyubov Institute for Theoretical  
Physics, Kiev

**Igor SOLOVTSOV**

Bogoliubov Lab at JINR, Dubna

**Yasutaka TAKANISHI**

Niels Bohr Institute, Copenhagen

**Gloria VUAGNIN**

INFN, Sezione di Trieste

**Jure ŽUPAN**

Jozef Stefan Institute, Ljubljana



# Some Recent Results of Electromagnetic Nucleon Form Factors Measurements Using Transfer of Polarization

Damir Bosnar (for the A1 collaboration at MAMI)

Department of Physics, Faculty of Science, University of Zagreb, Croatia

**Abstract.** Described are measurements of the electric form factor of the neutron, and modification of the proton form factor in the medium, using transfer of polarization. Main features of the continuous wave electron accelerator MAMI Mainz are outlined. Three high-resolution magnetic spectrometers, and proton and neutron polarimeters of the A1 collaboration are described. Recent measurements of the neutron electric form factor in the reaction  $D(\vec{e}, e' \vec{n})p$  and measurements of the medium modification of the proton factor in the reaction  ${}^4\text{He}(\vec{e}, e' \vec{p}){}^3\text{H}$  are presented.

## 1 Introduction

Understanding the structure of nucleons is of fundamental importance in the particle and nuclear physics. Presently the QCD, which is believed to be the theory of strong interactions, is not solvable at low energies and QCD-based theories have been developing. The ability of these theories to predict nucleon form factors and the influence of the nuclear medium upon them represents one of the most stringent tests of these theories, and hence precise data are required.

Polarization transfer experiments in electron scattering of good statistical accuracy became feasible with the development of electron accelerators with high luminosity, high duty factor and high polarized electron beams. New observables, shadowed in unpolarized experiments, become now available and reveal new and precise information regarding nucleon structure and the influence of the nuclear medium upon it.

In this contribution two examples of double polarization measurements at MAMI Mainz will be described: the determination of the neutron electric form factor, and the modification of proton form factor in the nuclear medium. Longitudinally polarized electron beam has been used in both experiments, and the polarization of the outgoing nucleon has been determined.

## 2 Mainz Microtron MAMI

The electron accelerator MAMI is located on the campus of the Johannes Gutenberg University in Mainz, Germany. MAMI [1] is a continuous-wave electron accelerator and consists of an injector linac followed by a cascade of three microtrons. The maximum available electron energy is 883 MeV and the maximum

current is 110  $\mu\text{A}$ . The polarized beam is available [2] with the maximum polarization of 80% and maximum current of 15  $\mu\text{A}$ . The helicity of the polarized beam can permanently be switched.

The upgrading of the accelerator is currently being undertaken. The already existing third stage of the microtron will be an input to the double sided-microtron. After the upgrade, which will be completed in 2003, the maximum electron energy is expected to be 1.5 GeV.

### 3 Magnetic Spectrometers and Nucleon Polarimeters

The A1 collaboration at MAMI Mainz has built three high-resolution magnetic spectrometers [3] and has been using them in the electron scattering experiments in order to explore nucleon and nuclei properties. In some experiments the magnetic spectrometers are complemented by additional detectors to achieve desired quantities. In the measurements described in this contribution, magnetic spectrometers have been used with nucleon (proton or neutron) polarimeters.

#### 3.1 Magnetic Spectrometers

The magnetic spectrometers, named A,B,C, have solid angles of 28 msr, 5.6 msr and 28 msr, respectively. They can detect electrons, pions, protons and other charged particle with the maximum momentum 735 MeV/c, 870 MeV/c, and 551 MeV/c, and have acceptance of 20 %, 15 %, 25 %, respectively. Deflecting magnet systems in A and C are built in the same way and consist of a quadrupole, a sextupole and two dipole magnets. The spectrometer B has a single clamshell dipole magnet. Detector packages in all three spectrometers are built in the same way and consist of two double-planes of vertical drift chambers (VDCs), two layers (3mm and 10mm thick) of scintillator counters and a Cherenkov counter. The magnetic spectrometers provide information regarding momentum of outgoing charged particles with the resolution better than  $10^{-4}$ , angles of outgoing charged particles with the resolution better than 3 mrad at the target, and information regarding the type of charged particles. Single measurements, as well as double and triple coincidence measurements are possible.

#### 3.2 Proton and Neutron Polarimeters

Measurements of proton and neutron polarizations are based on the same principle. The fact that the spin-orbit part and the radial part of the nuclear potential have the same order of magnitude is used. If the outgoing nucleons are polarized, their secondary scattering in the analyzer causes asymmetry in the cross section from which their polarization can be obtained.

In order to measure the proton polarization, the focal plane proton polarimeter has been built [4] and it can be put in the spectrometer A in place of the Cherenkov counter. The graphite analyzer has been used in this polarimeter. The large area horizontal drift chambers built for this polarimeter [5] determine

the scattering angles after passing analyzer, and standard VDCs in the spectrometer A determine proton trajectories before passing through the analyzer. The spin precession and information about all three polarization components of the protons at the target are provided by the passage of protons through the magnetic system of the spectrometer [6].

Neutrons are neutral particles, therefore the magnetic spectrometer supplemented with polarimeter cannot be used for their detection and polarization measurement. For these purposes a separate neutron polarimeter consisting of two walls of a plastic scintillator has been built [7]. The first wall of the plastic scintillator determines trajectories of outgoing neutrons and is used simultaneously as the analyzer [8]. The second wall of the plastic scintillator determines trajectories of the scattered neutrons in the analyzer. Between the polarimeter and the target there is a dipole magnet which provides controlled precession of neutron spins, and this is used to avoid calibration of effective analyzing power [9].

#### 4 Neutron Electric Form Factor and Double Polarization Measurements

The cross section for the elastic electron-nucleon scattering can be written in the Rosenbluth form using the Sachs form factors  $G_E$  and  $G_M$  [10]:

$$\frac{d\sigma}{d\Omega} = \left( \frac{d\sigma}{d\Omega} \right)_{Mott} \left( \frac{G_E^2 + \tau G_M^2}{1 + \tau} + 2\tau G_M^2 \tan^2 \frac{\theta_e}{2} \right), \quad (1)$$

where  $(\frac{d\sigma}{d\Omega})_{Mott}$  is the Mott cross section for the electron scattering off pointlike spin  $\frac{1}{2}$  particle,  $\theta_e$  is the electron scattering angle,  $\tau = \frac{Q^2}{4m_N^2}$  with  $m_N$  nucleon mass and  $Q^2 = -q^2 = \omega^2 - \vec{q}^2$ ,  $\omega$  energy and  $\vec{q}$  momentum of the virtual photon.

The proton form factors  $G_{E,M}^p$  have been successfully determined in the elastic electron-proton scattering. Measurements of neutron elastic form factors are more difficult because a free neutron target, which could be used in electron scattering experiments for this purpose, does not exist. One should use scattering off light nuclei where the influence of other nucleons must be accounted for. This method has been used to determine the neutron magnetic form factor  $G_M^n$ , but it cannot provide reliable results for the much smaller electric form factor  $G_E^n$ . This quantity becomes accessible as well by using measurements with the polarization transfer in exclusive electron scattering experiments [11]. In the ideal case of the  $n(\vec{\epsilon}, \epsilon' \vec{n})$ :

$$\frac{P_n^x}{P_n^z} = - \frac{1}{\sqrt{\tau + \tau(1 + \tau)\tan^2 \frac{\theta_e}{2}}} \frac{G_E^n}{G_M^n}, \quad (2)$$

where  $P_n^x$ ,  $P_n^z$  are components of neutron polarization in x and z directions, respectively. The x-axis of the coordinate system is in the electron scattering plane perpendicular to the direction of momentum transfer, y-axis is normal to

## Editors

Josip Trampetić  
Rudjer Boskovic Institute  
Theoretical Physics Division  
P.O.Box 180  
10 002 Zagreb  
Croatia

Julius Wess  
Sektion Physik der Ludwig-Maximilians-  
Universität  
Theresienstr. 37  
80333 München  
and  
Max-Planck-Institut für Physik  
(Werner-Heisenberg-Institut)  
Föhringer Ring 6  
80805 München  
Germany

---

*Cover Picture:* (see Fig.1 contribution by D. Denegri in this volume)

---

Library of Congress Cataloging-in-Publication Data.  
Cataloging-in-Publication Data applied for

Bibliographic information published by Die Deutsche Bibliothek Die Deutsche Bibliothek lists this publication in the Deutsche Nationalbibliografie; detailed bibliographic data is available in the Internet at <<http://dnb.ddb.de>>

ISSN 0075-8450

ISBN 3-540-00711-3 Springer-Verlag Berlin Heidelberg New York

This work is subject to copyright. All rights are reserved, whether the whole or part of the material is concerned, specifically the rights of translation, reprinting, reuse of illustrations, recitation, broadcasting, reproduction on microfilm or in any other way, and storage in data banks. Duplication of this publication or parts thereof is permitted only under the provisions of the German Copyright Law of September 9, 1965, in its current version, and permission for use must always be obtained from Springer-Verlag. Violations are liable for prosecution under the German Copyright Law.

Springer-Verlag Berlin Heidelberg New York  
a member of BertelsmannSpringer Science+Business Media GmbH

<http://www.springer.de>

© Springer-Verlag Berlin Heidelberg 2003  
Printed in Germany

The use of general descriptive names, registered names, trademarks, etc. in this publication does not imply, even in the absence of a specific statement, that such names are exempt from the relevant protective laws and regulations and therefore free for general use.

Typesetting: Camera-ready by the authors/editor  
Cover design: *design & production*, Heidelberg

measurements, and this causes significant differences between the neutron charge distributions in the Breit frame obtained from respective Fourier transforms of  $G_E^n$ .

## 5 Medium Modification Measurements of the Proton Form Factors

The polarization transfer reaction  $p(\vec{\epsilon}, e'\vec{p})$  can be used to measure the form factor ratio  $\frac{G_E^p}{G_M^p}$  by measuring the ratio of transverse and longitudinal polarization components of scattered protons [11]:

$$\frac{G_E^p}{G_M^p} = -\frac{P_x}{P_z} \frac{E + E'}{2m_p} \tan \frac{\theta_e}{2}, \quad (4)$$

where  $E$  and  $E'$  are energies of the incident and scattered electrons,  $\theta_e$  represents the electron scattering angle and  $m_p$  is the proton mass. The  $P_z$  and  $P_x$  are longitudinal and transverse polarization transfer observables, respectively. The  $z$ -axis is in the direction of the momentum transfer,  $y$ -axis normal to the electron scattering plane and  $x$ -axis is in the electron scattering plane normal to the direction of momentum transfer. We have measured the polarization transfer in the reaction  ${}^4\text{He}(\vec{\epsilon}, e'\vec{p}){}^3\text{H}$  at  $Q^2 = 0.4(\text{GeV}/c)^2$  and compared the ratio of transverse and longitudinal polarization components of ejected protons, to the same ratio for  $\vec{\epsilon}p$  scattering [20]. In this measurement protons were detected in the spectrometer A that was supplemented by the focal plane polarimeter described above, and electrons were detected in the spectrometer B.

Obtained results have been compared [20] with theoretical calculations and they favored models with a slightly modified form factor, but the statistical significance is not sufficient enough to exclude calculations without form factor modifications and the measurements with higher statistics are needed.

## References

1. H. Hermighaus et al., Proc. LINAC'90, 362 Albuquerque, New Mexico, USA (1990).
2. K. Aulenbacher et al., Nucl. Instr. and Meth. A **391**, 498 (1997).
3. K.I. Blomqvist et al. Nulc. Instr. and Meth. A **403**, 263 (1998).
4. Th. Pospischil et al., accepted by Nulc. Instr. and Meth. A.
5. Th. Pospischil et al., accepted by Nulc. Instr. and Meth. A.
6. Th. Pospischil, doctoral thesis, Mainz University 2000.
7. M. Seimetz, Dissertation in preparation, Institut für Kernphysik, Universität Mainz.
8. T. N. Taddeucci et al., Nucl. Instr. Meth. A **241**, 448 (1985).
9. M. Ostrick et al., Phys. Rev. Lett. **83**, 276 (1999).
10. R.G.Sachs, Phys. Rev. **126**, 2256 (1962).
11. R.G. Arnold, C. E. Carlson, F. Gross, Phys. Rev. C **23**, 363 (1981).
12. C. Herberg et al., Eur. Phys. J. A **5**, 131 (1999).

13. J. Becker et al., Eur. Phys. J. A **6**, 329 (1999).
14. J. Golak et al., Phys. Rev. C **63**, 034006 (2001).
15. D. Rohe et al., Phys. Rev. Lett. **83**, 4257 (1999).
16. J. Bermuth, doctoral thesis, Mainz University 2001.
17. T. Eden et al., Phys. Rev. C **50**, R1749 (1994).
18. I. Passchier et al., Phys. Rev. Lett. **82**, 4988 (1999).
19. H. Zhu et al., Phys. Rev. Lett. **87**, 081801 (2001).
20. S. Dieterich et al., Phys. Lett. B **500**, 47 (2001).

# Dyons in Nonabelian Born–Infeld Theory

Antun Balaž<sup>1</sup>, Maja Burić<sup>2</sup>, and Voja Radovanović<sup>2</sup>

<sup>1</sup> Institute of Physics, P. O. Box 57, 11001 Belgrade, Yugoslavia

<sup>2</sup> Faculty of Physics, University of Belgrade, P. O. Box 368, 11001 Belgrade, Yugoslavia

**Abstract.** We analyze the nonabelian extension of Born–Infeld lagrangian for  $SU(2)$  group. In the class of spherically symmetric solutions of finite energy, besides the Gal’tsov–Kerner glueballs we find only the analytic dyon solutions.

## 1 Action and Field Equations

The initial point of our analysis is the following nonabelian Born–Infeld [1,2] (NBI) action in Minkowski space:

$$S = \frac{1}{4\pi} \int d^4x (1 - \mathcal{R}) , \quad \mathcal{R} = \sqrt{1 + \frac{1}{2} F_{\mu\nu}^a F^{\mu\nu a} - \frac{1}{16} F_{\mu\nu}^a F^{*\mu\nu a}} . \quad (1)$$

The equations of motion which follow from the NBI action (1) are

$$D_\mu \frac{F^{\mu\nu} - G F^{*\mu\nu}}{\mathcal{R}} = 0 . \quad (2)$$

Here  $F^*$  denotes the Hodge-dual,  $F^{*\mu\nu} = \frac{1}{2} \epsilon^{\mu\nu\rho\sigma} F_{\rho\sigma}$ ,  $D_\mu$  is covariant derivative,  $a$  is the index of the gauge group and  $G = \frac{1}{4} F_{\mu\nu}^a F^{*\mu\nu a}$ . The equations of motion (2) can be complemented with the Bianchi identities,  $D_\mu F^{*\mu\nu} = 0$ .

In [2], spherically-symmetric configurations of finite energy for the action (1) were found. The ansatz for the gauge potentials was the monopole ansatz and it describes purely magnetic configurations. The usual splitting of the field strengths  $F_{\mu\nu}^a$  into “electric” and “magnetic” parts is:

$$E_i^a = F_{i0}^a , \quad B_i^a = \frac{1}{2} \epsilon_{ijk} F_{jk}^a . \quad (3)$$

We will generalize the monopole ansatz – in fact, we will consider the general spherically symmetric static potential for the  $SU(2)$  group (the so-called Witten’s ansatz, [3]). It is given by three real functions  $a_0(r)$ ,  $a_1(r)$ ,  $w(r)$  of the radial coordinate  $r$ . The components of the gauge potential read:

$$A_0^a = a_0(r) \frac{x^a}{r} , \quad A_i^a = a_1(r) \frac{x^a x^i}{r^2} + \epsilon_{aik} \frac{1 - w(r)}{r} \frac{x^k}{r} . \quad (4)$$

Here  $x^a$ ,  $x^i$  and  $x^k$  are the Cartesian coordinates. The field strengths for this ansatz are

$$E_i^a = a_0' \frac{x_i x_a}{r^2} - \frac{a_0 w}{r} \frac{x_i x_a - \delta_{ia} r^2}{r^2} ,$$

$$B_i^a = -2\delta_{ia} \frac{1-w}{r^2} + \frac{(1-w)^2}{r^2} \frac{x_i x_a}{r^2} + \left(\frac{1-w}{r^2}\right)' \frac{x_i x_a - \delta_{ia} r^2}{r} + \frac{a_1 w}{r^2} \epsilon_{iak} x_k ,$$

where prime denotes the derivative  $\frac{d}{dr}$ . The square root  $\mathcal{R}$  from (1) is

$$\mathcal{R} = \sqrt{1 + \frac{(1-w^2)^2}{r^4} + 2\frac{w'^2}{r^2} + 2\frac{a_1^2 w^2}{r^2} - 2\frac{a_0^2 w^2}{r^2} - a_0'^2 - \frac{[a_0(1-w^2)]'^2}{r^4}} .$$

We can now consider the condition of extremality of the action. After the integration of angular variables, the action is proportional to the lagrangian  $L$ ,

$$L = \int_0^\infty r^2 (\mathcal{R} - 1) dr . \quad (5)$$

Varying the unknown functions  $a_0$ ,  $a_1$  and  $w$ , we obtain the set of equations:

$$w^2 a_1 = 0 , \quad (6)$$

$$(1-w^2) \left( \frac{[a_0(1-w^2)]'}{r^2 \mathcal{R}} \right)' = \frac{2w^2 a_0}{\mathcal{R}} - \left( \frac{r^2 a_0'}{\mathcal{R}} \right)' , \quad (7)$$

$$w a_0 \left( \frac{[a_0(1-w^2)]'}{r^2 \mathcal{R}} \right)' = -\frac{2w(1-w^2)}{r^2 \mathcal{R}} - \left( \frac{2w'}{\mathcal{R}} \right)' - \frac{w a_0^2}{\mathcal{R}} + \frac{w a_1^2}{\mathcal{R}} . \quad (8)$$

## 2 NBI Dyons

The system of equations (6–8) is a complicated nonlinear system. We will search for particular solutions of this system with finite energy. The energy of the static configurations is equal to the negative value of the lagrangian,  $M = -L$ . The convergence of this integral on both boundaries imposes restrictions on the asymptotic behavior of the functions  $a_0$ ,  $a_1$  and  $w$ . We will discuss these restrictions later.

The simplest equation (6) implies essentially that  $a_1(r) = 0$ . Therefore, we will always assume this and denote  $a_0(r) = a(r)$  in the following.

The solutions with  $a(r) = 0$  were analyzed in [2] in detail. The simplest solution in this case is  $w(r) = \pm 1$  and it represents the pure gauge.  $w(r) = 0$  is also a solution: this is the embedded  $U(1)$  monopole. Its energy is finite:

$$M_e = \frac{\pi^{3/2}}{3\Gamma(3/4)^2} \approx 1.2360 . \quad (9)$$

There is also an infinite discrete set of finite energy solutions  $w_n(r)$  with the index  $n \in \mathbb{N}$ . These solutions can be found numerically using the condition that the function  $w(r)$  with the allowed asymptotic forms at  $r \rightarrow 0$  and  $r \rightarrow \infty$  match in the intermediate region. They are called Gal'tsov–Kerner glueballs.



The other simple possibility,  $w(r) = 0$ ,  $a(r) \neq 0$ , is also nontrivial. The equations of motion in this case reduce to

$$\left(\frac{a'}{r^2\mathcal{R}}\right)' = -\left(\frac{r^2a'}{\mathcal{R}}\right)', \quad \mathcal{R} = \sqrt{\frac{(1+r^4)(1-a'^2)}{r^4}}. \quad (10)$$

This equation can be solved explicitly and its solution is a two-parameter family

$$a(r; C, \alpha) = C \pm \int \sqrt{\frac{\alpha - 1}{\alpha + r^4}} dr, \quad (11)$$

where  $C$  and  $\alpha$  are the integration constants and  $\alpha > 1$ . The explicit form of the solution is given in terms of the elliptic integral. In accordance with the conditions of finiteness of energy and invariance of the equations under the change  $a(r) \rightarrow -a(r)$ , we will take  $C = 0$  and the  $+$  sign in front of the square root. The function  $a(r)$  for different values of  $\alpha$  is shown in Fig. 1. The limiting value of the parameter,  $\alpha = 1$ , gives  $a(r) = \text{const}$ , a configuration which is gauge equivalent to the embedded monopole  $w(r) = 0$ ,  $a(r) = 0$ . The energy of the solution (11) is

$$M(\alpha) = \frac{\pi^{3/2}}{\Gamma(3/4)^2} \frac{1}{2\alpha^{1/4}} \left(1 - \frac{\alpha}{3}\right). \quad (12)$$

The energy is unbounded below and its maximum is  $M_e$  at  $\alpha = 1$ . We observe that the existence of the electric field decreases the total energy.

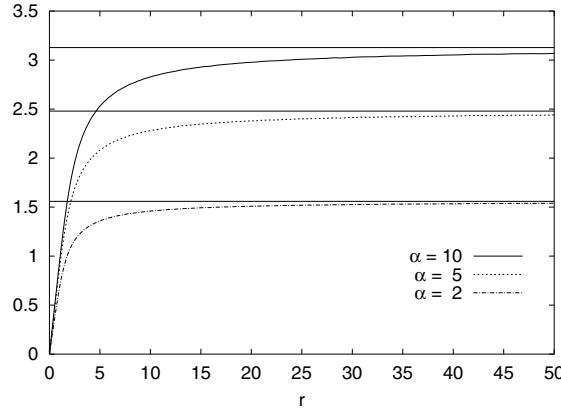


**Fig. 1.** Dyon solutions

We will call the solution (11) dyon [4], as in the asymptotic region  $r \rightarrow \infty$  the behavior of the electric and magnetic fields is given by

$$E_i^a \sim \sqrt{\alpha - 1} \frac{x_i x_a}{r^4}, \quad B_i^a \sim -\frac{x_i x_a}{r^4}, \quad (13)$$

and describes the field strenghts of point-like sources. The “electric charge” of the source is proportional to  $\sqrt{\alpha - 1}$ , while the “magnetic charge” is 1.

### 3 Conclusions

The condition of finiteness of energy in the general case of spherically symmetric NBI configurations restricts the possible behavior of the functions  $w(r)$  and  $a(r)$ . Along with the cases discussed above, there is one interesting solution which behaves as 't Hooft-Polyakov monopole (i.e.  $a(r) \rightarrow \text{const}$  and  $w(r) \rightarrow 0$  for  $r \rightarrow \infty$ ). It can be obtained by numerical integration starting from  $r = 0$  for some values of initial parameters denoted as  $w_2$  and  $a_1$ . The outcome of the integration for  $w_2 = -10$  and  $a_1 = 0.5$  with the integration step  $h = 10^{-5}$  is shown in Fig. 2. However, this solution is numerically unstable: if we keep the same values for the parameters  $w_2$  and  $a_1$ , but decrease the integration step  $h$ , we see that the oscillations of  $w(r)$  increase to the larger region of  $r$  and that the asymptotic value of  $a(r)$  at infinity increases. We conclude that the solutions of this type are probably nonanalytic. The analysis of the energy confirms this conclusion, too: the values of energy differ for orders of magnitude for different integration steps. We see that in the NBI case, as in the pure Yang–Mills theory,  $w(r) = 0$  and  $w(r) = 1$  are separated by infinite energy barrier and it is impossible to find the solution of finite energy which interpolates between them.

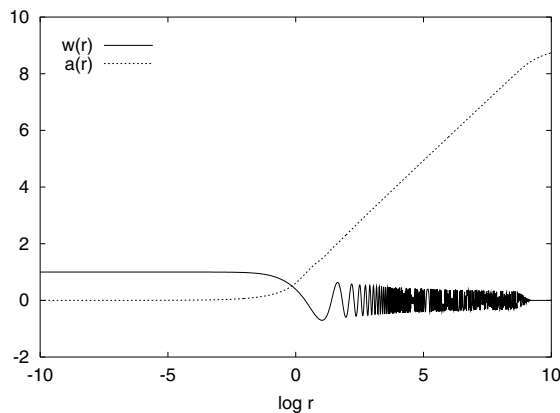


Fig. 2. Would-be NBI monopole

Further numerical analysis of the other allowed asymptotics strongly indicates that, besides Gal'tsov–Kerner glueballs and analytic dyons, there are no finite energy solutions.

### References

1. M. Born and L. Infeld, Proc. Roy. Soc. **A144**, 425 (1934).
2. D. Gal'tsov and R. Kerner, Phys. Rev. Lett. **84**, 5955 (2000).
3. M. S. Volkov and D. V. Gal'tsov, Phys. Rep. **319**, 1 (1999).
4. B. Julia and A. Zee, Phys. Rev. D **11**, 2227 (1975).

# One-Loop Finite Relations in the Standard Model

Martin Buysse

Institut de Physique Théorique, Université Catholique de Louvain, 2, Chemin du  
Cyclotron, B-1348 Louvain-La-Neuve, Belgium

**Abstract.** We establish the existence of *one-loop finite relations* between the Cabibbo angle and the quark mass ratios, in a Standard Model with one Higgs doublet and two quark generations. The argument is based on the calculation of the divergent one-loop radiative corrections to the quark mass matrices<sup>1</sup>.

## 1 Introduction

One of the outstanding questions raised by the Standard Model (SM) of elementary particles concerns the set of free parameters it seems to involve. Many of those parameters find their origin in the Yukawa sector of the theory: six quark masses, three mixing angles and one phase, not to mention the leptons. Furthermore, their empirical values show a strongly hierarchical pattern. Since the early times of its discovery, one has tried to complete the SM in order to reduce the size of its set of free parameters and hence propose an explanation for this observed hierarchy. The simplest way to reach this goal is to look for potential relations between apparently free parameters. But one has to make sure that those relations are preserved by the renormalization; they must be *natural* [2] [3], or at least, finite. Until now, most attempts consisted in enlarging the symmetry group of the SM by adding a horizontal component to it [4] [5] [6] [7]. The horizontal symmetry imposes constraints on the structure of the Yukawa couplings. After spontaneous breakdown of the symmetry, the fermion mass matrices that are generated still bear the stamp of those constraints and through bidiagonalization, they give rise to relations between mass ratios and mixing angles. Such an implementation guarantees that the relations survive to renormalization; they are called *natural*. However one soon realized [8] [9] [10] [11] that it could not be achieved without extending the particle content – by considering models with more than one Higgs doublet, thereby increasing the number of couplings...

We present an alternative way to envisage naturalness in the Yukawa sector [1]. We assume the existence of a tree-level relation between some apparently free parameters, such that it is not spoiled by divergent one-loop radiative corrections. The condition is not sufficient, but it is necessary (to be sufficient, the relation should hold at all orders in perturbation theory). Moreover, instead of one-loop naturalness, we talk about one-loop finiteness, since the obtained result

---

<sup>1</sup> This contribution is largely inspired by [1].

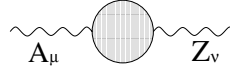
is not necessarily correlated with the presence of an extra symmetry group in the SM.

A first section is devoted to the presentation of a situation (evoked in [12]) where the use of a one-loop argument happens to be quite promising. We show how such a kind of argument, applied to the weak mixing angle  $\theta_W$ , within the SM, may give an insight of some higher scale *vertical* symmetry, and suggest the existence, at that scale, of a Grand Unified Theory (GUT).

In the second section we focus on the Cabibbo mixing angle and the quark mass ratios in a SM with one Higgs doublet and two quark generations. We establish a method to find out the one-loop finite relations between the *a priori* free parameters. We show that there are indeed one-loop finite relations (expressing the Cabibbo angle  $\theta_C$  as a function of the quark mass ratios  $m_u/m_c$  and  $m_d/m_s$ ) in a one-Higgs-doublet SM. We conclude that those relations cannot originate from any additionnal horizontal symmetry.

## 2 The Weak Angle

The weak angle  $\theta_W$  mixes the neutral bosons  $W_\mu^3$  and  $B_\mu$ , isospin eigenstates, to end up with the neutral bosons  $Z_\mu^0$  and  $A_\mu$ , mass eigenstates of the  $SU(2) \otimes U(1)$  Standard Model. This angle is radiatively corrected by the following vacuum polarization diagram:



$$(1)$$

Now imagine some theory, beyond the SM, in which the weak angle is no longer a free parameter. The radiative corrections to it would be finite. In particular, among them, the radiative corrections proportional to the number  $n$  of fermion generations would be finite.

Hence, if the fermion content of the theory of which we have assumed the existence is identical to the one of the SM, one can put the divergent fermionic contributions of the diagram (1) to zero, and obtain a constraint on the weak angle. At the one-loop level, without considering the finite parts, one has for  $\delta\theta_W$

$$\begin{aligned} n \sum_{\text{fermions}} \text{diagram (1)} &= n \sum_{\text{fermions}} \frac{Q(\frac{T_3}{2} - Q \sin^2 \theta_W)}{\cos \theta_W \sin \theta_W} \cdot \Pi_{\mu\nu} \\ &= n \frac{1 - \frac{8}{3} \sin^2 \theta_W}{\cos \theta_W \sin \theta_W} \cdot \Pi_{\mu\nu} \end{aligned} \quad (2)$$

where  $\Pi_{\mu\nu}$  is the photon self-energy in QED (whose divergent part does not depend on the mass of the fermion running in the loop), and where the sum has to be performed on the fermions of one single generation.

Hence, putting those divergent contributions to zero amounts to impose the constraint

$$\sin^2 \theta_W = \frac{3}{8} \quad (3)$$

which is precisely the value of  $\sin^2 \theta_W$  at the GUT scale. This means that, within the SM, without knowing anything of GUT's, one can use a one-loop argument to get some information about them, as far as they exist.

### 3 The Cabibbo Angle

We consider the two-fermion-generation SM in its minimal realization, namely built up with one single Higgs doublet. The hadronic Yukawa sector, which we are interested in, contains three useful free parameters: the Cabibbo angle  $\theta_C$  and the two mass ratios  $r_u = m_u/m_c$  and  $r_d = m_d/m_s$ . We assume the existence of a relation between the Cabibbo angle and the mass ratios, whose general form reads:

$$F(\theta_C) = G(r_u, r_d) \quad (4)$$

so that

$$F(\theta_C + \delta \theta_C) = G(r_u + \delta r_u, r_d + \delta r_d) \quad (5)$$

where  $\delta \theta_C$ ,  $\delta r_u$  and  $\delta r_d$  are the divergent parts of the radiative corrections to  $\theta$ ,  $r_u$  and  $r_d$  respectively. To be finite, (4) cannot be broken by infinite radiative corrections. That is, (5) must be verified. Thus

$$F_{\theta_C} \delta \theta_C = G_{r_u} \delta r_u + G_{r_d} \delta r_d \quad (6)$$

where  $f_x$  denotes the (partial) derivative of  $f$  with respect to  $x$ . Computing the one-loop radiative corrections<sup>2</sup>, one obtains:

$$\delta \theta_C = \epsilon \left[ \frac{1 + r_u^2}{1 - r_u^2} (m_d^2 - m_s^2) + \frac{1 + r_d^2}{1 - r_d^2} (m_u^2 - m_c^2) \right] \sin \theta_C \cos \theta_C \quad (8)$$

<sup>2</sup> The calculation of the divergent one-loop radiative corrections to the quark mass matrices, exclusively involves self-energy and tadpole diagrams. More precisely, since we are interested in relations between up-type quark mass ratios and down-type quark mass ratios on the one hand, and mixing angles on the other hand, we only need to compute the divergent one-loop radiative corrections to those specific parameters. This considerably simplifies our task. One indeed notices that neither QED nor QCD, which are flavour-blind, will bring in divergent contributions that would affect the mixing angle or the mass ratios. The same argument holds for the diagrams involving the transverse polarizations of the  $Z^0$  and of the  $W^\pm$  vector bosons, as well as the tadpoles. In other words, the only diagrams one has to consider are the quark self-energies due to the exchange of the scalars (Higgs and would-be-Goldstone bosons), that is, diagrams of the following type



$$\quad (7)$$

where the dashed line stands for the boson line. This is not astonishing since the scalars are the only fields that know about the difference between the fermion families. We are looking for a special structure inside the Yukawa couplings (or the mass matrices), hence the fact that the Yukawa sector is the only one responsible for the naturalness of this structure will come as no surprise. See [1] for the details of the calculation. to the Yukawa couplings

$$\delta r_u = \epsilon r_u [(m_d^2 - m_s^2) \cos 2\theta_C - (m_u^2 - m_c^2)] \quad (9)$$

$$\delta r_d = \epsilon r_d [(m_u^2 - m_c^2) \cos 2\theta_C - (m_d^2 - m_s^2)] \quad (10)$$

with  $\epsilon = \frac{3}{4} \frac{2}{v^2} \left( \frac{1}{4\pi^2} \ln \frac{\Lambda^2}{\mu^2} \right)$ ,  $\Lambda$  being a cut-off,  $\mu$  an arbitrary energy scale and  $v$  the vacuum expectation value of the scalar field. Let us bear in mind that we do not care about the finite part of the corrections. Introducing those expressions into equation (5) splits it into two independent equations (since we are not interested in considering relations involving mass ratios different from  $r_u$  and  $r_d$ ):

$$F_{\theta_C} \sin \theta_C \cos \theta_C \frac{1 + r_u^2}{1 - r_u^2} = G_{r_u} r_u \cos 2\theta_C - G_{r_d} r_d \quad (11)$$

$$F_{\theta_C} \sin \theta_C \cos \theta_C \frac{1 + r_d^2}{1 - r_d^2} = G_{r_d} r_d \cos 2\theta_C - G_{r_u} r_u \quad (12)$$

which turn out to be compatible if and only if

$$\cos 2\theta_C = \frac{\frac{1-r_u^2}{1+r_u^2} r_d G_{r_d} - \frac{1-r_d^2}{1+r_d^2} r_u G_{r_u}}{\frac{1-r_u^2}{1+r_u^2} r_u G_{r_u} - \frac{1-r_d^2}{1+r_d^2} r_d G_{r_d}} \quad (13)$$

Now this *must* be the relation (4) whose existence has been supposed, i.e.<sup>3</sup>

$$F(\theta_C) = \cos 2\theta_C \quad (14)$$

and

$$G(r_u, r_d) = \frac{\frac{1-r_u^2}{1+r_u^2} r_d G_{r_d} - \frac{1-r_d^2}{1+r_d^2} r_u G_{r_u}}{\frac{1-r_u^2}{1+r_u^2} r_u G_{r_u} - \frac{1-r_d^2}{1+r_d^2} r_d G_{r_d}} \quad (15)$$

Exploiting the remaining information in (11) and (12), and using (13) and (14), yields

$$\frac{1 + r_u^2}{1 - r_u^2} G - r_u G_{r_u} + \frac{1 + r_d^2}{1 - r_d^2} = 0 \quad (16)$$

$$\frac{1 + r_d^2}{1 - r_d^2} G - r_d G_{r_d} + \frac{1 + r_u^2}{1 - r_u^2} = 0 \quad (17)$$

This system – from which one obviously recovers equation (15) – is integrable, and the general solution reads

$$G(r_u, r_d) = \frac{-(1 + r_u^2)(1 + r_d^2) + 2\lambda r_u r_d}{(1 - r_u^2)(1 - r_d^2)} \quad (18)$$

---

<sup>3</sup> One checks that the arbitrary character of those identifications will not show itself in the expected solution. To prove it, we imagine (14) would rather read  $f(F(\theta_C)) = \cos 2\theta_C$ . One should then replace  $G$  by  $f(G)$  in the left-hand side of (15). But the right-hand side of it is invariant under  $G \mapsto f(G)$ . Namely, one can solve (15) with respect to the variable  $f(G)$  which we finally identify to  $f(F(\theta_C)) = \cos 2\theta_C$ .

where  $\lambda$  is the integration constant. One concludes that, if a relation of the kind suggested in (4) exists, it necessarily belongs to the following class:

$$\cos 2\theta_C = \frac{-(m_u^2 + m_c^2)(m_d^2 + m_s^2) + 2\lambda m_u m_c m_d m_s}{(m_u^2 - m_c^2)(m_d^2 - m_s^2)} \quad (19)$$

## 4 Conclusion

We have found an infinite number of one-loop finite relations inside the Yukawa sector. This set is parametrized by a dimensionless constant  $\lambda$ . One has no further theoretical argument to constrain the value of  $\lambda$ ; and one cannot evade the difficulty by asking one of the quark masses to vanish, since it would lead to a cosine smaller than minus one.

Stating that several finite relations potentially exist in a one-Higgs-doublet model apparently contradicts previous results obtained in the context of family symmetries [8] [9] [10] [11]. But since we do not appeal to such kind of symmetries, we do not expect our result to respect the conclusions derived in their context. Namely, the one-loop finite relations (19) cannot be associated with the presence of any extra horizontal symmetry. One should examine the validity of the results at higher loop level; then look for some possible “determination principle” of it outside or beyond the SM – just as the  $SU(5)$  GUT determines the “one-loop conjectured” value of the weak angle  $\theta_W$  at the GUT scale.

We should stress that the evidence of the existence of such a set of one-loop finite relations, namely the evidence of the existence of non-trivial solutions to the system (17), crucially relies on the expression of the divergent one-loop radiative corrections to the Yukawa parameters, and would definitively be invalidated if one modifies a single coefficient in those corrections.

The analysis we have conducted here can be applied to the leptons, provided that the neutrinos are massive, their mass being of the Dirac type exclusively. The result, since it depends on the sole structure of the Yukawa sector, is strictly identical.

The extension of the present calculation to a three-quark-generation SM seems to be doomed to failure because of the complexity of the one-loop radiative corrections to the Cabibbo-Kobayashi-Maskawa parameters [13] [14]. Those corrections are indeed too cumbersome to be manipulated and introduced into a solvable partial differential equations system. We will however expound, in a forthcoming paper, an alternative approach to derive similar results in a  $n$ -quark-generation SM.

## Acknowledgments

We would like to thank the organizers of the meeting, as well as J.-M. Gérard and J. Weyers for their comments, and the *Fonds pour la Formation à la Recherche dans l'Industrie et dans l'Agriculture* (FRIA) for supporting this work.

## References

1. M. Buysse. hep-ph/0104244.
2. S. Weinberg. *Rev. Mod. Phys.*, 46:255–277, 1974.
3. S. Weinberg. *Trans. New York Acad. Sci.*, 38:185–201, 1977.
4. H. Fritzsch. *Phys. Lett.*, B70:436, 1977.
5. H. Harari, H. Haut, and J. Weyers. *Phys. Lett.*, B78:459, 1978.
6. S. Pakvasa and H. Sugawara. *Phys. Lett.*, B73:61, 1978.
7. H. Fritzsch and J. Plankl. *Phys. Lett.*, B237:451, 1990.
8. D. Wyler. *Phys. Rev.*, D19:330, 1979.
9. R. Barbieri, R. Gatto, and F. Strocchi. *Phys. Lett.*, B74:344–346, 1978.
10. R. Gatto, G. Morchio, and F. Strocchi. *Phys. Lett.*, B83:348–350, 1979.
11. R. Gatto, G. Morchio, and F. Strocchi. *Phys. Lett.*, B80:265, 1979.
12. G. C. Branco and J. M. Gerard. *Phys. Lett. B* **124**, 415 (1983).
13. N. Cabibbo. *Phys. Rev. Lett.* **10**, 531 (1963).
14. M. Kobayashi and T. Maskawa. *Prog. Theor. Phys.* **49**, 652 (1973).



# Gravitational Wave Bursts from Brane World Neutrino Oscillations During Supernova Collapse

Herman J. Mosquera Cuesta<sup>1,2,3</sup>, Amol S. Dighe<sup>4</sup>, and André C. de Gouvêa<sup>4</sup>

<sup>1</sup> Abdus Salam International Centre for Theoretical Physics, Strada Costiera 11, Miramare 34014, Trieste, Italy

<sup>2</sup> Centro Brasileiro de Pesquisas Físicas, Laboratório de Cosmologia e Física Experimental de Altas Energias, Rua Dr. Xavier Sigaud 150, CEP 22290-180 Urca, Rio de Janeiro, RJ, Brazil

<sup>3</sup> Centro Latinoamericano de Física (CLAF), Avenida Wenceslau Braz 173, Botafogo, Rio de Janeiro, RJ, Brazil

<sup>4</sup> CERN Theory Division, 1122 CH, Genève 23, Suisse

**Abstract.** In braneworld-like solutions of the hierarchy problem gravitons and right-handed (sterile) neutrinos are in principle the unique non-standard model fields allowed to propagate into the bulk, thus their coupling is naturally expected. Since active-to-sterile neutrino oscillations can take place during the core bounce of a supernova collapse, then gravitational waves must be produced over the oscillation length through anisotropic neutrino flow. Because the oscillation feeds mass-energy up into (or takes it out of) the target species, the large mass-squared difference between species makes a huge amount of energy to be given off as gravity waves, which is larger than from neutrino convection and cooling, or quadrupole moments of neutron star matter. The strength of these bursts would turn them the more sure supernova gravitational-wave signal detectable by interferometers, for distances out to the VIRGO cluster of galaxies.

## 1 Astrophysical Motivation

As an attempt to solve the critical hierarchy problem between the Planck scale ( $10^{19}\text{GeV}$ ) and the electro-weak (standard model-SM) scale ( $1 - 10\text{TeV}$ ) revolutionary approaches have been proposed, in which the large extra-dimensions of Arkani-Hamed, Dimopoulos and Dvali (ADD)[1–3] and Randall-Sundrum (RS) braneworlds[4,5] come into play. In those scenarios the standard model fields are supposed to exist in a 3+1 dimensional *brane* embedded in a higher dimensional *bulk* where gravity (and non-SM fields) is allowed to propagate. Since the sterile neutrino is also that *blind bulk* fermion [Mohapatra and Pérez-Lorenzana, Nucl. Phys. B 576, 466 (2000); Caldwell, Mohapatra and Yellin, Phys. Rev. Lett. 87, 041601 (2001)], then, in both the ADD scenarios and RS models [4,5], the graviton-right-handed neutrino ( $\nu$ ) coupling is to take place. Next we attempt to pave the pathway to this fundamental issue and to make the case for it, to show (including discussion on experimental and observational constraints) that neutrino oscillations in ADD and RS scenarios do produce gravitational radiation, and more important that these gravity waves (GWs) are likely detectable by GWs interferometers as LIGO, VIRGO, GEO-600, and TAMA-300, and also by the TIGAs network of resonant-mass detectors.

## 2 Graviton-Sterile Neutrino Coupling

Because of the validity of Newton's law up to length scales down to 1 mm, the extra-dimensions should appear at a smaller scale[1–3]. Admitting the existence of extra dimensions, it follows that the 4-D graviton must be supplemented by a *tower* of Kaluza-Klein (KK) modes that corresponds to the phase space thus available in the bulk. The KK modes for the graviton that can be the GWs to detect from the neutrino oscillations could be similar in nature, and must correspond to a subset of long wavelength KK modes of the tower. It has been suggested that these KK modes might be emitted during a supernova (SN) core collapse (our study case)[7], and radiatively to decay to form a cosmological background mainly of  $\gamma$ -rays ( $E_\gamma \leq 100\text{MeV}$ ), electron-positron and  $\nu, \bar{\nu}$  pairs, susceptible of being detected[8]. The KK modes then released would compete with the SN neutrino cooling by shorten the observable signal if the radius of the (1) extra dimension is  $R \leq 0.66\mu\text{m}$ , for an extra dimension energy scale  $M_{P,n+4} \geq 31\text{MeV}$ .

In *braneworld* models of string phenomenology[4,5] the neutrino sector is indicated as the most likely messenger of CPT violation to the rest of the standard model. This is because the source of dynamical or spontaneous CPT violation should lie in the bulk, while the standard model effects are expected to be visible only through couplings of SM fields, supposed to reside on branes, to suitable bulk messengers. The generic bulk messengers are the graviton and the right-handed  $\nu$ . In models with not infinite extra-dimensions gravity effects can still be visible, while the sterile neutrino can still have potentially observable Dirac mass couplings[9], although the resulting neutrino oscillation physics is irrelevant to account for the solar or atmospheric neutrino problems. Thus again, because the graviton and sterile singlet neutrino may co-exist in the bulk they might couple. Consequently, oscillations of active into sterile  $\nu$ s must produce gravitational waves, while in general oscillations among active  $\nu$  species cannot. In fact, in [10], and based upon most robust considerations of SN core physics, we showed that this seems to be case: no GWs from active-to-active  $\nu$  oscillations during a SN core bounce.

To illustrate this coupling we follow the paper by Grossman and Neubert[11] in which, for the case of a RS model; where a interesting neutrino phenomenology can develop, the action exhibiting the graviton ( $g_{vis}^{\mu\nu}$ ) and sterile neutrino ( $e_{R0}$ ) coupling reads as[11]

$$S = \int d^4x \sqrt{-g_{vis}} \left\{ g_{vis}^{\mu\nu} \partial_\mu H_0^\dagger \partial_\nu H_0 - \lambda(|H_0|^2 - v_0^2)^2 \right\} \\ + \int d^4x \sqrt{-g_{vis}} \left\{ \bar{L}_0 \gamma^\mu \partial_\mu L_0 + \bar{e}_{R0} \gamma^\mu \partial_\mu e_{R0} - (y_e \bar{L}_0 H_0 e_{R0} + h.c.) \right\}, \quad (1)$$

where  $g_{vis}^{\mu\nu} = e^{2kr_c\pi} \eta_{\mu\nu}$  is the induced metric on the brane, with  $\sqrt{g_{vis}} = \det(-g_{vis}^{\mu\nu}) = e^{4kr_c\pi}$ ,  $\gamma^\mu = E_a^\mu(\phi = \pi) \gamma^a = e^{kr_c\pi} \gamma^\mu$ . In (1)  $H = (\phi_1, \phi_2)$  is the Higgs doublet and  $L = \nu_L, e_L$  is a left-handed lepton doublet (the reader is addressed to [11] for a thorough discussion and definitions of the quantities

appearing in (2)). This action, (1), is obtained after integration over the fifth dimension of the action describing the blind bulk fermion of mass  $m$  coupling minimally to gravity

$$S_{\text{fermion}}^{\text{graviton}}|_{\text{bulk}} = \int d^4x \int d\phi \sqrt{G} \left\{ E_a^A \left[ \frac{i}{2} \bar{\Psi}^a (\partial_A - \partial_A) \Psi + \frac{\omega_{bcA}}{8} \bar{\Psi} \{^a, \sigma^{bc}\} \Psi \right] - m \text{sgn}(\phi) \bar{\Psi} \Psi \right\}. \quad (2)$$

The coupling is mediated by the *spin connection*  $\omega_{bcA}$ , in a 5-dim space of metric:  $ds^2 = e^{-2kr_c|\phi|} \eta_{\mu\nu} dx^\mu dx^\nu - r_c d\phi$ .

To settle the remaining basics, we also recall the way the neutrino flux couples to neutron star matter, as needed for the oscillations to take place. This coupling has been shown[12] to be the ultimate process responsible for the neat kick given to a nascent pulsar during a SN collapse (see Mosquera Cuesta [Phys. Rev. D. 65, 061503(R) (2002)]). The electroweak coupling of neutrons ( $N^0$ ) and  $\nu$ s inside the PNS is described by the Lagrangean

$$L_{N^0 \leftrightarrow \nu}^{\text{int}} = \left[ \frac{G_F}{\sqrt{2}} \right] (\bar{N}^0 \gamma_\mu (1 - \gamma_5) N^0) [\bar{\nu} \gamma^\mu (1 - \gamma_5) \nu], \quad (3)$$

with the  $\nu$  field satisfying the time-dependent Dirac equation

$$\left( i\gamma^0 \partial_0 + i\gamma^\alpha \partial_\alpha + \rho(t) v_\beta \gamma^\beta \left[ \frac{(1 - \gamma_5)}{2} \right] - m_\nu \right) \Psi = 0. \quad (4)$$

Above  $G_F$  is the Fermi constant, and  $v_\beta$  the  $\nu$  4-velocity. In dense matter (at rest) the neutron 4-vector current density  $J^\mu = \langle \bar{N}^0 \gamma_\mu (1 - \gamma_5) N^0 \rangle \equiv (\rho, 0, 0, 0)$  acquires a non-zero expectation value. Here  $\rho = \frac{G_F}{\sqrt{2}} N_n^0$ , with  $N_n^0$  the neutron number density.

### 3 Enlarged $\nu$ and GWs Luminosity from $\nu$ Oscillations

#### 3.1 Supernova Neutrinos and Flavor Conversions

That the neutrino outflow from a proto-neutron star (PNS) core bounce is a source of GWs is a well-known issue[14,13,15–17,10]. Numerical simulations by Müller and Janka[16] have shown that, in general, the fraction of the total binding energy emitted as GWs by pure neutrino convection is:  $E_{GW}^\nu \sim [10^{-10} - 10^{-13}] M_\odot c^2$ , for a  $\nu$  luminosity:  $L_\nu \sim 10^{53} \text{erg s}^{-1}$  (see [16] for further details).

Unlike GWs produced by convection of neutrinos [16], in the production of GWs by neutrino oscillations[10] from active-to-sterile there exists two main reasons for expecting a major enhancement in the GWs luminosity during the transient: a) the conversion itself, which makes it the overall luminosity of a given neutrino species to grow by a large factor:  $L_\nu \leq 10\% L_\nu^{\text{total}}$ , see below. The enhancement stems from the mass-energy being given to, or drained from,

the new species into which oscillations take place. This augment gets reflected in the species mass-squared difference (energy conservation), and their relative numbers: one species is number-depleted while the other gets its number enlarged. But, even if the energy increase is smaller, b) the abrupt conversion over the transition time,  $\Delta T_{\text{osc}} \sim 10^{-4}\text{s}$ , which is set up by the oscillation length,  $\lambda_{\text{osc}}$ , and the convective neutrino diffusion velocity, ( $\bar{V}_\nu \sim 10^9 \text{ cms}^{-1}$  [16]), also magnifies transiently  $L_\nu$ . Being the neutrino flavor transition the *key piece* to produce GWs by this mechanism, it is needed to estimate how many of them can actually oscillate. This quantity is measured by the transition probability:  $P_{a \rightarrow s}(|\mathbf{x} - \mathbf{x}_0|)$ , which we estimate next in considering the way the neutrino couples to the neutron matter so as to make it viable these  $\nu_a \longleftrightarrow \nu_s$  oscillations.

### 3.2 $\nu$ Oscillations in Dense Matter

It was shown in [10] that vacuum flavor conversions among active  $\nu$ s cannot increase significantly the amount of escaping neutrinos from the “frozen” SN core, and thus no GWs burst is generated. However, interaction with matter, as in (3), may help in allowing more  $\nu$ s to escape if resonant conversions into sterile  $\nu$ s occur inside the neutrinosphere of the active  $\nu$ s (see [10] from where the next discussion is briefly updated). In the case of  $\nu_e \leftrightarrow \nu_s$  oscillations, the resonance occurs if

$$\sqrt{2}G_F \left[ N_e(x) - \frac{1}{2}N_n(x) \right] \equiv V(x) = \frac{\Delta m^2}{2E_\nu} \cos 2\theta. \quad (5)$$

Here  $N_e(x)$  is the electron number density (given by  $N_{e^-} - N_{e^+}$ ), and  $N_n(x)$  is the neutron number density. In the case of  $\nu_{\mu,\tau} \leftrightarrow \nu_s$  the  $N_e$  term is absent, while in the case of antineutrinos, the potential changes by an overall sign. Numerically, for  $\nu_e \leftrightarrow \nu_s$  oscillations,

$$V(x) = 7.5 \times 10^6 \left( \frac{\text{eV}^2}{\text{MeV}} \right) \left( \frac{\rho_m(x)}{10^{14} \text{g/cm}^3} \right) \left( \frac{3Y_e}{2} - \frac{1}{2} \right), \quad (6)$$

where  $Y_e$  is the electron number fraction. For  $\nu_{\mu,\tau} \leftrightarrow \nu_s$  oscillations, the last term in parenthesis is changed to  $(\frac{Y_e}{2} - \frac{1}{2})$ , assumed henceforth to be of order one.

Neutrino conversions in the resonance region can be strong if the adiabaticity condition is fulfilled: the oscillation probability is  $P_{as} = \cos^2 2\theta$ , which is close to 1 in the case of small mixing angles. Moreover, after the resonance region, the newly created sterile  $\nu$ s have very a small probability ( $P_{sa}^{\text{average}} = \frac{1}{2} \sin^2 2\theta$ ) of oscillating back to active  $\nu$ s, which could be potentially trapped. For the resonance condition to be satisfied, we require:  $10^4 \text{eV}^2 \leq \Delta m^2 \cos 2\theta (\frac{10 \text{MeV}}{E_\nu}) \leq 10^8 \text{eV}^2$ , while the adiabaticity condition is satisfied for:

$$\frac{\Delta m^2 \sin^2 2\theta}{2E_\nu \cos 2\theta} \left( \frac{1}{\rho} \frac{d\rho}{dx} \right)_{x=x_{\text{res}}}^{-1} \gg 1, \quad (7)$$

where  $x_{\text{res}}$  is the position of the resonance layer. Inside the core:  $(\frac{1}{\rho} \frac{d\rho}{dx})_{x=x_{\text{res}}}^{-1} \equiv \lambda_{\text{osc}} \sim 1 \text{km}$ , and therefore the adiabaticity condition is satisfied if  $\Delta m^2 \frac{\sin^2 2\theta}{\cos 2\theta} \gg$

$10^{-3}\text{eV}^2(\frac{E_\nu}{10\text{MeV}})$ , which is easily satisfied by  $\Delta m^2 \geq 10^4\text{eV}^2$  as long as  $\sin^2 \theta \gg 10^{-7}$ . Thus, we find that a substantial fraction of  $\nu_s$  may get converted to sterile  $\nu_s$ , and escape the core of the star, if the sterile  $\nu_s$  mass is such that  $10^4\text{eV}^2 \leq \Delta m_{as}^2 \leq 10^8\text{eV}^2$ . Such a mass difference cannot solve the observed solar and atmospheric neutrino problem, but the possibility of three active neutrinos explaining these anomalies and a heavy sterile neutrino of mass  $m_{\nu_s} \sim \text{keV}$  still stays open. In compensation,  $\sim 10\text{keV}$  sterile neutrinos have been shown to make a relevant contribution to the solution of the dark matter problem in the universe[18,20]. The number of  $\nu_s$  escaping, and their angular distribution, is sensitive to the instantaneous distribution of production sites. It was argued that these inhomogeneities can give rise to quadrupole moments that generates GWs[10,16], and dipole moments that could drive the runaway pulsar kicks. [10] also showed that the *fraction* of sterile  $\nu_s$  that can actually escape in the first few milliseconds is:  $P_{a \rightarrow s}(|\mathbf{x} - \mathbf{x}_0|) \leq 10\%$  of the total  $\nu$ -flux, which corresponds to an energy:  $\Delta E_{\nu_a \rightarrow \nu_s} \sim 3 \times 10^{52}\text{erg}$ .

### 3.3 Experimental and Observational Bounds

A note on experimental oscillation constraints is pertinent then: a) at very low values of the mixing angle ( $\sin^2 2\theta \leq 10^{-2}$ ), the CHOOZ experiment does not put any constraints on the neutrino mass. b) the tritium  $\beta$  decay experiment indicates  $\sin^2 2\theta_{es} m_{\nu_s}^2 \leq (2.5)^2\text{eV}^2$ , which is consistent with  $m_{\nu_s}^2 \geq 10^4\text{eV}^2$  and  $\sin^2 2\theta_{es} \leq 10^{-4}$  (note that the adiabaticity condition (3.2) holds at this value of  $\theta_{es}$ ). c) the neutrinoless double beta decay constraint  $\sin^2 2\theta_{es} m_{\nu_s} \leq 0.2\text{eV}$ , is satisfied for  $m_{\nu_s} \geq 10^2\text{eV}$  and  $\sin^2 2\theta_{es} \leq 10^{-3}$ [6]. Meanwhile, the cosmological constraint, which comes from the requirement that the universe should not be overclosed by heavy neutrinos, can be sidestepped if  $\nu_s$  has a small enough lifetime, which would require physics beyond the standard model, as the braneworld models, here called for. The bounds from the big bang nucleosynthesis still allow one species of sterile neutrinos[18].

In addition, studies of supernova physics have also focused on the potential rôle of oscillations between active and sterile neutrinos. In particular, there are limits on the  $\nu_e \leftrightarrow \nu_s$  conversion rate inside the supernova core from the detected electron neutrino flux from SN1987A [19]. According to [19], the time spread and the number of detected  $\nu_e$  events constrain  $\nu_e \leftrightarrow \nu_s$  oscillations with:  $10^6 \leq \Delta m^2 \leq 10^8\text{eV}^2$  for  $10^{-3} \leq \sin^2 2\theta_{es} \leq 10^{-7}$ , in striking agreement with our previous results. More stringent constraints stem from arguing that if there were too many “escaping neutrinos”, the supernova explosion itself would not take place [19]. Such bounds are, however, model dependent. One should keep in mind that the mechanism through which the explosion takes place is, in fact, not well established[15]. On the other hand, it is very likely that, if the results of [19] are indeed in the right pathway, there is no hope of achieving  $P_{\text{esc}}$  larger than 10%.

From the precedent discussion it becomes clear that once the oscillation occurs almost all the sterile  $\nu_s$  being created escape the star taking a huge amount of energy (and momentum) density ( $\leq 10\%\rho^\nu$ ) away with them. The coupling energy to matter of the former active  $\nu_s$  that convert into steriles is lost in

the transition. As shown by Mosquera Cuesta[12], this outflow breaks the PNS equilibrium, generating the GWs burst that may make it to pulsate, rotate and move due to a rocket-like thrust. The force imparted to the escaping neutrinos:  $\bar{F}_\nu^{back} = L_\nu/\bar{V}_\nu$ , applies back to the remaining active  $\nu$ -fluid, and from the coupling  $\nu - N^0$  to the neutron matter, as described by (3), to finally push the star away.

## 4 Gravitational Wave Energetics and Detectability

Whenever the  $\nu$  oscillations do take place in the SN core, the GWs signal most likely detectable should be produced over the time interval for which the conditions for conversions to take place are maintained, i.e.  $\sim (1 - 2)$ ms, or equivalently for frequencies  $f_{\text{GWs}} \sim [0.5 - 1]$ kHz. This frequency range corresponds to the optimal bandwidth for detection of ground-based detectors. For a 1ms conversions time span the neutrino luminosity reads

$$L_\nu \equiv \frac{\Delta E_{\nu_a \rightarrow \nu_s}}{\Delta T_{\text{osc}}} \sim \frac{3 \times 10^{52} \text{erg}}{1 \times 10^{-3} \text{s}} = 3 \times 10^{55} \frac{\text{erg}}{\text{s}}. \quad (8)$$

Note that this  $L_\nu$  agrees quite well with the one numerically computed by Pons, Steiner, Prakash and Lattimer[21] (see their Figure 3), and also with data for  $L_\nu$  from SN1987A during its first 15 seconds, as seen by IMB detector[19,21]. Hence, the GWs luminosity,  $L_{\text{GWs}}$ , as a function of the  $\nu$  luminosity can be obtained by relating the GWs flux:

$$\frac{c^3}{16\pi G} \left| \frac{dh}{dt} \right|^2 = \frac{1}{4\pi R^2} L_{\text{GWs}}, \quad (9)$$

to the GWs amplitude from the neutrino outflow,  $h_\nu$ , which can be computed from the neutrino luminosity after Refs.[17,13,16]

$$h_{ij}^{TT} = \frac{2G}{c^4 R} \int_\infty^{t-R/c} dt' L_\nu(t') \alpha(t') e_i \otimes e_j, \quad (10)$$

where  $e_i \otimes e_j$  is the GW polarization tensor. (10) can be recast in an approximate manner as:  $h_\nu = \frac{2G}{c^4 R} [\Delta t \times L_\nu \times \alpha]$ . The two last equations can be recast to obtain the GWs amplitude produced by the non-spherical outgoing front of the  $\nu_s$ -neutrinosphere. It yields[10,13,16]

$$h_\nu \simeq 1.5 \times 10^{-21} \text{Hz}^{-1/2} \left[ \frac{55 \text{kpc}}{R} \right] \left[ \frac{\Delta T}{10^{-3} \text{s}} \right] \left( \frac{L_\nu}{3 \times 10^{55} \frac{\text{erg}}{\text{s}}} \right) \left[ \frac{\alpha}{4 \times 10^{-1}} \right], \quad (11)$$

or equivalently

$$h_\nu \simeq |A| \text{Hz}^{-1/2} \left[ \frac{55 \text{kpc}}{R} \right] \left( \frac{\Delta E_{\text{GWs}}}{10^{-6} \text{M}_\odot c^2} \right)^{1/2} \left[ \frac{10^3 \text{Hz}}{f_{\text{GWs}}} \right]^{1/2}. \quad (12)$$

where  $|A| = 1.5 \times 10^{-21}$  is the proper GWs amplitude. A GWs signal with this amplitude will likely be detectable by the first generation of GWs interferometers, if an event at the distance of the Large Magellanic Cloud (SN1987A) takes place in the near future. It can also be detected by advanced interferometers (i.e. LIGO-II), and quantum limit operating resonant-mass detectors, over distances up to the VIRGO cluster of galaxies. Its imprint in the GWs waveform (GWs “light curve” from the PNS formed in the SN collapse) may resemble a spike of large amplitude, and timewidth of  $\sim(1-3)$ ms.

From (11) the GWs luminosity turns out to be

$$L_{\text{GWs}} = 4 \times 10^{50} \frac{\text{erg}}{\text{s}} \left[ \frac{L_\nu}{3 \times 10^{55} \frac{\text{erg}}{\text{s}}} \right]^2 \left( \frac{\alpha}{4 \times 10^{-1}} \right)^2, \quad (13)$$

where  $0.2 < \alpha < |-0.8|$  is the anisotropy parameter as defined by Burrows and Hayes[13]. It turns out that the GWs energy radiated in the process:  $E_{\text{GWs}} \equiv L_{\text{GWs}} \times \Delta T_{\text{osc}} \sim 4 \times 10^{47} \text{erg}$ , is almost similar to both the one sterile neutrinos carry away:  $E_\nu = 10^{57} |\nu_s \times 10^4 \text{eV}| \nu_s \left[ \frac{10^{-33} \text{g}^2}{\text{eV}} \right] \sim 2 \times 10^{-6} M_\odot c^2$ , and the one estimated to be necessary to explain the proper motion of pulsars as due to pure GWs kicks:  $E_{\text{surveys}}^{\text{Pulsar}}(\text{GWs}) \sim 4 \times 10^{-6} M_\odot c^2$ [22]. The quoted GWs energy also is  $\sim 10^5$  larger than both the current estimates from the fluid motion of the PNS constituents[16]. With so much an energy it is possible to kick the PNS up to the observed velocities of pulsars[23], as shown by Mosquera Cuesta[12].

## 5 Discussion and Closing Remarks

In summary, one can see that if neutrino flavor conversions actually take place during the SN core-bounce, the GWs signal from the process should irradiate much more GWs energy than standard mechanisms driving the neutron star dynamics at birth. This large GWs luminosity would turn these bursts the more sure detectable GWs signal from the next supernova explosion that would come to occur up to the VIRGO cluster distance,  $R \sim 20 \text{Mpc}$ . The radiation reaction of the outbursts could be the thruster mechanism of the Galaxy runaway pulsars[23] and black holes[24], as pointed out in [12].

Note, however, that equations (11) and (12) exhibit a strong dependence on two parameters: a) the neutrino luminosity, or equivalently the time scale over which the neutrino oscillations are expected to take place, and more notoriously on b) the asymmetry parameter  $\alpha$ . In respect to the  $\nu$  luminosity one can have rough confidence on the numbers presented here, which agree quite impressively with the numerical calculations by Pons et al. [21], because the conditions for the conversions to keep on occurring are met for no longer than (1-3)ms. In particular, for oscillations taking place mostly over the oscillation time,  $10^{-4} \text{s}$ , implying very high frequency GWs:  $f_{\text{GWs}} \sim 10^4 \text{Hz}$  (that perhaps would require special detection techniques), we get:  $L_\nu = 3 \times 10^{56} \frac{\text{erg}}{\text{s}}$ ,  $L_{\text{GWs}} = 4 \times 10^{52} \frac{\text{erg}}{\text{s}}$ , and  $E_{\text{GWs}} = 4 \times 10^{48} \text{erg}$ , which are still much larger than conventional estimates of GWs from neutron stars and supernovae. Aside from this, the asymmetry

dependence is more critical for the detectability of the bursts. Other numerical simulations of supernova explosions[16] have indicated that its value could be as small as  $\alpha \sim 5 \times 10^{-3}$ . This asymmetry would imply, according to (11), an effective GWs amplitude two orders of magnitude smaller than the one just computed, this way shortening the distance upto to potential sources. Nonetheless, even for this lower degree of asymmetry the computations show that still the GWs energy released during the conversions would dominate over the PNS mass motions or neutrino convection and diffusion.

## References

1. N. Arkani-Hamed, S. Dimopoulos, G. Dvali, Phys. Lett. B 429, 263 (1998).
2. I. Antoniadis, et al., Phys. Lett. B 436, 257 (1998).
3. N. Arkani-Hamed, S. Dimopoulos, G. Dvali, Phys. Rev. D 59, 086004 (1999).
4. L. Randall, R. Sundrum, Phys. Rev. Lett. 83, 4690 (1999).
5. L. Randall, R. Sundrum, Phys. Rev. Lett. 83, 3370 (1999).
6. R. N. Mohapatra, A. Perez-Lorezana, Nucl. Phys. B 576, 466 (2000). See also D. O. Caldwell, R. N. Mohapatra, S. J. Yellin, Phys. Rev. Lett 87, 041601 (2001). R. N. Mohapatra, A. Perez-Lorezana, C. S. Pires, Phys. Lett. B 491, 143 (2000).
7. C. Hanhart, et al., Nucl. Phys. B 595, 335 (2001). See also C. Hanhart et al., astro-ph/0102063 (2001).
8. S. Hannestad, G. G. Raffelt, Phys. Rev. Lett. 87, 051301 (2001).
9. G. Barenboim, et al., hep-ph/0108199, 30 Aug. (2001).
10. H. J. Mosquera Cuesta, Ap. J. Lett. 544, L61 (2000).
11. Y. Grossman, M. Neubert, Phys. Lett. B 474, 361 (2000).
12. H. J. Mosquera Cuesta, *Back-reaction of Einstein's gravitational waves as the origin of natal pulsars kicks*, Phys. Rev. D., Rapid Comm., in press (2001).
13. A. Burrows, J. Hayes, Phys. Rev. Lett. 76, 352 (1996).
14. A. Burrows, et al., Astrophys. J. 450, 830 (1995).
15. H.-Th. Janka, E. Müller, Astron. Astrophys. 306, 167 (1996). See also: Astron. Astrophys. 290, 290 (1994).
16. E. Müller, H.-Th. Janka, Ast. Astrophys. 317, 140 (1997).
17. R. I. Epstein, MNRAS 188, 305 (1978).
18. M. Patel, G. M. Fuller, What are sterile neutrinos good for?, report hep-ph/0003034 (v1) 5 Mar (2000).
19. H. Nunokawa, Phys. D. 56, 1704 (1997), and Nucl. Phys. Proc. Suppl. 95, 193 (2000).
20. S. Pakvasa, Discussion section on Adriatic Conference on *Particle Physics in the New Millenium*, Dubrovnik, Croatia, Sept 4-14 (2001).
21. J. A. Pons, et al., Phys. Rev. Lett. 86, 5223 (2001).
22. S. Nazin, M. Postnov, Astron. Astrophys. 317, L79 (1997).
23. A. G. Lyne, D. R. Lorimer, Nature 369, 127 (1994).
24. I. F. Mirabel, et al., Nature 413, 139-141 (2001).



# Towards Adelic Noncommutative Quantum Mechanics

Goran S. Djordjević<sup>1,2</sup> and Ljubiša Nešić<sup>1</sup>

<sup>1</sup> Department of Physics, University of Niš, Yugoslavia

<sup>2</sup> Sektion Physik, Universität München, Theresienstr. 37, D-80333 München, Germany

**Abstract.** A motivation of using noncommutative and nonarchimedean geometry on very short distances is given. Besides some mathematical preliminaries, we give a short introduction in adelic quantum mechanics. We also recall to basic ideas and tools embedded in  $q$ -deformed and noncommutative quantum mechanics. A rather fundamental approach, called deformation quantization, is noted. A few relations between noncommutativity and nonarchimedean spaces as well as similarities between corresponding quantum theories on them are pointed out. An extended Moyal product in a proposed form of adelic noncommutative quantum mechanics is considered. We suggest some question for future investigations.

## 1 Introduction

It is widely accepted that standard picture of space-time should be changed around and beyond Planck scale. “Measuring” of spacetime geometry under distances smaller than Planck length  $l_p$  is not accessible even to Gedanken experiments. It serves an idea of “quantization” and “discretization” of spacetime and a natural cutoff when using a quantum field theory to describe related phenomena. We are pointing out two possibilities for a reasonable mathematical background of a quantum theory on very small distances, The *first* one comes from the idea of spacetime coordinates as noncommuting operators

$$[\hat{x}^i, \hat{x}^j] = i\theta^{ij}. \quad (1)$$

Some noncommutativity of configuration space should not be a surprise in physics since quantum phase space with the canonical commutation relation

$$[\hat{x}^i, \hat{k}^j] = i\hbar\delta^{ij}, \quad (2)$$

where  $x^i$  are coordinates and  $k^j$  are the corresponding momenta, is the well-known example of noncommutative (pointless) geometry. This relation is connected in a natural way with the uncertainty principle and a “fuzzy” spacetime pictures at distances  $\theta^{1/2}$ . Although, it seems to have good physical sense for  $\theta^{1/2} \sim l_p$ , characteristic noncommutative distances could be related to gauge couplings [1], closer to observable distances. It should be noted that deriving of uncertainty relation ( $\delta x > l_p$ ) leads to an “strange” notion of quantum line and probably beyond archimedean geometry, because a coordinate always commute with itself [2]!

The *second* promising approach to the physics at the Planck scale, based on non-archimedean geometry was suggested [3]. The simplest way to describe such a geometry (oftenly called also ultrametric) is by using  $p$ -adic number fields  $\mathbb{Q}_p$  ( $p$  is a prime). On the basis of the Ostrovski theorem [4] there is no other nontrivial possibilities (besides field of real numbers  $\mathbb{R}$ ) to complete field of rational numbers  $\mathbb{Q}$  in respect to a (nontrivial) norm. Remind that all physical numerical experimental data belong  $\mathbb{Q}$ .

There have been many interesting applications of  $p$ -adic numbers and non-Archimedean geometry in various parts of modern theoretical and mathematical physics (for a review, see [4,5]). However we restrict ourselves here mainly to  $p$ -adic [6] and adelic [7] quantum mechanics (QM). It should be noted that adelic QM have appeared quite useful in quantum cosmology. The appearance of space-time discreteness in adelic formalism (see, e.g. [8]), as well as in noncommutative QM, is an encouragement for the further investigations. We emphasize the role of Feynman's  $p$ -adic path integral method on nonarchimedean spaces.

The  $p$ -adic analysis and noncommutativity also play a role in some areas of "macroscopic" physics [9]. We list shortly a few of similarities between non-Archimedean and noncommutative structures them and discuss in more details a new observed relation between an ordering on commutative ring in frame of deformation quantization [10] and an ordering on  $p$ -adic spaces in an intention to develop path integration on  $p$ -adics by "slicening" of trajectories [11].

## 2 $p$ -adic Numbers and Adeles

Any  $x \in \mathbb{Q}_p$  can be presented in the form [4]

$$x = p^\nu(x_0 + x_1p + x_2p^2 + \dots), \quad \nu \in \mathbb{Z}, \quad (3)$$

where  $x_i = 0, 1, \dots, p-1$  are digits.  $p$ -Adic norm of any term  $x_i p^{\nu+i}$  in the canonical expansion (3) is  $|x_i p^{\nu+i}|_p = p^{-(\nu+i)}$  and the strong triangle inequality holds, *i.e.*  $|a+b|_p \leq \max\{|a|_p, |b|_p\}$ . It follows that  $|x|_p = p^{-\nu}$  if  $x_0 \neq 0$ . Derivatives of  $p$ -adic valued functions  $\varphi : \mathbb{Q}_p \rightarrow \mathbb{Q}_p$  are defined as in the real case, but with respect to the  $p$ -adic norm. There is no integral  $\int \varphi(x)dx$  in a sense of the Lebesgue measure [4], but one can introduce  $\int_a^b \varphi(x)dx = \Phi(b) - \Phi(a)$  as a functional of analytic functions  $\varphi(x)$ , where  $\Phi(x)$  is an antiderivative of  $\varphi(x)$ . In the case of map  $f : \mathbb{Q}_p \rightarrow \mathbb{C}$  there is well-defined Haar measure. One can use the Gauss integral

$$\int_{\mathbb{Q}_v} \chi_v(ax^2 + bx)dx = \lambda_v(a)|2a|_v^{-\frac{1}{2}} \chi_v\left(-\frac{b^2}{4a}\right), \quad a \neq 0, \quad v = \infty, 2, 3, 5, \dots, \quad (4)$$

where index  $v$  denotes real ( $v = \infty$ ) and  $p$ -adic cases,  $\chi_v$  is an additive character:  $\chi_\infty(x) = \exp(-2\pi i x)$ ,  $\chi_p(x) = \exp(2\pi i \{x\}_p)$ , where  $\{x\}_p$  is the fractional part of  $x \in \mathbb{Q}_p$ .  $\lambda_v(a)$  is the complex-valued arithmetic function [4]. An adele [12] is an infinite sequence  $a = (a_\infty, a_2, \dots, a_p, \dots)$ , where  $a_\infty \in \mathbb{R} \equiv \mathbb{Q}_\infty$ ,  $a_p \in \mathbb{Q}_p$  with a restriction that  $a_p \in \mathbb{Z}_p$  for all but a finite set  $S$  of primes  $p$ . The set of all

adeles  $\mathbb{A}$  may be regarded as a subset of direct topological product  $\mathbb{Q}_\infty \times \prod_p \mathbb{Q}_p$ .  $\mathbb{A}$  is a topological space, and can be considered as a ring with respect to the componentwise addition and multiplication. An elementary function on adelic ring  $\mathbb{A}$  is

$$\varphi(x) = \varphi_\infty(x_\infty) \prod_p \varphi_p(x_p) = \prod_v \varphi_v(x_v) \quad (5)$$

with the main restriction that  $\varphi(x)$  must satisfy  $\varphi_p(x_p) = \Omega(|x_p|_p)$  for all but a finite number of  $p$ . Characteristic function on  $p$ -adic integers  $\mathbb{Z}_p$  is defined by  $\Omega(|x|_p) = 1$ ,  $0 \leq |x|_p \leq 1$  and  $\Omega(|x|_p) = 0$ ,  $|x|_p > 1$ .

The Fourier transform of the characteristic function (vacuum state)  $\Omega(|x_p|)$  is  $\Omega(|k_p|)$ . All finite linear combinations of elementary functions (5) make the set  $\mathcal{D}(\mathbb{A})$  of the Schwartz-Bruhat functions. The Hilbert space  $L_2(\mathbb{A})$  is a space of complex-valued functions  $\psi_1(x), \psi_2(x), \dots$ , with the scalar product and norm.

### 3 Adelic Quantum Mechanics

In foundations of standard QM one usually starts with a representation of the canonical commutation relation (2). In formulation of  $p$ -adic QM [6] the multiplication  $\hat{q}\psi \rightarrow x\psi$  has no meaning for  $x \in \mathbb{Q}_p$  and  $\psi(x) \in \mathbb{C}$ . In the real case momentum and hamiltonian are infinitesimal generators of space and time translations, but, since  $\mathbb{Q}_p$  is disconnected field, these infinitesimal transformations become meaningless. However, finite transformations remain meaningful and the corresponding Weyl and evolution operators are  $p$ -adically well defined.

Canonical commutation relation (2) in  $p$ -adic case can be represented by the Weyl operators ( $\hbar = 1$ )

$$\hat{Q}_p(\alpha)\psi_p(x) = \chi_p(\alpha x)\psi_p(x) \quad (6)$$

$$\hat{K}_p(\beta)\psi(x) = \psi_p(x + \beta). \quad (7)$$

$$\hat{Q}_p(\alpha)\hat{K}_p(\beta) = \chi_p(\alpha\beta)\hat{K}_p(\beta)\hat{Q}_p(\alpha). \quad (8)$$

It is possible to introduce the family of unitary operators

$$\hat{W}_p(z) = \chi_p(-\frac{1}{2}qk)\hat{K}_p(\beta)\hat{Q}_p(\alpha), \quad z \in \mathbb{Q}_p \times \mathbb{Q}_p, \quad (9)$$

that is a unitary representation of the Heisenberg-Weyl group. Recall that this group consists of the elements  $(z, \alpha)$  with the group product  $(z, \alpha) \cdot (z', \alpha') = (z + z', \alpha + \alpha' + \frac{1}{2}B(z, z'))$ , where  $B(z, z') = -kq' + qk'$  is a skew-symmetric bilinear form on the phase space. Dynamics of a  $p$ -adic quantum model is described by a unitary operator of evolution  $U(t)$  formulated in terms of its kernel  $K_t(x, y)$ ,  $U_p(t)\psi(x) = \int_{\mathbb{Q}_p} K_t(x, y)\psi(y)dy$ . In this way [6]  $p$ -adic QM is given by a triple  $(L_2(\mathbb{Q}_p), W_p(z_p), U_p(t_p))$ .

Keeping in mind that standard QM can be also given as the corresponding triple, ordinary and  $p$ -adic QM can be unified in the form of adelic QM [7]

$$(L_2(A), W(z), U(t)). \quad (10)$$

$L_2(\mathbb{A})$  is the Hilbert space on  $\mathbb{A}$ ,  $W(z)$  is a unitary representation of the Heisenberg-Weyl group on  $L_2(\mathbb{A})$  and  $U(t)$  is a unitary representation of the evolution operator on  $L_2(\mathbb{A})$ . The evolution operator  $U(t)$  is defined by

$$U(t)\psi(x) = \int_{\mathbb{A}} K_t(x, y)\psi(y)dy = \prod_v \int_{\mathbb{Q}_v} K_t^{(v)}(x_v, y_v)\psi^{(v)}(y_v)dy_v. \quad (11)$$

Note that any adelic eigenfunction has the form

$$\Psi(x) = \Psi_\infty(x_\infty) \prod_{p \in S} \Psi_p(x_p) \prod_{p \notin S} \Omega(|x_p|_p), \quad x \in \mathbb{A}, \quad (12)$$

where  $\Psi_\infty \in L_2(\mathbb{R})$ ,  $\Psi_p \in L_2(\mathbb{Q}_p)$ . In the low-energy limit adelic QM becomes ordinary one.

A suitable way to calculate propagator in  $p$ -adic QM is by  $p$ -adic generalization of Feynman's path integral [6]. There is no natural ordering on  $\mathbb{Q}_p$ . However, a bijective continuous map  $\varphi$  from the set of  $p$ -adic numbers  $\mathbb{Q}_p$  to the subset  $\varphi(\mathbb{Q}_p)$  of real numbers  $\mathbb{R}$  [4] was proposed. This map can be defined by (for an older injective version see [11])

$$\varphi(x) = |x|_p \sum_{k=0}^{\infty} x_k p^{-2k}. \quad (13)$$

Then, a linear order on  $\mathbb{Q}_p$  is given by the following definition:  $x < y$  if  $|x|_p < |y|_p$  or when  $|x|_p = |y|_p$  there exists such index  $m \geq 0$  that digits satisfy  $x_0 = y_0, x_1 = y_1, \dots, x_{m-1} = y_{m-1}, x_m < y_m$ . One can say:  $\varphi(x) > \varphi(y)$  iff  $x > y$ .

In the case of harmonic oscillator [11], it was shown that there exists the limit

$$K_p(x'', t''; x', t') = \lim_{n \rightarrow \infty} K_p^{(n)}(x'', t''; x', t') = \lim_{n \rightarrow \infty} N_p^{(n)}(t'', t') \times \int_{\mathbb{Q}_p} \cdots \int_{\mathbb{Q}_p} \chi_p \left( -\frac{1}{h} \sum_{i=1}^n \bar{S}(q_i, t_i; q_{i-1}, t_{i-1}) \right) dq_1 \cdots dq_{n-1}, \quad (14)$$

where  $N_p^{(n)}(t'', t')$  is the corresponding normalization factor for the harmonic oscillator. The subdivision of  $p$ -adic time segment  $t_0 < t_1 < \cdots < t_{n-1} < t_n$  is made according to linear order on  $\mathbb{Q}_p$ . In a similar way we have calculated path integrals for a few quantum models. For the references see [13]. Moreover, we were able to obtain general expression for the propagator of the systems with quadratic action (for the details see [14]), without ordering

$$K_p(x'', t''; x', t') = \lambda_p \left( -\frac{1}{2h} \frac{\partial^2 \bar{S}}{\partial x'' \partial x'} \right) \Big|_p \frac{1}{h} \frac{\partial^2 \bar{S}}{\partial x'' \partial x'} \Big|_p^{\frac{1}{2}} \chi_p \left( -\frac{1}{h} \bar{S}(x'', t''; x', t') \right). \quad (15)$$

Replacing an index  $p$  with  $v$  in (15) we can write quantum-mechanical amplitude  $K$  in ordinary and all  $p$ -adic cases in the same, compact (and adelic) form.

#### 4 Relations Between Noncommutative and $p$ -adic QM

Noncommutative geometry is geometry which is described by an associative algebra  $\mathcal{A}$  which is usually noncommutative and in which the set of points, if it exists at all, is relegated to a secondary role. Noncommutative spaces have arisen in investigation of brane configurations in string and M-theory. Since the one-particle sector of field theories leads to QM, a study of this topic has attracted much of interest. For single particle QM, the corresponding Heisenberg algebra is needed. In addition to (1) and (2) one chooses

$$[p^i, p^j] = i\Phi^{ij} \quad (16)$$

There are a lot of possibilities in choosing  $\theta$  and  $\Phi$ . Although one can take  $\theta^{ij}$  and  $\Phi^{ij}$  are antisymmetric nonconstant tensors (matrices), often, the simplest nontrivial case is considered:  $\theta^{ij} = \text{const}$  and  $\Phi^{ij} = 0$ . Another realization of noncommutativity is possible by  $q$ -deformation of a space, for example, *Manin plane*  $xy = qyx$  and  $q$ -deformed “classical” phase space  $px = qpx$ . This approach leads to a latticelike (discrete) structure of space-time [15].

A field  $\Psi(x)$  as a function of the noncommuting coordinates  $x$  can be used as Schrodinger wave function obeying the free field equation. Other realization, based on star product ( $v * \Psi$ ) instead of standard multiplication ( $V \cdot \Psi$ ) of a potential and wave function have been considered in corresponding Schrödinger equation too (i.e. see [16]).

The passage from one level of physical theory to more refined another, using what mathematicians call deformation theory is nothing extraordinary new. In a similar way, there is an old idea that QM is some kind of deformed classical mechanics. For a review see [17]. In fact, deformation quantization is closely related to Weyl quantization, shortly sketched in the previous section.

One direction of the investigation led to Moyal bracket and Moyal (star) product, widely used now in noncommutative QM

$$f *_m g = \chi_\infty \left( -\frac{\hbar}{8\pi^2} P \right) (f, g) = fg + \sum_{r=1}^{\infty} \left( \frac{i\hbar}{4\pi} \right)^r P^r(f, g). \quad (17)$$

Several integral formulas have been introduced for the star product and an (formal) parameter of deformation is finally related to some form of Planck constant  $\hbar$ . Quantisation can be taken as a deformation of the standard associative and commutative product, now called a star product, of classical observables driven by the Poisson bracket  $P$ . By the intuition, classical mechanics is understood as the limit QM when  $\hbar \rightarrow 0$ .

Some connections between  $p$ -adic analysis and quantum deformations have been noticed during the last ten years. It has been observed that the Haar measure on  $SU_q(2)$  coincides with the Haar measure on the field of  $p$ -adic numbers  $\mathbb{Q}_p$  if  $q = p^{-1}$  [2]. There is a potential such that the spectrum of the  $p$ -adic Schrödinger-like (diffusion) equation [4]

$$D\psi(x) + V(|x|_p)\psi(x) = E\psi(x) \quad (18)$$

is the same one as in the case of  $q$ -deformed oscillator found by Biedenharn [18] for  $q = 1/p$ . For more details see [2].

In a develop of the representation theory for the star product algebras in deformation quantization some non-Archimedean behavior is noted [10]. We find this relation very intrigue and discuss it in more details. Recall, that a star product  $*$ , on a Poisson manifold  $(M, \pi)$  is a (formal) associative  $\mathbb{C}[[\lambda]]$  - bilinear product for  $C^\infty(M)[[\lambda]]$

$$f * g = \sum_{r=0}^{\infty} \lambda^r C_r(f, g), \quad (19)$$

with bidifferential operators  $C_r$ .  $\mathbb{C}[[\lambda]]$  is an algebra of *formal* (in a formal parameter  $\lambda$ ) series  $\sum_{r=0}^{\infty} \lambda^r C_r$ ,  $C_r \in \mathbb{C}$  (a convergence of this series is still not under a consideration).  $C^\infty(M)[[\lambda]]$  is the space of formal series of smooth functions ( $x \in M$ ,  $f_r(x) \in C^\infty(M)$ ), for a fixed but variable  $x$ . With interpretation  $\lambda \leftrightarrow \hbar$  we identify  $C^\infty(M)[[\lambda]]$  with the algebra of observables of the quantum system corresponding to  $(M, \pi)$ . Let  $R$  be on an ordered (commutative associative unital) ring  $R$  [10], Let us note, that a concept of ordered ring is necessary one wish to define the positive functionals on a  $C^*$  algebra ( $C = R(i) = \{a + bi, a, b \in R\}$ ). It is related with Gelfand-Naimark's theorem on commutative spaces. By means of the positive functionals on  $C^*$  algebras we can reconstruct the (points on) "starting" manifold, that one on which an algebra of complex function will give the "original"  $C^*$  algebra. This is a motivation for generalization on noncommutative space. In this case, the corresponding product of formal functions will be the  $*$  product. Now,  $R[[\lambda]]$  will be an algebra of formal series on the ordered ring  $R$ . Then, if  $R$  is an ordered ring,  $R[[\lambda]]$  will be ordered in a canonical way, too, by the definition

$$\sum_{r=r_0}^{\infty} \lambda^r a_r > 0, \quad \text{if } a_{r_0} > 0. \quad (20)$$

In other words, a formal series in  $R[[\lambda]]$  will be a "positive" one, if first nonzero coefficient (an element of ordered ring  $R$  is positive).

It should be noted that the concept of ordered ring fits naturally to formal power series and thus to Gerstenhaber's deformation theory [19]. Then  $R[[\lambda]]$  will be *non-Archimedean*. For example, if we take that  $a_0 = -1$ , and  $a_1 = n$  ( $n \in \mathbb{N}$ , because for any commutative ordered ring with unit, set of integers is embedded in  $R$ ,  $\mathbb{N} \subset R$ , all others coefficients can be zero, we have  $-1 + n\lambda < 0$  or  $n\lambda < 1$  for all  $n \in \mathbb{Z}$ ). The interpretation in formal theory is that the deformation parameter  $\lambda$  is "very small" compared to the other numbers in  $R$ . We see that Waldmann's definition of the ordered algebra of formal series on ordered ring  $R$  immediately leads to the non-archimedean "structure". It could be a good indication to use ultrametric spaces and  $p$ -adics when physical deformation parameter is very small. We would like to underline that Zelmanov's ordering by means of map (13)  $\mathbb{Q}_p$ , i.e. on normed, ultrametric algebra, in frame of  $p$ -adic QM for  $\lambda = 1/p^2$  is related to the ordering of formal series on ordered rings in the frame of deformation quantization!

## 5 The Adelic Moyal Product and Noncommutative QM

The presented connections noncommutative vs. “nonarchimedean” QM suggest a need to formulate a quantum theory that may connect as much as possible nonarchimedean and noncommutative effects and structures. At the present level of quantum theory on adèles, a formulation of Noncommutative Adelic QM seems as the most promising attempt.

An enough simple frame for that might be representation of an algebra of operators (1), (2) and (16). It could be done by linear transformations on corresponding symplectic structure and deformed and extended bilinear product  $B$ . Correspondance between classical functions and quantum operators would be provided by Weyl quantisation. An equivalent formulation of noncommutative adelic QM by the triple  $(L_2(A_\theta), W_\theta(z), U_\theta(t))$ , does not seem to have principles obstacles. In this approach an adele of coordinates  $x_A$  would be replaced by a serie of noncommutative operators  $\hat{x}_A$ , where adelic properties of corresponding eigenvalues is still “conserved”.

Now, we has to consider a  $p$ -adic and adelic generalization of the Moyal product. Let us consider classical space with coordinates  $x^1, x^2, \dots, x^D$ . Let  $f(x)$  be a classical function  $f(x) = f(x^1, x^2, \dots, x^D)$ . Then, with the respect to the Fourier transformations and the usual Weyl quantization, we have

$$\hat{f}(x) = \int_{\mathbb{Q}_\infty^D} dk \chi_\infty(-k\hat{x}) \tilde{f}(k) \equiv f(\hat{x}). \quad (21)$$

Let us now have two classical functions  $f(x)$  and  $g(x)$  and we are interested in operator product  $\hat{f}(x)\hat{g}(x)$ . In the real case this operator product is

$$(\hat{f} \cdot \hat{g})(x) = \int \int dk dk' \chi_\infty(-k\hat{x}) \chi_\infty(-k'\hat{x}) \tilde{f}(k) \tilde{g}(k'). \quad (22)$$

Using the Baker-Campbell-Hausdorff formula, the relation (1) and then the coordinate representation one finds the Moyal product in the form

$$(f * g)(x) = \int_{\mathbb{Q}_p^D} \int_{\mathbb{Q}_p^D} dk dk' \chi_v \left( -(k + k')x + \frac{1}{2} k_i k'_j \theta^{ij} \right) \tilde{f}(k) \tilde{g}(k'). \quad (23)$$

Note that we already used our generalization from  $\mathbb{Q}_\infty$  to  $\mathbb{Q}_v$ . In the real case we use  $k_i \rightarrow -(i/2\pi)(\partial/\partial x^i)$  and obtain the well known form  $(f * g)(x) = \chi_\infty \left( -\frac{\theta^{ij}}{2(2\pi)^2} \frac{\partial}{\partial y^i} \frac{\partial}{\partial z^j} \right) f(y)g(z)|_{y=z=x}$ . In the  $p$ -adic case such an straightforward generalization is not possible (but, some kind of psudodifferentiaton could be useful). Thus, as the  $p$ -adic Moyal product we take

$$(f * g)(x) = \int_{\mathbb{Q}_p^D} \int_{\mathbb{Q}_p^D} dk dk' \chi_p(-(x^i k_i + x^j k'_j) + \frac{1}{2} k_i k'_j \theta^{ij}) \tilde{f}(k) \tilde{g}(k'). \quad (24)$$

We can writedown the adelic Moyal product of “classical” adelic functions  $f_A = (f_\infty, f_2, \dots, f_p, \dots)$ ,  $g_A = (g_\infty, g_2, \dots, g_p, \dots)$  on  $\mathbb{R} \times \prod_{p \in S} \mathbb{Q}_p \times \prod_{p \notin S} \mathbb{Z}_p$  space

$$(f * g)(x) = \int_{\mathbb{A}^D} \int_{\mathbb{A}^D} dk dk' \chi(-(x^i k_i + x^j k'_j) + \frac{1}{2} k_i k'_j \theta^{ij}) \tilde{f}_A(k) \tilde{g}_A(k') \quad (25)$$

Taking into account (5), (22) and the property of the Fourier transform of  $\Omega$  function, one has

$$\begin{aligned}
(f * g)(x) &= \chi_\infty \left( -\frac{\theta^{ij}}{2(2\pi)^2} \frac{\partial}{\partial y^i} \frac{\partial}{\partial z^j} \right) f(y)g(z)|_{y=z=x} \\
&\times \prod_{p \in S} \int_{\mathbb{Q}_p^D} \int_{\mathbb{Q}_p^D} dk dk' \chi_p(-(x^i k_i + x^j k'_j) + \frac{1}{2} k_i k'_j \theta^{ij}) \tilde{f}_p(k) \tilde{g}_p(k') \\
&\times \prod_{p \notin S} \int_{\mathbb{Z}_p^D} \int_{\mathbb{Z}_p^D} dk dk' \chi_p(-(x^i k_i + x^j k'_j) + \frac{1}{2} k_i k'_j \theta^{ij}). \tag{26}
\end{aligned}$$

It can be shown that if for all  $p$ ,  $\varphi(x) = \Omega(x)$ , the adelic Moyal product becomes real one.

### Acknowledgments

G.Dj. is partially supported by DFG Project “Noncommutative space-time structure - Cooperation with Balkan Countries”. We would like to thank P. Aschieri, I. Bakovic, B. Jurco and S. Waldmann for useful discussions.

### References

1. W. Behr, N. G. Deshpande, G. Duplancic, P. Shupp, J. Trampetic, J. Wess, *The  $Z \rightarrow \gamma\gamma$ ,  $gg$  Decays in the Noncommutative Standard Model*, hep-ph/0202121.
2. I.Ya. Aref'eva and I. V. Volovich, Phys. Lett. **B268**, 179 (1991).
3. I.V. Volovich, Class. Quantum Grav. **4**, L83 (1987).
4. V.S. Vladimirov, I.V. Volovich and E.I. Zelenov, *p-Adic Analysis and Mathematical Physics*, (World Scientific, Singapore, 1994).
5. L. Brekke and P.G.O. Freund, Phys. Rep. **233**, 1 (1993).
6. V.S. Vladimirov and I.V. Volovich, Comm. Math. Phys. **123**, 659 (1989).
7. B. Dragovich, Int. J. Mod. Phys. **A10**, 2349 (1995).
8. G. S. Djordjevic, B. Dragovich, Lj. D. Nešić, I. V. Volovich, *p-Adic and Adelic Minisuperspace Quantum Cosmology*, gr-qc/0105050.
9. R. Jackiw, *Physical instances of noncommuting coordinates*, hep-th/0110057.
10. S. Waldmann: *On the Representation Theory of Deformation Quantization*, math.QA/0107112.
11. E.I. Zelenov, J. Math. Phys. **32**, 147 (1991).
12. I.M. Gel'fand, M.I. Graev and I.I. Pyatetskii-Shapiro, *Representation Theory and Automorphic Functions*, (Saunders, London, 1966).
13. G.S. Djordjevic, B. Dragovich, Lj. Nešić, *Adelic Quantum Mechanics: Nonarchimedean and Noncommutative Aspects*, hep-th/0111088.
14. G.S. Djordjević and B. Dragovich, Mod. Phys. Lett. **A12**, 1455 (1997).
15. B.L. Cherchiai, S. Schraml and J. Wess, Int. J. Mod. Phys. **B13**, 3049 (1997).
16. L. Mezincescu, *Star operation in Quantum Mechanics*, hep-th/0007046.
17. G. Dito, D. Sternheimer, *Deformation quantization: genesis, developments and metamorphoses*, math.QA/0201168.
18. L.C. Biedenharn, J. Phys. A: Math. Gen. **22**, L873 (1989).
19. M. Gerstenhaber, D.S. Schack: ‘Algebraic Cohomology and Deformation Theory’, *Deformation Theory of Algebras and Structures and Applications*, ed by M. Hazewinkel, M. Gerstenhaber, (Kluwer, Dordrecht 1988) pp. 13-264.



# Three Loop Leading Top Mass Contributions to the $\rho$ Parameter

Michael Faisst

Institut für Theoretische Teilchenphysik, Universität Karlsruhe, D-76128 Karlsruhe, Germany

**Abstract.** We present analytic results for the three loop heavy top quark contributions of the electroweak  $\rho$  parameter. The calculation is carried out using the standard model lagrangian with vanishing gauge couplings. Within this gaugeless limit the masses of the Higgs boson  $M_H$  and of the top quark  $m_t$  are the single relevant mass scales. In the present calculation [1] we have investigated the behaviour of the  $\rho$  parameter in the limit of a Higgs mass equal to zero.

## 1 Introduction

The standard model predicts heavy top quark corrections in the low energy limit of four-fermion processes by means of virtual effects in the W and Z boson self energies [2]. The precise knowledge of such heavy particle effects is important in the context of searches for small effects originating from Higgs bosons or possible contributions from new physics.

The heavy top quark corrections to the W and Z self energies emerge in particular in a deviation of the so called  $\rho$  parameter from the tree level result.

The  $\rho$  parameter is usually defined by the ratio of neutral current  $J^{\text{NC}}$  to charged current  $J^{\text{CC}}$  at zero momentum transfer:

$$\rho = \frac{1}{1 - \Delta\rho} = \frac{J^{\text{NC}}(0)}{J^{\text{CC}}(0)}. \quad (1)$$

$J^{\text{CC}}(0)$  is given by the Fermi coupling constant  $G_F$  determined from the  $\mu$  decay rate and  $J^{\text{NC}}(0)$  is measured by neutrino scattering on electrons or hadrons.

This definition of the  $\rho$  parameter is not process independent as the radiative corrections depend on the value of the hypercharge of the particles involved in the studied processes. However, the leading terms in the yukawa coupling are process independent and can be related to the transversal parts of the self energies of the exchanged vector bosons W and Z by

$$\rho = \frac{1}{c^2} \frac{M_W^2 - \Pi_T^{WW}(0)}{M_Z^2 - \Pi_T^{ZZ}(0)}. \quad (2)$$

Here  $c = M_W^2/M_Z^2$  represents the cosine of the weak mixing angle, defined in the standard on-shell scheme. Corrections from vertex and box diagrams always involve extra powers of the weak coupling constant  $g_{\text{weak}}$  and are therefore suppressed by powers of  $g_{\text{weak}}/g_{\text{Yukawa}}^{\text{top}}$ , i.e.  $M_W/m_t$ .

Within this formula  $\Pi_T^{WW}(0)$  and  $\Pi_T^{ZZ}(0)$  can be taken as the bare irreducible graphs. In this form the results would appear infinite, but these infinities are canceled by the Higgs mass, top mass and W boson mass renormalization. Up to the two loop level the leading yukawa coupling correction to  $\rho$  can be expressed in a number of equivalent ways, i.e. in terms of  $G_F^2 m_t^4$  or  $m_t^4/M_W^4$ . At the three loop level one must be more precise. At this level the difference between low energy parameters and on-shell vector boson masses plays a role even in the leading  $m_t$  effects. In the following the final result is expressed in terms of the on-shell top mass and the low energy Fermi constant  $G_F$  from  $\mu$ -decay.

An outline of the calculation, including a short discussion of the renormalization, is given in the next section. In Sect. 3 we present our current results.

## 2 Treatment of Diagrams and Renormalization

In the investigated limit  $M_H = 0$  we are able to treat all particles besides the top quark as massless. Due to this fact we are faced with different types of diagrams containing just a sole mass scale. As stated in equation (2) the leading top mass contributions to  $\rho$  stem from the transversal part of the W and Z boson self energy. We have calculated the relevant three loop self energy diagrams using an asymptotic expansion [3] with respect to the small external momentum.

The second class of diagrams we had to deal with were on-shell self energy diagrams of the Higgs boson and the top quark. As far as the mass renormalization of Higgs boson is concerned the diagrams were computed in the limit of vanishing external momentum. In addition, this mass renormalization is only needed up to the one loop order in our calculation. By contrast, the mass renormalization of the top quark in the on-shell scheme leads to two loop on-shell diagrams. As these diagrams contain only one mass scale, they can be computed by using the packages TARCER [4] and ONSHELL2 [5].

The renormalization of the vacuum expectation value of the Higgs field is fixed by the requirement of vanishing Higgs tadpoles. It also influences the Higgs mass renormalization and the mass renormalization of the goldstone bosons. We need this renormalization constant up to two loops and the computation of the tadpoles is straightforward.

The whole calculation is done using dimensional regularization and anti-commuting  $\gamma_5$ . This prescription preserves the Ward-Takahashi identities which relate the self energies of the gauge bosons to the non-diagonal self energies of the gauge-to-goldstone and the goldstone boson self energies, as we checked explicitly.

Throughout this computation we have used several computer programs and packages. The diagrams were generated using QGRAF [6] and the asymptotic expansion in limit of a large Higgs mass was performed by EXP [7]. The resulting three loop integrals were evaluated with the help of the program packages MINCER [8] and MATAD [9] written in FORM [10].

### 3 Results

We have reproduced the one and two loop results for the  $\rho$  parameter at orders  $G_F$ ,  $G_F^2$  and  $G_F\alpha_s$  that can be found in [2,11–13]. Providing a better survey we are parameterizing the radiative corrections to  $\Delta\rho$  as

$$\begin{aligned}\Delta\rho = & n_c x_t + n_c x_t^2 (19 - 12\zeta_2) \\ & + n_c x_t^3 \Delta\rho^{(n_c x_t^3)} + n_c^2 x_t^3 \Delta\rho^{(n_c^2 x_t^3)} \\ & + \frac{\alpha_s}{\pi} C_F n_c x_t \left(-\frac{1}{2} - \zeta_2\right) + \frac{\alpha_s}{\pi} C_F n_c x_t^2 \Delta\rho^{(n_c \alpha_s x_t^2)} + \dots\end{aligned}\quad (3)$$

Here  $x_t$  is the typical parameter of the problem given by

$$x_t = \frac{G_F m_t^2}{8\sqrt{2}\pi^2} \approx 3.2 \cdot 10^{-3} \quad (4)$$

and  $\alpha_s$  is the strong coupling constant. In addition  $n_c$  represents the number of quark colours and  $C_F = (n_c^2 - 1)/(2n_c)$  is the casimir operator of the fundamental representation of the quark colour group. In the limit  $M_H = 0$  the analytical results for the leading top mass contributions to the  $\rho$  parameter are given by [1]:

$$\begin{aligned}\Delta\rho^{(n_c \alpha_s x_t^2)} = & \frac{185}{3} - 48\zeta_2 \ln 2 - 48\zeta_2 \ln^2 2 - \frac{151}{6}\zeta_2 + 29\zeta_3 - 102\zeta_4 \\ & + 27\sqrt{3}\text{Cl}_2 + 8\ln^4 2 + 192\text{Li}_4\left(\frac{1}{2}\right)\end{aligned}\quad (5)$$

$$\begin{aligned}\Delta\rho^{(n_c x_t^3)} = & 68 + 96\zeta_2 \ln 2 + 288\zeta_2 \ln^2 2 + 6\zeta_2 - 396\zeta_3 + 657\zeta_4 \\ & + 108\sqrt{3}\text{Cl}_2 - 216\text{Cl}_2^2 - 48\ln^4 2 - 1152\text{Li}_4\left(\frac{1}{2}\right)\end{aligned}\quad (6)$$

$$\Delta\rho^{(n_c^2 x_t^3)} = -\frac{6572}{15} + \frac{1472}{15}\zeta_2 + 440\zeta_3 - \frac{648}{5}\sqrt{3}\text{Cl}_2 \quad (7)$$

where  $\zeta_n$  is used for the values of the Riemann  $\zeta$ -function at  $n$ . The abbreviation  $\text{Cl}_2$  stands for  $\text{Cl}_2(\pi/3) = \text{Im}[\text{Li}_2(e^{i\pi/3})]$  where  $\text{Li}_2$  and  $\text{Li}_4$  represent the Di- and Quadri-logarithm respectively. Numerically we find

$$\begin{aligned}\Delta\rho = & 3x_t - 2.2176x_t^2 + 249.74x_t^3 \\ & - 8.5797\frac{\alpha_s}{\pi}x_t + 0.9798\frac{\alpha_s}{\pi}x_t^2.\end{aligned}\quad (8)$$

The pure electroweak three loop contribution leads to a correction of 36% of the two loop result to the  $\rho$  parameter. In contrast, the order  $\alpha_s x_t^2$  yields an enhancement of about 4% in comparison with the order  $x_t^2$  and is therefore negligible.

The program packages mentioned above allow for an extension of the presented analysis to the case of  $M_H = m_t$  and the limit  $M_H \gg m_t$ . Analytical results for the corresponding three loop contributions will appear elsewhere [14].

### Acknowledgments

The author thanks the organizers of the Adriatic 2001 meeting for their kind hospitality and the pleasant atmosphere during the workshop. I am grateful to my collaborator T. Seidensticker with whom this calculation has been worked out, and to K.G. Chetyrkin and J.H. Kühn for useful discussions.

This work is supported by the *Graduiertenkolleg "Hochenergiephysik und Teilchenastrophysik"* and the *DFG-Forscherguppe 'Quantenfeldtheorie, Computeralgebra und Monte-Carlo-Simulation'* (contract FOR 264/2-1).

### References

1. J. J. van der Bij, K. G. Chetyrkin, M. Faisst, G. Jikia and T. Seidensticker, *Phys. Lett. B* **498** (2001) 156.
2. M. Veltman, *Nucl. Phys. B* **123** (1977) 89.
3. For a review see, e.g.  
V.A. Smirnov, *Mod. Phys. Lett. A* **10** (1995) 1485 and references therein.
4. R. Mertig, *Comp. Phys. Commun.* **111** (1998) 265.
5. J. Fleischer and M.Yu. Kalmykov, *Comp. Phys. Commun.* **128** (2000) 531.
6. P. Nogueira, *J. Comp. Phys.* **105** (1993) 279.
7. T. Seidensticker, Diploma thesis (University of Karlsruhe, 1998), unpublished.
8. S.A. Larin, F.V. Tkachov, and J.A.M. Vermaseren, preprint NIKHEF-H/91-18 (1991).
9. M. Steinhauser, *Comp. Phys. Commun.* **134** (2001) 335; see also PhD thesis (University of Karlsruhe), Shaker Verlag, Aachen, 1996.
10. J.A.M. Vermaseren, Symbolic Manipulation with FORM, CAN (1991).
11. A. Djouadi and C. Verzegnassi, *Phys. Lett. B* **195** (1990) 265;  
A. Djouadi, *Nuovo Cim.* **100A** (1988) 357.
12. J.J. van der Bij and F. Hoogeveen, *Nucl. Phys. B* **283** (1987) 477.
13. J. Fleischer, O. V. Tarasov and F. Jegerlehner, *Phys. Lett. B* **319** (1993) 249.
14. M. Faisst and T. Seidensticker, in preparation.

# $\Delta S = 2$ Decays of $B^-$ Meson

Svetlana Fajfer<sup>1</sup> and Paul Singer<sup>2</sup>

<sup>1</sup> Physics Department, University of Ljubljana and J. Stefan Institute, 1000 Ljubljana, Slovenia

<sup>2</sup> Department of Physics, Technion - Israel Institute of Technology, Haifa 32000, Israel

**Abstract.** The  $\Delta S = 2$  transitions of the  $B$  mesons in the Standard Model are very rare. We investigate the three - body  $B^- \rightarrow K^- K^- \pi^+$  and two - body  $B^- \rightarrow K^{*-} \bar{K}^{*0}$ ,  $B^- \rightarrow K^- \bar{K}^0$ ,  $B^- \rightarrow K^{*-} \bar{K}^0$ ,  $B^- \rightarrow K^- \bar{K}^{*0}$  decays in the Standard Model and in the Minimal Supersymmetric Model with and without  $\mathcal{R}$  parity conservation. All five modes are found to have branching ratios of the order of  $10^{-13} - 10^{-11}$  in the Standard Model, while the expected branching ratio in the different extensions vary between  $10^{-9} - 10^{-6}$ , for a reasonable set of assumed parameters.

The rare  $B$  meson decays are very important in current searches of physics beyond Standard Model (SM) at low energies [1]. Recently, the decays  $b \rightarrow ss\bar{d}$  or  $b \rightarrow dd\bar{s}$  have been analyzed [2–4] to investigate possible effects of new physics. As shown in [2], the  $b \rightarrow ss\bar{d}$  transition is mediated in the standard model by the box-diagram and its calculation results in a branching ratio of nearly  $10^{-11}$ , the exact value depending on the relative unknown phase between  $t$ ,  $c$  contributions in the box. The authors of [2,3] have calculated the  $b \rightarrow ss\bar{d}$  transition in various extensions of the SM. It appears that for certain plausible values of the parameters, this decay may proceed with a branching ratio of  $10^{-8} - 10^{-7}$  in the minimal supersymmetric standard model (MSSM) [3]. Thus, decays related to the  $b \rightarrow ss\bar{d}$  transition which was calculated to be very rare in the Standard Model, provide a good opportunity for investigating beyond the Standard Model physics. Moreover, when one considers supersymmetric models with  $\mathcal{R}$ -parity violating couplings, it turned out that the existing bounds on the involved couplings of the superpotential did not provide any constraint on the  $b \rightarrow ss\bar{d}$  mode [2]. Recently, the OPAL collaboration [5] has set lower bounds on a combination of these couplings from the establishment of an upper limit for the  $B^- \rightarrow K^- K^- \pi^+$  decay  $BR(B^- \rightarrow K^- K^- \pi^+) \leq 8.8 \times 10^{-5}$ . The BELLE Collaboration has lowered this limit to  $3.2 \times 10^{-6}$  [6].

Here we describe an investigation of this decay mode in MSSM, with and without  $\mathcal{R}$  parity and two Higgs doublet models as possible alternatives to the SM. Then we comment on another possibility for the observation of the  $b \rightarrow ss\bar{d}$  transition: the two body decays of  $B^-$ . First, we proceed to describe the framework used in our analysis in which we concentrate on MSSM, with and without  $\mathcal{R}$  parity and two Higgs doublet models.

The minimal supersymmetric extension of the Standard Model leads to the following effective Hamiltonian describing the  $b \rightarrow ss\bar{d}$  transition [2,7]

$$\mathcal{H} = \tilde{C}_{MSSM}(\bar{s}\gamma^\mu d_L)(\bar{s}\gamma_\mu b_L), \quad (1)$$

where we have denoted

$$\tilde{C}_{MSSM} = -\frac{\alpha_s^2 \delta_{12}^{d*} \delta_{23}^d}{216 m_{\tilde{d}}^2} [24x f_6(x) + 66 \tilde{f}_6(x)] \quad (2)$$

with  $x = m_{\tilde{g}}^2/m_{\tilde{d}}^2$ , and the functions  $f_6(x)$  and  $\tilde{f}_6(x)$  are given in [7]. The couplings  $\delta_{ij}^d$  parametrize the mixing between the down-type left-handed squarks. At the scale of  $b$  quark mass and by taking the existing upper limits on  $\delta_{ij}^d$  from [7] and [2] the coupling  $\tilde{C}_{MSSM}$  is estimated to be  $|\tilde{C}_{MSSM}| \leq 1.2 \times 10^{-9} \text{ GeV}^{-2}$  for an average squark mass  $m_{\tilde{d}} = 500 \text{ GeV}$  and  $x = 8$ , which leads to an inclusive branching ratio for  $b \rightarrow ss\bar{d}$  of  $2 \times 10^{-7}$  [2]. The corresponding factor calculated in SM, taking numerical values from [8] and neglecting the CKM phases is estimated to be  $|C_{SM}| \simeq 4 \times 10^{-12}$  [2].

The authors of [2] have also investigated beyond MSSM cases by including  $R$ -parity violating interactions. The part of the superpotential which is relevant here is  $W = \lambda'_{ijk} L_i Q_j d_k$ , where  $i, j, k$  are indices for the families and  $L, Q, d$  are superfields for the lepton doublet, the quark doublet, and the down-type quark singlet, respectively. Following notations of [9] and [2] the tree level effective Hamiltonian is

$$\mathcal{H} = - \sum_n \frac{f_{QCD}}{m_{\tilde{\nu}_n}^2} [\lambda'_{n32} \lambda_{n21}^* (\bar{s}_R b_L) (\bar{s}_L d_R) + \lambda'_{n21} \lambda_{n32}^* (\bar{s}_R d_L) (\bar{s}_L b_R)]. \quad (3)$$

The QCD corrections were found to be important for this transition [10]. For our purpose it suffices to follow [2] retaining the leading order QCD result  $f_{QCD} \simeq 2$ , for  $m_{\tilde{\nu}} = 100 \text{ GeV}$ .

Most recently an upper bound on the specific combination of couplings entering (12) has been obtained by OPAL from a search for the  $B^- \rightarrow K^- K^- \pi^+$  decay [5]  $C_{\mathcal{R}} = \sum_n (|\lambda'_{n32} \lambda_{n21}^*|^2 + |\lambda'_{n21} \lambda_{n32}^*|^2)^{1/2} < 10^{-4}$ . Here we take the order of magnitude, while the OPAL result is  $5.9 \times 10^{-4}$  based on a rough estimate  $\Gamma(B^- \rightarrow K^- K^- \pi^+) \simeq 1/4 \Gamma(b \rightarrow ss\bar{d})$ .

We proceed now to study the effect of Hamiltonians (9), (12) on the various  $\Delta S = 2$  decays of charged  $B$  - mesons. In order to calculate the matrix elements of the operators appearing in the effective Hamiltonian, we use the factorization approximation [12–14], which requires the knowledge of the matrix elements of the current operators or the density operators. Here we use the standard form factor representation [12,13] of the matrix elements described in detail in [4,16].

For the  $F_1$  and  $F_0$  form factors appearing in the decomposition of the matrix element of the weak current between two pseudoscalar states, one usually assumes pole dominance [13,15]. For the vector and axial vector form factor, appearing in the decomposition of the matrix element of the weak current between the vector and pseudoscalar states, we use again pole dominance [13,15]. The relevant parameters are taken from [12,14]  $F_0^{BK}(0) = 0.38$ ,  $A_0^{BK*}(0) = 0.32$ . For the calculations of the density operators we use derivatives of the vector or axial-vector currents [16]. In our numerical calculation we use  $f_K = 0.162 \text{ GeV}$ ,  $g_{K^*} = 0.196 \text{ GeV}^2$  [14]. Now we turn to the analysis of the specific modes.

We denote  $\mathcal{O} = (\bar{s}\gamma^\mu(1 - \gamma_5)d) (\bar{s}\gamma_\mu(1 - \gamma_5)b)$ , and then we use  $\mathcal{H} = C\mathcal{O}$  with  $C$  being  $1/4\tilde{C}_{MSSM}$ ,  $1/4C_{SM}$  [16]. Using factorization and introducing  $s = (p_B - k_1)^2$ ,  $t = (p_B - k_2)^2$  and  $u = (p_B - p_\pi)^2$ , one finds for the  $B^- \rightarrow K^- K^- \pi^+$  decay

$$\begin{aligned} \langle K^-(k_1)K^-(k_2)\pi^+(p_\pi)|\mathcal{O}|B^-(p_B)\rangle &= F_1^{K\pi}(s)F_1^{BK}(s)[m_B^2 + 2m_K^2 - s - 2t - \\ &\quad - \frac{m_K^2 - m_\pi^2}{s}(m_B^2 - m_K^2)] \\ &\quad + F_0^{K\pi}(s)F_0^{BK}(s)\frac{m_K^2 - m_\pi^2}{s}(m_B^2 - m_K^2). \end{aligned} \quad (4)$$

Within MSSM the branching ratio is found to be

$$BR(B^- \rightarrow K^- K^- \pi^+)_{MSSM} \leq 4.7 \times 10^{-9}, \quad (5)$$

while SM gives this rate to be  $5.2 \times 10^{-14}$ . The MSSM which includes  $\mathcal{R}$  parity breaking terms can occur in this decay. The matrix element of the operator  $\mathcal{O}_{\mathcal{R}} = (\bar{s}(1 \pm \gamma_5)d) (\bar{s}(1 \mp \gamma_5)b)$  is found to be

$$\begin{aligned} \langle K^-(k_1)K^-(k_2)\pi^+(p_\pi)|\mathcal{O}_{\mathcal{R}}|B^-(p_B)\rangle &= \\ F_0^{K\pi}(s)F_0^{BK}(s)\frac{(m_B^2 - m_K^2)(m_K^2 - m_\pi^2)}{(m_s - m_d)(m_b - m_s)}. \end{aligned} \quad (6)$$

Taking the values of the quark masses as in [12]  $m_b = 4.88 \text{ GeV}$ ,  $m_s = 122 \text{ MeV}$ ,  $m_d = 7.6 \text{ MeV}$  and using the bound given above, we estimate the upper limit of the branching ratio  $BR(B^- \rightarrow K^- K^- \pi^+)_{\mathcal{R}} \leq 1.8 \times 10^{-7}$  for  $C_{\mathcal{R}} < 10^{-4}$ . This limit is raised to  $6 \times 10^{-6}$  for the upper bound on  $C_{\mathcal{R}}$  of  $5.9 \times 10^{-4}$  given in [5].

The long distance effects (LD) are usually suppressed in the  $B$  meson decays. However, in any search of new physics one has to include their contributions also [4]. In the case of  $B^- \rightarrow K^- K^- \pi^+$  decay, we have analyzed two contributions [4]: (I) the box diagram, which is essentially the LD analog of the SD calculation in the standard model [2] of the  $b \rightarrow s\bar{s}d$  transition. (II) the contribution of virtual " $D^0$ " and " $\pi^0$ " mesons, via the chain  $B^- \rightarrow K^- D^0$  (" $\pi^0$ ")  $\rightarrow K^- K^- \pi^+$ . This contribution arises as a sequence of two  $\Delta S = 1$  transitions and may lead to final  $K^- K^- \pi^+$  state as well. It is therefore necessary to have an estimate of its relevance vis - à - vis the "direct"  $\Delta S = 2$  transition. The box diagrams contributes to the real and imaginary part of the amplitude for the  $B^- \rightarrow K^- K^- \pi^+$  decay.

The final result for the decay rate is

$$\Gamma(B^- \rightarrow K^- K^- \pi^+) = \frac{1}{2(2\pi)^3 32m_B^3} \int_{(m_\pi + m_K)^2}^{(m_B - m_K)^2} ds_2 \int_{(s_1)_1}^{(s_1)_2} ds_1 |\mathcal{A}|^2, \quad (7)$$

where

$$\begin{aligned} (s_1)_{1,2} &= m_K^2 + m_\pi^2 - \frac{1}{2s_2}[(s_2 - m_B^2 + m_K^2)(s_2 + m_\pi^2 - m_K^2) \\ &\quad \pm \lambda^{1/2}(s_2, m_B^2, m_K^2)\lambda^{1/2}(s_2, m_\pi^2, m_K^2)] \end{aligned} \quad (8)$$

and  $\lambda(a, b, c) = a^2 + b^2 + c^2 - 2ab - 2ac - 2ab$ . The  $\mathcal{A}_r^{box}$  denotes the leading term of the amplitude, which results after using the primitive cut-off regularization:

$$\mathcal{A}_r^{box}(B^- \rightarrow K^- K^- \pi^+) \simeq G^2 V_{cb} V_{cs}^* V_{cd} V_{cs}^* \frac{1}{16\pi^2} \Lambda^2 (m_D^2 - m_\pi^2). \quad (9)$$

There is obviously the uncertainty in the value to be taken for  $\Lambda$ . The momentum in the box cannot exceed  $m_B$ , and by taking  $\Lambda \simeq 10$  GeV we obtain

$$BR(B^- \rightarrow K^- K^- \pi^+)_{(r)}^{(box)} \simeq 8 \times 10^{-15} \quad (10)$$

for the real part of this contribution, using  $\Gamma(B^- \rightarrow all) = 4 \times 10^{-13}$  GeV [8]. Turning now to the imaginary part of the  $B^- \rightarrow K^- K^- \pi^+$  amplitude provided by the  $DD$  and  $D\pi$  intermediate states, it is given by [4]

$$\begin{aligned} \mathcal{A}_i^{box}(B^- \rightarrow K^- K^- \pi^+) &= -\frac{G^2}{32\pi^2} V_{cb} V_{cs}^* V_{cd} V_{cs}^* \\ &\int d^4 q_1 \delta(q_1^2 - m_D^2) [\delta((q_1 - k_1 - k_2)^2 - m_D^2) - \delta((q_1 - k_1 - p_\pi)^2 - m_\pi^2)] \\ &\{ -q_1^4 + (-2k_2 \cdot q_1 q_1^2 + 2p_\pi \cdot q_1 q_1^2 + q_1^2(m_K^2 + 2k_1 \cdot p_\pi + m_B^2 - 2k_2 \cdot p_B) \\ &+ 2p_\pi \cdot q_1 2k_2 \cdot q_1 + 2p_\pi \cdot q_1(-m_B^2 + 2k_2 \cdot p_B) \\ &+ 2k_2 \cdot q_1(m_K^2 + 2p_\pi \cdot k_1) + (-m_B^2 + 2k_2 \cdot p_B)(m_K^2 + 2k_1 \cdot p_\pi) \\ &+ (k_1 \leftrightarrow k_2) \}. \end{aligned} \quad (11)$$

Introducing now  $s_1 = (p_B - k_1)^2 = (k_2 + p_\pi)^2$  and  $s_2 = (p_B - k_2)^2 = (k_1 + p_\pi)^2$  one arrives at

$$\begin{aligned} \mathcal{A}_i^{box}(B^- \rightarrow K^- K^- \pi^+) &= -\frac{G^2}{32\pi^2} V_{cb} V_{cs}^* V_{cd} V_{cs}^* \\ &\times \{ F(m_D^2, s_1, s_2) - F(m_\pi^2, s_1, s_2) + (s_1 \leftrightarrow s_2) \}, \end{aligned} \quad (12)$$

with

$$\begin{aligned} F(m_P, s_1, s_2) &= \frac{\lambda^{1/2}(m_D^2, m_P^2, s_1)}{m_D^2 - m_P^2 + s_1} \\ &\{ -m_D^4 + m_D^2(2s_1 - \frac{3}{2}m_K^2 - \frac{3}{2}m_\pi^2 - \frac{1}{2}s_2) + (s_1 - m_\pi)(-s_1 + m_K^2) \\ &+ (s_1 \leftrightarrow s_2) \}. \end{aligned} \quad (13)$$

Using the expression for the decay width we find

$$BR(B^- \rightarrow K^- K^- \pi^+)_{(i)}^{(box)} \simeq 6 \times 10^{-12}. \quad (14)$$

The part of the decay amplitude due to the " $D^0$ " pole is then given by

$$\begin{aligned} \mathcal{A}_{D^0}^{pole}(B^- \rightarrow K^- K^- \pi^+) &= -\frac{G^2}{2} V_{cb} V_{cs}^* V_{cd} V_{cs}^* a_1^{(b)} a_1^{(c)} f_K f_\pi \\ &\times F_0^{BD}(m_K^2) F_0^{DK}(m_\pi^2) \frac{(m_B^2 - q^2)(q^2 - m_K^2)}{q^2 - m_D^2 + im_D \Gamma_D}. \end{aligned} \quad (15)$$



The decay width due to this contribution is given by

$$\begin{aligned} \Gamma(B^- \rightarrow K^- K^- \pi^+) &= \frac{1}{2(2\pi)^3 32m_B^3} |C|^2 |F_0^{BD}(m_K^2) F_0^{DK}(m_\pi^2)|^2 \\ &\times \int_{(m_\pi+m_K)^2}^{(m_B-m_K)^2} ds \frac{(m_B^2 - s)^2 (s - m_K^2)^2}{(s - m_D^2)^2 + (m_D \Gamma_D)^2} \\ &\times \frac{1}{s} \lambda^{1/2}(s, m_B^2, m_K^2) \lambda^{1/2}(s, m_\pi^2, m_K^2), \end{aligned} \quad (16)$$

with  $C = (G^2/2) V_{cb} V_{cs}^* V_{cd} V_{cs}^* a_1^{(b)} a_1^{(c)} f_K f_\pi$ , for the resonance in a  $s$  channel and the same for the resonance in a crossed channel.

Using for  $a_1^{(b)}$ ,  $a_1^{(c)}$ ,  $F_0^{DK}$  and  $F_0^{BD}$  the value of Bauer, Stech and Wirbel [14] we calculate the virtual " $D^0$ " contribution by deleting a width of  $2\Delta$  around  $D$  mass in the  $s$  variable. The size of  $\Delta$  is related to the experimental accuracy of the  $D$  - determination in the final  $K^- \pi^+$  state. In the various experiments it ranges between 1 and 10 MeV. One should keep in mind that average accuracy of  $D^0$  - mass determination is 0.5 MeV [8]. Thus, in order to delete the physical  $D^0$ 's one must take at least  $\Delta = 1$  MeV. However, we shall check the  $\Delta$  dependence for a range of values to make sure that our conclusions are not affected.

For  $\Delta = 20, 5, 1, 0.1$  MeV we find the nonresonant  $D^0$  contribution to be [4]

$$BR(B^- \rightarrow K^- K^- \pi^+)_{(D^0)}^{pole} = (0.31; 1.2; 6.2; 61) \times 10^{-15}. \quad (17)$$

In all cases the result is much smaller than (13), though one should remember that  $\Delta = (1 - 5)$  MeV is the realistic option. A similar calculation for  $\pi^0$  intermediate contribution, i.e.  $B^- \rightarrow K^- \pi^0 \pi^0 \rightarrow K^- \pi^+$  yields a value smaller by four orders of magnitude, especially as a result of CKM angles. The pole contribution is therefore considerably smaller than the LD box contribution calculated with  $DD$  and  $D\pi$  intermediate states; thus the total branching ratio from all diagrams we included is [4]

$$BR(B^- \rightarrow K^- K^- \pi^+)_{LD} = 6 \times 10^{-12}. \quad (18)$$

As a check, we used our  $\mathcal{A}_{(D^0)}^{pole}$  amplitude to calculate  $B^- \rightarrow K^- K^- \pi^+$  as given by decay via a physical  $D^0$  and we find a branching ratio of  $7 \times 10^{-6}$ . This agrees very well with the experimental expectation of  $(9.9 \pm 2.8) \times 10^{-6}$ , obtained by using  $BR(B^- \rightarrow D^0 K^-) = (2.57 \pm 0.65 \pm 0.32) \times 10^{-4}$  and  $BR(D^0 \rightarrow K^- \pi^+) = 3.85 \times 10^{-2}$  [8]. Therefore, we have shown that the long - distance contributions to  $B^- \rightarrow K^- K^- \pi^+$  in the SM are smaller or comparable to the short - distance box diagram, and have the branching ratio in a  $10^{-12} - 10^{-11}$  range. This is a most welcome feature since it strengthens the suitability of the  $B^- \rightarrow K^- K^- \pi^+$  decay as an ideal testing ground for physics beyond the standard model, as originally suggested in [2].

We briefly discuss the various two - body  $\Delta S = 2$  decays of  $B^-$  meson. Using factorization and the definitions given above, one finds the following helicity amplitudes for the  $B^- \rightarrow K^{*-} \bar{K}^{*0}$  decay [16]

$$H_{00}(B^- \rightarrow K^{*-} \bar{K}^{*0}) = C g_{K^*}(m_B + m_{K^*}) [\alpha A_1^{BK^*}(m_{K^*}^2) - \beta A_2(m_{K^*}^2)] \quad (19)$$

$$H_{\pm\pm}(B^- \rightarrow K^{*-} \bar{K}^{*0}) = Cg_{K^*}(m_B + m_{K^*})[\alpha A_1^{BK^*}(m_{K^*}^2) \mp \gamma V^{BK^*}(m_{K^*}^2)] \quad (20)$$

where

$$\alpha = \frac{1 - 2r^2}{2r^2}, \quad \beta = \frac{k^2}{2r^2(1+r)^2}, \quad \gamma = (1 - 4r^2) \quad (21)$$

with  $r = m_{K^*}/m_B$ ,  $k^2 = 1 + r^4 + t^4 - 2r^2 - 2t^2 - 2r^2t^2$ . The decay width is then

$$\Gamma(B^- \rightarrow K^{*-} \bar{K}^{*0}) = \frac{|\mathbf{p}|}{8\pi m_B^2} [|H_{00}|^2 + |H_{++}|^2 + |H_{--}|^2]. \quad (22)$$

Within MSSM model the branching ratio becomes  $\leq 6.2 \times 10^{-9}$ , while SM gives this rate to be  $6.8 \times 10^{-14}$ . The  $\mathcal{R}$  - parity term described by the effective Hamiltonian cannot be seen in this decay mode when factorization approach is used, since the density operator matrix element  $\langle \bar{K}^{*0} | (\bar{s}d) | 0 \rangle$  vanishes.

Turning now to  $B^- \rightarrow PV$  decays we have

$$\langle \bar{K}^0(k_0) K^{*-}(k_-, \epsilon) | \mathcal{O} | B^-(p_B) \rangle = -2m_{K^*} f_K A_0^{BK^*}(m_{K^*}^2) \epsilon^* \cdot k_0. \quad (23)$$

Denoting the  $B^- \rightarrow K^0 K^{*-}$  decay amplitude by  $\mathcal{A}$ , one finds

$$\sum_{pol} |\mathcal{A}|^2 = |C|^2 f_K^2 |A_0(m_K^2)|^2 \lambda(m_B^2, m_K^2, m_{K^*}^2) \quad (24)$$

with the  $\lambda(a, b, c) = a^2 + b^2 + c^2 - 2(ab + bc + ac)$ . The branching ratio is straightforwardly found to be  $BR(B^- \rightarrow K^{*-} \bar{K}^0)_{MSSM} \leq 1.6 \times 10^{-9}$ , which is comparable to the SM prediction of [12] for the  $\Delta S = 0$   $B^- \rightarrow K^{*-} K^0$  decay, given as  $BR(B^- \rightarrow K^{*-} K^0) = 1 \times 10^{-9}$ ,  $5 \times 10^{-9}$ ,  $2 \times 10^{-9}$  obtained for the number of colours  $N_c = 2$ ,  $N_c = 3$ ,  $N_c = \infty$ , respectively.

The SM calculation for the  $\Delta S = 2$  transition leads to  $BR(B^- \rightarrow K^{*-} \bar{K}^0)_{SM} = 1.7 \times 10^{-14}$  [16]. The MSSM which includes  $\mathcal{R}$  parity breaking terms can occur in this decay. The matrix element of the operator  $\mathcal{O}_{\mathcal{R}} = (\bar{s}(1 + \gamma_5)d)(\bar{s}(1 - \gamma_5)b)$  can be found to be [16]

$$\begin{aligned} \langle \bar{K}^0(k_0) K^{*-}(k_-, \epsilon) | \mathcal{O}_{\mathcal{R}} | B^-(p_B) \rangle &= \\ \frac{m_K^2 f_K}{(m_s + m_d)(m_s + m_b)} (2m_{K^*} \epsilon^* \cdot k_0) A_0^{BK^*}(m_K^2). \end{aligned} \quad (25)$$

Taking the values of the quark masses as in [12]  $m_b = 4.88 \text{ GeV}$ ,  $m_s = 122 \text{ MeV}$ ,  $m_d = 7.6 \text{ MeV}$  and using the constraint on the  $\mathcal{R}$  parity breaking parameter  $C_{\mathcal{R}} < 10^{-4}$ , we obtain the estimation of the upper limit of the branching ratio  $BR(B^- \rightarrow K^{*-} \bar{K}^0)_{\mathcal{R}}$  to be  $4.4 \times 10^{-8}$ . This limit is raised to  $1.5 \times 10^{-6}$  for the upper bound on  $C_{\mathcal{R}}$  of  $5.9 \times 10^{-4}$  given in [5]. For the other possible  $VP$  decay with  $\Delta S = 2$   $B^- \rightarrow K^- \bar{K}^{*0}$ , the relevant operator is

$$\langle \bar{K}^{*0}(k_0, \epsilon) K^-(k_-) | \mathcal{O} | B^-(p_B) \rangle = 2g_{K^*} f_K F_1^{BK^*}(m_{K^*}^2) \epsilon^* \cdot k_- \quad (26)$$

giving the branching ratio in MSSM with an upper limit

$$BR(B^- \rightarrow K^- \bar{K}^{*0})_{MSSM} < 5.9 \times 10^{-9} \quad (27)$$

in comparison with SM result  $6.5 \times 10^{-14}$ .

Finally, for the  $B^- \rightarrow PP$  case one has

$$\langle \bar{K}^0(k_0) K^-(k_-) | \mathcal{O} | B^-(p_B) \rangle = i f_K F_0^{BK} (m_K^2) (m_B^2 - m_K^2). \quad (28)$$

The multiplication with the corresponding  $1/4\tilde{C}_{MSSM}$  gives the required amplitude  $\tilde{\mathcal{A}}$ . The branching ratio is then

$$\Gamma(B^- \rightarrow K^- \bar{K}^0) = \frac{1}{16\pi m_B^2} \sqrt{m_B^2 - 4m_K^2} |\tilde{\mathcal{A}}|^2, \quad (29)$$

The branching ratio for MSSM is found to be  $BR(B^- \rightarrow K^- \bar{K}^0)_{MSSM} \leq 2.3 \times 10^{-9}$ , in comparison with the  $2.5 \times 10^{-14}$  found in the SM. The matrix element of the  $R$  parity breaking MSSM operator leads to the decay width

$$\begin{aligned} \Gamma(B^- \rightarrow K^- \bar{K}^0)_{\mathcal{R}} &= \frac{1}{16\pi m_B^2} \sqrt{m_B^2 - 4m_K^2} |\langle K^- \bar{K}^0 | \mathcal{O}^{(1)} | B^- \rangle / 4|^2 \\ &\times \frac{f_{QCD}^2}{m_{\tilde{\nu}}^4} \left( \sum_{i=n} |\lambda'_{n32} \lambda'^*_{n21}|^2 + |\lambda'_{n21} \lambda'^*_{n32}|^2 \right) \end{aligned} \quad (30)$$

where we have used  $\mathcal{O}^{(1)} = (\bar{s}\gamma_5 d)(\bar{s}b)$  [16]. The corresponding branching ratio  $BR(B^- \rightarrow K^- \bar{K}^0)_{\mathcal{R}}$  can be as large as  $3.3 \times 10^{-6}$ .

One might wonder if the long distance effects are important in two - body  $\Delta S = 2$   $B^-$  decays. We have estimated the tree level contribution of the  $D(D^*)$  which then goes into  $K(K^*)$  via weak annihilation. We found that these contributions give a branching ratio of the order  $10^{-18}$  and therefore they can be safely neglected. One might think that the exchange of two intermediate states  $D(D^*)$ ,  $K(K^*)$  can introduce certain long distance contributions. In decay  $B \rightarrow "D" "K" \rightarrow "K" "K"$  the first weak vertex arises from the decay  $B \rightarrow "D" "K"$  and the second weak vertex (see e.g. [4]) can be generally obtained from the three body decays of  $D \rightarrow KKK$ . Therefore, we are quite confident to suggest that the long distance effects are not important in the two - body  $\Delta S = 2$   $B$  decays.

At this point we have to emphasize that although in principle two body decays would appear to be simpler to analyze, there is the process of  $K^0 - \bar{K}^0$  mixing which complicates the possibility of detection.

We can summarize that in the  $B^- \rightarrow K^- K^- \pi^+$  and two - body  $B^-$  decays, the MSSM with the chosen set of parameters gives rates of the order  $10^{-9} - 10^{-8}$ , while the  $\mathcal{R}$  parity breaking terms in the MSSM can be seen only in the  $B^- \rightarrow K^- K^- \pi^+$ ,  $B^- \rightarrow K^{*-} \bar{K}^0$  and  $B^- \rightarrow K^- \bar{K}^0$  decays. Presently, the experimental limit on  $C_{\mathcal{R}}$  allows these modes to have branching ratios as high as  $10^{-6}$ , mainly due to possible  $\mathcal{R}$ -parity terms in MSSM. Turning to the possibility of detecting these decay modes, the  $B^- \rightarrow K^- K^- \pi^+$  seems to be the

best candidate, since in the other modes we discussed, having  $\bar{K}^0$  in the final states complicates the possibility of a detection because of  $K^0 - \bar{K}^0$  mixing [16].

Thus, among the  $\Delta S = 2$  decay modes of the  $B^-$  meson, the  $B^- \rightarrow K^- K^- \pi^+$  decay is the ideal candidate to look for physics beyond SM, while  $B^- \rightarrow K^{*-} \bar{K}^{*0}$ ,  $B^- \rightarrow K^- \bar{K}^{*0}$  decays offer this possibility too, although for a more restricted set of models.

## References

1. For reviews, see A. Masiero, L. Silvestrini in Proc. *2nd Intern. Conf. on B Physics and CP Violation* (BCONF 97), Honolulu, HI 1997, T. E. Browder, F. A. Harris, S. Pakvasa eds (World Scientific, Singapore 1998), p.172. Y. Grossman, Y. Nir, R. Rattazzi in *Heavy Flavours* 2nd edn. Edition, A. J. Buras and M. Lindner eds, p. 755 (World Scientific, Singapore 1998).
2. K. Huitu, C. -D.Lü, P. Singer, D. -X. Zhang: Phys. Rev. Lett. **81**, 4313 (1998).
3. K. Huitu, C. -D.Lü, P. Singer, D. -X. Zhang: Phys. Lett. B **445**, 394(1999).
4. S. Fajfer and P. Singer: Phys. Lett. B **478**, 185 (2000).
5. G. Abbiendi et al., OPAL Collaboration: Phys. Lett. B **476**, 233 (2000).
6. K. Abe et al., BELLE Collaboration, hep-ex/0201007.
7. F. Gabbiani, E. Gabrielli, A. Masiero, L. Silvestrini: Nucl. Phys. B **477**, 321 (1996).
8. Particle Data Group, D. E. Groom et. al: Europ. Phys. Journal C **15**, 1 (2000).
9. D. Choudhury and P. Roy: Phys. Lett. B **378**, 153 (1996).
10. J. L. A. Bagger, K.T. Matchev, and R.J. Zhang: Phys. Lett. B **412**, 77 (1997).
11. T. P. Cheng, M. Sher: Phys. Rev. D **35**, 3484 (1987); M. Sher, Y. Yuan: Phys. Rev. D **41**, 1461 (1991).
12. A. Ali, G. Kramer and C. D. Lü: Phys. Rev. D **58**, 094009 (1998).
13. M. Wirbel, B. Stech and M. Bauer, Z. Phys. C **29**, 637 (1985).
14. M. Bauer, B. Stech, M. Wirbel: Z. Phys. C **34**, 103 (1987); F. Buccella, M. Forte, G. Miele, G. Ricciardi: Z. Phys. C **48**, 47 (1990); P. Lichard: Phys. Rev. D **55**, 5385 (1997).
15. S. Fajfer, J. Zupan: Int. J. Mod. Phys. A **14** 4161 (1999).
16. S. Fajfer and P. Singer: Phys. Rev. D **62**, 117702 (2000); Nucl. Phys. B **93**, 134 (2001).

# Charmonium Hadro-Production at HERA-*B*

Olga Igonkina (for the HERA-*B* collaboration)

Institute for Theoretical and Experimental Physics, Cheremushkinskaja, 25, 117259  
Moscow, Russia

**Abstract.** HERA-*B* is a fixed target experiment at DESY(Hamburg). The target consists of 8 thin wires of various materials inside the HERA proton beam. The trigger is primarily designed to select  $J/\psi \rightarrow l^+l^-$  events. The detection of both charged and neutral tracks permits reconstruction of excited charmonium states such as  $\chi_c$ ,  $\eta'_c$ ,  $h_c$  and therefore allows studies of their production mechanism. The acceptance of the detector covers the largely uncharted region of negative  $x_F$  as well as the more common positive  $x_F$ . The negative  $x_F$  acceptance and the variation of target material allows a systematic study of nuclear suppression models.

The potential of HERA-*B* for measurements of charmonium production as well as preliminary results of data taking in the year 2000 are presented.

## 1 Introduction

The charmonium system and its production in hadronic collisions has recently attracted considerable attention from both theoretical and experimental sides due to two different problems, namely, understanding of the production mechanism and the influence of the nucleus on production rates.

The production mechanism includes the creation of a  $c\bar{c}$  pair in the interaction of gluons and/or quarks and the formation of a charmonium state from an unbound pair. The first step is calculated in pQCD. However the process of formation of the bound state is not understood. Three different models compete to describe production of heavy quarkonium: the Color Singlet Model (*CSM*)[1], non relativistic QCD (*NRQCD*)[2] and the Color Evaporation Model (*CEM*)[3]. To distinguish between the models new measurements are required, such as the production rates of all charmonium states below  $D\bar{D}$  threshold as a function of transverse momentum  $p_T$ , the Feynman variable  $x_F$ <sup>1</sup>, and the polarization.

The production rate is also influenced by the presence of the nucleus. The (anti)nuclear shadowing[4], energy loss[5], or an intrinsic charm component[6] affect initial parton density distributions. Those effects influence also other processes, e.g. Drell-Yan production. The absorption of the produced  $c\bar{c}$  by the nucleus[7], comovers[8], or energy loss by the  $c\bar{c}$  pair[9] have been claimed to be responsible for the observed charmonium suppression.

It has been suggested that the change in the production rate of charmonium due to the presence of the nucleus factorizes with the production mechanism and

---

<sup>1</sup>  $x_F$  is the longitudinal momentum fraction  $x_F = p_z/p_z^{max}$  in the c.m. system.

can be expressed by the function

$$\sigma_{pA} = \sigma_{pN} \cdot A^\alpha, \quad (1)$$

where  $\sigma_{pN}$  is the production cross section of a given state in proton–nucleon interactions and  $A$  is the atomic mass of the nucleus. The parameter  $\alpha$  represents the combination of different nuclear effects. To distinguish between models one could study the dependence of  $\alpha$  on  $x_F$  [10]. As was shown in [11] the  $\chi_c$  states are more sensitive to nuclear effects than  $J/\psi$  or  $\psi'$ .

Measurements of the hadro–production of different charmonium states are available only for  $J/\psi$  and  $\psi'$  and only in the positive  $x_F$  region. Measurements of the fraction of  $J/\psi$  produced via  $\chi_c$  states are very limited. No measurement of the nuclear dependence of  $\chi_c$  production is available.

## 2 Detector

HERA- $B$  is a fixed target experiment located at the HERA proton storage ring at DESY (Hamburg). The energy of the proton beam is 920 GeV which gives the energy in the c.m. frame  $\sqrt{s} = 41.6$  GeV. The target consists of 8 wires of different materials, namely C, Al, Ti, W. During operation, the wires are inserted into the halo of the beam. Good resolution of reconstructed vertices allows for separation of the primary interactions between the different wires. The interaction rate varies in the range 5–20 MHz. At 5 MHz interaction rate one event contains in average 0.5 primary interactions distributed according to Poissonian statistics.

The detector scheme is presented in Fig.1. The tracker consists of 3 parts : a silicon vertex detector, micro strip gas chambers (the inner tracker) and honey-comb drift chambers (the outer tracker). The 2.2 Tm magnet is positioned in the middle of the spectrometer and gives a 0.64 GeV/c transverse momentum kick to the charged particles. Particle identification devices include a ring imaging

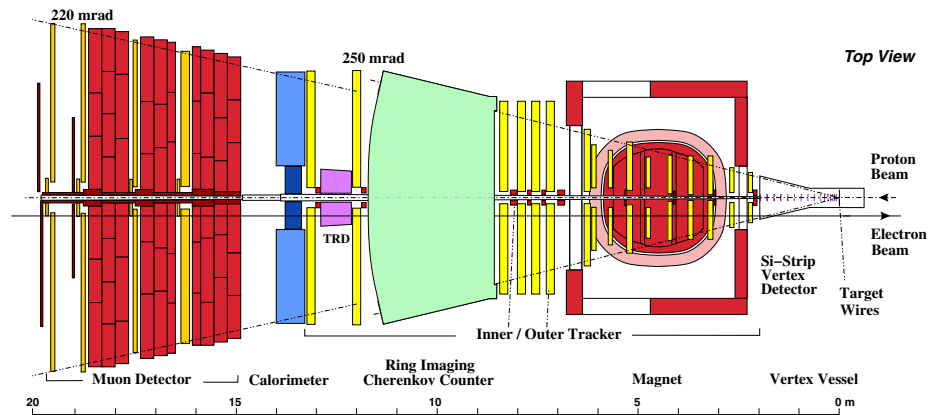


Fig. 1. The HERA- $B$  detector

Cherenkov counter (*RICH*), an electromagnetic calorimeter and a muon system. A detailed description of the detector can be found elsewhere[12].

The detector covers a large pseudo-rapidity interval  $\eta \in [2, 5]$ , corresponding to the  $x_F^{J/\psi}$  interval  $[-0.4, 0.3]$ . During the year 2000 run the inner part of the tracker was not in use and therefore the coverage of detector was restricted to  $x_F^{J/\psi} \in [-0.4, 0.1]$ .

The detector allows complete event reconstruction including the neutral particles  $\gamma$  and  $\pi^0$ . Therefore, HERA-B can search for excited charmonium states such as  $\chi_c, \eta'_c \rightarrow J/\psi + \gamma$ ,  $\psi' \rightarrow J/\psi + \pi\pi$ ,  $h_c(1P_1) \rightarrow J/\psi + \pi^0$ .

The cross section for  $J/\psi$  production is small compare to the inelastic cross section  $\sigma_{J/\psi}/\sigma_{in} = 3 \cdot 10^{-5}$ . HERA-B uses a  $J/\psi$  oriented trigger which selects lepton pairs  $e^+e^-$ ,  $\mu^+\mu^-$  with a high invariant mass. Tracks with hits in at least three muon superlayers are classified as muon tracks. The transverse momentum of muons is required to be greater than 0.7 GeV/c. For the electron trigger the transverse energy deposited in the calorimeter by each candidate is required to be greater than 1 GeV/c. HERA-B also makes use of triggers of other kinds (e.g. hard photon or single lepton triggers) which are not discussed in this article.

### 3 Analysis

The year 2000 data were collected in parallel with commissioning of the detector. Only the carbon and titanium wires were used. The collected sample consists of about  $16 \cdot 10^6$  events with varying trigger conditions. Among them we have reconstructed approximately 4000  $J/\psi \rightarrow \mu^+\mu^-$  decays and  $10^5$   $J/\psi \rightarrow e^+e^-$ . The detailed analysis of the events included a precise calculation of track parameters, a common vertex constraint, and particle identification. The muon identification included data from the muon system, *RICH*, and tracker. Electron identification was based on the calorimeter and tracker information. To reduce background from hadrons, the presence of a bremsstrahlung cluster in the direction of the track in front of the magnet was required for at least one of the 2 electron candidates.

The invariant mass distribution is shown in Fig.2. The main background contribution is due to random combinations of hadrons misidentified as muons or electrons. The Drell-Yan contribution is estimated to be at the level of a few percent. The fraction of charm or beauty decays with 2 muons or electrons in the final state is negligible. The mass resolution  $\sigma(M_{\mu\mu}) \approx 50 \text{ MeV}/c^2$ ,  $\sigma(M_{ee}) \approx 130 \text{ MeV}/c^2$  agrees with the expectation based on full detector simulation. The larger width of the mass in the electron channel is explained by significant loss of energy in the magnet area which was not recovered.

### 4 Preliminary Results

The total cross section of  $J/\psi$  production in  $p$ -C interactions was measured with a subsample of the  $J/\psi \rightarrow e^+e^-$  candidates. The obtained value is  $\sigma(J/\psi)_{tot} =$

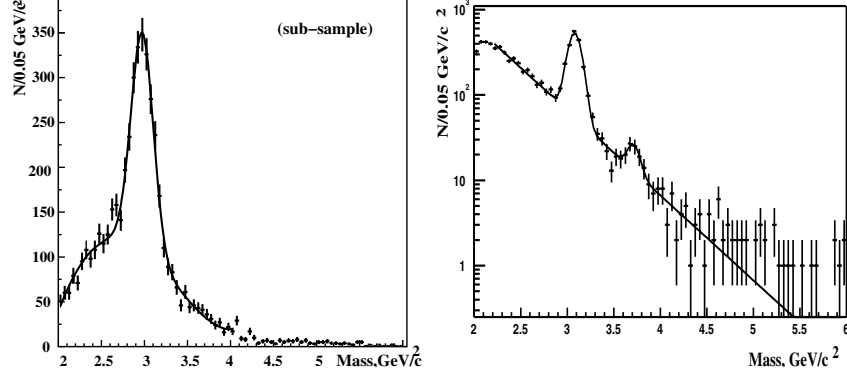


**Fig. 2.** Invariant mass distribution (a)  $e^+e^-$ , (b)  $\mu^+\mu^-$

$403 \pm 52 \pm 103$  nb/nucleon where we assumed nuclear dependence according to (1) with  $\alpha = 0.94$ . A comparison of the HERA-B result with the measurements of other experiments is shown in Fig.3. As the data were taken in parallel to detector and trigger commissioning, the data taking conditions were relatively unstable which results in a large systematic uncertainty. The results are in agreement with measurements of experiments E771[13] and E789[14], which ran at a similar c.m. energy. The prediction of NRQCD tuned at other energies is higher than the HERA-B measurement but it is closer to the data than the CSM prediction.

The muon channel data was used to measure the  $p_T, x_F$  spectra of  $J/\psi$  (see Fig.4). The data were fit with functions used by E789:

$$\frac{dN}{dp_T^2} = a \left( 1 + \left( \frac{p_T}{p_0} \right)^2 \right)^{-6}, \quad (2a)$$

$$\frac{dN}{dx_F} = b (1 - |x_F|)^c. \quad (2b)$$

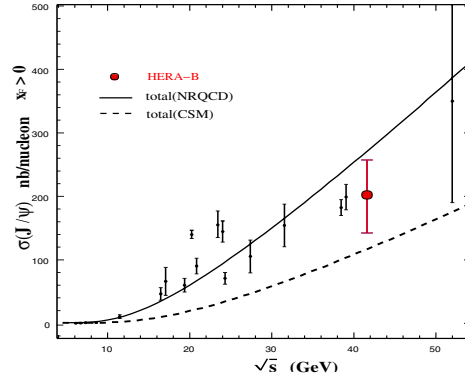


**Fig. 3.** Measured total cross section of  $J/\psi$  as a function of the c.m.s energy



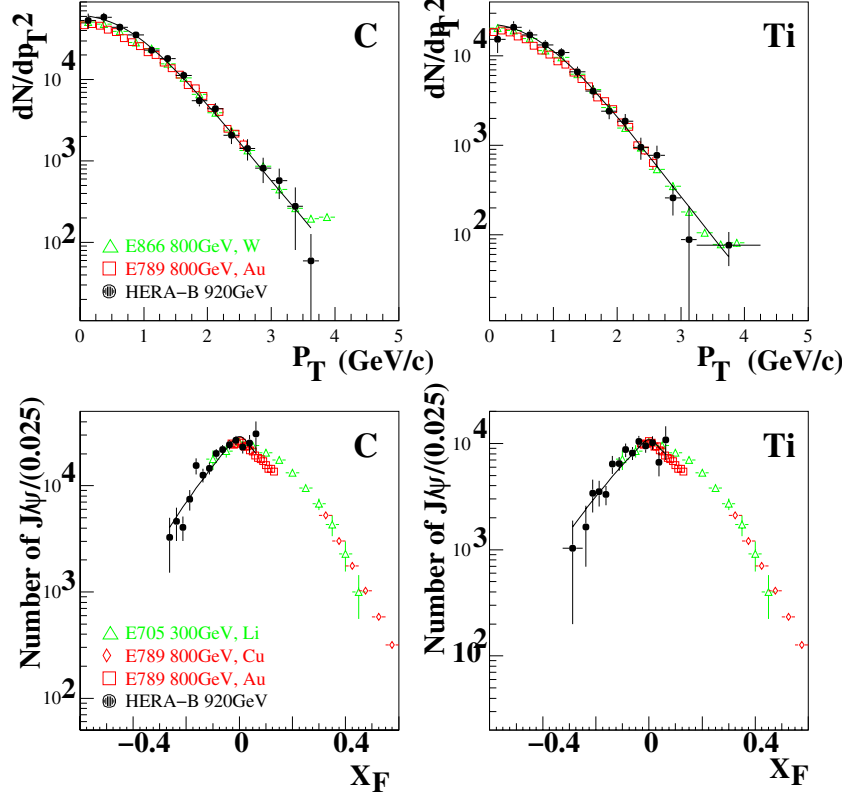


**Fig. 4.** Number of  $J/\psi$  observed as a function of  $p_T, x_F$  for C and Ti data. The results of E789[14] and E866[15] are normalized to the total number of  $J/\psi$  observed by HERA-B

The shapes of the distributions are determined by parameters  $p_0$  and  $c$ . The average transverse momentum  $\langle p_T \rangle$  is of interest to study  $\langle p_T \rangle$  broadening as a function of nucleus and  $\sqrt{s}$  [17]. Using (2a) it is determined as  $\langle p_T \rangle = 35\pi p_0/256$ . The HERA-B results are summarized in Table 1.

The nuclear dependence of  $J/\psi$  hadro-production can be extracted from the comparison of  $J/\psi$  rates for  $p$ -C and  $p$ -Ti collisions. Using formula 1 we estimated the parameter  $\alpha$  to be  $1.027 \pm 0.043 \pm 0.02$  where the first error is statistical

**Table 1.** Parameters of the  $p_T$  and  $x_F$  distributions of  $J/\psi$ . Only the statistical errors are shown

Interaction	$p_0$	$\langle p_T \rangle$	$c$
p-C	$2.71 \pm 0.06$	$1.16 \pm 0.03$	$6.24 \pm 0.48$
p-Ti	$2.90 \pm 0.09$	$1.25 \pm 0.04$	$6.31 \pm 0.60$

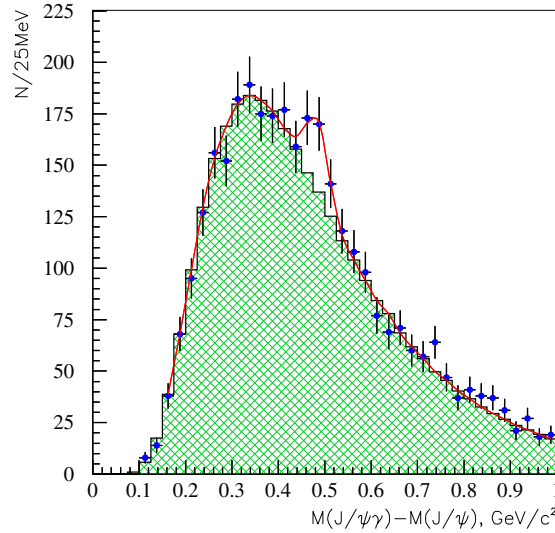


**Fig. 5.** Difference of the invariant mass of  $(l^+l^-\gamma)$  and the mass of  $(l^+l^-)$  where  $l$  is electron or muon. The hatched histogram shows the invariant mass of  $J/\psi$  candidates and photons from the different events.

and the second one is systematic. The value corresponds to the kinematic range of  $J/\psi$  shown in Fig.4. The result is in good agreement with more precise measurements of other experiments [15],[16] estimated for positive  $x_F$  region.

Figure 5 shows the  $\chi_c$  signal reconstructed in the  $J/\psi+\gamma$  channel for  $J/\psi$  candidates within a  $J/\psi$  invariant mass window of 2 standard deviations. The data corresponds to interactions on the carbon wire. The photons from  $\chi_c$  are reconstructed in the calorimeter with an efficiency ( $\varepsilon_\gamma$ ) of 22%. The signal is seen both in electron and muon samples. The shifts of the mass signals from  $\chi_c$  are explained by the high occupancy of low energy clusters in the calorimeter, which increases the energy of the photon from  $\chi_c$  but hardly affects energetic leptons from  $J/\psi$ . The random combinations of  $J/\psi$  and photons from different events describe the background under  $\chi_c$  very well. Analysis of  $J/\psi$  sidebands does not reveal any excess in the  $\chi_c$  mass region. The estimated fraction of  $J/\psi$  produced via  $\chi_{c1}$  and  $\chi_{c2}$  is  $0.42 \pm 0.12$  where the major uncertainty is determined by the statistical error. A comparison of the HERA-B result with other experiments and theoretical predictions is shown in Fig.6.

## 5 Outlook

During the year 2002 we aim to collect about  $10^6$   $J/\psi$  in both channels. Running conditions will be more stable than in the year 2000, therefore, the systematic error in estimation of the total cross section or in the ratio of  $J/\psi$  for different wires will be significantly reduced. The statistics collected will be enough to provide a measurement of the nuclear dependence of charmonium hadro-production

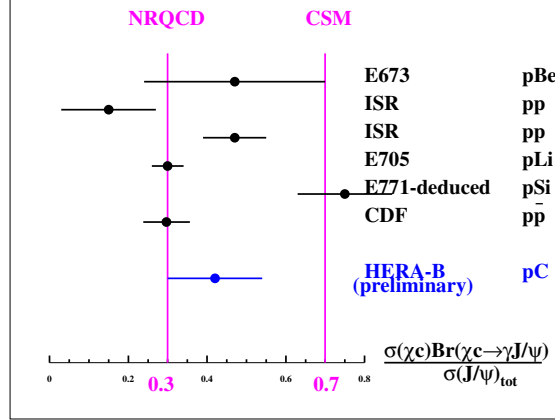


**Fig. 6.** Comparison of the HERA-B results with theoretical predictions and the results of other experiments. The value of E771 is deduced from the published cross sections of  $\sigma(J/\psi)_{\text{tot}}, \sigma(\chi_{c1}), \sigma(\chi_{c2})$ . The references could be found at [18].

as a function of  $p_T$  and  $x_F$ . It will be a first measurement in the negative  $x_F$  region while the positive  $x_F$  region can be used for comparison with E866 results.

The fraction of  $J/\psi$  produced via  $\chi_c$  channels is an important observable to distinguish between different models of  $J/\psi$  hadro-production and nuclear suppression. We expect to reconstruct of the order of  $10^5$   $\chi_c$  events which will be by far the largest sample of recorded  $\chi_c$  produced in proton-nucleus interactions.

### Acknowledgments

This work was supported in part by the Alexander von Humboldt Stiftung and Max Planck Society via the Max Planck research award.

### References

1. C. H. Chang: Nucl.Phys. **B172** 425 (1980) R. Baier, R. Rückl: Phys.Lett. **B102** 364 (1981) Z.Phys. **C19** 251 (1983)
2. P. Cho, A. Leibovich: Phys.Rev. **D53** 6203 (1996) M. Beneke, I. Z. Rothstein, Phys.Rev. **D54** 2005 (1996)
3. H. Fritzsch: Phys.Lett. **B67** 217 (1977)
4. J. J. Aubert et al.: Nucl.Phys. **B293** 740 (1987) M. Arneodo: Phys.Rep. **240** 301 (1994)
5. S. Gavin, J. Milana: Phys.Rev.Lett. **68** 1834 (1992) S. J. Brodsky, P. Hoyer: Phys.Lett. **B298** 165 (1993)
6. S. J. Brodsky et al.: Phys.Lett. **B93** 451 (1980); S. J. Brodsky et al.: Phys.Rev. **D23** 2745 (1981) S. J. Brodsky et al.: Phys.Lett. **B63** 1566 (1989)
7. D. Kharzeev, H. Satz: Phys.Lett. **B366** 316 (1996)
8. S.Gavin, R.Vogt: Nucl.Phys. **B345** 104 (1990)
9. D.Kharzeev, H.Satz: Z.Phys. **C60** 389 (1993)

10. R.Vogt: Phys.Rev. **C61** 035203 (2000)
11. R.Vogt: hep-ph/0107045 (2001)
12. HERA-*B* collaboration: DESY-PRC-95-01 (2001)
13. T. Alexopoulos et al.: Phys.Lett. **B374** 271 (1996)
14. M. H. Schub et al.: Phys.Rev. **D52** 1307 (1995)
15. M. J. Leitch et al.: Phys.Rev.Lett. **84** 3256 (2000)
16. D. M. Alde et al.: Phys.Rev.Lett. **66** 133 (1991) M. J. Leitch et al.: Phys.Rev. **D52** 4251 (1995)
17. A. Gribushin et al.: Phys.Rev. **D62** 012001 (2000) P. Hoyer, S. Peigné: Phys. Rev. **D57** 1864 (1998)
18. A. G. Clark et al.: Nucl.Phys. **B142** 29 (1978) D. A. Bauer et al.: Phys.Rev.Lett. **54** 753 (1985) L. Antoniazzi et al.: Phys.Rev.Lett. **70** 383 (1993) T. Alexopoulos et al.: Phys.Rev. **D62** 032006 (2000) F. Abe et al.: Phys.Rev.Lett. **79** 578 (1997)

# Finite Chern-Simons Matrix Model – Algebraic Approach

Larisa Jonke\* and Stjepan Meljanac

Theoretical Physics Division, Rudjer Bošković Institute, P.O. Box 180, HR-10002  
Zagreb, Croatia

**Abstract.** We analyze the algebra of observables and the physical Fock space of the finite Chern-Simons matrix model. We observe that the minimal algebra of observables acting on that Fock space is identical to that of the Calogero model. Our main result is the identification of the states in the  $l$ -th tower of the Chern-Simons matrix model Fock space and the states of the Calogero model with the interaction parameter  $\nu = l + 1$ .

## 1 Introduction

It is well known that the canonical quantization of the system of particles in a strong magnetic field gives a natural realization of noncommutative space. A nice discussion of that physical situation is given by R. Jackiw in this proceedings. One can speculate whether it is possible to describe a real physical system – Quantum Hall fluid – using quantum field theory on noncommutative plane. It was conjectured [1] that the Laughlin state of electrons at a filling fraction<sup>1</sup>  $1/k$  was described by the noncommutative version of the  $U(1)$  Chern-Simons theory at level  $k$ . The fields in that theory were infinite matrices corresponding to an infinite number of electrons on infinite plane. Later, Polychronakos [2] proposed a regularized version of the same model that could describe a finite number of electrons localized on a plane. The complete minimal basis of exact wavefunctions for the theory at an arbitrary level  $k$  and rank  $N$  was given in [3]. Using the properties of the energy eigenvalues of the Calogero model [4], an orthogonal basis for the Chern-Simons (CS) matrix model was identified [5].

The relation between the Calogero model and Quantum Hall (QH) physics was investigated using the algebraic approach [6,7] and the collective-field theory [8]. In [6] it was conjectured and then proved in [7] that one could map anyons in the lowest Landau level into the Calogero model, using the complex representation of the  $S_N$ -extended Heisenberg algebra underlying the Calogero model. On the other hand, it was shown in [8] that the correlation functions of the QH edge state and the Calogero model were related for the integer interaction parameter  $\nu$ . Also, the relation between the Calogero model and the matrix model was established [9]. Finally, an interesting link between noncommutative CS theory and QH fluid was provided using branes in massive Type IIA string

---

\* talk given by L. Jonke

<sup>1</sup> Actually, it was shown by Polychronakos that owing to the quantum effects the corresponding filling fraction is  $1/(k + 1)$ .

theory [10]. Taking into consideration all these relations between the Calogero model, the matrix model and QH physics, one hopes that this intricate network of connections between the apparently different physical systems will provide useful insight into common underlying structure.

## 2 Calogero Model

First, we give a short overview of the Calogero model. The Hamiltonian of the (rational) Calogero model describes  $N$  identical particles (bosons) interacting through an inverse square interaction subjected to a common confining harmonic force:

$$H = -\frac{\hbar^2}{2m} \sum_{i=1}^N \frac{\partial^2}{\partial x_i^2} + \frac{m\omega^2}{2} \sum_{i=1}^N x_i^2 + \frac{\nu(\nu-1)\hbar^2}{2m} \sum_{i \neq j}^N \frac{1}{(x_i - x_j)^2}. \quad (1)$$

After performing a similarity transformation on the Hamiltonian (1), we obtain the reduced Hamiltonian acting on the space of symmetric functions:

$$H' = \prod_{i < j}^N |x_i - x_j|^\nu H \prod_{i < j}^N |x_i - x_j|^{-\nu} = \sum_{i=1}^N a_i^\dagger a_i + E_0, \quad (2)$$

where the ground-state energy is  $E_0 = \omega N[1 + (N-1)\nu]/2$ . Here, we have introduced the creation and annihilation operators

$$\begin{aligned} a_i^\dagger &= \frac{1}{\sqrt{2}} \left( -\partial_i - \nu \sum_{j, j \neq i}^N \frac{1}{x_i - x_j} (1 - K_{ij}) + \omega x_i \right), \\ a_i &= \frac{1}{\sqrt{2}} \left( \partial_i + \nu \sum_{j, j \neq i}^N \frac{1}{x_i - x_j} (1 - K_{ij}) + \omega x_i \right), \end{aligned} \quad (3)$$

satisfying the following commutation relations

$$[a_i, a_j] = [a_i^\dagger, a_j^\dagger] = 0, \quad [a_i, a_j^\dagger] = \left( 1 + \nu \sum_{k=1}^N K_{ik} \right) \delta_{ij} - \nu K_{ij}. \quad (4)$$

The elementary generators  $K_{ij}$  of the symmetry group  $S_N$  exchange labels  $i$  and  $j$ . The Fock space representation is defined by  $a_i|0\rangle = 0$  and  $K_{ij}|0\rangle = |0\rangle$ . The physical Fock space is defined by  $S_N$ -symmetric states  $F_{\text{symm}}^{\text{Cal}} = \{\prod_{n_k} B_k^{\dagger n_k} |0\rangle\}$ , where  $B_k = \sum_i a_i^k$  are collective,  $S_N$ -symmetric operators. Then one can write

$$H' \prod_{n_k} B_k^{\dagger n_k} |0\rangle_\nu = [E_0 + \omega \sum_{k=1}^N k n_k] \prod_{n_k} B_k^{\dagger n_k} |0\rangle_\nu. \quad (5)$$

The  $S_N$ -symmetric observables  $B_n^\dagger$  creating the symmetric Fock space satisfy the following commutation relations:

$$\begin{aligned} [B_m, B_n] &= [B_m^\dagger, B_n^\dagger] = 0, \\ [B_m, B_n^\dagger] &= n \sum_{r=0}^{m-1} \sum_{i=1}^N a_i^r a_i^{\dagger n-1} a_i^{m-r-1} = m \sum_{s=0}^{n-1} \sum_{i=1}^N a_i^{\dagger s} a_i^{m-1} a_i^{n-s-1}. \end{aligned} \quad (6)$$

Including the observables of the type  $B_{m,n} = \sum a_i^{\dagger m} a_i^n$ ,  $m+n \leq N$  into consideration leads to the closed polynomial Lie algebra  $\mathcal{B}_N^{\text{Cal}}$  described in [11].

The the observables  $B_n$  satisfy the following algebraic relation:

$$[B_{i_1}, [B_{i_2}, [\dots, [B_{i_n}, B_n^\dagger] \dots]] = n! \prod_{\alpha=1}^n i_\alpha B_{I-n}, \quad (7)$$

where  $I = \sum_{\alpha=1}^n i_\alpha$  and  $i_1, \dots, i_n, n = 1, 2, \dots, N$ . The representation of algebra (19) in  $F_{\text{sym}}(\nu)$  is completely characterized by the minimal set of the generalized vacuum conditions:

$$\begin{aligned} B_2 B_2^\dagger |0\rangle_\nu &= 2N(N\nu + 1 - \nu) |0\rangle_\nu, \\ B_3 B_3^\dagger |0\rangle_\nu &= 3N[2(\nu - 1)^2 + \nu - 3N\nu(\nu - 1) + N^2\nu^2] |0\rangle_\nu = y |0\rangle_\nu, \\ B_3 B_3^{\dagger 2} |0\rangle_\nu &= 54\{\nu B_1^\dagger B_2^\dagger + [N + (N - 2)(\nu - 1) + y/27] B_3^\dagger\} |0\rangle_\nu. \end{aligned} \quad (8)$$

One can show that all other generalized vacuum conditions can be calculated using the algebra (19) and relations (8). The action on  $B_n$  on any state in the  $S_N$ -symmetric Fock space, and all matrix elements of the form  ${}_\nu \langle 0 | (\prod B_i^{n_i}) (\prod B_j^{\dagger n_j}) | 0 \rangle_\nu$  are uniquely determined by (19) and (8).

### 3 CS Matrix Model

#### 3.1 Introduction – The Physical Fock Space

Let us start from the action proposed in [2]:

$$S = \int dt \frac{B}{2} \text{Tr} \left\{ \varepsilon_{ab} \left( \dot{X}_a + i [A_0, X_a] \right) X_b + 2\theta A_0 - \omega X_a^2 \right\} + \Psi^\dagger \left( i\dot{\Psi} - A_0 \Psi \right). \quad (9)$$

Here,  $A_0$  and  $X_a$ ,  $a = 1, 2$ , are  $N \times N$  hermitian matrices and  $\Psi$  is a complex  $N$ -vector. The eigenvalues of the matrices  $X_a$  represent the coordinates of electrons,  $A_0$  is a gauge field, and  $\Psi$  acts like a boundary field. We choose the gauge  $A_0 = 0$  and impose the equation of motion for  $A_0$  as a constraint:

$$-iB [X_1, X_2] + \Psi \Psi^\dagger = B\theta. \quad (10)$$

The trace part of (10) gives

$$\Psi^\dagger \Psi = NB\theta. \quad (11)$$

Notice that the commutators have so far been classical matrix commutators. After quantization, the matrix elements of  $X_a$  and the components of  $\Psi$  become operators satisfying the following commutation relations:

$$\begin{aligned} [\Psi_i, \Psi_j^\dagger] &= \delta_{ij}, \\ [(X_1)_{ij}, (X_2)_{kl}] &= \frac{i}{B} \delta_{il} \delta_{jk}. \end{aligned} \quad (12)$$

It is convenient to introduce the operator  $A = \sqrt{\frac{B}{2}}(X_1 + iX_2)$  and its hermitian conjugate  $A^\dagger$  obeying the following commutation relations:

$$[A_{ij}, A_{kl}^\dagger] = \delta_{il} \delta_{jk}, \quad [A_{ij}, A_{kl}] = [A_{ij}^\dagger, A_{kl}^\dagger] = 0. \quad (13)$$

Then, one can write the Hamiltonian of the model at hand as

$$H = \omega \left( \frac{N^2}{2} + \text{Tr}(A^\dagger A) \right) = \omega \left( \frac{N^2}{2} + \mathcal{N}_A \right), \quad (14)$$

$\mathcal{N}_A$  being the total number operator associated with  $A$ 's. Upon quantization, the constraints (10) become the generators of unitary transformations of both  $X_a$  and  $\Psi$ . The trace part (11) demands that (the l.h.s. being the number operator for  $\Psi$ 's)  $B\theta \equiv l$  be quantized to an integer. The traceless part of the constraint (10) demands that the wavefunction be invariant under  $SU(N)$  transformations, under which  $A$  transforms in the adjoint<sup>2</sup> and  $\Psi$  in the fundamental representation.

Energy eigenstates will be  $SU(N)$  singlets; generally, some linear combinations of terms with at least  $lN(N-1)/2$   $A^\dagger$  operators and  $Nl$   $\Psi^\dagger$  fields. Explicit expressions for the wavefunctions were written in [3]:

$$|\Phi\rangle = \prod_{j=1}^N (\text{Tr} A^{\dagger j})^{c_j} C^{\dagger l} |0\rangle, \quad (15)$$

where

$$C^\dagger \equiv \varepsilon^{i_1 \dots i_N} \Psi_{i_1}^\dagger (\Psi^\dagger A^\dagger)_{i_2} \dots (\Psi^\dagger A^{\dagger N-1})_{i_N}, \quad (16)$$

and  $A_{ij}|0\rangle = \Psi_i|0\rangle = 0$ .

The system contains  $N^2 + N$  oscillators coupled by  $N^2 - 1$  constraint equations in the traceless part of (10). Effectively, we can describe the system with  $N + 1$  independent oscillators. Therefore, the physical Fock space that consists

<sup>2</sup> Note that as  $A$  transforms in the reducible representation  $(N^2 - 1) + 1$ , with the singlet  $B_1 \equiv \text{Tr} A$ , one can introduce a pure adjoint representation as  $\bar{A}_{ij} = A_{ij} - \delta_{ij} B_1/N$ . This slightly modifies the commutator (13), and completely decouples  $B_1$  from the Fock space. Physically, this correspond to the separation of the centre-of-mass coordinate as it has been done for the Calogero model in [11]. For the sake of simplicity, this will not be done here.



of all  $SU(N)$ -invariant states can be spanned by  $N + 1$  algebraically independent operators:  $B_n^\dagger \equiv \text{Tr} A^{\dagger n}$  with  $n = 1, 2, \dots, N$ , and  $C^\dagger$ . The operators  $B_k^\dagger$  for  $k > N$  can be expressed as a homogeneous polynomial of total order  $k$  in  $\{B_1^\dagger, \dots, B_N^\dagger\}$ , with constant coefficients which are common to all operators  $A^\dagger$  [14]. Since

$$\text{Tr} A^k C^{\dagger l} |0\rangle \equiv B_k C^{\dagger l} |0\rangle = 0, \quad \forall k, \forall l, \quad (17)$$

the state  $C^{\dagger l} |0\rangle \equiv |0, l\rangle$  can be interpreted as a ground state – vacuum with respect to all operators  $B_k$ . Note that the vacuum is not normalized to one, i.e.,  $\langle 0, l | 0, l \rangle \neq 1$ . The whole physical Fock space can be decomposed into towers (modules) built on the ground states with different  $l$ :

$$F_{\text{phys}}^{\text{CS}} = \sum_{l=0}^{\infty} F_{\text{phys}}^{\text{CS}}(l) = \sum_{l=0}^{\infty} \left\{ \prod B_k^{\dagger n_k} |0, l\rangle \right\}.$$

Clearly, the states from different towers are mutually orthogonal.

The action of the Hamiltonian (14) on the states in the physical Fock space is

$$H \prod B_k^{\dagger n_k} |0, l\rangle = \omega \left[ \frac{N^2}{2} + \sum_k k n_k + l \binom{N}{2} \right] \prod B_k^{\dagger n_k} |0, l\rangle, \quad (18)$$

and the ground-state energy is  $E_0(l) = \omega[N^2 + lN(N-1)]/2$ . Comparing this result with the known one for the Calogero model (see (18)) we see that the spectra of the two models are identical provided  $\nu = l + 1$ . This has already been noticed in Refs.[9,5]. However, from the identification of spectra it only follows

$$\left( \prod B_i^{\dagger n_i} \right)^{\mathcal{N}} |0, l\rangle = \sum \left( \prod B_k^{\dagger n_k} \right)^{\mathcal{N}} |0\rangle_{l+1},$$

where the r.h.s. of this relation is, in general, a sum of different terms of total order  $\mathcal{N}$  in the observables of the Calogero model. We use the same letter to denote observables in both models. In CS matrix model,  $B_n = \text{Tr} A^n$  and in the Calogero model,  $B_n = \sum_i a_i^n$ , but from the context it should be clear what  $B_n$  represent. The vacuum in the CS matrix model is denoted as  $|0, l\rangle$  and the vacuum in the Calogero model is denoted as  $|0\rangle_\nu$ .

### 3.2 Algebraic Structure of the CS Matrix Model

We restrict ourselves to the minimal algebra including only observables of the type  $B_n$  and  $B_n^\dagger$ , defined with the following relations (including corresponding hermitian conjugate relations):

$$[B_{i_1}, [B_{i_2}, [\dots, [B_{i_n}, B_n^\dagger] \dots]] = n! \prod_{\alpha=1}^n i_\alpha B_{I-n}, \quad (19)$$

where  $I = \sum_{\alpha=1}^n i_\alpha$  and  $i_1, \dots, i_n, n = 1, 2, \dots, N$ . These relations can be viewed as a generalization of triple operator algebras defining para-Bose and para-Fermi

statistics [15]. The identical successive commutators relations (19) holds for the observables acting on the  $S_N$ -symmetric Fock space of the Calogero model [11]. The action of  $B_k$  on any state in the Fock space is of the form:

$$B_k \prod_i B_i^{\dagger n_i} |0, l\rangle = \sum \left( \prod_j B_j^{\dagger n_j} \right)^{\mathcal{N}-k} |0, l\rangle, \quad \mathcal{N} = \sum_i n_i \geq k, \quad (20)$$

In order to calculate the precise form of the r.h.s. of (9) we apply the hermitian conjugate relation (19) on the l.h.s. of (9) shifting the operator  $B_k$  to the right, at least for one place. We repeat this iteratively as long as the number of  $B^{\dagger}$ 's on the right from  $B_k$  is larger or equal to the index  $k$ . For  $k > \sum n_i$ , one directly calculates a finite set of relations from (13), the so-called generalized vacuum conditions. We show that the *minimal* set of generalized vacuum conditions needed to completely define the representation of the algebra (19) on the Fock space is

$$\begin{aligned} B_2 B_2^{\dagger} |0, l\rangle &= 2N(N + lN - l) |0, l\rangle, \\ B_3 B_3^{\dagger} |0, l\rangle &= 3N[N^2 + 1 + l(N - 1)(2N - 1) + l^2(N - 1)(N - 2)] |0, l\rangle = y |0, l\rangle, \\ B_3 B_3^{\dagger 2} |0, l\rangle &= 54\{(l + 1)B_1^{\dagger} B_2^{\dagger} + [N + (N - 2)l + y/27]B_3^{\dagger}\} |0, l\rangle. \end{aligned} \quad (21)$$

Namely, the operators  $B_2$ ,  $B_3$  and hermitian conjugates play a distinguished role in the algebra, since all other operators  $B_n$ ,  $B_n^{\dagger}$  for  $n \geq 4$  can be expressed as successive commutators (19), using only  $B_2$ ,  $B_3$  and their hermitian conjugates. Therefore, one can derive all other generalized vacuum conditions using (19) and (21).

The relations (19) and the generalized vacuum conditions (21) represent the minimal algebraic structure defining the complete physical Fock space representation. Using these relations one can calculate the action of  $B_n$  on any state in the physical Fock space, and calculate all matrix elements (scalar product) of the form  $\langle 0, l | (\prod_i B_i^{n_i}) (\prod_j B_j^{\dagger n_j}) |0, l\rangle$ , up to the norm of the vacuum.

## 4 Results

Our main observation is that the generalized vacuum conditions for the CS matrix model (21) and for the Calogero model (8) coincide for  $\nu = l + 1$ . This follows entirely from the common algebraic structure (19) and the structure of the vacuum conditions. As we have already said, the algebraic relations (19) and the generalized vacuum conditions uniquely determine the action of observables on the Fock space, so we conclude that

$$B_k (\prod_i B_i^{\dagger n_i}) |0, l\rangle = B_k (\prod_i B_i^{\dagger n_i}) |0\rangle_{l+1}, \quad (22)$$

and that all scalar products in  $F_{\text{phys}}^{\text{CS}}$  can be identified with the corresponding matrix elements in the Fock space of the Calogero model:

$$\langle 0, l | (\prod_i B_i^{n_i}) (\prod_j B_j^{\dagger n_j}) |0, l\rangle = {}_{l+1} \langle 0 | (\prod_i B_i^{n_i}) (\prod_j B_j^{\dagger n_j}) |0\rangle_{l+1}. \quad (23)$$

Note that the vacuum is unique in both models, so we set  $|0, l\rangle = |0\rangle_{l+1}$ , up to the norm. Now we can identify all states in  $F_{\text{phys}}^{\text{CS}}(l)$  with the corresponding states in  $F_{\text{symm}}^{\text{Cal}}(l+1)$  as

$$(\prod B_k^{\dagger n_k})|0, l\rangle = (\prod B_k^{\dagger n_k})|0\rangle_{l+1}. \quad (24)$$

One can prove these results in different ways. For example, we can restrict ourselves to the subspace of the Fock space generated by  $\{B_1^{\dagger}, B_2^{\dagger}, B_3^{\dagger}\}$  and prove the relations (22), (23) and (24) in this subspace, by straightforward calculation and by induction. Then, using the algebraic relation (19) we simply generate the rest of the needed results on the full (physical) Fock space. The other way to obtain our result is to notice that from the equivalence of spectra it follows  $\nu = l + 1$ . Also, from the fact that the algebraic relations (19) hold for both models we know that the states in the Calogero model and the CS matrix model are identical, but we have no information on the relation between  $l$  and  $\nu$ . The combination of these two results leads again to the identification of the states in  $F_{\text{phys}}^{\text{CS}}(l)$  and  $F_{\text{symm}}^{\text{Cal}}(l+1)$ , (24). We point out that our algebraic proof of (22), (23) and (24) relies only on the identical algebra (19) and the identical minimal set of generalized vacuum conditions for both models, and not on the structure of their Hamiltonians.

In conclusion, we have discussed the Fock-space picture in detail and elucidated the  $A$ -representation of the CS matrix model. We have precisely formulated the connection between the states in the Fock spaces of the CS matrix and the Calogero model. We stress that although the models have similar Fock spaces and a common minimal algebraic structure, the complete algebraic structures are quite different. [18].

### Acknowledgment

This work was supported by the Ministry of Science and Technology of the Republic of Croatia under contract No. 00980103.

### References

1. L. Susskind, *The Quantum Hall Fluid and Non-Commutative Chern Simons Theory*, hep-th/0101029.
2. A. P. Polychronakos, J. High Energy Phys. **04** (2001) 011.
3. S. Hellerman and M. Van Raamsdonk, J. High Energy Phys. **10** (2001) 039.
4. F. Calogero, J. Math. Phys. **10** (1971) 2191, 2197; J. Math. Phys. **12** (1971) 419.
5. D. Karabali and B. Sakita, Phys. Rev. D **65** (2002) 075304.
6. T. H. Hansson, J. M. Leinaas and J. Myrheim, Nucl. Phys. B **384** (1992) 559.
7. L. Brink, T. H. Hansson, S. Konstein and M. A. Vasiliev, Nucl. Phys. B **401** (1993) 591.
8. S. Iso and S. J. Rey, Phys. Lett. B **352** (1995) 111.
9. A. P. Polychronakos, Phys. Lett. B **264** (1991) 362.

10. O. Bergman, J. Brodie and Y. Okawa, *The Stringy Quantum Hall Fluid*, hep-th/0107178.
11. L. Jonke and S. Meljanac, Phys. Lett. B **511** (2001) 276.
12. L. Jonke and S. Meljanac, Phys. Lett. B **526** (2002) 149.
13. S. B. Isakov and J. M. Leinaas, Nucl. Phys. B **463** (1996) 194; J. M. Leinaas, *Generalized statistics and the algebra of observables*, hep-th/9611167; S. B. Isakov et. al., Phys. Lett. B **430** (1998) 151.
14. A. J. Macfarlane and H. Pfeiffer, J. Math. Phys. **41** (2000) 3192; L. Jonke and S. Meljanac, *The algebra of the observables in the Calogero model and in the Chern-Simons matrix model*, Phys. Rev. B (2002) to appear.
15. Y. Ohnuki and S. Kamefuchi, *Quantum Field Theory and Parastatistics*, Tokyo University Press 1982.
16. A. P. Polychronakos, Mod. Phys. Lett. A **11** (1996) 1273.
17. A. P. Polychronakos, J. High Energy Phys. **06** (2001) 070.
18. L. Jonke, S. Meljanac, J. High Energy Phys. **01** (2002) 008.

# Expectations for Charged Higgs in CMS

Ritva Kinnunen

Helsinki Institute of Physics, Helsinki, Finland

**Abstract.** Expectations for the production of the heavy charged Higgs in the CMS experiment are discussed in the associated production channel  $gb \rightarrow tH^\pm$  with  $H^\pm \rightarrow \tau\nu$  and  $H^\pm \rightarrow tb$  decay and in the  $s$ -channel process  $q\bar{q}' \rightarrow H^\pm$  with the  $H^\pm \rightarrow \tau\nu$  decay. The  $pp \rightarrow tH^\pm + X$ ,  $H^\pm \rightarrow \tau\nu$  channel with fully hadronic final state is found to be the most promising for the charged Higgs search at LHC. The expected discovery ranges are evaluated for CMS for the integrated luminosity of  $30fb^{-1}$ .

## 1 Introduction

While a variety of decay channels and final states have been shown to serve for the discovery of the neutral MSSM Higgs bosons at LHC [1] only few decay channels, mainly  $H^\pm \rightarrow \tau\nu$  and  $H^\pm \rightarrow tb$ , seem to be useful for the search of the charged MSSM Higgs boson. However, the discovery of the charged Higgs is highly desirable in an early stage of LHC running as it provides the most straightforward way to disentangle between the SM and MSSM Higgs boson spectra. Here we discuss two SM decay modes and demonstrate that the charged Higgs can be found in a large part of the MSSM parameter space already with  $30fb^{-1}$  and a specially clean signature is expected in the the  $H^\pm \rightarrow \tau\nu$  decay channel from  $pp \rightarrow tH^\pm + X$  as has been proposed in ref. [2].

If charged Higgs is light,  $m_{H^\pm} < m_{top}$ , it can be produced in top decays through  $t \rightarrow H^\pm b$  in the  $t\bar{t}$  production. The expected discovery range using the  $H^\pm \rightarrow \tau\nu$  decay channel has been shown to be for  $m_A \lesssim 160$  GeV almost independent on  $\tan\beta$  [3]. The main production processes for a heavy Higgs,  $m_{H^\pm} > m_{top}$ , are the production in association with a top quark in  $gb \rightarrow tH^\pm$  and  $gg \rightarrow tbH^\pm$  processes and the  $s$ -channel production  $q\bar{q}' \rightarrow H^\pm$ . At low masses and large  $\tan\beta$ , before opening of the  $H^\pm \rightarrow tb$  decay mode,  $H^\pm$  decays almost exclusively to  $\tau\nu$ . Above the  $H^\pm \rightarrow tb$  threshold the branching ratio to  $\tau\nu$  decreases rapidly to about 10% at  $\tan\beta \sim 10$ , the  $H^\pm \rightarrow tb$  is at  $\sim 70\%$  level and the SUSY decay channels start to dominate with increasing Higgs mass especially at low  $\tan\beta$  values. The branching ratios at high  $\tan\beta$  are found to be insensitive to the amount of stop mixing and the sign of the  $\mu$  parameter.

The PYTHIA (version 6.1) [4] is used to generate the events for the associated production. The SUSY parameter spectrum used in LEP2 Higgs searches is assumed with  $M_{SUSY} = 1$  TeV,  $M_2 = -\mu = 200$  GeV,  $m_{\tilde{g}} = 800$  GeV and  $X_t = 0$  (no-mixing) or  $X_t = 2450$  GeV (maximal stop mixing) [5]. The polarized  $\tau$  decays are included using TAUOLA package [6]. The jets and the missing transverse

energy are reconstructed with the fast CMS detector response simulation package CMSJET [7]. For b-tagging the impact parameter method is used with tagging efficiencies from full simulation and reconstruction of the CMS tracker [8].

CMS experiment has developed an efficient hadronic  $\tau$  trigger, based on Level-1 calorimeter selection, Level-2 electromagnetic calorimeter isolation [4] and a Level-3 tracking (isolation) [5]. This trigger, combined with a multi-jet trigger, will allow an efficient triggering and control of the background rates even for the fully hadronic final states discussed here.

## 2 $pp \rightarrow tH^\pm + X, H^\pm \rightarrow \tau\nu$

The processes  $g\bar{b} \rightarrow \bar{t}H^\pm$  and  $gg \rightarrow \bar{t}bH^\pm$  contribute to the production in association with a top quark at LHC. The first process has larger cross section but the calculation of the cross section is more difficult due to the large uncertainty of the b-quark structure function in the proton. The production cross sections of ref. [11] are calculated eliminating the double counting between the two processes. Event generation in PYTHIA is performed through the process  $gb \rightarrow tH^\pm$  alone. The cross sections evaluated with the CTEQ5L structure functions for  $m_{H^\pm} = 200$  and 400 GeV at  $\tan\beta = 40$  are  $\sim 8$  pb and  $\sim 0.9$  pb, respectively. The corresponding cross sections from ref. [11] are  $\sim 4.2$  pb and  $\sim 0.9$  pb. For this work the Pythia cross sections are used although there is a significant disagreement relative to the theoretical calculations at low Higgs masses.

The main backgrounds are due to the  $t\bar{t}$  events with  $W_1 \rightarrow \tau\nu$ ,  $W_2 \rightarrow qq'$ ,  $W + jet$  events with  $W \rightarrow \tau\nu$  and  $Wt$  events with  $W_1 \rightarrow \tau\nu$ ,  $W_2 \rightarrow qq'$ . When purely hadronic events are selected, the reconstructed transverse mass  $m_T(\tau - jet, E_t^{miss})$  has an endpoint at  $m_W$  for the backgrounds, i.e. much below the endpoint for the signal. Since all these backgrounds contain the  $W \rightarrow \tau\nu$  decay they can be reduced efficiently thanks to the  $\tau$  polarization when appropriate  $\tau$  selection cuts are used. A detailed discussion of the polarization effects in  $H^\pm \rightarrow \tau\nu$  and  $W^\pm \rightarrow \tau\nu$  decay can be found in ref. [2].

The  $\tau^+$  from  $H^\pm \rightarrow \tau^+\nu$  is produced in a left-handed polarization state. In the simplest case of  $\tau^+ \rightarrow \pi^+\bar{\nu}$  decay the right-handed  $\bar{\nu}$  is preferentially emitted in the direction opposite to the  $\tau^+$  in the  $\tau$  rest frame to preserve the polarization. In the dominant  $t\bar{t}$  background the  $\tau^+$  from the  $W^+ \rightarrow \tau^+\nu$  decay is produced right-handed due to the vector nature of  $W$  forcing the  $\bar{\nu}$  from  $\tau^+ \rightarrow \pi^+ \overline{\text{neutrino}}$  to be emitted in the direction of the  $\tau^+$  in the  $\tau$  rest frame. Thus harder pions are expected from the  $H^\pm$  decays than from the  $W^\pm$  decays in the case of  $\tau$  decaying to one charged pion.

The  $\tau^\pm \rightarrow \pi^\pm\bar{\nu}$  decay represents a 12.5% fraction of the  $\tau$  decays. The one charged prong final states can also be produced through the  $\tau^\pm \rightarrow \rho^\pm\bar{\nu}$  and  $\tau^\pm \rightarrow a_1^\pm\bar{\nu}$  decays with branching ratios of 26% and 7.5%, respectively. In these decays harder pions are produced from the longitudinal vector meson components relative to the background while the situation is opposite for the transverse components. As a consequence the polarization effects are smeared for the  $\tau^\pm \rightarrow \rho^\pm\bar{\nu}$  and  $\tau^\pm \rightarrow a_1^\pm\bar{\nu}$  channels as compared to the  $\tau^+ \rightarrow \pi^+\bar{\nu}$  channel.

In order to suppress the backgrounds with real  $\tau$ 's more than 80% of the energy of the  $\tau$  jet candidate, reconstructed in the calorimeter in a cone of  $\Delta R < 0.4$ , is required to be carried by a single charged pion,  $r = p^\pi / E^{\tau jet} > 0.8$ . Figure 1a shows the variable  $r$  for the signal events with  $m_{H^\pm} = 200$  and 400 GeV and for the  $t\bar{t}$  events including all hadronic  $\tau$  decay modes. Efficiency of this  $\tau$  selection including the jet  $E_t$  threshold ( $E_t^{\tau-jet} > 100$  GeV) is  $\sim 8\%$  for  $m_{H^\pm} = 200$  GeV,  $\sim 20\%$  for  $m_{H^\pm} = 400$  GeV whilst it is only 0.3% for the  $t\bar{t}$  events.

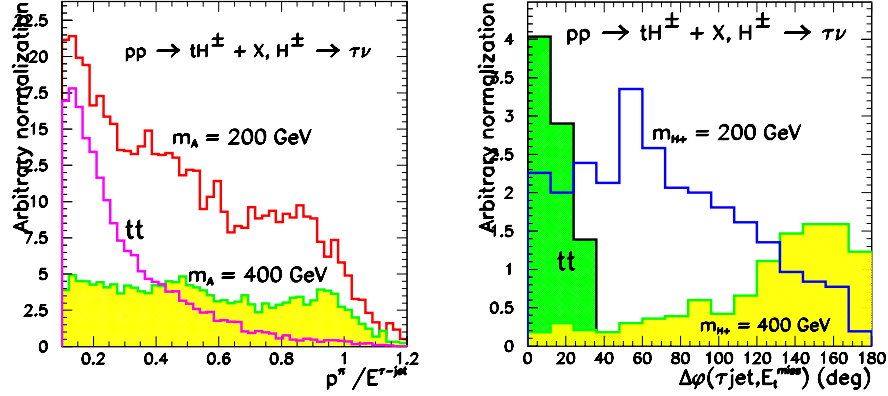
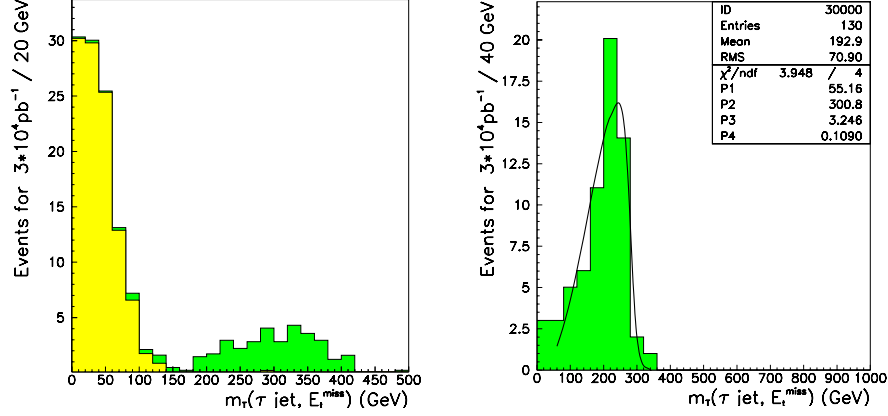


Fig. 1. a) Distribution of  $p^\pi / E^\tau$  with  $E_t^{\tau-jet} > 100$  GeV for  $gb \rightarrow tH^\pm, H^\pm \rightarrow \tau\nu$  with  $m_{H^\pm} = 200$  and 400 GeV and for the  $t\bar{t}$  events with  $W^\pm \rightarrow \tau\nu$ , b) Distribution of the azimuthal angle in the transverse plane between the  $\tau$ -jet and the  $E_t^{miss}$  vector with  $E_t^{\tau-jet}, E_t^{miss} > 100$  GeV for  $m_{H^\pm} = 200$  and 400 GeV and for the  $t\bar{t}$  events.

To suppress further the potentially large  $W + jet$  and  $QCD$  backgrounds the mass of the associated top quark is reconstructed from a tagged  $b$ -jet and two other remaining jets. The efficiency for tagging a  $b$ -jet in the signal events is  $\sim 58\%$  while the mistagging rate in the  $W + jet$  events is  $\sim 2\%$ . Further reduction of the  $t\bar{t}$  background is still possible using a veto an additional jet with  $E_t > 40$  GeV and  $|\eta| < 2.5$  or (and) a veto on the second top present in the  $t\bar{t}$  events. For the reconstruction of the second top from the  $\tau$  jet, missing energy and one of the remaining jets the longitudinal component of the missing energy is first resolved from the  $W$  mass constraint selecting the smaller of the two solutions for  $p_L^\nu$ . Distribution of the relative azimuthal angle in the transverse plane between the  $\tau$  jet and the  $E_t^{miss}$  vector,  $\Delta\phi(\tau - jet, E_t^{miss})$ , is shown in Fig. 1b for the signal with  $m_{H^\pm} = 400$  and 200 GeV and for the  $t\bar{t}$  events. The mass difference between  $W$  and  $H^\pm$ , and the hard  $E_t$  cuts ( $E_t^{\tau-jet}, E_t^{miss} > 100$  GeV), are reflected in the  $\Delta\phi$  distribution which for the background events (with  $W \rightarrow \tau\nu$ ) is limited to small opening angles. A cut in the  $\Delta\phi$  angle ( $\Delta\phi \gtrsim 60^\circ$ ) practically eliminates the low mass background.

The distribution of the transverse mass from the  $\tau$  jet and the missing transverse energy  $m_T^2 = 2 E_t^{\tau-jet} E_t^{miss} (1 - \cos\phi(\tau - jet, E_t^{miss}))$  superimposed on the total background after the  $\tau$  selection cuts, top mass reconstruction,  $b$ -



**Fig. 2.** a) Transverse mass reconstructed from  $\tau$  jet and  $E_t^{miss}$  for  $gb \rightarrow tH^\pm$ ,  $H^\pm \rightarrow \tau\nu$  with  $m_{H^\pm}=400$  GeV and  $\tan\beta=40$  superimposed on the total background for  $30\text{ fb}^{-1}$ . b) the same as in a) but with the cut  $\Delta\phi(\tau - \text{jet}, E_t^{miss}) > 60^\circ$  and for  $m_{H^\pm}=300$  GeV,  $\tan\beta=25$  including the a fit with the function of (1).

tagging and the jet and second top veto cuts is shown in Fig. 2a for  $m_{H^\pm} = 400$  GeV and  $\tan\beta = 40$ . The signal component is well separated at high  $m_T$  values from the bulk of the background events. The sharp endpoint of the  $m_T$  spectrum allows to determine the Higgs mass in this channel. For this the  $m_T$  distribution is fitted with the following 4-parameter function:

$$m_T = F_0 \times \int_0^1 \frac{D(z)}{\sqrt{(m_{fit}^2 - m_T^2)}} dz . \quad (1)$$

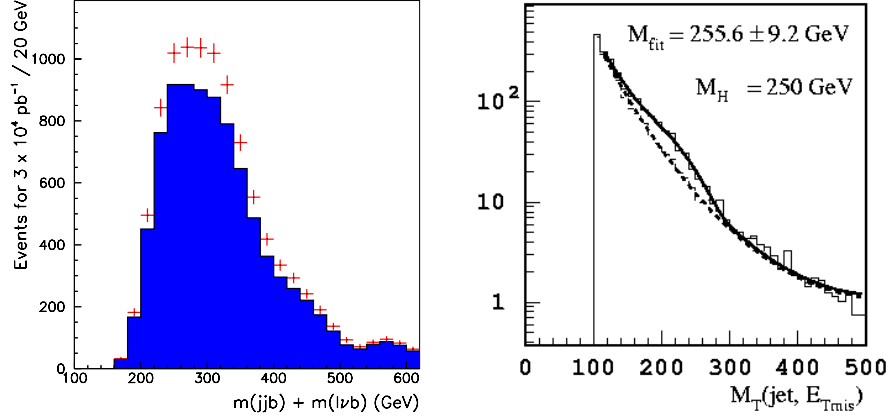
where  $D(z)$  is the  $\tau \rightarrow \text{jet}$  fragmentation function of the form  $D(z) \sim z^{1.02} \times (1-z)^{0.28}$ .

Figure 2b shows an example of the fit for  $m_{H^\pm} = 300$  GeV with  $\tan\beta = 25$ , which is a point near the limit of the expected discovery range. The statistical precision of the mass determination is better than 2 % for  $\tan\beta \gtrsim 15$  for this Higgs mass. The main source of the systematic uncertainty is the  $E_t^{miss}$  measurement presently under investigation in CMS.

### 3 $pp \rightarrow tH^\pm + X$ , $H^\pm \rightarrow tb$

The  $H^\pm \rightarrow tb$  decay channel profits from a large branching ratio for all  $\tan\beta$  values ( $\sim 70\%$ ) in the large Higgs mass range but extraction of the Higgs boson signal is difficult due to the background from  $t\bar{t}$  production in association of jets ( $t\bar{t}b\bar{b}$ ,  $t\bar{t}c\bar{c}$ ,  $t\bar{t}jj$ ...). This channels relies heavily on an efficient b-tagging capability as at least 3 b-jets has to be detected to identify the event and to reconstruct the Higgs boson mass. The events are required to contain one isolated lepton from the decay of one of the top quarks, 3 tagged b-jets with  $E_t > 30$  GeV and two non-b-jets with  $E_t > 20$  GeV from  $W \rightarrow qq'$  decay. The leptonic and hadronic





**Fig. 3.** a) Reconstructed Higgs mass for  $gb \rightarrow tH^\pm$ ,  $H^\pm \rightarrow tb$  with  $m_{H^\pm} = 250$  GeV and  $\tan\beta = 30$  superimposed on the total background for  $30\text{ fb}^{-1}$ , b) the same as in a) but for  $q\bar{q}' \rightarrow H^\pm$ ,  $H^\pm \rightarrow \tau\nu$  with  $m_{H^\pm} = 250$  GeV and  $\tan\beta = 50$ .

top are reconstructed. For the reconstruction of the leptonic top the  $W$  mass constraint is used.

Figure 3a shows the signal for  $m_{H^\pm} = 250$  GeV and  $\tan\beta = 30$  superimposed on the total background for  $30\text{ fb}^{-1}$ . The main background component is found to be the  $t\bar{t}$  events with two mistagged light quark or gluon jets. The signal distribution contains contribution from both the leptonic and the hadronic top. This combinatorics may be reduced by selecting the correct top quark by exploiting the somewhat harder  $p_t$  distribution of the top from  $H^\pm \rightarrow tb$  decay. Due to the hard  $E_t$  cuts applied the background is forced to peak in the signal region. Significantly softer  $E_t$  thresholds could improve the background shape but may not be possible due to additional backgrounds entering and due to the triggering requirements.

#### 4 $q\bar{q}' \rightarrow H^\pm$ , $H^\pm \rightarrow \tau\nu$

The cross section for the  $s$ -channel production of the charged Higgs at LHC from  $q\bar{q}' \rightarrow H^\pm$  is comparable to that for the associated production but the signal is embedded in an overwhelming direct  $W$  production. However, it is shown in ref. [12] that extraction of the Higgs boson signal is still possible in the  $H^\pm \rightarrow \tau\nu$  decay channel at high  $\tan\beta$  values. The cross section is calculated to the next to leading order including the  $2 \rightarrow 2$  and  $2 \rightarrow 3$  processes [12]. The cross section has strong dependence on the light quark mass through the  $m_u^2 \cot^2\beta + m_d^2 \tan^2\beta$  term. Assuming the Particle Data Group values [13] for the light quark masses the cross sections of  $\sim 5$  pb and  $\sim 1$  pb are obtained for  $\tan\beta = 50$  and  $m_{H^\pm} = 200$  and 400 GeV, respectively. Event generation is performed with the TopRex Monte-Carlo generator [14] using PYTHIA [4] for the fragmentation and TAUOLA [6] for the polarized  $\tau$  decays.

Main background is the direct  $W$  production with  $W \rightarrow \tau\nu$  decay. It can be efficiently reduced exploiting the  $\tau$  polarization requiring 80% of the  $\tau$ -jet energy to be carried by a single charged pion but remains still high under the signal component. Event selection for this channel is similar to the associated channel with  $H^\pm \rightarrow \tau\nu$  decay except somewhat softer  $E_t$  thresholds have to be applied for the  $\tau$  jet and for  $E_t^{miss}$ . Figure 3b shows an example of the reconstructed Higgs mass superimposed on the total background for  $m_{H^\pm} = 250$  GeV and  $\tan\beta = 50$  for an integrated luminosity of  $30 \text{ fb}^{-1}$ . The expected number of signal events is 344 with a total background of 1756 events.

In order to determine the Higgs mass in this channel the transverse mass distribution,  $m_T(\tau - \text{jet}, E_t^{miss})$ , is fitted with the 4 parameter function shown in (1). In this case the form  $\sim z^{6.5} \times (1.22 - z)^{3.5}$  is taken for the function  $D(z)$ . For the background the exponential 4-parameter function  $m_T = \exp(a_0 + a_1 \times m_T + a_2 \times m_T^d)$  is used.

The fits to the  $m_T$  distributions of a Higgs boson with  $m_{H^\pm} = 200$  GeV yield for the expected statistical error of the Higgs mass measurement  $\lesssim 6\%$  for  $\tan\beta > 15$ . The error expected for  $\tan\beta$  measurement is 5 - 65% for  $15 < \tan\beta < 50$ .

## 5 Conclusions

Figure 4 shows the expected  $5\sigma$ -discovery region for the MSSM Higgs bosons in the  $m_A, \tan\beta$  parameter plane for  $30 \text{ fb}^{-1}$  in CMS. The parameter space excluded by LEP in the maximal mixing scenario is also shown in the figure [15]. For the charged Higgs in  $pp \rightarrow tH^\pm + X$ ,  $H^\pm \rightarrow \tau\nu$  the discovery range is for  $\tan\beta \gtrsim 15$  around  $m_A=200$  GeV, for  $\tan\beta \gtrsim 20$  around  $m_A=400$  GeV and for  $\tan\beta \gtrsim 40$  around  $m_A=600$  GeV. The  $H^\pm \rightarrow tb$  decay channel and  $s$ -channel process with  $H^\pm \rightarrow \tau\nu$  have smaller reach in  $m_A$ ,  $m_A < 400$  GeV and  $m_A < 300$  GeV, respectively, with the lowest  $\tan\beta$  values about 20 for  $H^\pm \rightarrow tb$  and about 15 for the  $s$ -channel process around  $m_A=200$  GeV. The reach for the light charged Higgs in  $t\bar{t}$  events is for  $m_A \lesssim 160$  GeV.

For the  $H^\pm \rightarrow \tau\nu$  decay mode the  $\tau$  polarization, producing harder single pions from  $\tau$  decay when the  $\tau$  originates from  $H^\pm \rightarrow \tau\nu$  than in the case when the  $\tau$  is from the  $W^\pm \rightarrow \tau\nu$  can be used to reduce efficiently all the main backgrounds, by demanding that a single pion carries more than 80% of the  $\tau$  jet energy. With fully hadronic final states the transverse mass reconstructed from the  $\tau$ -jet and  $E_t^{miss}$  has a quasi-Jacobian peak shape with an endpoint at  $m_T \sim m_{H^\pm}$  for the signal, and at  $m_T \sim m_W$  for the backgrounds. For  $pp \rightarrow tH^\pm + X$ ,  $H^\pm \rightarrow \tau\nu$  an almost background-free signal is expected limited by the signal production rate. The source of possible background are the large accidental measurement errors in  $E_t^{miss}$  diluting the background  $m_T$  distribution towards large masses. B-tagging reduces the potentially large  $W + \text{jet}$  and QCD backgrounds and is a key element for the  $pp \rightarrow tH^\pm + X$ ,  $H^\pm \rightarrow tb$  channel where at least 3  $b$ -jets have to be detected. Search for charged Higgs is a challenge for the LHC experiments requiring excellent tracking and calorimetry.

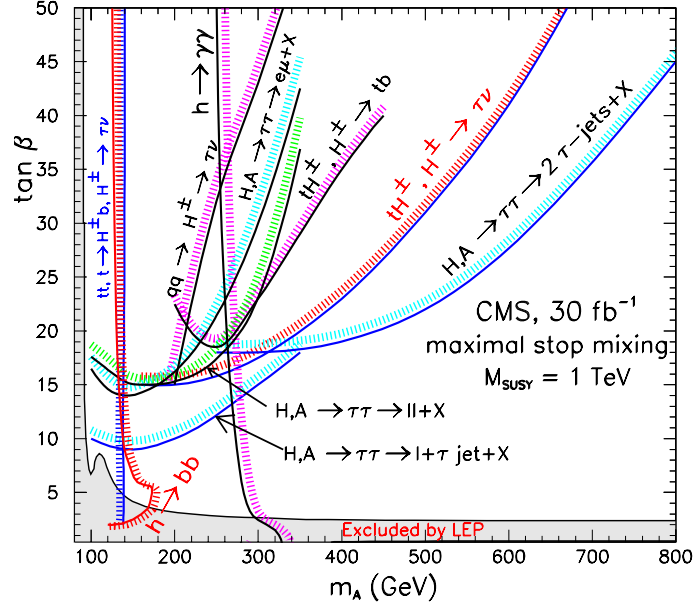


**Fig. 4.** Expected  $5\sigma$ -discovery limits for the MSSM Higgs bosons in CMS for  $30fb^{-1}$  assuming maximal stop mixing.

### Acknowledgements

I would like to thank Daniel Denegri, D.P. Roy and Sergei Slabospitsky for helpful discussions and S.S. for reading the manuscript.

### References

1. D. Denegri, V. Drollinger, R. Kinnunen, K. Lassila-Perini, S. Lehti, F. Moortgat, A. Nikitenko, S. Slabospitsky, N. Stepanov, Summary of the CMS Discovery Potential for the MSSM SUSY Higgses, CMS NOTE 2001/032, hep-ph/0112045.
2. D.P. Roy, The hadronic Tau decay signature of heavy charged Higgs boson at LHC, Phys. Lett. B459(1999) 607.
3. S. Banerjee and M. Maity, Search for the Charged Higgs in Top Decays in CMS, CMS NOTE 2000/039.
4. T. Sjostrand, Comp.Phys.Comm. 82 (1994) 74; CERN-TH.6488/92; CERN-TH.7112/93, S. Mrenna, SPYTHIA, A Supersymmetric Extension of PYTHIA5.7, ANL-HEP-PR-96-63.
5. M. Carena, S. Heynemeyer, C.E.M. Wagner and G. Weiglein, Successions for improved benchmark scenarion for Higgs-boson searches at LEP2, CERN-TH/99-374, DESY 99-186, hep-ph/9909435.
6. S. Jadach, Z. Was, R. Decker, M. Jezabek and J.H. Kuhn, CERN-TH-6793, 1992
7. S. Abdullin, A. Khanov and N. Stepanov, CMSJET, CMS TN/94-180.
8. CMS Collaboration, The tracker project, Technical Design Report, CERN/LHCC 98-6, CMS TDR 5, 26 February 1998.

9. S. Eno, W. Smith, S. Dasu, R. Kinnunen and A. Nikitenko, A Study of a First and Second Level Tau Trigger, CMS NOTE 2000/055.
10. D. Kotlinski, A. Nikitenko and R. Kinnunen, Study of a Level-3 Tau Trigger with the Pixel Detector, CMS NOTE 2001/017.
11. S. Moretti and D.P. Roy, Detecting heavy charged Higgs bosons at the LHC with triple b-tagging, hep-ph/9909435.
12. S. Slabospitsky, CMS NOTE 2002/010, hep-ph-0203094.
13. D.E. Groom et al., The European Physical Journal C15, 1 (2000).
14. S. Slabospitsky and L. Sonnenschein, CMS NOTE 2002/009, hep-ph-0201292.
15. The ALEPH, DELPHI, L3 and OPAL Collaborations, and the LEP Higgs Working Group, CERN-EP/2001-055 and hep-ex/0107030.

# Heavy Ion Physics in CMS

Olga Kodolova (for CMS collaboration)

Scobeltsyn Institute of Nuclear Physics Moscow State University, 119899, Moscow,  
Russia

**Abstract.** The possibility to measure dimuons from  $\Upsilon$  and  $J/\Psi$  families, hard jets and photons produced in ultra-relativistic heavy ion collisions at LHC energies have been investigated. The simulations were carried out for the CMS detector. A strong correlation between the transverse energy gathered in the calorimeters and event centrality is observed. The invariant mass spectrum for Pb-Pb events is presented and the signal to background ratios for  $\Upsilon$  and  $J/\Psi$  masses are calculated. Expected statistics will be large enough to look for the correlations with centrality of events and transverse momentum of the resonance state. The jets and photons with  $E_T > 100\text{GeV}$  will be measured with good efficiency and purity.  $\gamma$ -jet and Z-jet events give a good possibility to evaluate the energy losses of hard partons in dense matter.

The primary goal of the heavy ion physics program on LHC (Large Hadronic Collider) is to study the plasma of quarks and gluons (QGP). The critical temperature for deconfinement  $T_c \sim 170 - 260\text{ MeV}$  depending on the scenario is expected to be reached with heavy ion beams ( $E \sim 5.5\text{ TeV/n-n}$ ) [1]. One of strongest signatures proposed as evidence for QGP is the heavy quark vector mesons suppression [2]. At the same time, the detection of the  $Z \rightarrow \mu^+\mu^-$  will provide a good reference to estimate the suppression as long as the point-like Z-boson is supposed to remain unchanged even at the very high energy densities expected [3]. The other hard probe of QGP is the jet production as the energy loss of the gluon(quark) in traversing dense matter leads to a quenching, i.e. a suppression of high  $P_T$  jets. The dijet quenching and enhancement of the mono-jet/dijet ratio [4], as well as the study of jets in Z+jet [3] and  $\gamma$ +jet [5] channels are possible probes we intend to investigate.

## 1 Compact Muon Solenoid (CMS)

The CMS detector [6] was designed for the study of  $pp$  interactions, but some of its features provide in a unique way the possibility to search for the hard probes of deconfinement described above.

CMS is very well suited to study the  $\Upsilon$  family and to a lesser extent the  $J/\psi$  and  $\Psi'$ . The detector will have large acceptance for muons covering almost five units in pseudorapidity from -2.4 to 2.4. The large magnetic field allows to put calorimeters at the distance of about 1.3 m from the beam pipe which reduces in this way the background in the dimuon mass spectrum due to pion and kaon decays. A resolution in dimuon mass near 0.5 % obtained thanks to the high

precision tracker detector. So the different states of the  $\Upsilon$  and  $J/\Psi$  families can be resolved.

The hadron and electromagnetic calorimeters are located inside coil and cover (including Very Forward Calorimeter) from -5 to 5 pseudorapidity units. Almost 80% of transverse energy will be gathered in this rapidity range [7]. The design of calorimeters also allows to look for the hard jet production and the hard photon measurements in this wide pseudorapidity region.

## 2 Vector Meson Production

### 2.1 General Conditions for Background and Signal Simulation

Hard processes (production of heavy resonances) are superimposed on the “thermal” background events. Resonances suppression in the dense matter is not included. The cross-sections for the hard events are rescaled from the  $pp$  ones according to:

$$\sigma_{AA} = A^{2\alpha} \times \sigma_{pp} \quad (1)$$

with  $\alpha=0.9$  for  $(J/\Psi)$ ,  $\alpha=0.95$  for  $(\Upsilon)$ . The cross-sections in  $pp$  collisions are evaluated using the PYTHIA [8] event generator and extrapolations from CDF data [9].

Soft particles (mainly pions and kaons) generated in the heavy ion collision are one of the important sources of background [10], dominating in the dimuon mass spectrum in the Pb-Pb central events. The crucial parameters are the multiplicity and the transverse momentum distribution of particles.

The most pessimistic case is considered. We take 8000 charged particles per unit of rapidity in the central Pb-Pb collision, with a pseudorapidity shape distribution according to HIJING [11]; for the transverse momentum spectrum the SHAKER [12] parametrisation is used.

The next most important source of background for the dimuon spectrum are pairs from  $bb$  and  $cc$  decays, and the mixed cases where one muon is from the one source ( $\pi/K, \Upsilon$  decays) and the other from another source (semileptonic  $bb, cc$  decays).  $bb$  and  $cc$  decay events are generated with PYTHIA.

Both “thermal” and hard events are passed through the full GEANT simulation of the CMS detector, including all material interactions with low thresholds.

### 2.2 Dimuon Production

**Reconstruction Algorithm.** One of the key issues in the CMS Heavy Ion program is to recognize real  $\Upsilon \rightarrow \mu\mu$  in the condition of highly occupied tracker. Uncorrelated decays from soft pions and kaons are the main cause of mismatching muons and thus the main source of the false reconstructed pairs.

A reconstruction algorithm [13] based on  $\delta\phi, P_T$  roads has been developed for the central rapidity region ( $|y| < 1.2$ ). This algorithm allows to find and reconstruct heavy resonances with an efficiency varying from 90 % to 75 % depending on the event multiplicity (up to 8000 charged particles per rapidity unit

i.e. 60000 particles in the CMS tracker acceptance). At the same time it suppresses uncorrelated pairs from pions and kaons by a factor of 6 times (Table 1) for  $|\eta| < 0.8$  and about 2 times for  $0.8 < |\eta| < 1.2$ . The other background sources mentioned above are also suppressed when compared to the hard events.

The Z coordinate (longitudinal) of the primary vertex of the heavy ion event is determined with the two barrel pixel layers. The clusters obtained in the two pixel layers are combined to form track candidates, the transverse momentum of which is calculated assuming that the primary vertex transverse coordinates are (0,0). In order to increase the number of real tracks in the candidate sample only pairs with  $0.5 \text{ GeV}/c < P_T < 5 \text{ GeV}/c$  are selected. For each pair the Z-coordinate of the primary vertex is estimated by extrapolating a straight line in the  $(r, z)$  -plane to the beam axis. The distribution of Z-coordinates of the intersection point with beam line is shown in Fig.1 for two different particle multiplicities. The peak due to real tracks can easily be distinguished from the uniform back ground originating from fake (combinatorial) pairs.

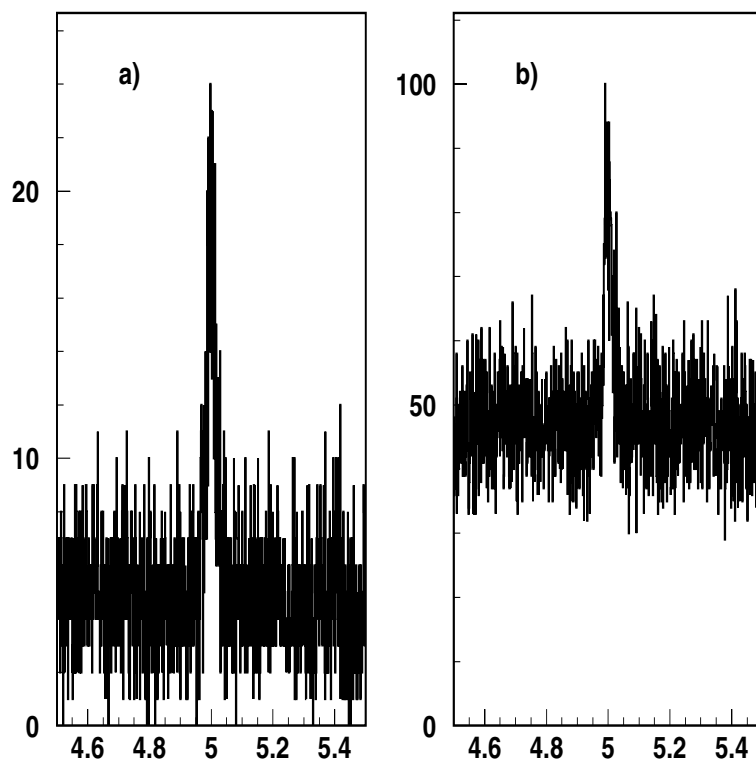


**Fig. 1.** Distribution of Z-position of the primary vertex. a)  $dN^{\pm}/dy=2500$ , b)  $dN^{\pm}/dy=8000$ .

A fit of these distributions using the following function:

$$F = \exp((Z - Z_0)/(2 \times \sigma^2)) + \text{const} \quad (2)$$

gives  $Z_0 = 5$  cm and  $\sigma = 140$   $\mu\text{m}$  (The events were generated at  $Z = 5$  cm.).

Muon reconstruction is seeded from muon chambers. Separate propagations are performed in the transverse (R/Z $\phi$ ) and longitudinal (RZ) planes. In the RZ plane, using a linear parametrization including the primary vertex one can predict the wheel of the cylinder or ring of the forward disks where the muon track can appear. In the transverse plane the parametrization of the trajectory in the tracker barrel and tracker endcap is different. In the tracker barrel region the difference between the azimuthal angles ( $d\phi(l, l+1)$ ) between two clusters of the trajectory located on different cylinders (with radius  $r_l$  and  $r_{l+1}$ ) is proportional to  $dr_{l,l+1}/P_T$

$$|d\phi_{l,l+1}| = \frac{k \times |r_l - r_{l+1}|}{P_T} \quad (3)$$

while in the forward region  $d\phi(l, l+1)$  is proportional to  $dZ/P_L$ .

$$|d\phi_{l,l+1}| = \left| \frac{k \times dZ}{P_L} \right| \quad (4)$$

The efficiency and sample purity for a multiplicity up to 3000 charged particles per unit of rapidity is found to be 90% and above 97% correspondingly. For higher multiplicity the efficiency starts to fall and reaches 75 % (with 97 % purity) for the case of central Pb Pb collisions assuming 8000 charged particles per rapidity unit.

**$\Upsilon$  and  $J/\Psi$  Mass Range.** The expected statistics and signal/background ratios for indicated luminosities and for different nuclei are shown in Table 1. The large statistics available should give the possibility to investigate the dependence on the impact parameter of event and transverse momentum of the resonances.

**Table 1.** Expected number of events and Signal/Background ratio for one month run with indicated luminosity.

	Resonances	$J/\Psi$	$J/\Psi'$	$\Upsilon$	$\Upsilon'$
CaCa	Statistics	220000	5800	340000	115000
$Lum. 10^{29}$	S/B	9.7		9.4	
PbPb	Statistics	10600	350	22000	7500
$Lum. 10^{27}$	S/B	1.0		1.6	

The dimuon mass spectrum in the  $\Upsilon$  mass range (Fig. 2a) is built using all combinations of track pairs from those reaching the muon stations and applying



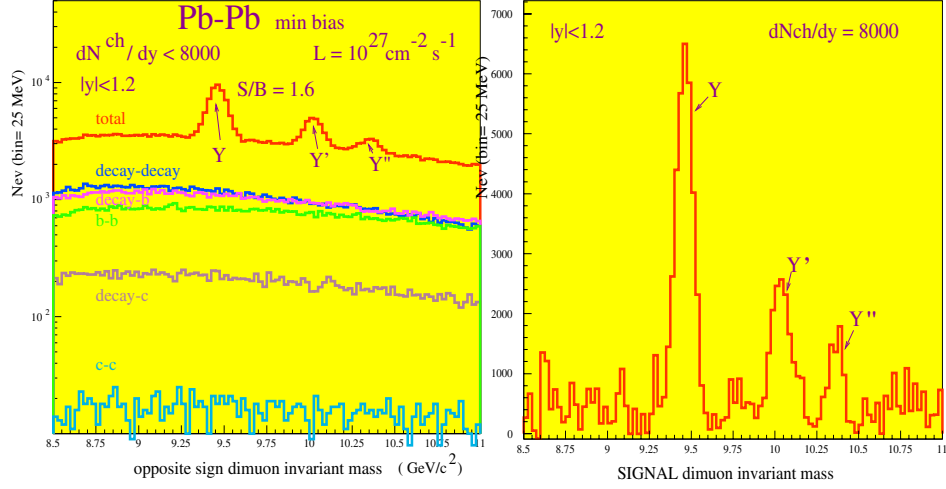


Fig. 2a. Dimuon mass spectrum.

Fig. 2b. Dimuon mass spectrum after background subtraction.

the reconstruction efficiency according to the track pair origin. The uncorrelated background can be subtracted using the like-sign dimuon spectrum:

$$S = OS - 2 \times \sqrt{N^{++}N^{--}} \quad (5)$$

where subtraction is made in each bin of the dimuon opposite-sign spectrum (Fig. 2b).

**Z Mass Range.** In the high dimuon invariant mass region  $M(\mu^+\mu^-) > 20\text{GeV}$  Drell-Yan, Z boson and semileptonic decays of the open flavors ( $cc, bb$ ) are the main sources of dimuons [16]. Applying a cut on the  $P_T$  of  $>$  than  $5\text{ GeV}/c$  makes the contribution of the uncorrelated decays from the soft particles negligible. A clear signal of  $Z \rightarrow \mu\mu$  decays is seen [3]. The expected number of the  $Z \rightarrow \mu\mu$  decays is 11000 and of  $(Z+\text{jet})$  events with  $E_T^{\text{jet}} > 50\text{GeV}$  is 600 for a one month Pb-Pb run. The spectrum of dimuons from B-decay is also an interesting object for investigation of medium-induced energy losses of quarks [14].

### 3 Jet Quenching

In case of quark gluon plasma formation the hard quark is expected to have an additional medium - induced loss, which leads to softening of the jet spectrum. As a result a number of effects are expected to be observed:

- the number of dijet events decreases significantly,
- the monojet/dijet ratio increases,
- the maximum of the distribution of  $E_T^\gamma - E_T^{\text{jet}}$  will be shifted,
- the jet energy flow will strongly depend on the angle between the jet and the reaction plane.

### 3.1 General Conditions for Signal and Background Simulation

The other important task is to extract hard jets and photons from the background of AA events which generates large energy deposition in CMS calorimeters. Jets spectrum is generated with PYTHIA and rescaled for AA events according to ratio (1) with  $\alpha = 1$ . The background is generated with either FRITIOF [15] or HIGING and SHAKER parametrisations as described above.

### 3.2 Jet Detection

The photon and jet reconstruction efficiency and energy resolution have been studied using detailed version of CMS calorimeters. Modified cone and window algorithms for hard jet extraction have been developed. The key point is to search for “jet-like” clusters above the average energy [17] deposition for tower/cell.

- In the first step the average transverse energy  $\overline{E_T^{cell}}(\eta)$  and dispersion  $D_T^{cell}(\eta)$  in a cell are calculated over all cells included in barrel and endcap parts of calorimeter as a function of pseudorapidity  $\eta$ .
- All possible rectangular windows (including overlaps) in calorimeter map in  $\eta - \varphi$  space are constructed. The window consists of an integer number of calorimeter cells. The number of cells in window in  $\eta$  ( $N_\eta^{wind}$ ) and in  $\varphi$  ( $N_\varphi^{wind}$ ) is calculated separately by expressions:

$$\begin{aligned} N_\eta^{wind} &= R * N_\eta^{total} / \eta_{max}, \\ N_\varphi^{wind} &= R * N_\varphi^{total} / 2\pi, \end{aligned}$$

where  $N_\eta^{total}$  and  $N_\varphi^{total}$  are the total number of cells in calorimeters in  $\eta$  and  $\varphi$ ;  $\eta_{max}$  is the maximal value of pseudorapidity  $\eta$ ;  $R$  is the external parameter of the algorithm.

- The window energy is calculated as the sum of cell transverse energies  $E_T^{cell}$  over all  $n_c$  cells included into this window minus the background energy per cell:

$$E_T^{wind} = \sum_{n_c} \{E_T^{cell} - [\overline{E_T^{cell}}(\eta) + D_T^{cell}(\eta)]\},$$

where  $\overline{E_T^{cell}}(\eta)$  is the average transverse energy,

$D_T^{cell}(\eta) = \sqrt{(\overline{E_T^{cell}(\eta)})^2 - \left(\overline{E_T^{cell}(\eta)}\right)^2}$  is the dispersion in cell as a function of  $\eta$ . If the value of transverse cell energy after subtraction of the background energy per cell becomes negative it is set equal to zero.

Then the search for a jet-containing window and the evaluation of the jet energy starts from the window with maximum transverse energy.

- The non-overlapping windows with energy  $E_T^{wind} > 2\sqrt{\sum D_c(\eta)^2}$  are considered as candidates for the jets.
- The center of gravity of the window is considered as the center of the jet.

- For correction of the jet axis, the cell with the maximum transverse energy in cone is chosen and considered as a new center of this jet.  
The correction procedure acts independently and can be added or removed from the algorithm.
- Cells of the cone within the radius  $R$  around the jet center are collected.
- The value  $\overline{E_T^{cell}(\eta)}$  and  $D_T^{cell}(\eta)$  are recalculated using cells which are not covered by jets.
- The jet energy is calculated as energies of collected cells minus mean background energy per cell:

$$E_T^{jet} = \sum \{E_T^{cell} - [\overline{E_T^{cell}(\eta)} + D_T^{cell}(\eta)]\}.$$

### 3.3 $\gamma$ +Jet Channel

Some investigations have been recently performed on possibility to observe the shift of the maximum in the difference between  $E_T$  of photon and  $E_T$  of jet with the CMS detector [18], see Fig. 3.

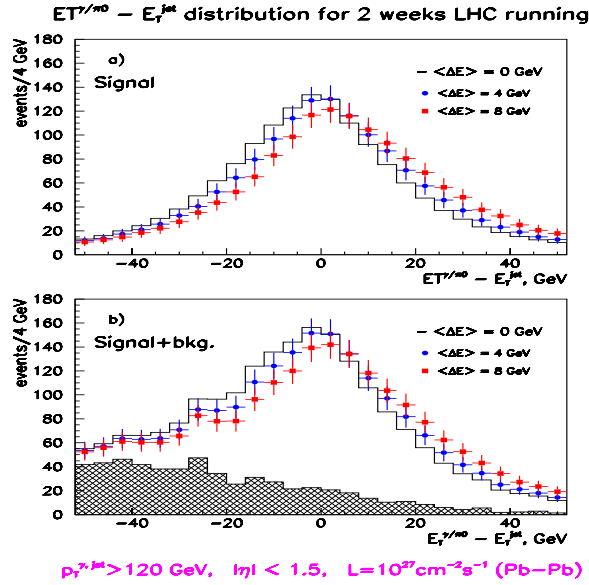


**Fig. 3.** Difference between  $E_T$  of photon and  $E_T$  of jet. a) without background. b) with background.

Jets with a transverse energy exceeding 100 GeV can be observed with excellent efficiency and purity. The shift of the mean value of the difference between the transverse energy of photon (or Z) and the hard jet gives the possibility to evaluate energy losses of hard partons. The main source of background for  $\gamma$ -jet events are jet-jet events, where one of the jets has a leading  $\pi^0$ .

## 4 Trigger and Data Acquisition

Muon,  $e/\gamma$  and jet trigger rates have been estimated for the case of Pb-Pb events assuming 1 or 2 experiments. In the case of 1 experiment, a single muon first level trigger gives a rate of 500 Hz and for 2 experiments the rate is 160 Hz. Dimuon first level trigger gives a 60 and 20 Hz rate correspondingly [19]. As for jets the first level trigger rate is found to be 400-200 Hz for thresholds 40-50 GeV; correspondingly the  $e$  and  $\gamma$  trigger algorithms used in pp and modified for conditions of high occupancy of electromagnetic calorimeter - and obtained rates already at level one are around 10 Hz [20]. The data acquisition system developed for pp interactions will allow to record 70 events/sec on tape [21].

## References

1. E.Laermann, Nucl.Phys., A **610**, 1 (1996); G.Boyd et al, Nucl.Phys., B **469**, 419(1996).
2. T.Matsui and H.Satz, Phys.Lett., B**178**, 416(1986).
3. V.Kartalishvili, R.Kvatadze, R.Shanidze, Phys.Lett., B**356**, 589(1995).
4. I.P.Lokhtin et al, CMS NOTE-1998/025, (1998).
5. X.-N Wang, Z.Huang, I.Sarcevic, Phys.Rev.Lett., **231**, 77(1996).
6. CMS Technical Proposal, CERN/LHCC 94-38, (1994).
7. R.Kvatadze, CMS CR 1997-015, (1997).
8. T. Sjostrand, CERN-TH.7112/93, (1993).
9. F. Abe *et al*, (CDF Collab.) Fermilab-Pub-95/271-E.
10. M. Bedjidian, O.Drapier CMS NOTE-99/052, (1999).
11. M. Guilassy, X.-N. Wang, Comp.Phys.Com. **83**, 307 (1994).
12. F.Antinori, Internal note, ALICE/MC, 93-09, (1993).
13. O. Kodolova, M.Bedjidian, CMS NOTE-99/004, (1999).
14. I.Lokhtin et al, CMS NOTE-2001/008, 2001.
15. B.Andersson et al, Z.Phys.C**57**, 485, 1993.
16. M.Bedjidian et al, CMS NOTE-1999/017, 1997.
17. I.Vardanyan et al, CMS NOTE submitted.
18. O.Kodolova et al, CMS NOTE-1998/063, 1998.
19. G.Wrochna CMS NOTE-1997/089, 1997.
20. O.Kodolova et al, CMS NOTE-1998/078, 1998.
21. A.Rasz et al, CMS NOTE-2000/027, 2000.

# Tracking in a High Rate Environment

Gordana Medin (for the HERA-B Collaboration)

Humboldt University in Berlin

**Abstract.** HERA-B, a fixed target experiment to study heavy flavour production in proton-nucleon interactions at HERA, has to cope with high particle densities. The reconstruction program for the main tracking system consisting of drift and microstrip gas chambers requires an efficient pattern recognition method. The method should be robust enough with respect to large occupancies and tracking detector imperfections like dead, inefficient and noisy channels. In this paper we present different track finding algorithms.

## 1 Introduction

The HERA-B experiment at DESY is a large acceptance spectrometer originally planned to detect B mesons produced in fixed target proton (920 GeV) nucleus interactions. The detector is designed to reconstruct 4 to 5 interactions per bunch crossing (every 96 ns) with about 120 charged tracks from primary interactions (and with a similar number of tracks from secondary interactions). This leads to a high particle density with a radial distribution of the particle flux ( $R$  is the distance from the beam) as shown in Fig. 1:

$$\phi \approx \frac{4 \cdot 10^7}{\text{cm}^2\text{s}} \frac{1}{R^2/\text{cm}^2} \quad (1)$$

Due to the strongly forward oriented kinematics the detector is build as a forward magnet spectrometer covering polar angles varying from about 10 to 200 mrad (see Fig. 1). The main detector components are the multi-wire target, the vertex detector system installed inside a vacuum vessel, the dipole magnet providing a magnetic-field integral of 2.2 Tm, the tracking system for the track reconstruction and momentum measurement, the Ring-Imaging Cherenkov counter (RICH) for kaon/pion/proton separation, an electromagnetic calorimeter (ECAL) for electron and photon measurement, and the muon system.

HERA-B has suffered significant delays compared to its ambitious original schedule. These delays were mainly due to operational problems of the tracking detectors in a harsh high-radiation environment. The detector were completed at the beginning of the year 2000. The first 6 months of data-taking were mainly devoted to the commissioning of the apparatus.

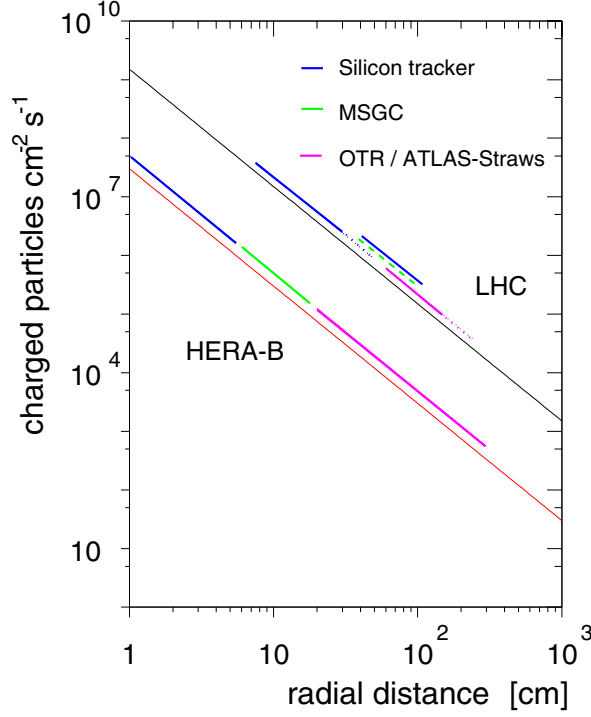


**Fig. 1.** Particle flux as a function of the radial distance from the beam for HERA-B and LHC experiments. The flux in the Outer Tracker region is comparable to the flux which the ATLAS TRT straws will see in LHC.

## 2 Main Tracking System

One of the challenging components of this spectrometer is the tracking system. It has to cope with the extremely high particle fluxes and high radiation doses which are comparable to LHC conditions. Because of a strong radial dependence of the particle flux on the distance to the beam pipe, different granularities for the tracking detectors had to be chosen to keep occupancies at a reasonable level. The different granularities were achieved by choosing different technologies for the inner and outer tracking region. MSGC-GEM detectors are used in the inner region (Inner Tracker) to cover the distance between 6cm and 30cm around the beam pipe. The outer region is covered by honeycomb drift chambers. The diameter of the honeycomb drift cells is 10mm for the outer and 5 mm for the inner sectors. The Outer Tracker consists of 13 planar superlayers comprising a total of about 115 000 channels. Each superlayer consists of six individual layers, and each of them is subdivided into 12 sectors to adjust the channel count to the track density. In half of the layers, the wires are vertical ( $0^\circ$  layers), the other layers are stereo ones with the wires rotated by  $\pm 5^\circ$ . Four MSGC-GEM detectors form one Inner Tracker layer. Similar to the outer tracker, the orientation of sensitive strips in a half of layers is vertical, the strips in the stereo layers are

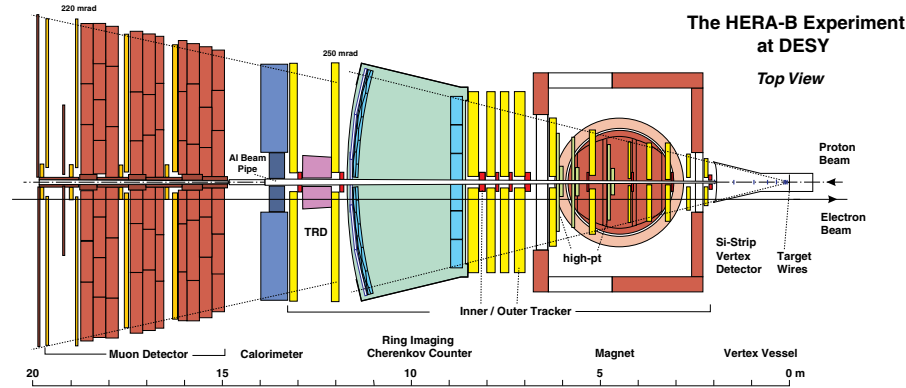


**Fig. 2.** Top view of the HERA-B spectrometer. The proton beam coming from the right.

rotated by  $\pm 5^\circ$ . The layers are grouped in three blocks: “magnet chambers” inside the dipole magnet, “pattern chambers” in the field-free region between the magnet and the RICH and “trigger chambers” in front of the ECAL. The pattern chambers have the highest density of single measuring planes and are used for pattern recognition. An isometric view of the multiplanar geometry of the pattern tracker is shown in Fig. 3.

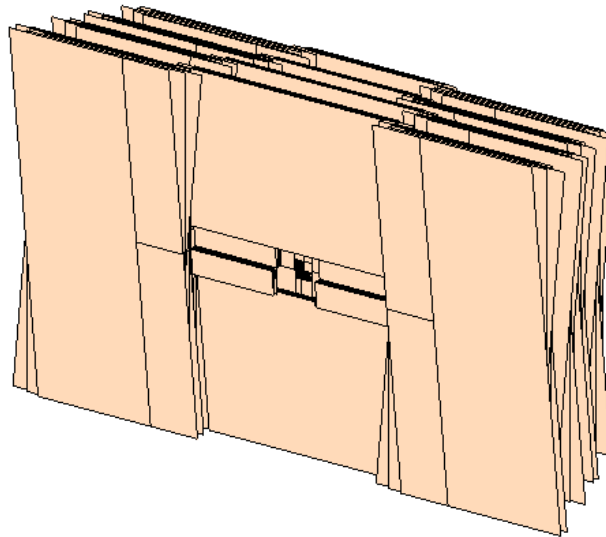


**Fig. 3.** Isometric view of the HERA-B pattern tracker.

### 3 Track Reconstruction

The pattern recognition, as the first step of the track reconstruction, starts in the field-free region of the pattern chambers. Using a Kalman Filter algorithm, track segments are reconstructed [1]. The tracks are continued further upstream using the magnet chambers and joined with reconstructed tracks from the vertex detector. This is illustrated in Figure 2. The downstream propagation of the tracks uses the trigger chambers in front of the ECAL. The track momentum is determined from a global fit to the full reconstructed track.

### 4 Methods for Track Recognition

In the past few years, members of the HERA-B collaboration have performed an extensive analysis of different track recognition methods. These efforts have resulted in the reconstruction packages RANGER [1] and OTR/ITR-CATS [2].

RANGER is based on the track following and concurrent track evolution approach. The pattern recognition procedure first searches for 2D straight track candidates in the  $xz$  projection using only the hit information from the  $0^\circ$  layers. Then it finds for each of these candidates the corresponding vertical track candidate in the  $yz$  projection using simultaneously the hit information from the  $\pm 5^\circ$

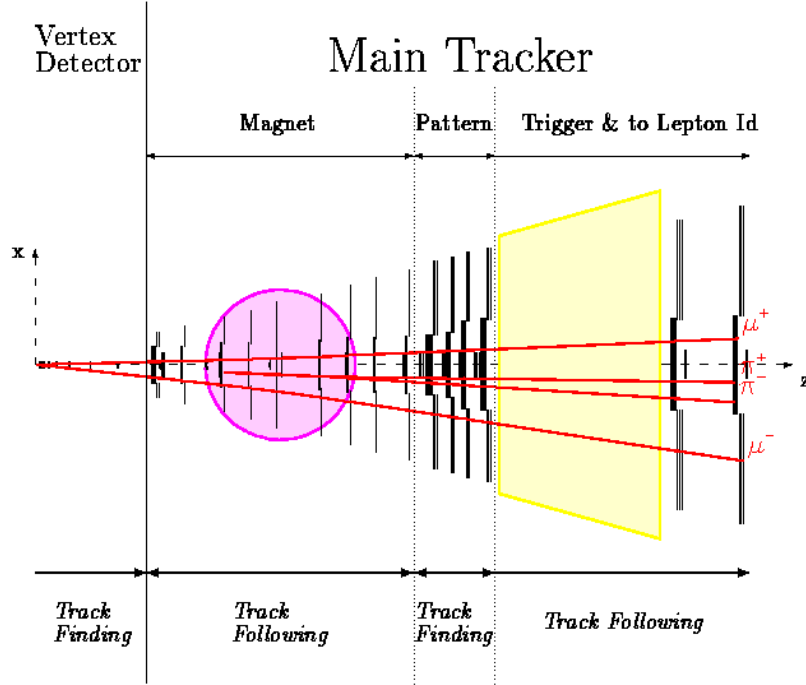
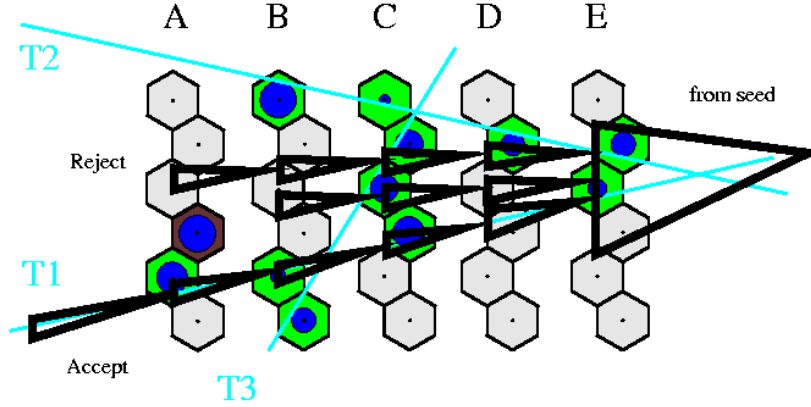


Fig. 4. Layout of the HERA-B vertex and main tracking system (top view) [1].





**Fig. 5.** Illustration of the concurrent track evolution strategy for an ambiguous situation caused by three nearby tracks in a superlayer of the HERA-B outer tracker. The propagation proceeds upstream from the right to the left [1]

stereo layers. After the vertical track candidate was found, its hits are combined with those of the  $xz$  projection, and a three-dimensional track candidate is fitted using a Kalman filter.

The concurrent track evolution strategy is illustrated in Fig. 3. A starting initial set of track parameters for a track candidate, called a “seed” is necessary. Given a seed, the algorithm performs the track following procedure in the course of which it tries to find the next hit and improves the track parameters with each new hit added. The method splits the tracks whenever more than one hit is observed in the neighbourhood of the predicted hit location. In order to keep the number of simultaneously propagated track branches at a reasonable level, the algorithm must discard some of them relying upon a quality index of the track. One of the problems with which the algorithm had to cope when applied to the first data was a lower hit efficiency and hit resolution than expected, and a large fraction of “dead” channels (caused by hardware problems). To provide a reasonable track reconstruction efficiency and ghost rate RANGER must work with a higher number of simultaneously explored track branches.

A new algorithm was developed as an alternative approach for track reconstruction that would be more robust and tolerant to hardware problems. The track reconstruction techniques implemented in OTR/ITR-CATS package combine features of cellular automata for track recognition with the advantages of the Kalman filter for track fitting. The input information for the cellular automaton is given by space-points which are considered as elementary units or cells. In the framework of the OTR/ITR-CATS algorithm, space-points are defined as short 3D track segments inside superlayers. The three-dimensional track segments inside superlayers are reconstructed by first searching for hit multiplets in the  $0^0$ - layers and then attaching multiplets in the stereo layers. The combined  $0^0$  and stereo multiplets are then fitted by a Kalman filter. To create track can-

didates of space-points and collect hits missed in the layers where space-points could not be reconstructed the cellular automaton procedure was performed. A cellular automaton is a discrete-time dynamical system that evolves in a phase space consisting of cells [2]. Disadvantage of this algorithm is that, if in an intermediate superlayer there is no neighbouring space-points, the cellular automaton cannot jump over such a hole, as caused by a dead region in the tracker. The solution is that a cellular automaton is accompanied by a track following procedure. As seeds are used the track candidates found by the cellular automaton and space-points for which the automaton could not find any neighbours.

The tracking efficiency is larger than 95 % for the reference tracks coming from the target region, and about 80-95% in average for all tracks. The ghost rate is roughly 14%.

## 5 Summary

The operation of tracking detectors under conditions close to what is expected at the LHC and efficient track reconstruction at detector occupancies of up to 20% makes the HERA-B apparatus a pioneer in the field of high-rate tracking. Two pattern recognition algorithms, described in this paper, show comparable results with high reconstruction efficiency, reasonable behaviour of CPU time consumption and robustness of the algorithm in case of low hit efficiencies of the detectors and increased track multiplicity.

## References

1. R. Mankel, HERA-B Note 97-082, *ranger - a Pattern Recognition Algorithm for the HERA-B Main Tracking System*
2. I. Abt, D. Emelianov, I. Gorbounov and I. Kisel, *Cellular Automaton and Kalman Filter Based Track Search in the Pattern Tracker of the HERA-B* (submitted to NIM A)

# Resonances from Strongly-Interacting Electroweak Symmetry Breaking Sector at Future $e^+e^-$ Colliders

Mikuláš Gintner and Ivan Melo

Physics Dept., University of Žilina, Veľký diel, 010 26 Žilina, Slovakia

**Abstract.** We study new strong resonances associated with the physics responsible for the strong electroweak symmetry breaking. We write down the lowest order effective chiral Lagrangians describing the couplings of these new resonances to the Standard Model fields and calculate signals for  $I = J = 0$   $S$ -resonances and for  $I = J = 1$   $\rho$ -resonances in the  $WWt\bar{t}$  scattering in the process  $e^+e^- \rightarrow \nu\bar{\nu}t\bar{t}$  at the Next Linear Collider. We also find low-energy constraints on the  $\rho$ -resonance couplings to the top quark.

## 1 Introduction

One of the most important problems of today's particle physics is the mechanism of electroweak symmetry breaking (ESB). The mechanism of ESB is responsible for giving the  $W$  and  $Z$  bosons their masses. Despite some progress in the experimental limits on the Higgs mass [1], the ESB sector of the Standard Model (SM) is still rather weakly constrained by the experimental data and the physics behind the mechanism of ESB remains unknown.

In this work we study some phenomenological consequences of the *strongly-coupled* ESB sector. Typical representatives of the strongly-coupled scenario are technicolor models built in analogy to chiral symmetry breaking in QCD. The strong ESB gives rise to massless Goldstone bosons — electroweak (EW) pions — which, just like QCD pions, are assumed to be bound states of some more fundamental strongly interacting objects (e.g. technifermions). According to Higgs mechanism, EW pions are absorbed by  $W$  and  $Z$  bosons and become their longitudinal components ( $W_L, Z_L$ ). Thus any collider process which involves the longitudinal weak gauge bosons can in principle give us an access to the interactions connected to the mechanism of ESB [2].

Since  $V_L V_L$  ( $V = W, Z$ ) scattering amplitudes start to violate unitarity at 1-3 TeV range we expect new strongly interacting ESB resonances (equivalent of lowest QCD resonances such as  $\rho$  and  $\omega$ ) to appear at or below this scale. We will not be able to see the substructure of these new resonances and EW pions at the Large Hadron Collider (LHC) and at the Next Linear Collider (NLC) operating at 1-3 TeV range, but the question is if we can distinguish at least the resonances themselves and measure their masses and couplings.

A lot of attention has been devoted to the testing of the strongly-interacting scenario in the longitudinal vector boson scattering  $V_L V_L \rightarrow V_L V_L$  [3]. The

studies concentrated on signatures of either a new  $I = J = 1$  ESB  $\rho$ -resonance or a new  $I = J = 0$  ESB  $S$ -resonance (parameters of the  $S$ -resonance can be tuned to immitate the SM Higgs boson — SM-like  $S$ -resonance) at either the NLC or the LHC. The results have shown that it will be possible to establish the presence of strong ESB at the LHC and the NLC and that, to a degree, it will be possible to distinguish new strong resonances [2].

Another potentially powerful process for the study of strong ESB is the scattering of longitudinal vector bosons to top quarks,  $V_L V_L \rightarrow t\bar{t}$ . Its main appeal is in the possibility to test whether the extraordinarily large top quark mass is generated by the same new strong interactions which are responsible for ESB, or by yet additional new strong interactions introduced just for that sake. In the former case (represented, e.g., by the extended technicolor theories [4]) we expect the top quark to couple significantly to the resonances which unitarize  $V_L V_L \rightarrow V_L V_L$  scattering [5,6]. This could lead to significant event rates in  $V_L V_L \rightarrow t\bar{t}$ . In the latter case, when the mechanism of the top mass generation is different from the  $W$  mass generation (as in topcolor-assisted technicolor models [4]), we expect that the top quark does not couple significantly to the new resonances of the strong ESB sector. This would imply that the new resonances observed in the  $V_L V_L \rightarrow V_L V_L$  channel are suppressed in the  $V_L V_L \rightarrow t\bar{t}$  channel [2,5].

When studying the  $V_L V_L \rightarrow t\bar{t}$  process, we can make use of another unique property of the top quark. Unlike all the other known quarks the top quark decays so rapidly that the information about its spin is transferred directly to the final state with negligible hadronization uncertainties. This raises an interesting possibility to measure polarized cross sections in  $V_L V_L \rightarrow t\bar{t}$  and use this information to distinguish between  $S$ - and  $\rho$  resonances which contribute to different helicity combinations of the top quarks [2,5].

For these reasons the  $V_L V_L \rightarrow t\bar{t}$  process at the NLC has recently attracted growing interest. There have been studies within the SM [7–9], within the Higgsless SM below the scale of new physics (no-resonance model) [10,6], and also within models above the scale of a new  $S$ -resonance and  $\rho$ -resonance [2,5,11,12].

In this work we study the new  $S$ - and  $\rho$ -resonances in the process  $W_L W_L \rightarrow t\bar{t}$  which is being considered as a subprocess of  $e^+e^- \rightarrow \nu\bar{\nu}t\bar{t}$  at the NLC with the CM energy of 1.5 TeV and 2 TeV. Three cases, the no-resonance, the  $S$ -resonance, and the  $\rho$ -resonance are considered with various values of parameters. We show the importance of low energy constraints for  $\rho$ -resonance signals at NLC. We calculate total and differential cross sections with polarized (anti-)top quarks in the final state using the Effective- $W$  Approximation and considering longitudinal weak gauge bosons only. The number of events obtained is for the assumed integrated luminosity of 200 fb<sup>-1</sup>.

This contribution is organized as follows. In Section 2 we introduce the lowest order effective chiral Lagrangians describing models with no resonance,  $S$ -resonance, and  $\rho$ -resonance. Our calculations and results obtained for the models under consideration are presented in Section 3 and conclusions in Section 4.

## 2 No-, $S$ - and $\rho$ -Resonance Models

Due to our ignorance of details of new strong physics behind ESB the most convenient approach to the analysis of its possible consequences is the effective field theory framework. In this approach, if energy available is below the threshold of new resonances production, one starts with EW pions as the only particles in the spectrum which are subject to new strong interactions. The Lagrangian of EW pions is the familiar nonlinear  $\sigma$ -model based on global  $SU(2)_L \times SU(2)_R$  spontaneously broken down to  $SU(2)_V$  custodial or isospin symmetry. This symmetry breaking pattern is supported by the relation  $M_W/M_Z = \cos \theta_W$  which is satisfied to high accuracy.

If we assume to have enough energy to produce a new resonance it must be added to the set of building elements of the effective Lagrangian. In our work beside the no-resonance case we also assume the production of either the  $S$ -resonance or  $\rho$ -resonance. They are added to the Lagrangian respecting chiral  $SU(2)_L \times SU(2)_R$  symmetry. For  $S$ -resonance it is a straightforward procedure, for  $\rho$ -resonance one can follow either Weinberg [13] or hidden symmetry approach [14]. The gauge interactions of the SM are introduced by requiring the  $S$  and  $\rho$  Lagrangians to be gauge invariant under  $SU(2)_L \times U(1)_Y$ .

Let us begin with the gauged no-resonance Lagrangian given by

$$\begin{aligned} \mathcal{L}_0 = & - \overbrace{v^2 \text{Tr}\{\mathcal{A}_\mu \mathcal{A}^\mu\}}^{\text{nonlinear } \sigma \text{ model}} - \overbrace{\bar{\psi}_L u^\dagger u^\dagger M \psi_R}^{t \text{ couples to } \pi; m_t, m_b} + h.c. + \mathcal{L}_{kin}(\tilde{\mathbf{W}}, \tilde{\mathbf{Y}}) \\ & + \bar{\psi}_L i\gamma^\mu [\partial_\mu + \tilde{\mathbf{W}}_\mu + \frac{i}{2}g'(B-L)Y_\mu] \psi_L \\ & + \bar{\psi}_R i\gamma^\mu [\partial_\mu + \tilde{\mathbf{Y}}_\mu + \frac{i}{2}g'(B-L)Y_\mu] \psi_R \end{aligned} \quad (1)$$

where  $\mathcal{A}_\mu = [u^\dagger(\partial_\mu + \tilde{\mathbf{Y}}_\mu)u - u(\partial_\mu + \tilde{\mathbf{W}}_\mu)u^\dagger]/2$ ;  $u = \exp(i\boldsymbol{\pi} \cdot \boldsymbol{\tau}/2v)$  with  $v = 246$  GeV,  $\boldsymbol{\pi}$  is the isospin triplet of the EW pions, and  $\boldsymbol{\tau}$  are Pauli matrices;  $\psi$  denotes fermion field doublet,  $(t, b)$ , the  $B-L$  is the baryon minus lepton number operator, and the  $M = \text{diag}(m_t, m_b)$  is the fermion doublet mass matrix.  $\mathcal{L}_{kin}(\tilde{\mathbf{W}}, \tilde{\mathbf{Y}})$  is the kinetic energy term of the  $SU(2)_L$  gauge field,  $W_\mu$  and the  $U(1)_Y$  gauge field,  $Y_\mu$ ;  $\tilde{\mathbf{W}}_\mu = ig\mathbf{W}_\mu \cdot \boldsymbol{\tau}/2$ ;  $\tilde{\mathbf{Y}}_\mu = ig'Y_\mu\tau^3/2$ .

The gauged  $S$ -resonance model can be described by the following leading order effective Lagrangian

$$\begin{aligned} \mathcal{L}_S = & \mathcal{L}_0 + \mathcal{L}_{kin}(S) - \frac{1}{2}M_S^2 S^2 - 2g'''v \text{Tr}\{\mathcal{A}_\mu \mathcal{A}^\mu\} S \\ & - \frac{\alpha}{v} \bar{\psi}_L u^\dagger u^\dagger M \psi_R S + h.c. \end{aligned} \quad (2)$$

where  $\mathcal{L}_0$  is given by (1), the  $\mathcal{L}_{kin}(S)$  is the kinetic energy term of the  $S$ -resonance,  $S$  denotes the scalar ( $I = J = 0$ ) ESB resonance field,  $M_S$  is its mass. The  $g'''$ ,  $\alpha$  and  $M_S$  are free parameters.

The gauged  $\rho$ -resonance model is given by

$$\mathcal{L}_\rho = \mathcal{L}_0 + \mathcal{L}_{kin}(\rho) - a \frac{v^2}{4} \text{Tr}[(\omega_\mu + \rho_\mu)(\omega^\mu + \rho^\mu)]$$

$$\begin{aligned}
& +b_1 \bar{\psi}_L i\gamma^\mu [u\partial_\mu - u\rho_\mu + u\frac{i}{2}g'(B-L)Y_\mu] u^\dagger \psi_L \\
& +b_2 \bar{\psi}_R P i\gamma^\mu [u\partial_\mu - u\rho_\mu + u\frac{i}{2}g'(B-L)Y_\mu] u^\dagger P \psi_R \\
& +\lambda_1 \bar{\psi}_L i\gamma^\mu u^\dagger \mathcal{A}_\mu \gamma^5 u \psi_L + \lambda_2 \bar{\psi}_R P i\gamma^\mu u \mathcal{A}_\mu \gamma^5 u^\dagger P \psi_R \quad (3)
\end{aligned}$$

where  $\omega_\mu = [u^\dagger(\partial_\mu + \tilde{\mathbf{Y}}_\mu)u + u(\partial_\mu + \tilde{\mathbf{W}}_\mu)u^\dagger]/2$ ;  $\rho_\mu = ig''\rho_\mu \cdot \boldsymbol{\tau}/2$ ,  $\rho_\mu$  denotes the vector ( $I = J = 1$ ) ESB  $\rho$ -resonance field,  $\mathcal{L}_0$  is given by (1), the  $\mathcal{L}_{kin}(\rho)$  is the kinetic energy term of the  $\rho$ -resonance, the  $a$ ,  $g''$ ,  $b_1$ ,  $b_2$ ,  $\lambda_1$  and  $\lambda_2$  are free parameters and  $P = \text{diag}(1, 0)$ . The  $P$  matrix ensures that the  $\rho$  only couples to the right-handed top quark but not to the right-handed bottom quark (to avoid constraints on the  $\rho$  couplings from the  $Zb\bar{b}$  vertex), which spoils the custodial symmetry in much the same fashion as does the top-bottom mass splitting.

The low energy experiments place the following constraints on the parameters of the  $\rho$ -resonance Lagrangian [15]:  $g'' \gtrsim 10$ ,  $|b_2 - \lambda_2| \lesssim 0.04$  and  $|b_1 - \lambda_1| \lesssim 0.01$ .

### 3 Signals from the $S$ - and the $\rho$ -Resonances at the NLC

The question is if the  $\rho$  coupling constants which respect constraints of Sec. 2 can generate significant signals in the  $W_L W_L \rightarrow t\bar{t}$  scattering at the NLC. Here we consider this scattering as a subprocess of the process  $e^+e^- \rightarrow \nu\bar{\nu}t\bar{t}$ , see Fig. 1.

We have chosen to calculate signals for three  $\rho$ -resonances of the same mass  $M_\rho = 1$  TeV but different couplings and widths  $\Gamma_\rho$ , summarized in Table 1. For comparison we also calculate signals from two  $S$ -resonances — 800 GeV SM-like Higgs boson with the width  $\Gamma_H = 285$  GeV ( $g''' = \alpha = 1$ ) and the nonstandard

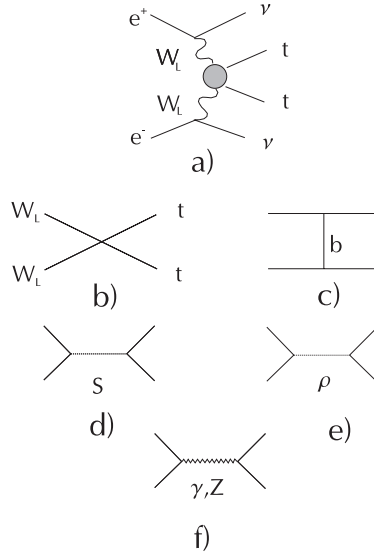


**Fig. 1.** Feynman diagrams for (a)  $e^+e^- \rightarrow \nu\bar{\nu}t\bar{t}$ , (b-f)  $W_L W_L \rightarrow t\bar{t}$

**Table 1.** Parameters of the three  $\rho$ -resonances;  $b_1 = \lambda_1 = 0$ ,  $\lambda_2 = 0.04$ .  $\Gamma_\rho$  is uniquely defined by  $M_\rho$  and the coupling constants

	$M_\rho(\text{TeV})$	$b_2$	$g''$	$\Gamma_\rho(\text{GeV})$
$\rho_1$	1	0.04	15	4.99
$\rho_2$	1	0.08	10	9.42
$\rho_3$	1	0.04	40	21.66

800 GeV  $S$ -resonance with the width  $\Gamma_S = 158$  GeV ( $g''' = 0.7, \alpha = 1$ ) — and from the no-resonance model.

To calculate cross sections of the process  $e^+e^- \rightarrow \nu\bar{\nu}t\bar{t}$  we used Effective- $W$  Approximation (EWA) [16] in which one convolutes the cross section for the subprocess  $W_L W_L \rightarrow t\bar{t}$  with the corresponding distribution functions of the  $W_L$  boson. For the EWA to be valid the invariant energy scales of the process should be much larger than the  $W$  mass. Since the distribution function for longitudinal  $W$ -bosons is largely independent of the  $W$  beam energies the EWA describes more accurately  $W_L$  contributions than contributions of transverse  $W$ -bosons. Fortunately, sensitivity of  $W_T$  channels to the ESB sector is much weaker than sensitivity of  $W_L$  channels. Therefore to extract the signal of new physics without having the transverse  $W$  contributions calculated the following quantity can be used [12]

$$\sigma_{\text{new physics}} - \sigma_{SM}(M_H = 100 \text{ GeV}) \quad (4)$$

Here the transverse  $W$  contributions are expected to subtract each other. Thus the difference (4) should be a good estimate of what we would get if much more complete calculations of the studied process were performed.

To calculate the subprocess cross sections we used the ET theorem according to which we replaced  $W_L$  boson with the corresponding EW pion  $\pi$ . The subprocess diagrams are shown in Figs. 1b – 1f. The main contribution comes from the diagrams 1b – 1e, while the contribution of the diagram 1f is small. We note that the helicity cross sections  $\sigma^{++} = \sigma^{--}$  (the signs refer to helicities of the  $t$  and  $\bar{t}$ , respectively) receive their contributions mainly from the diagrams 1b and 1d,  $\sigma^{+-}$  mainly from 1c and 1e while  $\sigma^{-+}$  is negligible.

We show the results of our calculations in Fig. 2. Figure 2a shows the total cross section  $\sigma^{+-}$  for the process  $e^+e^- \rightarrow \nu\bar{\nu}t\bar{t}$  in femtobarns as a function of the CM energy  $\sqrt{s}$  of the NLC. The signals from the  $\rho$  resonances rise above the solid line which represents both the  $S$ -resonances and the no-resonance model at the same time (they have approximately the same  $\sigma^{+-}$ ). The best signal comes from the  $\rho$ -resonance with the width  $\Gamma_\rho = 9.42$  GeV ( $b_2 = 0.08$ ,  $g'' = 10$ ) — for  $\sqrt{s} = 1.5$  TeV and  $\sqrt{s} = 2$  TeV we get cross sections 0.8 fb and 1.9 fb, respectively. Assuming integrated luminosity  $L = 200 \text{ fb}^{-1}$  we get for the  $\rho$ -resonance 160 events at  $\sqrt{s} = 1.5$  TeV and 380 events at  $\sqrt{s} = 2$  TeV. For  $S$ -resonances and the no-resonance model we get 102 events at  $\sqrt{s} = 1.5$  TeV

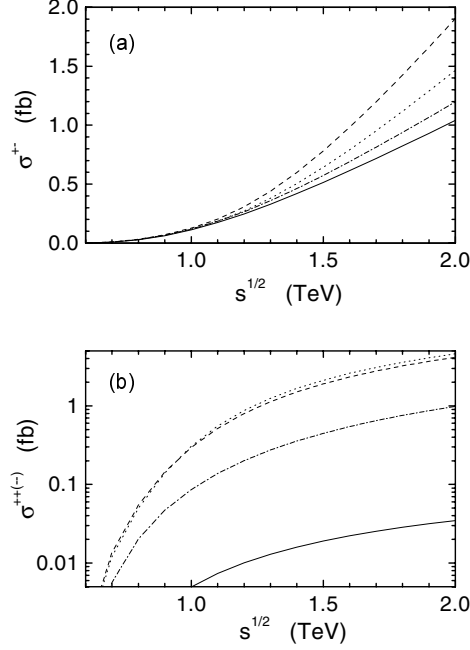


**Fig. 2.** Helicity cross sections for  $e^+e^- \rightarrow \nu \bar{\nu} t \bar{t}$  as a function of CM energy: (a)  $\sigma^{+-}$  for the three  $\rho$ -resonances of Table 1:  $\rho_1$  (dotted line),  $\rho_2$  (dashed line),  $\rho_3$  (dash-dotted line). The solid line is for both the  $S$ -resonance and the no-resonance signal; (b)  $\sigma^{++}$  ( $= \sigma^{--}$ ) for the nonstandard 800 GeV  $S$ -resonance with  $\Gamma_S = 158$  GeV (dotted line), the 800 GeV SM-like Higgs boson (dashed line), all  $\rho$ -resonances and the no-resonance model (dash-dotted line), the 100 GeV SM Higgs (solid line)

and 208 events at  $\sqrt{s} = 2$  TeV. We note that the only cut performed on data was the cut on the invariant mass of the  $t\bar{t}$  pair  $m_{t\bar{t}} > 500$  GeV. Further cuts are needed to reduce the backgrounds which are not treated here. Following previous studies [12] we estimate that the efficiency of these cuts for the signal is about  $\epsilon_{cut} = 80$  % and that the remaining events will be fully reconstructed (including  $b$ -tagging) with the efficiency of about  $\epsilon_{rec} = 30$  % [5]. Hence, for the final event numbers  $N_f = N \epsilon_{cut} \epsilon_{rec}$ . For the  $\rho$ -resonance we thus finally get 38 (91) events at 1.5 TeV (2 TeV), and for  $S$ -resonances and the no-resonance case 24 (50) events at 1.5 TeV (2 TeV).

In Fig. 2b we show the total cross section  $\sigma^{++} = \sigma^{--}$  for the process  $e^+e^- \rightarrow \nu \bar{\nu} t \bar{t}$  in femtobarns as a function of the CM energy  $\sqrt{s}$ . In this case the  $S$ -resonances dominate: for the SM-like Higgs we get  $\sigma^{++} + \sigma^{--} = 3.8$  (8.3) fb at  $\sqrt{s} = 1.5$  (2) TeV, while for the  $\rho$ -resonances and the no-resonance model we get the same results  $\sigma^{++} + \sigma^{--} = 0.9$  (1.8) fb at  $\sqrt{s} = 1.5$  (2) TeV. After the cuts and the reconstruction we get for the SM-like Higgs 182 (398) events at 1.5 (2) TeV and for the  $\rho$ - and the no-resonance case 43 (86) events at 1.5 (2) TeV.

Differential cross sections for  $e^+e^- \rightarrow \nu \bar{\nu} t \bar{t}$  as a function of the invariant mass  $m_{t\bar{t}}$  at  $\sqrt{s} = 1.5$  TeV are shown for  $(+-)$  helicity combination in Fig.



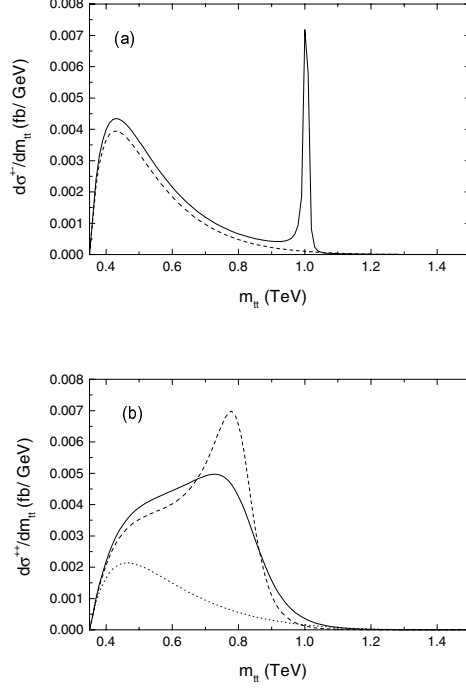


**Fig. 3.** Differential cross sections for  $e^+e^- \rightarrow \nu \bar{\nu} t \bar{t}$  as a function of the invariant mass  $m_{t\bar{t}}$  at  $\sqrt{s} = 1.5$  TeV: (a)  $\frac{d\sigma^{+-}}{dm_{t\bar{t}}}$  for  $\rho_2$  (solid line), the  $S$ -resonances and the no-resonance case (dashed line); (b)  $\frac{d\sigma^{++}}{dm_{t\bar{t}}}$  for the 800 GeV SM-like Higgs boson (solid line), the 800 GeV nonstandard  $S$ -resonance with  $\Gamma_S = 158$  GeV (dashed line), all  $\rho$ -resonances and the no-resonance model (dotted line)

3a and for  $(++)$  helicity combination in Fig. 3b. The measurement of these differential cross sections could provide the resonance mass if the resonance has a well defined peak with sufficient number of events contributing to the peak. For  $\rho_2$  (solid line in Fig. 3a), we get 37 events in the peak before the cuts and reconstruction, assuming integrated luminosity  $L = 200 \text{ fb}^{-1}$ .

## 4 Conclusions

We have studied the new strong resonances associated with the physics responsible for the strong electroweak symmetry breaking and signals of these resonances in the process  $e^+e^- \rightarrow \nu \bar{\nu} t \bar{t}$ . We have provided the comprehensive treatment of the  $\rho$  Lagrangian including the low-energy constraints on its parameters. The analysis presented in this work shows that the total signal from the  $\rho$ -resonance summed through all helicity channels at the energy of 1.5 TeV and the integrated luminosity of  $200 \text{ fb}^{-1}$  is 81 events after the cuts and reconstruction. The corresponding numbers for 800 GeV SM-like Higgs is 206 events and for the no-resonance case 67 events. The SM-like 800 GeV Higgs (and heavy  $S$ -resonances

in general) is thus well separated from the  $\rho$ -resonance and the no-resonance cases. To distinguish the  $\rho$ -resonance signal from the no-resonance one and to confirm the spin of the  $S$ -resonance it is very useful to study individual helicity channels and distributions in invariant mass  $m_{t\bar{t}}$ . The  $\rho$ -resonance contributes mainly to the helicity cross section  $\sigma^{+-}$  for the process  $e^+e^- \rightarrow \nu\bar{\nu}t\bar{t}$ , while the  $S$ -resonance contributes mainly to the cross section  $\sigma^{++}$ . This underlines the importance of the measurement of the top quark helicity (see [5] for more on this). Another way to improve on signals is to go to the CM energy of 2 TeV.

This work was supported by grant VEGA 1/8307/01.

## References

1. M. Swartz: Plenary talk presented at the XIX International Symposium on Lepton and Photon Interactions at High Energies, Stanford University, Aug. 9-14, 1999, [hep-ex/9912026]; L3 Collaboration, presentation at LEPC, CERN, November 1999, [<http://13www.cern.ch/conferences/talks99.html>].
2. T.L. Barklow et al.: Strong coupling Electroweak Symmetry Breaking, Working Group Summary Report from the 1996 DPF/DPB Summer Study New Directions for High Energy Physics Snowmass, Colorado, June 25–July 12, 1996, [hep-ph/9704217].
3. M. Golden, T. Han, G. Valencia: Report contributed to ESB & BSM Book, ed. by T. Barklow, S. Dawson, H. Haber, J. Siegrist, [hep-ph/9511206]; J. Bagger et al: *Phys. Rev.* **D49** (1994), 1246, [hep-ph/9306256]; R. Casalbuoni et al: *Z. Phys.* **C60** (1993), 315; See also [2] and references therein.
4. For a review of technicolor/extended technicolor theories and topcolor-assisted technicolor theories see K. Lane “Technicolor 2000”, [hep-ph/0007304].
5. E.R. Morales, M.E. Peskin: Proceedings of the International Workshop on Linear Colliders, Sitges, Barcelona, Spain, 28 April – 5 May, 1999, [hep-ph/9909383].
6. T. Lee: *Phys. Lett.* **B 315** (1993), 392.
7. R. P. Kauffman: *Phys. Rev.* **D41** (1990), 3343.
8. T.L. Barklow: “Using  $e^+e^- \rightarrow \nu\bar{\nu}t\bar{t}$  to probe strong EW symmetry breaking at the NLC”, report from the Proceedings of the 1996 DPF/DPB Summer Study, Snowmass, Colorado, June 25 – July 12, 1996.
9. M. Gintner, S. Godfrey: contribution to the Proceedings of the 1996 DPF/DPB Summer Study, Snowmass, Colorado, June 25 – July 12, 1996, [hep-ph/9612342].
10. F. Larios, C.-P. Yuan: *Phys. Rev.* **D55** (1997), 7218; F. Larios, T. Tait, C.P. Yuan: *Phys.Rev.* **D57** (1998), 3106.
11. M. Gintner, I. Melo: contribution to the Proceedings of the 13 th Conference of the Slovak and Czech physicists, Zvolen, Slovakia, Aug 1999.
12. T. Han, Y.J. Kim, A. Likhoded, G. Valencia: [hep-ph/0005306].
13. S. Weinberg: *Phys. Rev.* **166** (1968), 1568.
14. M. Bando, T. Kugo and K. Yamawaki: *Phys. Rep.* **164** (1988), 217.
15. M. Gintner, I. Melo: *Acta Phys. Slovaca* **51** (2001), 139.
16. S. Dawson: *Nucl. Phys.* **B249** (1985), 42.

# Predictions for Deeply Virtual Compton Scattering on a Spin-One Target

Axel Kirchner<sup>1</sup> and Dieter Müller<sup>2</sup>

<sup>1</sup> Institut für Theoretische Physik, Universität Regensburg, D-93040 Regensburg, Germany

<sup>2</sup> Fachbereich Physik, Universität Wuppertal, D-42097 Wuppertal, Germany

**Abstract.** We consider hard lepton production of a photon on a spin-one target and give the general azimuthal angular dependence of the differential cross section. Furthermore, we estimate the beam spin asymmetry for an unpolarized deuteron target at HERMES.

## 1 Introduction

Exclusive two-photon processes in the light-cone dominated region, i.e., in the generalized Bjorken limit, are most suitable for the exploration of the partonic content in hadrons, since in leading order (LO) both photons directly couple to one quark line [1]. In such processes one can measure, for instance, different photon-to-meson form factors, i.e.,  $\gamma^*\gamma \rightarrow M$ , the production of hadron pairs and also processes like  $\gamma^*N \rightarrow N\gamma$  or  $\gamma N \rightarrow Nl^+l^-$ . The latter two are denoted as deeply virtual Compton scattering (DVCS) in the space- and time-like regions [2–7].

The factorization of short- and long-range dynamics is formally given by the operator product expansion (OPE) of the time ordered product of two electromagnetic currents, which has been worked out at leading twist-two in next-to-leading order (NLO) and at twist-three level in LO of perturbation theory (for references see [7]). However, one should be aware that the partonic hard-scattering part, i.e., the Wilson coefficients, contains collinear singularities, which are absorbed in the non-perturbative distributions by a factorization procedure, which has been proven at twist-two level [8].

The non-perturbative distributions are defined in terms of light-ray operators with definite twist sandwiched between the corresponding hadronic states. These process dependent correlation functions are sensitive to different aspects of hadronic physics. Especially, in DVCS one can access the so-called generalized parton distributions (GPDs). The second moment of the flavour singlet GPDs is related to the expectation value of the energy momentum tensor. Thus, it gives in principle information on the angular orbital momentum fraction of the nucleon spin carried by quarks [9]. We should stress that this process is a new tool to probe the partonic content of the nucleon on the level of amplitudes and, thus, it provides us new information [10].

Recently, the DVCS process has been measured by the H1 collaboration [11] in the small  $x_B$  region (see also [12]) as well as in single beam spin asymmetries by the HERMES [13] and CLAS [14] collaborations. The theoretical predictions

depend on the GPDs, which are unknown. However, they are constrained by sum rules and the reduction to the parton densities in the forward kinematics. All experimental data are consistent with an oversimplified model, which satisfies the constraints and, thus, also with each other [7].

It is appealing to employ DVCS for the investigation of other hadrons and nuclei. An appropriate candidate is deuteron, which has been widely used as a target in lepto-scattering experiments. This nucleus has been extensively studied in both deep-inelastic [15] and elastic [16,17] scattering. From the theoretical point of view it would be desired to have complementary information, which could give us a deeper understanding of this nucleus in terms of its fundamental degree of freedom [18].

In this paper we outline the OPE approach applied to DVCS. Moreover, we determine the azimuthal angular dependence of the cross section for a spin-1 target. Relying on qualitative properties of GPDs, which are consistent with the DVCS data for the proton target, we estimate the size of the beam spin asymmetry for HERMES kinematics.

## 2 General Formalism

For the leptonproduction of a photon

$$l^\pm(k)h(P_1) \rightarrow l^\pm(k')h(P_2)\gamma(q_2) \quad (1)$$

on a hadronic target  $h$  with the mass  $M$  the five-fold cross section

$$\frac{d\sigma}{dx_B dy d|\Delta^2| d\phi d\varphi} = \frac{\alpha^3 x_B y}{16 \pi^2 Q^2 \sqrt{1 + \epsilon^2}} \left| \frac{\mathcal{T}}{e^3} \right|^2, \quad \epsilon \equiv 2x_B \frac{M}{Q}, \quad (2)$$

depends on the Bjorken variable  $x_B = Q^2/2P_1 \cdot q_1$ , where  $Q^2 = -q_1^2$  with  $q_1 = k - k'$ , the momentum transfer square  $\Delta^2 = (P_2 - P_1)^2$ , the lepton energy fraction  $y = P_1 \cdot q_1 / P_1 \cdot k$  and, in general, two azimuthal angle. We use the target rest frame, where the virtual photon three-momentum points towards the negative  $z$ -direction.  $\phi$  is the angle between the lepton and hadron scattering planes and  $\varphi = \Phi - \phi_N$  is the difference of the azimuthal angle  $\Phi$  of the spin vector

$$S^\mu = (0, \cos \Phi \sin \Theta, \sin \Phi \sin \Theta, \cos \Theta) \quad (3)$$

and the azimuthal angle  $\phi_N$  of the recoiled hadron (see [7]).

In the following we consider this process in the (generalized) Bjorken limit,  $Q^2 \sim P_1 \cdot q_1 = \text{large}$ ,  $\Delta^2$  and  $M^2$  are comparably small. The amplitude  $\mathcal{T}$  is the sum of the DVCS  $\mathcal{T}_{\text{DVCS}}$  and Bethe-Heitler (BH)  $\mathcal{T}_{\text{BH}}$  amplitudes:

$$\mathcal{T}^2 = \sum_{\lambda', \lambda'} \{ |\mathcal{T}_{\text{BH}}|^2 + |\mathcal{T}_{\text{DVCS}}|^2 + \mathcal{I} \}, \quad (4)$$

with the interference term

$$\mathcal{I} = \mathcal{T}_{\text{DVCS}} \mathcal{T}_{\text{BH}}^* + \mathcal{T}_{\text{DVCS}}^* \mathcal{T}_{\text{BH}}, \quad (5)$$

where the recoiled lepton ( $\lambda'$ ) and hadron ( $\lambda'$ ) polarization will not be observed.

Each of these three terms in (4) can be calculated in a straightforward manner by the contraction of a known leptonic tensor  $L_{\mu\dots}$  with the DVCS tensor  $T_{\mu\nu}^{\text{DVCS}}$  or/and hadronic current  $J_\alpha$ . The former one is given in terms of GPDs, while the latter one is parametrized in terms of elastic electromagnetic form factors. For instance, the interference term reads

$$\sum_{\lambda'} \mathcal{I} = \frac{\pm e^6}{Q^2 \Delta^2} L^{\mu\nu\alpha}(k, k') T_{\mu\nu}^{\text{DVCS}}(P, \Delta, q) J_\alpha^\dagger(\Delta) + \text{h.c.} \quad \begin{cases} + & \text{for } e^- \\ - & \text{for } e^+ \end{cases}, \quad (6)$$

where  $P = P_1 + P_2$  and  $q = (q_1 + q_2)/2$ . The resulting predictions for the spin-0 and -1/2 targets are presented at the twist-three level in [5,7].

Let us now consider the spin-1 target in more detail. The hadronic current

$$J_\mu = -\epsilon_2^* \cdot \epsilon_1 P_\mu G_1 + (\epsilon_2^* \cdot P \epsilon_{1\mu} + \epsilon_1 \cdot P \epsilon_{2\mu}^*) G_2 - \epsilon_2^* \cdot P \epsilon_1 \cdot P \frac{P_\mu}{2M^2} G_3 \quad (7)$$

is given by three form factors  $G_i(\Delta^2)$  with  $i = \{1, 2, 3\}$ , where  $\epsilon_{1\mu}$  ( $\epsilon_{2\mu}$ ) denote the three polarization vectors for the initial (final) hadron. The form factors  $G_i(\Delta^2)$  have been measured and their parametrizations are available in the literature, see [17] and references therein.

The DVCS hadronic tensor is given by the time-ordered product of the electromagnetic currents  $j_\mu$ , which is sandwiched between hadronic states with different momenta. In LO of perturbation theory and at twist-two accuracy it reads [4]

$$\begin{aligned} T_{\mu\nu}(\xi, \Delta^2, \mathcal{Q}^2) &= \frac{i}{e^2} \int dx e^{ix \cdot q} \langle P_2 | T j_\mu(x/2) j_\nu(-x/2) | P_1 \rangle \\ &= -\mathcal{P}_{\mu\sigma} g_{\sigma\tau} \mathcal{P}_{\tau\nu} \frac{q \cdot V_1}{P \cdot q} - \mathcal{P}_{\mu\sigma} i \epsilon_{\sigma\tau q\rho} \mathcal{P}_{\tau\nu} \frac{A_{1\rho}}{P \cdot q}, \end{aligned} \quad (8)$$

where the projection operator  $\mathcal{P}_{\mu\nu} = g_{\mu\nu} - q_{1\mu} q_{2\nu} / q_1 \cdot q_2$  ensures gauge invariance. For convenience we introduced the scaling variable  $\xi \approx \frac{x_B}{2-x_B}$ . At twist-two level the amplitudes  $V_1$  and  $A_1$  can be decomposed in a complete basis of nine Compton form factors (CFFs). Adopting the notation of [18], they read in the vector case

$$\begin{aligned} V_\mu &= -\epsilon_2^* \cdot \epsilon_1 P_\mu \mathcal{H}_1 + (\epsilon_2^* \cdot P \epsilon_{1\mu} + \epsilon_1 \cdot P \epsilon_{2\mu}^*) \mathcal{H}_2 - \epsilon_2^* \cdot P \epsilon_1 \cdot P \frac{P_\mu}{2M^2} \mathcal{H}_3 \\ &\quad + (\epsilon_2^* \cdot P \epsilon_{1\mu} - \epsilon_1 \cdot P \epsilon_{2\mu}^*) \mathcal{H}_4 + \left( \frac{2M^2 \{ \epsilon_2^* \cdot q \epsilon_{1\mu} + \epsilon_1 \cdot q \epsilon_{2\mu}^* \}}{P \cdot q} + \frac{\epsilon_2^* \cdot \epsilon_1}{3} P_\mu \right) \mathcal{H}_5, \end{aligned} \quad (9)$$

and in the axial-vector case

$$\begin{aligned} A_\mu &= i \epsilon_{\mu\epsilon_2^* \epsilon_1 P} \tilde{\mathcal{H}}_1 - \frac{i \epsilon_{\mu\Delta P \epsilon_1} \epsilon_2^* \cdot P + i \epsilon_{\mu\Delta P \epsilon_2^*} \epsilon_1 \cdot P}{M^2} \tilde{\mathcal{H}}_2 \\ &\quad - \frac{i \epsilon_{\mu\Delta P \epsilon_1} \epsilon_2^* \cdot P - i \epsilon_{\mu\Delta P \epsilon_2^*} \epsilon_1 \cdot P}{M^2} \tilde{\mathcal{H}}_3 - \frac{i \epsilon_{\mu\Delta P \epsilon_1} \epsilon_2^* \cdot q + i \epsilon_{\mu\Delta P \epsilon_2^*} \epsilon_1 \cdot q}{q \cdot P} \tilde{\mathcal{H}}_4, \end{aligned} \quad (10)$$

where  $1/Q$ -power suppressed effects have been neglected. The remaining logarithmic  $Q$ -dependence is governed by perturbation theory.

The CFFs in (9) and (10) are given by a convolution of perturbatively calculable coefficient functions  $C^{(\pm)}$  and twist-two GPDs via

$$\mathcal{H}_k(\xi) = \sum_{i=u,\dots} \int_{-1}^1 dx C_i^{(-)}(\xi, x) H_k^i(x, \eta)|_{\eta=-\xi}, \quad \text{for } k = \{1, \dots, 5\}, \quad (11)$$

$$\tilde{\mathcal{H}}_k(\xi) = \sum_{i=u,\dots} \int_{-1}^1 dx C_i^{(+)}(\xi, x) \tilde{H}_k^i(x, \eta)|_{\eta=-\xi}, \quad \text{for } k = \{1, \dots, 4\}. \quad (12)$$

For each quark species  $i$  we have nine GPDs. The two sets  $\{H_1^i, \dots, H_5^i\}$  and  $\{\tilde{H}_1^i, \dots, \tilde{H}_4^i\}$  are defined by off-forward matrix elements of vector and axial-vector light-ray operators. The coefficient functions  $C^{(\mp)}$  have perturbative expansion. In LO they read for the even  $(-)$  and odd  $(+)$  parity sectors

$$\xi C_{(0)i}^{(\mp)}(\xi, x) = \frac{Q_i^2}{1 - x/\xi - i0} \mp \frac{Q_i^2}{1 + x/\xi - i0}, \quad (13)$$

where  $Q_i$  is the fractional quark charge.

Employing the parametrizations (7), (9) and (10), the contractions of leptonic and hadronic tensors provide the kinematically exact expression for the squared BH term (of course, in tree approximation), while the interference term

$$\begin{aligned} \sum_{\lambda'} \mathcal{T}_{\text{BH}} \mathcal{T}_{\text{DVCS}}^* = & \quad (14) \\ & \frac{2 - 2y + y^2}{y^2 \mathcal{P}_1(\phi) \mathcal{P}_2(\phi)} \frac{4\xi}{\Delta^2 Q^4} \left( k^\sigma - \frac{q^\sigma}{y} \right) \left[ \left( J_\sigma + 2\Delta_\sigma \frac{q \cdot J}{Q^2} \right) q \cdot V_1^\dagger + 2i\epsilon_{\sigma q \Delta J} \frac{q \cdot A_1^\dagger}{Q^2} \right] \\ & + \frac{\lambda(2 - y)y}{y^2 \mathcal{P}_1(\phi) \mathcal{P}_2(\phi)} \frac{4\xi}{\Delta^2 Q^4} \left( k^\sigma - \frac{q^\sigma}{y} \right) \left[ \left( J_\sigma + 2\Delta_\sigma \frac{q \cdot J}{Q^2} \right) q \cdot A_1^\dagger + 2i\epsilon_{\sigma q \Delta J} \frac{q \cdot V_1^\dagger}{Q^2} \right], \end{aligned}$$

and the squared DVCS amplitude

$$\begin{aligned} \sum_{\lambda'} |\mathcal{T}_{\text{DVCS}}|^2 = & 8 \frac{2 - 2y + y^2}{y^2} \frac{\xi^2}{Q^6} \left( q \cdot V_1 \ q \cdot V_1^\dagger + q \cdot A_1 \ q \cdot A_1^\dagger \right) \\ & + 8 \frac{\lambda(2 - y)}{y} \frac{\xi^2}{Q^6} \left( q \cdot V_1 \ q \cdot A_1^\dagger + q \cdot A_1 \ q \cdot V_1^\dagger \right) \end{aligned} \quad (15)$$

are expanded with respect to  $1/Q$ . In contrast to the squared DVCS amplitude the interference as well as the squared BH terms have an additional  $\phi$ -dependence due to the (scaled) BH propagators

$$\mathcal{P}_1 \approx -\frac{1}{y} \{1 - y + 2K \cos(\phi)\}, \quad \mathcal{P}_2 \approx \frac{1}{y} \{1 + 2K \cos(\phi)\}. \quad (16)$$

The kinematical factor

$$K \approx \sqrt{-\frac{\Delta^2}{Q^2}(1-x_B)(1-y)} \left(1 - \frac{\Delta_{\min}^2}{\Delta^2}\right). \quad (17)$$

vanishes at the kinematical boundary  $\Delta^2 = \Delta_{\min}^2 \approx M^2 x_B^2 / (1-x_B)$ .

### 3 Observables for Leptoproduction of a Photon

In our frame the contractions of leptonic and hadronic tensors, see (6), yield finite sums of Fourier harmonics, whose form is governed by general principles. After summation over the final polarization states, which is not indicated below, the three parts of the squared amplitude read for massless leptons [7]:

$$|\mathcal{T}_{\text{BH}}|^2 = \frac{e^6(1+\epsilon^2)^{-2}}{x_B^2 y^2 \Delta^2 \mathcal{P}_1(\phi) \mathcal{P}_2(\phi)} \left\{ c_0^{\text{BH}} + \sum_{n=1}^2 [c_n^{\text{BH}} \cos(n\phi) + s_n^{\text{BH}} \sin(\phi)] \right\}, \quad (18)$$

$$|\mathcal{T}_{\text{DVCS}}|^2 = \frac{e^6}{y^2 Q^2} \left\{ c_0^{\text{DVCS}} + \sum_{n=1}^2 [c_n^{\text{DVCS}} \cos(n\phi) + s_n^{\text{DVCS}} \sin(n\phi)] \right\}, \quad (19)$$

$$\mathcal{I} = \frac{\pm e^6}{x_B y^3 \mathcal{P}_1(\phi) \mathcal{P}_2(\phi) \Delta^2} \left\{ c_0^{\mathcal{I}} + \sum_{n=1}^3 [c_n^{\mathcal{I}} \cos(n\phi) + s_n^{\mathcal{I}} \sin(n\phi)] \right\}, \quad (20)$$

where the  $+$  ( $-$ ) sign in the interference stands for the negatively (positively) charged lepton beam.

The Fourier coefficients can be calculated from (14), (15), and an analogous one for the squared BH amplitude by summing over the polarization  $\Lambda'$ , where we can employ the common projector technique. For a spin-1 particle we have (see for instance [19])

$$\begin{aligned} \epsilon_{1\mu}^*(\Lambda=0)\epsilon_{1\nu}(\Lambda=0) &= S_\mu S_\nu, \\ \epsilon_{1\mu}^*(\Lambda=\pm 1)\epsilon_{1\nu}(\Lambda=\pm 1) &= \frac{1}{2} \left( -g_{\mu\nu} + \frac{P_{1\mu}P_{1\nu}}{M^2} - S_\mu S_\nu + \frac{i\Lambda}{M} \epsilon_{\mu\nu P_1 S} \right), \end{aligned} \quad (21)$$

where  $\Lambda = \{+1, 0, -1\}$  denotes the magnetic quantum number with respect to the quantization direction given by the spin vector  $S_\mu$  defined in (3). Obviously, the spin sum of the recoiled hadron is

$$\sum_{\Lambda'=-1}^1 \epsilon_{2\mu}^*(\Lambda')\epsilon_{2\nu}(\Lambda') = -g_{\mu\nu} + \frac{P_{2\mu}P_{2\nu}}{M^2}. \quad (22)$$

As we see, for a spin-1 target the Fourier coefficients quadratically depend on the spin vector  $S_\mu$  and, thus, we find the following decomposition

$$\begin{aligned} c_n^T &= c_{n,\text{unp}}^T + c_{n,\text{LP}}^T \cos(\Theta) + c_{n,\text{TP}}^T(\varphi) \sin(\Theta) + c_{n,\text{LTP}}^T(\varphi) \sin(2\Theta) \\ &\quad + c_{n,\text{LLP}}^T \cos^2(\Theta) + c_{n,\text{TTP}}^T(\varphi) \sin^2(\Theta) \end{aligned} \quad (23)$$

for  $T = \{\text{BH}, \mathcal{I}, \text{DVCS}\}$ . An analogous decomposition holds true for the odd harmonics  $s_n^T$ . The unpolarized and the longitudinally polarized coefficients  $c/s_{n,\text{unp}}^T$ ,  $c/s_{n,\text{LP}}^T$ , and  $c/s_{n,\text{LLP}}^T$ , respectively, are independent of  $\varphi$ . The transverse coefficients  $c/s_{n,\text{TP}}^T$  and the transverse-longitudinal interference terms can be decomposed with respect to the first harmonics in the azimuthal angle  $\varphi$

$$c_{n,\text{TP}}^T(\varphi) = c_{n,\text{TP}+}^T \cos(\varphi) + s_{n,\text{TP}-}^T \sin(\varphi), \quad (24)$$

$$c_{n,\text{LTP}}^T(\varphi) = c_{n,\text{LTP}+}^T \cos(\varphi) + s_{n,\text{LTP}-}^T \sin(\varphi), \quad (25)$$

while  $c/s_{n,\text{TTP}}^T$  may be written as

$$c_{n,\text{TTP}}^T(\varphi) = c_{n,\text{TTP}\Sigma}^T + c_{n,\text{TTP}\Delta}^T \cos(2\varphi) + s_{n,\text{TTP}\pm}^T \sin(2\varphi). \quad (26)$$

Analogous equations hold true for the odd harmonics (just replace  $c \leftrightarrow s$ ). Let us add that with this notation the  $c(s)$  harmonics are given by the real (imaginary) part of certain linear combinations of form factors and/or CFFs.

Altogether we have for a given harmonic in  $\phi$  nine possible observables<sup>1</sup>. In principle, they can be measured by an appropriate adjustment of the spin vector and Fourier analysis with respect to the azimuthal angle  $\varphi$ . The interference term linearly depends on the CFFs and is, thus, of special interest. In facilities that have both kinds of leptons it can be separated by means of the charge asymmetry. The dominant harmonics are  $c/s_1^T$ , predicted at leading twist-two. We write them as product of leptonic prefactors  $\mathcal{L}$  and ‘universal’ functions  $\mathcal{C}_i^T$ :

$$\begin{Bmatrix} c_{1,i}^{\mathcal{I}} \\ s_{1,i}^{\mathcal{I}} \end{Bmatrix} = \begin{Bmatrix} \mathcal{L}_{1,i}^{\mathcal{I}c} \\ \mathcal{L}_{1,i}^{\mathcal{I}s} \end{Bmatrix} \begin{Bmatrix} \Re \\ \Im \end{Bmatrix} \mathcal{C}_i^{\mathcal{I}}, \quad \text{for } i = \{\text{unp}, \dots, \text{TTP}-\}. \quad (27)$$

As mentioned before, they depend on nine CFFs

$$\mathcal{C}_i^{\mathcal{I}} = (G_1 \cdots G_3) \mathcal{M}_i^{\mathcal{I}} \begin{pmatrix} \mathcal{H}_1 \\ \vdots \\ \tilde{\mathcal{H}}_4 \end{pmatrix}, \quad (28)$$

where the matrix  $\mathcal{M}$  will be presented elsewhere [20]. Single spin-flip and unpolarized as well as double spin-flip contributions provide the imaginary and real part, respectively, of the nine linear combinations  $\mathcal{C}_i^{\mathcal{I}}$ .

## 4 Estimate of the Beam-Spin Asymmetry

In this section we estimate the size of the beam spin asymmetry

$$A_{\text{LU}}(\phi) = \frac{d\sigma^\uparrow(\phi) - d\sigma^\downarrow(\phi)}{d\sigma^\uparrow(\phi) + d\sigma^\downarrow(\phi)}, \quad (29)$$

<sup>1</sup> Note that  $c_{n,\text{TTP}\Sigma}^T$  does not belong to an independent frequency, rather it can be included in the constant and  $\cos^2(\theta)$  terms of (23).



at large  $y$  and small momentum transfer for the HERMES experiment. We should also ensure that  $M^2/Q^2$  corrections are under control. Since  $M = 1875.6$  MeV we require  $Q^2 \geq 4$  GeV<sup>2</sup>. Because of large  $y$ , the BH amplitude dominates the DVCS one and thus the beam spin asymmetry is approximately determined by

$$A_{\text{LU}}(\phi) \sim \pm \frac{x_B}{y} \frac{s_{1,\text{unp}}^T}{c_{0,\text{unp}}^{\text{BH}}} \sin(\phi) \quad \text{with} \quad \begin{cases} + & \text{for } e^- \\ - & \text{for } e^+ \end{cases}. \quad (30)$$

For  $-\Delta_{\text{min}} \ll -\Delta^2 \ll M^2$  and  $x_B \lesssim 0.3$  the Fourier coefficients can be drastically simplified due a crude approximation of kinematical factors

$$A_{\text{LU}}(\phi) \sim \pm \sqrt{\frac{-\Delta^2}{Q^2} (1-y)} \frac{x_B \Im \mathcal{H}_1(\xi, \Delta^2, Q^2)|_{\xi=x_B/2}}{G_1(\Delta^2)} \sin(\phi). \quad (31)$$

For a spin-1/2 target one finds the analogous equation, i.e.,  $G_1 \rightarrow F_1$  and  $\mathcal{H}_1 \rightarrow \mathcal{H}$ . Note that the same rule

$$\int_{-1}^1 dx \left( Q_u \left\{ \frac{H_1}{H} \right\}_{u_v}(x, \xi, \Delta^2, Q^2) + Q_d \left\{ \frac{H_1}{H} \right\}_{d_v}(x, \xi, \Delta^2, Q^2) \right) = \left\{ \frac{G_1}{F_1} \right\}(\Delta^2) \quad (32)$$

suggest that the  $\Delta^2$ -dependence of the valence-quark GPDs is essentially given by  $G_1$  and  $F_1$ , respectively. The analyses of the H1, HERMES and CLAS data at LO indicate that the  $\Delta^2$  fall-off of the sea-quark GPDs is steeper than the valence quark ones. Thus, we neglect the sea quark contribution and write the valence like GPDs as a product of form factor and quark distribution function

$$\frac{\Im \mathcal{H}(\xi, \Delta^2)}{F_1(\Delta^2)} \sim \pi \{ Q_u^2 q_{u_v}(\xi) + Q_d^2 q_{d_v}(\xi) \}_{|\xi=x_B/2}, \quad (33)$$

$$\frac{\Im \mathcal{H}_1(\xi, \Delta^2)}{G_1(\Delta^2)} \sim \pi \frac{Q_u^2 + Q_d^2}{2} \{ q_{u_v}(\xi) + q_{d_v}(\xi) \}_{|\xi=x_B/2}. \quad (34)$$

For HERMES kinematics with central values  $\langle x_B \rangle = 0.11$ ,  $\langle \Delta^2 \rangle = -0.27$  GeV<sup>2</sup> and  $\langle Q^2 \rangle = 2.6$  GeV<sup>2</sup> we find with the MRS A' parametrization  $A_{\text{LU}}(\phi) \sim 0.3 \sin(\phi)$  for positron-proton scattering, which is consistent with experimental data [13]. For  $Q^2 = 4$  GeV<sup>2</sup>,  $x_B = 0.1$  and  $\Delta^2 = -0.3$  GeV<sup>2</sup> we estimate

$$\begin{aligned} A_{\text{LU}}(\phi) &\sim -0.13 \sin(\phi) && \text{for deuteron target,} \\ A_{\text{LU}}(\phi) &\sim -0.16 \sin(\phi) && \text{for proton target.} \end{aligned} \quad (35)$$

## 5 Summary

We gave the general azimuthal angular dependence of the leptonproduction cross section of a photon on a spin-1 target. Such experiments allow to study the deuteron from a new perspective. Compared to DIS or elastic lepton-deuteron scattering, they provide additional information, contained in the CFFs.

At twist-two level there are nine CFFs. In the case of a polarized beam and target, with an adjustable quantization direction, the imaginary and real part of all these CFFs can be separately measured by means of the charge asymmetry. Moreover, an appropriate Fourier analysis allows to eliminate the twist-three contamination. In this way one gets the maximal access to the deuteron GPDs at twist-two level, with a contamination of  $M^2/Q^2$  and  $\Delta^2/Q^2$  contributions.

As discussed, for certain kinematics the beam spin asymmetry is essentially determined by one CFF only. Although the approximations are rather crude, the result can serve to obtain a qualitative understanding of this GPD. The LO analysis of the pioneering measurements of DVCS [11,13,14] on the proton suggest for  $-\Delta^2 \sim 0.3 \text{ GeV}^2$  the dominance of valence-quark GPDs with no essential enhancement by the skewedness effect. Assuming the same features also for the deuteron GPDs, we estimated the size of the beam spin asymmetry.

## References

1. D. Müller, D. Robaschik, B. Geyer, F.-M. Dittes, and J. Hořejši, *Fortschr. Phys.* **42**, 101 (1994).
2. A. Radyushkin, *Phys. Lett. B* **380**, 417 (1996); X. Ji, *Phys. Rev. D* **55**, 7114 (1997).
3. M. Diehl, T. Gousset, B. Pire, and J. P. Ralston, *Phys. Lett. B* **411**, 193 (1997).
4. A. Belitsky, D. Müller, L. Niedermeier, and A. Schäfer, *Nucl. Phys. B* **593**, 289 (2001).
5. A. Belitsky, D. Müller, A. Kirchner, and A. Schäfer, *Phys. Rev. D* **64**, 116002 (2001).
6. E. R. Berger, M. Diehl, and B. Pire, *Timelike Compton scattering: Exclusive photoproduction of lepton pairs*, hep-ph/0110062 (2001).
7. A. V. Belitsky, D. Müller, and A. Kirchner, *Theory of deeply virtual compton scattering on the nucleon*, hep-ph/0112108 (2001).
8. J. Collins and A. Freund, *Phys. Rev. D* **59**, 074009 (1999); X. Ji and J. Osborne, *Phys. Rev. D* **58**, 094018 (1998).
9. X. Ji, *Phys. Rev. Lett.* **78**, 610 (1997).
10. J. Ralston and B. Pire, *Femto-photography of protons to nuclei with deeply virtual Compton scattering*, (2001).
11. C. Adloff et al., *Phys. Lett. B* **517**, 47 (2001).
12. P. R.B. Saull (ZEUS Coll.), *Prompt photon production and observation of deeply virtual compton scattering*, hep-ex/0003030 (2000).
13. A. Airapetian et al., *Phys. Rev. Lett.* **87**, 182001 (2001).
14. S. Stepanyan et al., *Phys. Rev. Lett.* **87**, 182002 (2001).
15. P. Hoodbhoy, R. Jaffe, and A. Manohar, *Nucl. Phys. B* **312**, 571 (1989).
16. S. Brodsky, C.-R. Ji, and G. Lepage, *Phys. Rev. Lett.* **51**, 83 (1983).
17. R. Gilman and F. Gross, *Electromagnetic structure of the deuteron*, nuc-th/0111015 (2001); M. Garçon and J. V. Orden, *The deuteron: structure and form factors*, nuc-th/0102049 (2001).
18. E. R. Berger, F. Cano, M. Diehl, and B. Pire, *Phys. Rev. Lett.* **87**, 142302 (2001).
19. G. Passarino, *Nucl. Phys. B* **237**, 249 (1984).
20. A. Kirchner and D. Müller, *in preparation*.

# $H \rightarrow \tau\tau$ Studies in CMS

Alexander Nikitenko

Imperial College, London, UK

**Abstract.** We present a current status of the studies on possibility to observe with CMS detector  $A$  and  $H$  bosons (in the framework of the Minimal Super Symmetry Model) decaying into two  $\tau$  leptons and Standard Model Higgs boson produced via weak boson fusion and decaying into two  $\tau$ 's.

## 1 CMS Reach on SUSY $A$ , $H \rightarrow \tau\tau$

It has been shown with fast simulations of the CMS detector that  $A$ ,  $H \rightarrow \tau\tau$  decay may be a discovery mode in a significant region of  $M_A$ ,  $\tan(\beta)$  parameter space already with  $30 \text{ fb}^{-1}$  of the data [1–3]. CMS is currently optimising with full simulations the trigger and off-line selections for all final states : lepton-lepton, lepton+ $\tau$  jet and two  $\tau$  jets. We describe here the most recent results on selection of Higgs decays with two  $\tau$  jets.

$A, H \rightarrow \tau\tau$  with 2  $\tau$  jet hadronic final states have been shown to extend significantly the SUSY Higgs discovery reach into the large mass (600 - 800 GeV) range [2]. To exploit fully the 2  $\tau$  jet final states - especially in the low ( $\sim 200$  GeV) mass range - an efficient hadronic  $\tau$  trigger has been developed based on Level-1 calorimeter selection, Level-2 electromagnetic calorimeter isolation [4] and a Level-3 tracking (isolation) using the only pixel detector information [5].

Level-1 calorimeter single or double Tau trigger with thresholds 80 and 65 GeV for  $L = 2 \times 10^{33} \text{ cm}^{-2} \text{ s}^{-1}$  selects  $A, H \rightarrow \tau\tau \rightarrow 2\tau$  jet events useful for off-line analysis with an efficiency of about 0.9 while giving an output QCD background rate of about 6 kHz. A further reduction of the QCD background rate by a factor  $\sim 10^3$  is possible at the High Level Trigger path (Level2 calorimeter and Level3 Pixels) with an efficiency of  $\sim 40\%$  for the signal at  $m_H = 200$  and 500 GeV [6] as one can see in Fig. 1. Similar performance is expected using the regional tracking option of the CMS High Level Trigger once the CPU performance is proven to be satisfactory. For the off-line  $\tau$  identification the tracker information is used. The fast simulation of the CMS detector [7] is used to study the signal to background ratios. The track reconstruction efficiency evaluated with full simulation of CMS tracker is included as a function of  $p_t$  and  $\eta$  for the track. The  $\tau$  jet candidate ( $E_t > 60$  GeV) is required to contain a hard ( $p_t > 40$  GeV) charged track within  $\Delta R < 0.1$  around the calorimeter jet axis. Around this leading track in a cone of  $\Delta R < 0.03$  two other tracks with  $p_t > 1$  GeV are accepted to include the 3-prong  $\tau$  decays. This narrow cone with one or

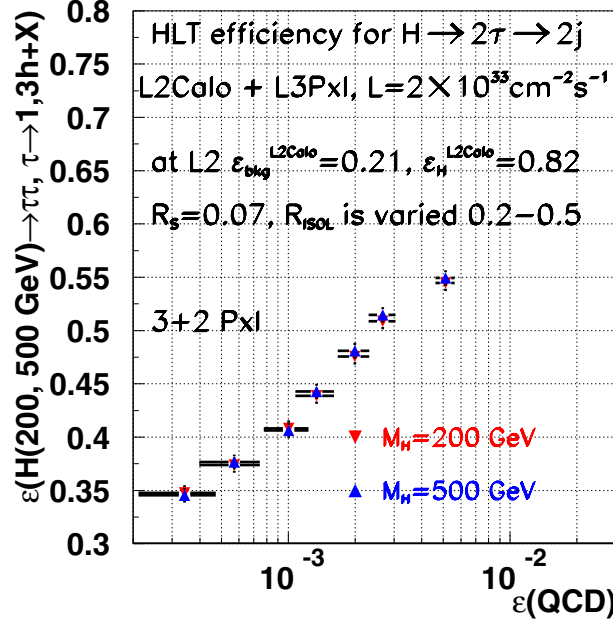


**Fig. 1.** Efficiency of QCD background and Higgs signal at High Level Trigger when the size of the pixel isolation cone is varied.

three hard tracks is required to be isolated demanding that no track with  $p_t > 1$  GeV is found in the surrounding larger cone of  $\Delta R < 0.4$ . Efficiency for this  $\tau$  selection is 7.2% for  $m_A = 200$  GeV and 34% for  $m_A = 500$  GeV. Accepting the 3-prong decays in the narrow cone of  $\Delta R < 0.03$  increases the event rate for  $A, H \rightarrow \tau\tau \rightarrow 2\tau$  jets in the high mass range ( $m_A = 500$  GeV) by  $\sim 1.7$  but also degrade significantly the QCD rejection factor for hard QCD jets. Figure 2 (left plot) shows the rejection factor against the QCD jets for the 1/3 prong selection a function of  $E_t$  jet compared to the one prong selection with one hard ( $p_t > 40$  GeV) charged track within  $\Delta R(jet, track) < 0.1$ . Optimisation is still needed for the low mass range for more efficient selection mainly by increasing the size of the narrow cone.

A further suppression can be obtained exploiting the  $\tau$  lifetime using  $\tau$  vertex reconstruction or impact parameter measurement or a combination of them. A full simulation study indicates that an additional rejection factor of  $\sim 5$  against the 3-prong QCD jets and an efficiency of  $\sim 80\%$  for the  $\tau$  jets can be obtained with  $\tau$  vertex reconstruction as it is shown in Fig. 2 (right plot). Promising results are also obtained from the impact parameter method in the channel  $A, H \rightarrow \tau\tau \rightarrow \ell^+\ell^- + X$  using full simulation combining the impact parameter measurements for the two leptons from  $\tau$  decays to reduce the backgrounds with  $W \rightarrow \ell\nu$  and  $Z \rightarrow \ell\ell$  decays [3].

The resolution of the reconstructed Higgs mass and even more so the mass reconstruction efficiency in  $A, H \rightarrow \tau\tau$  events is very sensitive to the  $E_t^{miss}$

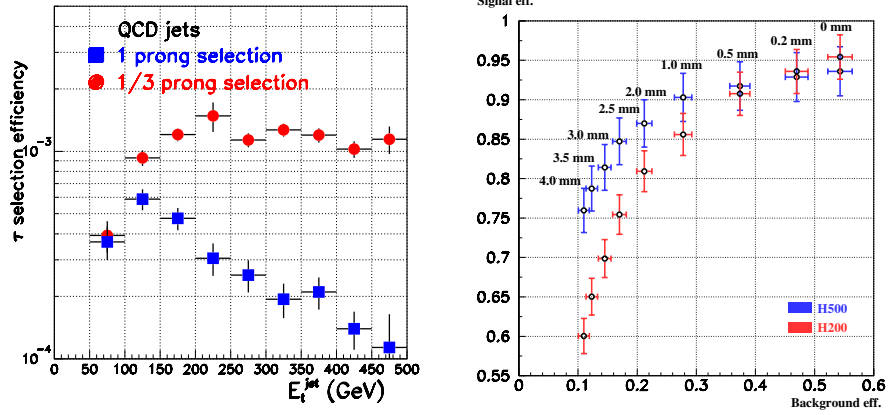


**Fig. 2.** Left plot - rejection factor against the QCD jets as a function of  $E_t^{jet}$  for the 1 and 1/3 prong  $\tau$  selection; Right plot - rejection factor against the QCD jet v.s. efficiency for  $\tau$  jet with cut on the distance between reconstructed primary and the secondary vertex of  $\tau$  jet candidate

measurement. The absolute value of  $E_t^{miss}$  is relatively small in these events making the mass reconstruction and background reduction with a cut in  $E_t^{miss}$  a difficult task. Figure 3 (left plot) shows the Higgs mass reconstructed with full simulation for  $b\bar{b}A$ ,  $A \rightarrow \tau\tau \rightarrow 2\tau$  jets with  $m_A = 500$  GeV and  $\tan\beta = 20$  [8]. Resolution of the reconstructed Higgs mass is 14.5% for  $m_A = 200$  GeV and 14.9% for  $m_A = 500$  GeV and the corresponding reconstruction efficiencies are 37% and 36%, respectively (including  $\Delta\phi < 175^\circ$  cut and requiring positive neutrino energies). This confirms the earlier results of the fast simulation study [2].

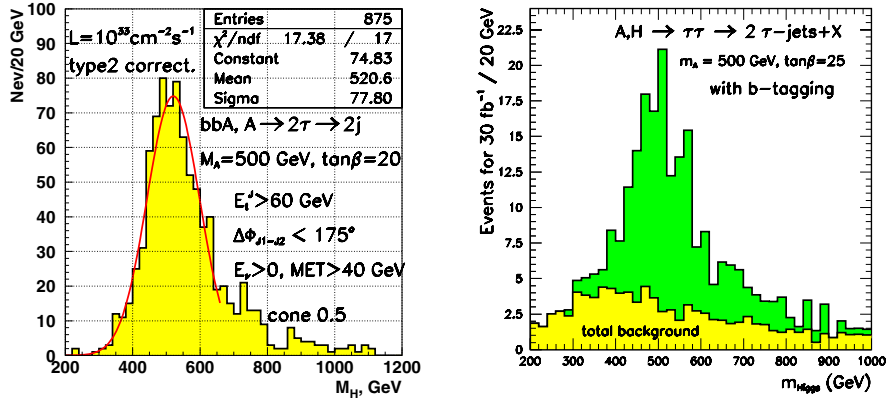


**Fig. 3.** Left plot - reconstructed Higgs mass for  $b\bar{b} H \rightarrow \tau\tau \rightarrow 2\tau$  jets with  $m_H = 500$  GeV; Right plot - Higgs mass for  $H \rightarrow \tau\tau \rightarrow 2\tau$  jets with  $m_H = 500$  GeV and  $\tan\beta = 25$  superimposed on the total background for  $30 \text{ fb}^{-1}$ . One tagged b-jet is required.

The large  $Z, \gamma^* \rightarrow \tau\tau$  background can be reduced efficiently only with b-tagging in the associated production processes  $b\bar{b}H_{SUSY}$ . The associated b-jets are soft and uniformly distributed over  $|\eta| < 2.5$ . Nevertheless, a study with full simulation shows that a b-tagging efficiency of  $\sim 34\%$  per jet can be obtained for the signal events with a mistagging rate less than 1% for  $Z + jets$  events [3]. Requiring one tagged b-jet reduces efficiently also QCD background thus improving significantly the signal visibility. Figure 3 (right plot) shows the signal for  $m_H = 500$  GeV and  $\tan\beta = 25$  superimposed on the total background with b-tagging. The missing transverse energy  $E_t^{miss}$  plays a major role in the Higgs mass reconstruction as discussed above. However, a cut in  $E_t^{miss}$  does not improve significantly the mass resolution and therefore, in order to retain the signal statistics, is not used in this study. Figure 4 shows the expected discovery reach for 30  $\text{fb}^{-1}$  assuming maximal stop mixing scenario [9]. The expectations for other important MSSM Higgs discovery channels in CMS [10] and the exclusion region from LEP II [11] are also shown in the figure. The  $A, H \rightarrow \tau\tau$  channels are found to be insensitive for stop mixing, the SUSY scale and for the sign of the Higgsino mass parameter  $\mu$  for high enough  $\tan\beta$  ( $\gtrsim 10$ ). A systematic study of the  $A, H \rightarrow \tau\tau$  with  $\ell^+\ell^-$  and lepton+ $\tau$  jet final states is also presently in progress in CMS including full simulation the combined triggers,  $\tau$  identification,  $\tau$  tagging with impact parameter and vertex reconstruction, Higgs mass reconstruction and b-tagging in the associated production channels.

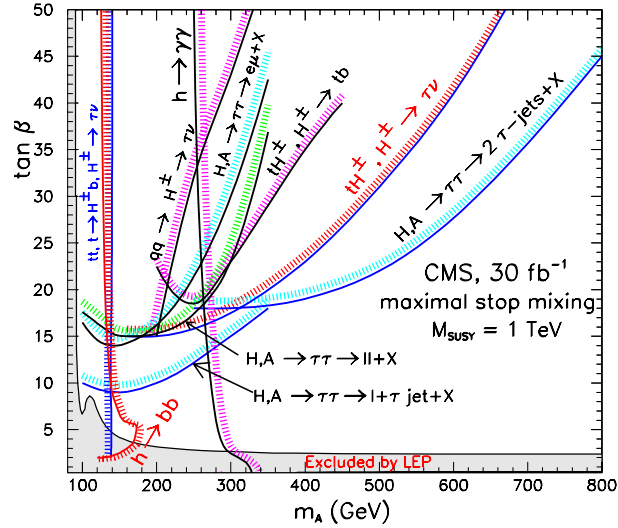


**Fig. 4.** Expected  $5\sigma$  discovery reach for the MSSM Higgs bosons in CMS in the maximal mixing scenario for  $30\text{fb}^{-1}$  as a function of  $m_A$  and  $\tan\beta$ . The shaded area is excluded by LEP

## 2 Observability of SM Higgs $qq \rightarrow qqH, H \rightarrow \tau\tau$

It has been shown in [12] that observability at LHC of the light Standard Model Higgs boson produced via weak boson fusion and decaying into  $\gamma\gamma, \tau\tau$  and  $WW$  may significantly extend the measurement of the Higgs boson couplings. We present here the CMS fast simulation study on  $\tau\tau$  mode with lepton+ $\tau$  jet final state and comparison with parton level simulation done in [14].

### 2.1 Signal and Background Generation

Higgs events produced via weak boson fusion have been generated with PYTHIA5.7 [13]. Backgrounds considered in this study are QCD and EW production of  $Z + jj$  ( $Z \rightarrow \tau\tau \rightarrow l + \tau$  jet) and  $W + 3j$  ( $W \rightarrow e(\mu) + \nu$ ). We didn't consider  $b\bar{b} + jj$  background, however it's expected to be relatively small [14]. QCD  $Z + jj$  production has been generated with LO matrix element from D. Zeppenfeld interfaced with PYTHIA. EW  $Z + jj$  production has been simulated with COMPHEP [15] interfaced with PYTHIA.  $W + 3j$  events have been produced with PYTHIA which may underestimate cross-section.

Fast detector simulation with CMSJET [7] has been performed both for the signal and background events. One of the key point of all searches for the light Higgs produced via weak boson fusion is a mini jet veto : veto events with additional soft ( $E_T > 20$  GeV) jet(s) inside rapidity gap between two tagging jets. An efficiency of mini jet veto is extremely sensitive to a such effects as calibration, electronic noise and readout thresholds, interaction of soft particles in the tracker in front of the calorimeter, magnetic field, pile up activity. Since we didn't expect that fast CMSJET simulation can properly reproduce some of those effects, we did not evaluate mini jet veto efficiency from CMSJET simulation. We use instead the efficiency of mini jet veto  $P_{surv}$  taken from [16] : 0.87 for the signal and EW  $Z + jj$  background and 0.28 for QCD backgrounds as a multiplicative factor.  $P_{surv}$  calculated in [16] is a probability to radiate an additional jet (parton) in the rapidity gap between two tagging jets. It's assumed that a such jets is reconstructed with 100 % efficiency. CMS full simulation study on soft jet reconstruction [17] shows that with a dedicated window algorithm it's possible to reconstruct 20 GeV jets at low luminosity with a good purity and about 100 % efficiency. The problem of the false jet reduction however has still to be investigated.

We use off-line  $\tau$  jet identification efficiency with calorimeter and tracker 0.32 and jet misidentification as  $\tau$  jet 0.0019 obtained from the full simulations [18]. A realistic efficiency of the lepton triggering and reconstruction of 0.9 is used.

### 2.2 Event Selections and Results

In the event selection the following cuts are applied:

- $p_T^l > 15\text{GeV}, |\eta_l| < 2.4;$
- $E_T^{\tau-jet} > 30\text{GeV}, |\eta_{\tau-jet}| < 2.4;$

- $\eta_{j \min} + 0.7 < \eta_{l, \tau\text{-jet}} < \eta_{j \max} - 0.7$ ;
- $|\eta_{j1} - \eta_{j2}| > 4.4, \quad \eta_{j1}\eta_{j2} < 0$ ;
- $M_{j1j2} > 1000 \text{ GeV}$ ;
- $m_t(l, \not{p}_T) < 30 \text{ GeV}$ ;
- $0 < x_{\tau l} < 0.75, \quad 0 < x_{\tau h} < 1$ ;
- $|m_{\tau\tau} - m_H| < 15 \text{ GeV}$ ;

where  $x_{\tau l}$  and  $x_{\tau h}$  is a fraction of the visible (measured) energy of  $\tau$  leptons and  $j_1$  and  $j_2$  means tagging jets.

Number of signal events for  $M_H=135 \text{ GeV}$  and number of different background events expected after all selections for an integrated luminosity  $30 \text{ fb}^{-1}$  are shown in Table 1. An errors correspond to MC statistics used in this study. For comparison a number of events estimated in [14] are also shown in the second row.

**Table 1.** Number of signal and different background events expected after all selections for an integrated luminosity  $30 \text{ fb}^{-1}$

Higgs, $M_H=135 \text{ GeV}$	QCD Z+jj	EW Z+jj	W+3j
$6.7 \pm 0.3$	$0.63 \pm 0.10$	$0.74 \pm 0.08$	$0.14 \pm 0.05$
6.2 (from [14])	total background from [14] is 1.1		

**Table 2.** Number of signal and total number of background events expected after all selections for an integrated luminosity  $30 \text{ fb}^{-1}$ . Higgs production cross-section in pb and  $Br(H \rightarrow \tau\tau)$  as calculated by VV2H and HDECAY are shown in the first two rows

$M_H, \text{ GeV}$	115	125	135	145
$\sigma(qq \rightarrow qqH), \text{ pb}$	4.49	4.15	3.81	3.57
$Br(H \rightarrow \tau\tau), \%$	7.2	6.1	4.5	2.6
Signal	12.6	9.9	6.7	3.6
Total background	5.5	2.3	1.5	1.1

Number of signal and total number of background events expected after all selections for an integrated luminosity  $30 \text{ fb}^{-1}$  are shown in Table 2. Higgs production cross-section in pb and  $Br(H \rightarrow \tau\tau)$  as calculated by VV2H and HDECAY packages [19] are presented in the first two rows of Table 2.

The reconstructed effective mass of two  $\tau$  leptons for the background QCD and EW  $Z + jj$  ( $Z \rightarrow \tau\tau \rightarrow l + \tau \text{ jet}$ ) and Higgs of  $M_H=135 \text{ GeV}$  is shown in Fig. 5. Distributions are normalised on expected number of events after all selections (not including  $m_{\tau\tau}$  window) for integrated luminosity  $30 \text{ fb}^{-1}$ .



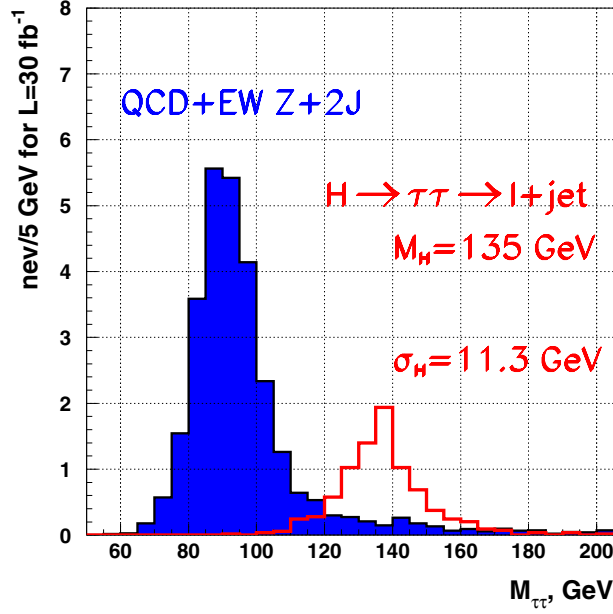


**Fig. 5.** Reconstructed effective mass of two  $\tau$  leptons for background QCD and EW  $Z+jj$  ( $Z \rightarrow \tau\tau \rightarrow l+\tau$  jet) and Higgs of  $M_H=135$  GeV. Distributions are normalised on expected number of events after all selections (not including  $m_{\tau\tau}$  window) for integrated luminosity  $30 \text{ fb}^{-1}$

### Acknowledgements

I would like to thank Ritva Kinnunen, Daniel Denegri and Laury Wendland for a big pleasure to work together on  $A, H \rightarrow \tau\tau$  channels. I would like to thank S. Ilin for generation with COMPHEP EW  $Z+jj$  background and D. Zeppenfeld for matrix element input for generation of QCD  $Z+jj$  background, checking COMPHEP EW  $Z+jj$  cross-section and for very useful discussions on weak boson fusion channels.

### References

1. R. Kinnunen and A. Nikitenko, Study of  $H, A \rightarrow \tau\tau \rightarrow \ell + \tau \text{ jet} + E_t^{\text{miss}}$  in CMS, CMS NOTE 1997/106.
2. R. Kinnunen and D. Denegri, Study of  $H, A \rightarrow \tau\tau \rightarrow h^+ + h^- + X$  in CMS, CMS NOTE 1999/037.
3. Sami Lehti, Prospects for the Detection of the MSSM Higgs Bosons Decaying into Tau Leptons in the CMS Detector, Dissertation, University of Helsinki, Report Series in Physics, HU-P-D93, 2001.
4. S. Eno, W. Smith, S. Dasu, R. Kinnunen and A. Nikitenko, A Study of a First and Second Level Tau Trigger, CMS NOTE 2000/055.
5. D. Kotlinski, A. Nikitenko and R. Kinnunen, Study of a Level-3 Tau Trigger with the Pixel Detector, CMS NOTE 2001/017.

6. A. Nikitenko and D. Kotlinski, CMS NOTE in preparation.
7. S. Abdullin, A. Khanov and N. Stepanov, CMSJET, CMS TN/94-180, <http://cmsdoc.cern.ch/~abdullin/cmsjet.html>
8. A. Nikitenko, S. Kunori and R. Kinnunen, Missing Transverse Energy Measurement with Jet Energy Corrections, CMS NOTE 2001/040.
9. M. Carena, S. Heynemeyer, C.E.M. Wagner and G. Weiglein, Suggestions for improved benchmark scenarios for Higgs-boson searches at LEP2, CERN-TH/99-374, DESY 99-186, hep-ph/9909435.
10. D. Denegri, V. Drollinger, R. Kinnunen, K. Lassila-Perini, S. Lehti, F. Moortgat, A. Nikitenko, S. Slabospitsky, N. Stepanov, Summary of the CMS Discovery Potential for the MSSM SUSY Higgses, CMS NOTE 2001/032.
11. The ALEPH, DELPHI, L3 and OPAL Collaborations, and the LEP Higgs Working Group, CERN-EP/2001-055 and hep-ex/0107030.
12. D. Zeppenfeld, R. Kinnunen, A. Nikitenko, E. Richter-Was, Phys.Rev. **D62** (2000) pp.13009, CERN-TH-2000-039.
13. <http://www.thep.lu.se/~torbjorn/Pythia.html>
14. D. Rainwater, D. Zeppenfeld and K. Hagiwara, Phys.Rev. **D59** (1999) 014037; T. Plehn, D. Rainwater and D. Zeppenfeld, Phys.Rev. **D61** (2000) 093005.
15. A.S.Belyaev et al., hep-ph/0101232
16. D. Rainwater, PhD thesis, report hep-ph/9908378
17. I. Vardanian, O. Kodolova, S. Kunori and A. Nikitenko, CMS Note in preparation.
18. R. Kinnunen, A. Nikitenko, Study of Tau Jet identification in CMS, CMS Note 1997/002
19. A.Djouadi, J. Kalinowski and M. Spira, HDECAY: a Program for Higgs Boson Decays in the Standard Model and its Supersymmetric Extension, Comput. Phys. Commun. 108 (1998) 5.

# Self-gravitating Bosons at Finite Temperature

Hrvoje Nikolić

Theoretical Physics Division, Rudjer Bošković Institute, P.O.B. 180, HR-10002  
Zagreb, Croatia

**Abstract.** A general-relativistic formalism describing a system of self-gravitating charged bosons is given. It describes the system at zero as well as at finite temperature and chemical potential. A phase transition (Bose-Einstein condensation) occurs at some critical temperature.

## 1 Introduction

Boson stars are candidates for dark matter ([6]). They are composed of massive spin 0 particles, such as Higgs, axion, and supersymmetric partners. Their description is based on the assumption that non-gravitational interactions can be neglected ([2]). In this paper we study their properties at finite temperature, assuming thermodynamical equilibrium with the rest of the Universe. Today,  $T \ll m$ , so the temperature effects are irrelevant to their present properties. However, in an early stage of the Universe evolution,  $T \sim m$ , so the temperature effects are important for understanding the formation of boson stars.

A maximal mass  $M$ , above which the pressure cannot compensate for the gravitational attraction, is typical of systems described by general relativity. The mass is related to the radius  $r$  of the system as

$$GM \sim r. \quad (1)$$

Denoting the energy density by  $\rho$  and using  $M \sim \rho r^3$ , we find

$$r \sim (\rho G)^{-1/2}, \quad (2)$$

$$M \sim (\rho G^3)^{-1/2}. \quad (3)$$

A boson condensate at  $T = 0$  is described by the Klein-Gordon equation, so we estimate

$$r \sim m^{-1}, \quad (4)$$

$$M \sim M_{\text{Pl}}^2/m, \quad (5)$$

$$\rho \sim m^2 M_{\text{Pl}}^2, \quad (6)$$

where

$$M_{\text{Pl}} = \sqrt{\hbar c/G} = G^{-1/2} \quad (7)$$

is the Planck mass.

In the gas phase, bosons have the Bose-Einstein distribution, so for  $T \sim m$  we estimate

$$\rho \sim m^4, \quad (8)$$

$$M \sim M_{\text{Pl}}^3/m^2, \quad (9)$$

$$r \sim M_{\text{Pl}}/m^2. \quad (10)$$

The transition from one phase to another occurs through a phase transition. In this paper we present the formalism that describes both phases at finite temperature. The formalism determines the order and temperature of the transition, as well as the dependence of the mass, entropy and radius on the temperature and number of particles.

## 2 Einstein Equations

The metric is described by the Einstein equations

$$\frac{1}{2}g_{\mu\nu}\mathcal{R} - R_{\mu\nu} = 8\pi G T_{\mu\nu}. \quad (11)$$

In the case of spherical symmetry and time independence, the metric takes the form

$$ds^2 = e^{\nu(r)}dt^2 - e^{\lambda(r)}dr^2 - r^2(d\vartheta^2 + \sin^2\vartheta d\varphi^2). \quad (12)$$

In this case, the Einstein equations reduce to

$$\nu' = -8\pi G T_r^r r e^\lambda + \frac{1}{r}(e^\lambda - 1), \quad (13)$$

$$\lambda' = 8\pi G T_0^0 r e^\lambda - \frac{1}{r}(e^\lambda - 1). \quad (14)$$

In the case of a perfect fluid, the energy-momentum tensor takes the form

$$T_\nu^\mu = (\rho + p) u^\mu u_\nu - g_\nu^\mu p. \quad (15)$$

Therefore,  $T_0^0 = \rho$ ,  $T_r^r = -p$ .

We define the function  $\mathcal{M}(r)$  through the relation

$$e^\lambda = \frac{1}{1 - 2G\mathcal{M}/r}. \quad (16)$$

This implies that  $\mathcal{M}(r)$  is the mass contained inside the radius  $r$ , i.e.

$$\mathcal{M}(r) = \int_0^r dr \, 4\pi r^2 \rho. \quad (17)$$

### 3 Complex Scalar Field in Curved Space-Time for $T = 0$

The action of the complex scalar field is

$$S = \int d^4x \sqrt{-g} [g^{\mu\nu} (\partial_\mu \phi^*) (\partial_\nu \phi) - m^2 \phi^* \phi] . \quad (18)$$

We study a particular class of solutions of the corresponding equation of motion, such that it takes a form

$$\phi(r, t) = e^{-i\omega t} \frac{P(r)}{\sqrt{2}} . \quad (19)$$

The equation of motion (Klein-Gordon equation in curved space-time) reduces to

$$P'' + \left( \frac{\nu' - \lambda'}{2} + \frac{2}{r} \right) P' + e^\lambda (\omega^2 e^{-\nu} - m^2) P = 0 . \quad (20)$$

The relevant components of the energy-momentum tensor resulting from (18) and (19) are

$$T_0^0 \equiv \rho = \frac{1}{2} [\omega^2 P^2 e^{-\nu} + P'^2 e^{-\lambda} + m^2 P^2] , \quad (21)$$

$$-T_r^r \equiv p = \frac{1}{2} [\omega^2 P^2 e^{-\nu} + P'^2 e^{-\lambda} - m^2 P^2] . \quad (22)$$

Similarly, the corresponding conserved current is

$$j^\mu = ig^{\mu\nu} (\phi^* \partial_\nu \phi - \phi \partial_\nu \phi^*) \quad (23)$$

$$= \left( \frac{1}{g_{00}} 2\omega \phi^* \phi, 0, 0, 0 \right) . \quad (24)$$

The soliton solutions  $P(r)$  of the equations given above are extensively discussed by [2].

### 4 Generalization to Finite Temperature

The system at finite temperature is described by the partition function

$$Z = \text{Tr} e^{-\beta(H - \mu N)} = \int [dg][d\Phi][d\Phi^*] e^{-S_g - S_{\text{KG}}} , \quad (25)$$

where  $\beta = 1/T$  is the inverse temperature,  $H$  is the Hamiltonian,  $\mu$  is the chemical potential and  $N$  is the conserved number of particles (charge). The action ([4])

$$S_g = -\frac{1}{16\pi G} \int_Y d^4x \sqrt{g} \mathcal{R} - \frac{1}{8\pi G} \int_{\partial Y} d^3x \sqrt{g^{(3)}} (K(g) - K(\eta)) \quad (26)$$

is the effective Euclidean gravitational action. Here

$$\int_Y d^4x = \int_0^\beta d\tau \int_\Sigma dx^1 dx^2 dx^3 , \quad (27)$$

so the variable  $\tau$  is related to finite temperature, not to the physical-time evolution. The boundary term in the action appears because the integration is over a manifold with a boundary, which is related to finite  $\beta = 1/T$  and finite radius  $R$ . The Klein-Gordon effective action is

$$S_{\text{KG}} = \int_Y d^4x \sqrt{g} (g^{\mu\nu} \partial_\mu \Phi^* \partial_\nu \Phi + m^2 |\Phi|^2) , \quad (28)$$

where ([5])

$$\partial_0 \Phi^* \equiv \left( \frac{\partial}{\partial \tau} + \mu \right) \Phi^* , \quad (29)$$

$$\partial_0 \Phi \equiv \left( \frac{\partial}{\partial \tau} - \mu \right) \Phi . \quad (30)$$

We decompose  $\Phi(x)$  as

$$\Phi(x) = \phi(x) + \psi(x) , \quad (31)$$

where  $\phi$  is the condensate equal to the expected value of  $\Phi$ . The field  $\phi$  extremizes the action, i.e. satisfies the classical equation of motion. The field  $\psi$  is a fluctuation about the expected value. In our calculations we neglect the metric fluctuations, so the partition function can be written as

$$Z = Z_g Z_{\text{cd}} Z_{\text{th}} , \quad (32)$$

where

$$Z_g = e^{-S_g} , \quad Z_{\text{cd}} = e^{-S_{\text{cd}}} \quad (33)$$

are classical actions and

$$Z_{\text{th}} = \int [d\psi] [d\psi^*] e^{-S_{\text{KG}}[\psi, \psi^*]} \quad (34)$$

describes the thermal fluctuations. It can be written as

$$\ln Z_{\text{th}} = \int d^3x \sqrt{g^{(3)}} \ln z(x) , \quad (35)$$

where

$$\ln z(x) = - \int \frac{d^3q}{(2\pi)^3} [\ln(1 - e^{-\bar{\beta}(E - \bar{\mu})}) + \ln(1 - e^{-\bar{\beta}(E + \bar{\mu})})] \quad (36)$$

has a form similar to that in flat space-time. Here

$$E = \sqrt{q^2 + m^2} , \quad \bar{\mu}(x) = \mu / \sqrt{g_{00}(x)} , \quad \bar{\beta}(x) = \beta \sqrt{g_{00}(x)} , \quad (37)$$

where  $\bar{\mu}(x)$  and  $\bar{\beta}(x)$  are the local chemical potential and the local inverse temperature, respectively. The thermal contributions to the pressure, energy density, particle-number density and entropy density are given by

$$p_{\text{th}} = \frac{1}{\bar{\beta}} \ln z , \quad (38)$$

$$\rho_{\text{th}} = - \frac{\partial}{\partial \bar{\beta}} \ln z \Big|_{\bar{\beta}\bar{\mu}} , \quad (39)$$

$$n_{\text{th}} = \frac{1}{\bar{\beta}} \frac{\partial}{\partial \bar{\mu}} \ln z , \quad (40)$$

$$\sigma = \bar{\beta}(p_{\text{th}} + \rho_{\text{th}} - \bar{\mu}n_{\text{th}}) , \quad (41)$$

respectively. Recall that the particle-number density actually represents the density of the difference of the number of particles and that of antiparticles.

We introduce the thermodynamical potential given by

$$\Omega(\beta, \mu) = -\frac{1}{\beta} \ln Z = M - \int_{\Sigma} d^3x \sqrt{g} [g^{00} \omega^2 P^2 + p_{\text{th}} + \rho_{\text{th}}] , \quad (42)$$

and the free energy

$$F(\beta, N) = \Omega(\beta, \mu) + \mu N . \quad (43)$$

For  $\omega = \mu$ , which corresponds to the thermodynamic equilibrium in which the periodic condition  $\phi(\beta) = \phi(0)$  is satisfied, (43) becomes

$$F = M - TS , \quad (44)$$

which is a relation well known from thermodynamics because the mass  $M$  is equal to the total energy of the system. The free energy is an important quantity because, at a given temperature, the system in thermodynamic equilibrium takes the configuration which has the minimal free energy.

## 5 Details of the Model

Since all equations have to be solved numerically, it is convenient to introduce the dimensionless variables  $x$ ,  $\varphi$ ,  $\tilde{\mathcal{M}}$ ,  $\tilde{N}$ ,  $\tilde{F}$ , defined by

$$x = mr , \quad \varphi = \frac{P}{M_{\text{Pl}}} , \quad (45)$$

$$\mathcal{M} = \frac{M_{\text{Pl}}^2}{m} \tilde{\mathcal{M}} , \quad N = \frac{M_{\text{Pl}}^2}{m^2} \tilde{N} , \quad F = \frac{M_{\text{Pl}}^2}{m} \tilde{F} . \quad (46)$$

We also introduce dimensionless parameters

$$\alpha = \frac{\mu}{T} , \quad \gamma = \frac{\omega}{\mu} , \quad \eta = \frac{m^2}{M_{\text{Pl}}^2} . \quad (47)$$

While other dimensionless parameters are chosen such that they are of the order of unity, the parameter  $\eta$  is typically a very small parameter. The dimensionless energy density is

$$\tilde{\rho} = \frac{\rho}{m^2 M_{\text{Pl}}^2} = \frac{1}{2} \left[ (\chi + 2) \varphi^2 + \frac{x - 2\tilde{\mathcal{M}}}{x} \left( \frac{d\varphi}{dx} \right)^2 \right] + \eta \tilde{\rho}_{\text{th}} . \quad (48)$$

The dimensionless thermal contribution to the energy density  $\tilde{\rho}_{\text{th}}$  is chosen such that it is of the order of unity ([1]). We see that the thermal contributions to the energy density are suppressed because  $\eta$  is very small. Similar relations are also valid for the pressure  $p$  and the particle density  $n$  ([1]).

We introduce a new variable  $\chi$  defined by

$$e^{\nu(x)} = \frac{\omega^2}{m^2} \frac{1}{\chi(x) + 1} . \quad (49)$$

To avoid the divergences at  $x = 0$ , we have to require

$$\tilde{\mathcal{M}}(0) = 0, \quad \left. \frac{d\varphi}{dx} \right|_{x=0} = 0 . \quad (50)$$

The other two initial conditions  $\varphi(0)$  and  $\chi(0)$  are simultaneously found from the requirement that  $\varphi(\infty) = 0$  and that the total particle-number  $\tilde{N}$  is fixed.

The radius  $R$  is not fixed by the model itself. To fix it, we use the following physical arguments. In an early stage of the Universe evolution, bosons are in a purely gas phase, in lumps with a huge number of particles and a huge radius:

$$N_{\text{gas}} \sim M_{\text{Pl}}^3 / m^3 , \quad (51)$$

$$R_{\text{gas}} \sim M_{\text{Pl}} / m^2 . \quad (52)$$

By cooling, the initial huge lump of bosons decays into a number of small boson stars  $N_{\text{stars}} \sim N_{\text{gas}} / N_{\text{cd}} \sim M_{\text{Pl}} / m$ . The volume occupied by each of these small boson stars is of the order  $V \sim R_{\text{gas}}^3 / N_{\text{stars}}$ , so the radius  $R \sim V^{1/3}$  is

$$R \sim \frac{1}{\eta^{1/3} m} . \quad (53)$$

We see that, for  $\eta \ll 1$ ,

$$R_{\text{cd}} \ll R \ll R_{\text{gas}} . \quad (54)$$

For  $T \sim m$ , the contributions to the total number of particles from gas and the condensed phase are of the same order inside the radius  $R$ .

The results of detailed numerical calculations are presented in the paper of [1]. It appears that the quantities like the mass  $M$  and the entropy  $S$  change continuously and smoothly at the critical temperature of the phase transition, provided that  $\eta \ll 1$ . This corresponds to a second-order phase transition. However, when  $\eta$  is comparable to 1, then  $M$  and  $S$  do not change continuously at the critical temperature of the phase transition, which corresponds to a first-order phase transition.



## 6 Conclusions

Boson stars are candidates for dark matter. A phase transition (Bose-Einstein condensation) occurs by cooling the self-gravitating system of bosons. If the mass of the boson is much smaller than the Planck mass, then the density of gas is much smaller than the condensed-soliton density, so the influence of gravity on the gas phase is negligible. Consequently, the phase transition is a second-order transition, similarly to the case of non-interacting bosons ([3]). If the mass of the boson is close to the Planck mass, then the transition is a first-order transition.

## Acknowledgment

This work was supported by the Ministry of Science and Technology of the Republic of Croatia under Contract No. 00980102.

## References

1. Bilić and Nikolić (2000) Bilić N., Nikolić H. (2000): Nucl. Phys. B **590**, 575
2. Friedberg et al. (1987) Friedberg R., Lee T.D., Pang Y. (1987): Phys. Rev. D **35**, 3640
3. Haber and Weldon (1982) Haber H.E., Weldon H.A. (1982): Phys. Rev. D **25**, 502
4. Hawking (1979) Hawking S.W. (1979): in *General relativity: An Einstein centenary survey*, edited by Hawking S.W. and Israel W. (Cambridge University Press, Cambridge)
5. Kapusta (1989) Kapusta J.I. (1989): *Finite-temperature field theory* (Cambridge University Press, Cambridge)
6. Mielke and Schunck (2000) Mielke E.W., Schunck F.E. (2000): Nucl. Phys. B **564**, 185

# BLM Scale for the Pion Transition Form Factor<sup>\*</sup>

Blaženka Melić<sup>1,2,3</sup>, Bene Nžić<sup>3</sup>, and Kornelija Passek<sup>3</sup>

<sup>1</sup> Institut für Physik, Universität Mainz, D-55099 Mainz, Germany

<sup>2</sup> Institut für Theoretische Physik, Universität Würzburg, D-97074 Würzburg, Germany

<sup>3</sup> Theoretical Physics Division, Rudjer Bošković Institute, P.O. Box 180, HR-10002 Zagreb, Croatia

**Abstract.** We review the determination of the NLO Brodsky-Lepage-Mackenzie (BLM) renormalization scale for the pion transition form factor. We argue that the prediction for the pion transition form factor is independent of the factorization scale at every order in the strong coupling constant.

## 1 Introduction

The pion transition form factor, the simplest exclusive quantity, offers an excellent testing ground for QCD. For large virtualities of the photons (or at least for one of them) perturbative QCD (PQCD) is applicable [1]. A specific feature of this process is that the leading-order (LO) prediction is zeroth order in the QCD coupling constant, and one expects that PQCD for this process may work at accessible values of spacelike photon virtualities.

The pion transition form factor  $F_{\gamma\pi}(Q^2)$  is defined in terms of the amplitude  $\gamma^*(q, \mu) + \gamma(k, \nu) \rightarrow \pi(P)$

$$\Gamma^{\mu\nu} = i e^2 F_{\gamma\pi}(Q^2) \epsilon^{\mu\nu\alpha\beta} P_\alpha q_\beta, \quad (1)$$

and for large-momentum transfer  $Q^2 = -q^2$ , it can be represented [2,1] as a convolution

$$F_{\gamma\pi}(Q^2) = \Phi^*(x, \mu_F^2) \otimes T_H(x, Q^2, \mu_F^2), \quad (2)$$

where  $\otimes$  stands for the usual convolution symbol ( $A(z) \otimes B(z) = \int_0^1 dz A(z) B(z)$ ). In (2), the function  $T_H(x, Q^2, \mu_F^2)$  is the hard-scattering amplitude for producing a collinear  $q\bar{q}$  pair from the initial photon pair;  $\Phi^*(x, \mu_F^2)$  is the pion distribution amplitude (DA) representing the probability amplitude for finding the valence  $q\bar{q}$  Fock state in the final pion with the constituents carrying fractions  $x$  and  $(1-x)$  of the meson's total momentum  $P$ ;  $\mu_F^2$  is the factorization (or separation) scale at which soft and hard physics factorize. In this standard hard-scattering approach, pion is regarded as consisting only of valence Fock states, transverse quark momenta are neglected as well as quark masses.

The hard-scattering amplitude  $T_H$  is obtained by evaluating the  $\gamma^*\gamma \rightarrow q\bar{q}$  amplitude, and has a well-defined expansion in  $\alpha_S(\mu_R^2)$ , with  $\mu_R^2$  being the renormalization (or coupling constant) scale of the hard-scattering amplitude. Thus,

---

<sup>\*</sup> Talk given by K. Passek at the 8th Adriatic Meeting, Dubrovnik 2001.

one can write

$$T_H(x, Q^2, \mu_F^2) = T_H^{(0)}(x, Q^2) + \frac{\alpha_S(\mu_R^2)}{4\pi} T_H^{(1)}(x, Q^2, \mu_F^2) + \frac{\alpha_S^2(\mu_R^2)}{(4\pi)^2} T_H^{(2)}(x, Q^2, \mu_F^2, \mu_R^2) + \dots \quad (3)$$

The process-independent function  $\Phi(x, \mu_F^2)$  is intrinsically nonperturbative, but it satisfies an evolution equation of the form

$$\mu_F^2 \frac{\partial}{\partial \mu_F^2} \Phi(x, \mu_F^2) = V(x, u, \alpha_S(\mu_F^2)) \otimes \Phi(u, \mu_F^2), \quad (4)$$

where  $V(x, u, \alpha_S(\mu_F^2))$  is the perturbatively calculable evolution kernel. If the distribution amplitude  $\Phi(x, \mu_0^2)$  is determined at an initial momentum scale  $\mu_0^2$  (using some nonperturbative methods), then the differential-integral evolution equation (4) can be integrated using the moment method to give  $\Phi(x, \mu_F^2)$ .

The perturbative expansion of the pion transition form factor takes the form

$$F_{\gamma\pi}(Q^2) = F_{\gamma\pi}^{(0)}(Q^2) + \frac{\alpha_S(\mu_R^2)}{4\pi} F_{\gamma\pi}^{(1)}(Q^2) + \frac{\alpha_S^2(\mu_R^2)}{(4\pi)^2} F_{\gamma\pi}^{(2)}(Q^2, \mu_R^2) + \dots \quad (5)$$

The choice of the expansion parameter represents the major ambiguity in the interpretation of the perturbative QCD predictions. We see that the coupling constant  $\alpha_S(\mu_R^2)$ , as well as, the coefficients  $F_{\gamma\pi}^{(i)}$  ( $i > 1$ ) from (5), depend on the definition of the renormalization scale and scheme. The truncation of the perturbative expansion at any finite order causes the residual dependence of the prediction on the choice of the renormalization scale and scheme, and introduces the theoretical uncertainty. If one can optimize the choices of the scale and scheme according to some sensible criteria, the size of the higher-order correction as well as the size of the expansion parameter, i.e. the QCD running coupling constant, can then serve as sensible indicators of the convergence of the perturbative expansion.

The simplest and widely used choice (the justification for the use of which is mainly pragmatic), is to take the  $\mu_R^2$  scale equal to characteristic momentum transfer of the process, i.e. in our case  $\mu_R^2 = Q^2$ . But since each external momentum entering an exclusive reaction is partitioned among many propagators of the underlying hard-scattering amplitude, the physical scales that control these processes are inevitably much softer than the overall momentum transfer.

Several scale setting procedure were proposed in the literature [3–5]. In the Brodsky-Lepage-Mackenzie (BLM) procedure [5], all vacuum-polarization effects from the QCD  $\beta$ -function are resummed into the running coupling constant. According to BLM procedure, the renormalization scale best suited to a particular process in a given order can be, in practice, determined by computing vacuum-polarization insertions in the diagrams of that order, and by setting the scale demanding that  $n_f$ -proportional terms should vanish. The optimization of the renormalization scale and scheme for exclusive processes by employing the BLM

scale fixing was elaborated in [6]. The renormalization scales in the BLM method are physical in the sense that they reflect the mean virtuality of the gluon propagators and the important advantage of this method is “pre-summing” the large  $(\beta_0 \alpha_S)^n$  terms, i.e., the infrared renormalons associated with coupling constant renormalization ([6] and references therein).

In our recent work [7] we have determined the BLM scale for the pion transition form factor, i.e., for the  $\gamma^* \gamma \rightarrow \pi$  process. The LO prediction for the pion transition form factor is zeroth order in the QCD coupling constant, the NLO corrections [8] represent leading QCD corrections and the vacuum polarization contributions appearing at the next-to-next-to-leading order (NNLO) were needed to fix the BLM scale from the requirement

$$F_{\gamma\pi}^{(2,n_f)}(Q^2, \mu_R^2 = \mu_{BLM}^2) = 0, \quad (6)$$

where  $F_{\gamma\pi}^{(2,n_f)}(Q^2, \mu_R^2)$  represents the  $n_f$ -proportional NNLO term from (5).

In this work we outline important points of this calculation and present the results that follow from the consistent calculation up to  $n_f$ -proportional NNLO contributions to both the hard-scattering and the distribution amplitude.

## 2 Analytical Calculation

We first outline the calculational procedure and its ingredients which are illustrated in Fig. 1.

The  $\gamma^* + \gamma \rightarrow q\bar{q}$  amplitude denoted by  $T$  contains collinear singularities, and it factorizes as

$$T(u, Q^2) = T_H(x, Q^2, \mu_F^2) \otimes Z_{T,col}(x, u; \mu_F^2). \quad (7)$$

Here,  $\mu_F^2$  denotes a factorization scale at which the separation of collinear singularities takes place, and all collinear singularities are factorized in  $Z_{T,col}$ , since  $T_H$  is, by definition, a finite quantity.

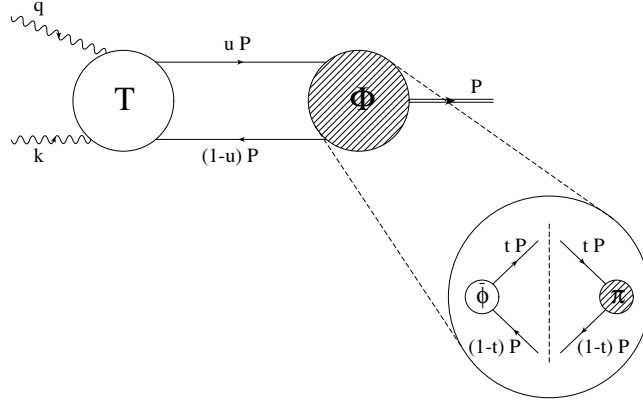


**Fig. 1.** Pictorial representation of the pion transition form factor calculational ingredients.

On the other hand, a process-independent distribution amplitude for a pion in a frame where  $P^+ = P^0 + P^3 = 1$ ,  $P^- = P^0 - P^3 = 0$ , and  $P_\perp = 0$  is defined [1,9] as

$$\Phi(u) = \int \frac{dz^-}{2\pi} e^{i(u-(1-u))z^-/2} \left\langle 0 \left| \bar{\Psi}(-z) \frac{\gamma^+ \gamma_5}{2\sqrt{2}} \Omega \Psi(z) \right| \pi \right\rangle_{(z^+ = z_\perp = 0)}, \quad (8)$$

where  $\Omega = \exp \left\{ ig \int_{-1}^1 ds A^+(zs) z^-/2 \right\}$  is a path-ordered factor making  $\Phi$  gauge invariant. The unrenormalized pion distribution amplitude  $\Phi(u)$  given in (8) and the distribution amplitude  $\Phi(v, \mu_F^2)$  renormalized at the scale  $\mu_F^2$  are related by a multiplicative renormalizability equation

$$\Phi(u) = Z_{\phi,ren}(u, v; \mu_F^2) \otimes \Phi(v, \mu_F^2). \quad (9)$$

By convoluting the “unrenormalized” (in the sense of collinear singularities) hard-scattering amplitude  $T(u, Q^2)$  with the unrenormalized pion distribution amplitude  $\Phi(u)$ , given by (7) and (9), respectively, one obtains

$$F_{\gamma\pi}(Q^2) = \Phi^\dagger(u) \otimes T(u, Q^2). \quad (10)$$

The divergences of  $T(u, Q^2)$  and  $\Phi(u)$  cancel

$$Z_{T,col}(x, u; \mu_F^2) \otimes Z_{\phi,ren}(u, v; \mu_F^2) = \delta(x - v), \quad (11)$$

and the usual expression (2) emerges. It is worth pointing out that the scale  $\mu_F^2$  representing the boundary between the low- and high-energy parts in (2) is, at same time, the separation scale for collinear singularities in  $T(u, Q^2)$ , on the one hand, and the renormalization scale for UV singularities appearing in  $\Phi(u)$ , on the other hand.

We note also that the pion distribution amplitude as given in (8), with  $|\pi\rangle$  being the physical pion state, of course, cannot be determined using perturbation theory. We can write  $\Phi(u)$  as

$$\Phi(u) = \tilde{\phi}(u, t) \otimes \langle q\bar{q}; t | \pi \rangle, \quad (12)$$

where  $\tilde{\phi}(u, t)$  is obtained from (8) by replacing the meson state  $|\pi\rangle$  by a  $|q\bar{q}; t\rangle$  state composed of a free quark and antiquark. The amplitude  $\tilde{\phi}$  can be treated perturbatively, making it possible to investigate the high-energy tail of the pion DA, to obtain  $Z_{\phi,ren}$  and to determine the DA evolution.

We proceed to calculation. This is the first calculation of the hard-scattering amplitude  $T(u, Q^2)$  of an exclusive process with the NNLO terms taken into account. The subtraction (separation) of collinear divergences at the NNLO is significantly more demanding than that at the NLO. Owing to the fact that the process under consideration contains one pseudoscalar meson, the calculation is further complicated by the  $\gamma_5$  ambiguity related to the use of the dimensional regularization method to treat UV and collinear divergences. The consistent calculation of  $T$  and  $\tilde{\phi}$  enable us to resolve these problems and, hence, we have calculated the LO, NLO, and  $n_f$ -proportional NNLO contributions to the perturbative expansions of both the hard-scattering amplitude and the perturbatively calculable part of the distribution amplitude.

### 3 Discussing the Factorization Scale Independence of the Finite Order Result

The dependence of pion distribution amplitude  $\Phi(x, \mu_F^2)$  on  $\mu_F^2$  is specified by the evolution equation (4). This dependence is completely contained in the evolutionary part  $\phi_V$

$$\Phi(v, \mu_F^2) = \phi_V(v, s; \mu_F^2, \mu_0^2) \otimes \Phi(s, \mu_0^2), \quad (13)$$

which satisfies the evolutionary equation

$$\mu_F^2 \frac{\partial}{\partial \mu_F^2} \phi_V(v, s, \mu_F^2, \mu_0^2) = V(v, s'; \mu_F^2) \otimes \phi_V(s', s, \mu_F^2, \mu_0^2), \quad (14)$$

while  $\Phi(s, \mu_0^2)$  represents the nonperturbative input determined at the scale  $\mu_0^2$ .

By differentiating (2) with respect to  $\mu_F^2$  and by taking into account (4), one finds that the hard-scattering amplitude satisfies the evolution equation

$$\mu_F^2 \frac{\partial}{\partial \mu_F^2} T_H(x, Q^2, \mu_F^2) = -T_H(y, Q^2, \mu_F^2) \otimes V(y, x; \mu_F^2), \quad (15)$$

which is similar to (4). The  $\mu_F^2$  dependence of  $T_H(x, Q^2, \mu_F^2)$  can be, analogous to (13), factorized in the function  $\phi_V(y, x, Q^2, \mu_F^2)$  as

$$T_H(x, Q^2, \mu_F^2) = T_H(y, Q^2, \mu_F^2 = Q^2) \otimes \phi_V(y, x, Q^2, \mu_F^2). \quad (16)$$

Using (14) one can show by partial integration that (16) indeed represents the solution of the evolution equation (15).

By substituting (13) and (16) in (2), we obtain

$$F_{\gamma\pi}(Q^2) = T_H(y, Q^2, Q^2) \otimes \phi_V(y, s, Q^2, \mu_0^2) \otimes \Phi^*(s, \mu_0^2), \quad (17)$$

where

$$\phi_V(y, x, Q^2, \mu_F^2) \otimes \phi_V(x, s, \mu_F^2, \mu_0^2) = \phi_V(y, s, Q^2, \mu_0^2), \quad (18)$$

has been taken into account. It is important to realize that the expression (18) is valid at every order of a PQCD calculation, and this can be easily shown (see [7]). Hence, the factorization scale  $\mu_F^2$  disappears from the final prediction at every order in  $\alpha_S$  and therefore does not introduce any theoretical uncertainty. The crucial point is that both the resummation of  $(\alpha_S \ln(\mu_F^2/\mu_0^2))^n$  terms in  $\Phi$  as well as the resummation of  $(\alpha_S \ln(Q^2/\mu_F^2))^n$  terms in  $T_H$ , have to be performed using (13) and (16) along with the results from (14). We note here that by adopting the common choice  $\mu_F^2 = Q^2$ , we avoid the need for the resummation of the  $(\alpha_S \ln(Q^2/\mu_F^2))^n$  terms in the hard-scattering part, making the calculation simpler.

## 4 Numerical Predictions

We refer to [7] for the complete analytical expressions for the pion transition form factor calculated up to  $n_f$  proportional NNLO terms.

The prediction for the pion transition form factor and the BLM scale  $\mu_{BLM}^2$  depend on the form of the distribution amplitude. There is increasing theoretical evidence coming from different calculations [10] that the low energy pion distribution amplitude does not differ much from its asymptotic form.

The expression for the pion transition form factor  $Q^2 F_{\gamma\pi}(Q^2)$  corresponding to the asymptotic distribution reads

$$Q^2 F_{\gamma\pi}(Q^2) = 2C_\pi f_\pi \left\{ 3 + \frac{\alpha_S(\mu_R^2)}{4\pi}(-20) + \frac{\alpha_S^2(\mu_R^2)}{(4\pi)^2} \times \left[ \left( -\frac{2}{3}n_f \right) \left( -43.47 - 20 \ln \frac{\mu_R^2}{Q^2} \right) + \dots \right] + \dots \right\}, \quad (19)$$

where  $C_\pi = \sqrt{2}/6$  is a flavour factor, while  $f_\pi = 0.131$  GeV. The  $n_f$ -proportional NNLO contribution determines the value of the BLM scale

$$\mu_R^2 = (\mu_{BLM}^2)^{as} \approx \frac{Q^2}{9}. \quad (20)$$

One notes that this scale is considerably softer than the total momentum transfer  $Q^2$ , which is consistent with partitioning of  $Q^2$  among the pion constituents.

The NLO predictions obtained in the  $\overline{MS}$  scheme are displayed in Fig. 2. The predictions based on the asymptotic DA are, in contrast to the ones obtained using the CZ DA [11], in good agreement with the experimental data [12].

Nevertheless, the rather low BLM scale given in (20), and consequently the large  $\alpha_S(\mu_{BLM}^2)$ , questions the applicability of the perturbative prediction at

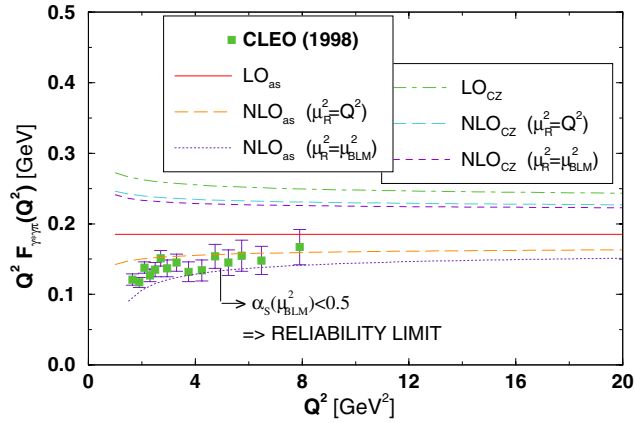


**Fig. 2.** The LO and NLO predictions for the pion transition form factor obtained using the  $\overline{MS}$  scheme (and the usual one-loop formula for  $\alpha_S$  with  $\Lambda_{\overline{MS}} = 0.2$  GeV<sup>2</sup>).

experimentally accessible momentum transfers. The NLO predictions obtained assuming the asymptotic DA and the BLM scale (20) satisfy the requirement  $\alpha_S(\mu_R^2) < 0.5$  for  $Q^2 \geq 6 \text{ GeV}^2$ . This reliability limit is indicated on Fig. 2. The transition to the more physical  $\alpha_V$  scheme, may offer a way out of this problem.

In [6] the exclusive hadronic amplitudes were analysed in the  $\alpha_V$  scheme, in which the effective coupling  $\alpha_V(\mu^2)$  is defined from the heavy-quark potential  $V(\mu^2)$ . The  $\alpha_V$  scheme is a natural, physically based scheme, which by definition automatically incorporates vacuum polarization effects into the coupling. The  $\mu_V^2$  scale reflects the mean virtuality of the exchanged gluons.

If use is made of the scale-fixed relation between the couplings  $\alpha_{\overline{MS}}$  and  $\alpha_V$  [6] then, to the order we are calculating, the NLO prediction in the  $\alpha_V$  scheme is obtained by taking  $\mu_R^2 = \mu_V^2 = e^{5/3} \mu_{BLM}^2$ , i.e. for the asymptotic DA

$$(\mu_V^2)^{as} = e^{5/3} (\mu_{BLM}^2)^{as} \approx \frac{Q^2}{2}. \quad (21)$$

The NLO prediction for  $Q^2 F_{\gamma\pi}(Q^2)$  obtained in  $\alpha_V$  scheme is depicted in Fig. 3. As can be seen, it is in good agreement with experimental data. We note that, since  $\alpha_V$  is an effective running coupling defined from the physical observable, it must be finite at low momenta, and the appropriate parameterization of the low-energy region should in principle be included (see [13] for various proposals).

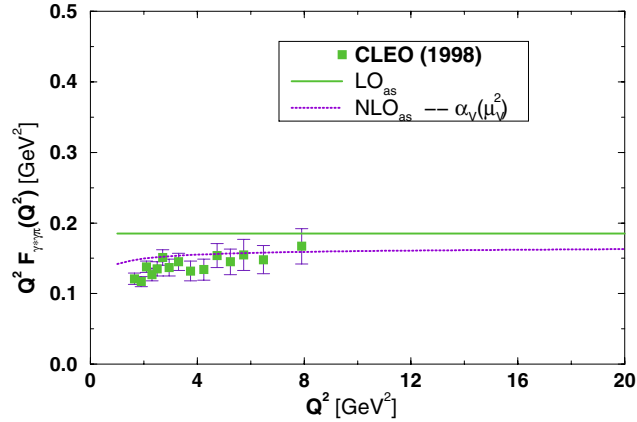


**Fig. 3.** The LO and NLO predictions for the pion transition form factor in the  $\alpha_V$  scheme ( $\Lambda_V = 0.16 \text{ GeV}^2$ ).

## 5 Conclusions

In this paper we have reviewed the determination of the NLO BLM scale for the pion transition form factor. A consistent calculation of both the hard-scattering and the perturbatively calculable part of the pion distribution amplitude has been performed up to  $n_f$ -proportional NNLO terms.



It has been demonstrated that the prediction for the pion transition form factor is independent of the factorization scale  $\mu_F^2$  at every order in the strong coupling constant  $\alpha_S$ . Provided both the hard-scattering and the distribution amplitude are treated consistently regarding their  $\mu_F^2$  dependence, the factorization scale disappears from the final prediction at every order in  $\alpha_S$  without introducing any theoretical uncertainty. One can use  $\mu_F^2 = Q^2$  to simplify the calculation, but any other choice would lead to the same result.

The renormalization scale  $\mu_R^2$  fixed according to the BLM scale setting prescription within the  $\overline{MS}$  scheme and corresponding to the asymptotic pion distribution amplitude, turns out to be  $\mu_{BLM}^2 \approx Q^2/9$ . Thus, in the region of  $Q^2 < 8 \text{ GeV}^2$ , in which the experimental data exist,  $\mu_{BLM}^2 < 1 \text{ GeV}^2$ . Consequently, the prediction obtained with  $\mu_R^2 = \mu_{BLM}^2$  cannot, in this region, be considered reliable.

In addition to the results calculated in the  $\overline{MS}$  renormalization scheme, the numerical prediction assuming the same distribution but in the  $\alpha_V$  scheme, with the renormalization scale  $\mu_R^2 = \mu_V^2 = e^{5/3} \mu_{BLM}^2 \approx Q^2/2$ , has also been obtained. It is displayed in Fig. 3 and, as seen, is in good agreement with experimental data. Due to the fact that the scale  $\mu_V^2$  reflects the mean gluon momentum in the NLO diagrams, it is to be expected that the higher-order QCD corrections are minimized, so that the leading order QCD term gives a good approximation to the complete sum.

### Acknowledgments

One of us (B.M.) acknowledges the support by the Alexander von Humboldt Foundation. This work was supported by the Ministry of Science and Technology of the Republic of Croatia under Contract No. 0098002.

### References

1. G. P. Lepage and S. J. Brodsky, Phys. Rev. D **22**, 2157 (1980)
2. G. P. Lepage and S. J. Brodsky, Phys. Lett. B **87**, 359 (1979); A. V. Efremov and A. V. Radyushkin, Phys. Lett. B **94**, 245 (1980); A. Duncan and A. H. Mueller, Phys. Lett. B **90**, 159 (1980)
3. G. Grunberg, Phys. Rev. D **29**, 2315 (1984)
4. P. M. Stevenson, Nucl. Phys. B **231**, 65 (1984)
5. S. J. Brodsky, G. P. Lepage and P. B. Mackenzie, Phys. Rev. D **28**, 228 (1983)
6. S. J. Brodsky, C. Ji, A. Pang and D. G. Robertson, Phys. Rev. D **57**, 245 (1998)
7. B. Melić, B. Nizić and K. Passek, Phys. Rev. D **65**, 053020 (2002); hep-ph/0107311
8. F. del Aguila and M. K. Chase, Nucl. Phys. **B193**, 517 (1981); E. Braaten, Phys. Rev. D **28**, 524 (1983); E. P. Kadantseva, S. V. Mikhailov and A. V. Radyushkin, Yad. Fiz. **44**, 507 (1986) [Sov. J. Nucl. Phys. **44**, 326 (1986)]
9. G. R. Katz, Phys. Rev. D **31**, 652 (1985); S. J. Brodsky, P. Damgaard, Y. Frishman and G. P. Lepage, Phys. Rev. D **33**, 1881 (1986)
10. V. Braun and I. Halperin, Phys. Lett. B **328**, 457 (1994); R. Jakob, P. Kroll and M. Raulfs, J. Phys. G **22**, 45 (1996); A. V. Radyushkin, Few Body Syst. Suppl. **11**, 57 (1999); A. Schmedding and O. Yakovlev, Phys. Rev. D **62**, 116002 (2000); A. P. Bakulev, S. V. Mikhailov and N. G. Stefanis, Phys. Lett. B **508**, 279 (2001)

11. V. L. Chernyak and A. R. Zhitnitsky, Phys. Rept. **112**, 173 (1984)
12. J. Gronberg *et al.* [CLEO Collaboration], Phys. Rev. D **57**, 33 (1998)
13. J. M. Cornwall, Phys. Rev. D **26**, 1453 (1982); A. Donnachie and P. V. Landshoff, Nucl. Phys. **B311**, 509 (1989); D. V. Shirkov and I. L. Solovtsov, Phys. Rev. Lett. **79**, 1209 (1997)

# Radiatively Induced Conversions of Massive Neutrinos\*

Krešimir Kumerički\*\* and Ivica Picek\*\*\*

Department of Physics, Faculty of Science, University of Zagreb, P.O.B. 331,  
HR-10002 Zagreb, Croatia

## 1 Massive Neutrinos and Lepton Mixing

In the present exciting moment of neutrino physics we have two important pieces of evidence for neutrino conversions:

- (i) A conversion of  $\nu_\mu$  dominantly to  $\nu_\tau$ , from  $\nu_\mu$  deficit in atmospheric neutrinos [1], with the up/down asymmetry established in  $\nu_\mu$  induced events;
- (ii) A conversion of the solar  $\nu_e$  into  $\nu_\mu$  or  $\nu_\tau$ , inferred by combining SuperKamiokande [1] and SNO [2] data.

This robust evidence can be accommodated within the standard model (SM) by assuming masses and mixing of three standard (active) neutrinos, as follows.

The known matter fields are grouped, generation by generation, within five different representations of the Standard Model *gauge* group  $G_{\text{SM}} = SU(3)_C \times SU(2)_L \times U(1)_Y$ ,

$$\begin{aligned} Q_{Li}^I(3, 2)_{+1/6}, \quad u_{Ri}^I(3, 1)_{+2/3}, \quad d_{Ri}^I(3, 1)_{-1/3}, \\ L_{Li}^I(1, 2)_{-1/2}, \quad \ell_{Ri}^I(1, 1)_{-1}, \quad [\text{no } N_{Ri}] . \end{aligned}$$

Here the index  $I$  denotes gauge-interaction eigenstates, and the index  $i = 1, 2, 3$  is the generation index. The easiest way to introduce neutrino masses is to go slightly beyond the minimal SM, by introducing additional  $SU(2)_L$ -singlet, “sterile”, right-handed neutrinos  $N_{Ri}^I(1, 1)_0 \equiv \nu_{Ri}^I$ . This results in the Dirac neutrino mass matrix

$$(M_\nu^D)_{ij} \overline{\nu_{Li}^I} \nu_{Rj}^I . \quad (1)$$

The mass matrix of charged leptons  $M_l$  and the Dirac neutrino mass matrix  $M_\nu^D$  can be diagonalized by bi-unitary transformations

$$\begin{aligned} M_l^{\text{diag}} &= V_{lL} M_l V_{lR}^\dagger = \text{diag}\{m_e, m_\mu, m_\tau\} , \\ M_\nu^{D\text{diag}} &= V_{\nu L} M_\nu^D V_{\nu R}^\dagger = \text{diag}\{m_1, m_2, m_3\} . \end{aligned}$$

---

\* Presented by I.Picek at 8th Adriatic Meeting, *Particle Physics in the New Millennium*, Dubrovnik, Croatia, September 4–14, 2001

\*\* e-mail: kkumer@phy.hr

\*\*\* e-mail: picek@phy.hr

In the basis of the neutrino mass eigenstates  $(\nu_1, \nu_2, \nu_3)$ , there is a  $3 \times 3$  flavour mixing matrix entering the charged lepton current interactions,

$$U_{\text{MNS}} \equiv V_{\text{IL}} V_{\nu\text{L}}^\dagger,$$

which in the standard parametrization of the mixing among neutrinos reads

$$U_{\text{MNS}} = \begin{pmatrix} 1 & 0 & 0 \\ 0 & c_{23} & s_{23} \\ 0 & -s_{23} & c_{23} \end{pmatrix} \begin{pmatrix} c_{13} & 0 & s_{13}e^{-i\delta} \\ 0 & 1 & 0 \\ -s_{13}e^{i\delta} & 0 & c_{13} \end{pmatrix} \begin{pmatrix} c_{12} & s_{12} & 0 \\ -s_{12} & c_{12} & 0 \\ 0 & 0 & 1 \end{pmatrix}. \quad (2)$$

This leptonic analogue of the Cabibbo-Kobayashi-Maskawa (CKM) matrix,

$$\begin{pmatrix} \nu_e \\ \nu_\mu \\ \nu_\tau \end{pmatrix} = U_{\text{MNS}} \begin{pmatrix} \nu_1 \\ \nu_2 \\ \nu_3 \end{pmatrix} = \begin{pmatrix} U_{e1} & U_{e2} & U_{e3} \\ U_{\mu1} & U_{\mu2} & U_{\mu3} \\ U_{\tau1} & U_{\tau2} & U_{\tau3} \end{pmatrix} \begin{pmatrix} \nu_1 \\ \nu_2 \\ \nu_3 \end{pmatrix}, \quad (3)$$

generalizes the  $2 \times 2$  lepton flavour mixing, first introduced by Maki, Nakagawa and Sakata [3].

An input from short-baseline reactor neutrino experiments [4,5], the small value  $|U_{e3}| = s_{13} \leq 0.16$  which decouples solar and atmospheric neutrino oscillations, enables the separate two-flavour fits:

$$\begin{aligned} \Delta m_{12}^2 &\leq 2 \cdot 10^{-4} \text{ eV}^2 && \text{(solar neutrino oscillations)}; \\ \Delta m_{23}^2 &\simeq 3 \cdot 10^{-3} \text{ eV}^2 && \text{(atmospheric neutrino oscillations)}. \end{aligned}$$

Basically, this will give  $\nu_3$  mass eigenstate above or below the “solar doublet” ( $\nu_1$  and  $\nu_2$ ). In addition, one can construct the lepton flavour mixing matrix with a reasonable accuracy [6]. The preferable solution corresponds to the oscillation in matter with a large mixing angle. This LMA solution to the solar neutrino problem (where only moduli of the elements can be shown [6])

$$U_{\text{MNS}} = \begin{pmatrix} 0.74 - 0.90 & 0.45 - 0.65 & < 0.16 \\ 0.22 - 0.61 & 0.46 - 0.77 & 0.57 - 1/\sqrt{2} \\ 0.14 - 0.55 & 0.36 - 0.68 & 1/\sqrt{2} - 0.82 \end{pmatrix}, \quad (4)$$

shows a “democratic” mixing, very different from the “hierarchical” one in the quark sector. Apart from being unanticipated, this bears some profound consequences [7]. Note that all matrix elements are of the order unity, with an exception of the already mentioned upper-right entry  $|U_{e3}|$ . Essentially, the LMA solution provides a rather restrictive scenario with small neutrino masses, so that the most significant observable effect of the mixing is that of neutrino oscillations. Neutrino decay and spin resonant rotation are not completely excluded, as well as more exotic possibilities, such as non-standard flavour-changing interactions or violation of equivalence principle.

## 2 Radiative Corrections to Neutrino–Electron Scattering

Is there some information which neutrino decays could give us on the lepton mixing? In fact, this will depend very much on the values of neutrino masses. For example, the  $\nu_H(P) \rightarrow \nu_L(p)e^+(k_+)e^-(k_-)$  decay (originally considered in [8], and reconsidered more recently in [9]), was used [10] for constraining the  $|U_{e3}|$  MNS matrix element. Although allowed by the existing *direct* laboratory mass limit of  $\sim 18$  MeV for  $\nu_\tau$ , the global fit which leads to (4) requires simultaneously sub-eV mass eigenstates that exclude this decay. Accordingly, one is left with the scattering variant of this process which might play some role in astrophysical environments.

The S-matrix for scattering of the massive neutrinos on the electron contains the diagrams in Figs. 1 and 2 which will generate the nondiagonal, heavy( $\nu_H$ )-to-light( $\nu_L$ ), transition

$$\mathcal{H}^{\text{HL}}(x) = \frac{G_F}{\sqrt{2}} \bar{e} \gamma^\mu (f_V - f_A \gamma_5) e \bar{\nu}_L \gamma_\mu (1 - \gamma_5) \nu_H. \quad (5)$$

We study the form-factors  $f_V$  and  $f_A$  in the adopted framework for massive neutrinos, which is the standard electroweak theory extended by extra parameters. Recently, we employed the same framework (providing also charged-lepton, flavour-violating transitions) in calculating the radiative annihilation of muonium [11,12]. Here, the quantities  $f_V$  and  $f_A$  are finite and calculable within such a renormalizable gauge theory.

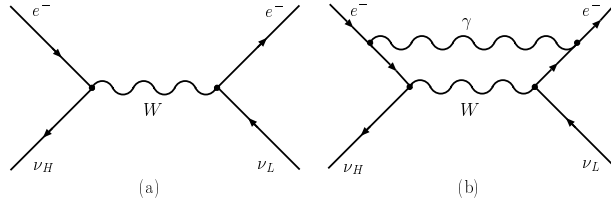


**Fig. 1.** Tree-level Feynman diagram (a), describing the nondiagonal neutrino electron interaction, and the corresponding radiative correction diagram (b)

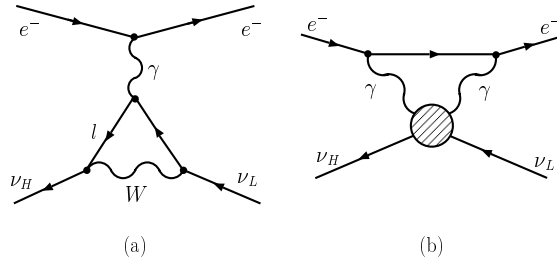


**Fig. 2.** One-loop nondiagonal radiative neutrino-electron interaction (a), and the photonic-loop diagram (b) induced by the  $\nu_H \nu_L \gamma \gamma$  vertex (the shaded circle)

The referent tree-level amplitude corresponding to the diagram on Fig. 1(a) reads (after a Fierz transformation)

$$\mathcal{A}_{\text{tree}} = \frac{G_F}{\sqrt{2}} \sum_{\alpha=\mu,\tau} \lambda_\alpha \bar{u}(p) \gamma^\mu (1 - \gamma_5) u(P) \times \bar{u}(k_-) \gamma_\mu (1 - \gamma_5) v(k_+) , \quad (6)$$

where the summation over combinations  $\lambda_\alpha \equiv U_{\alpha H} U_{\alpha L}^*$  appears on account of the unitarity of  $U_{\text{MNS}}$ .

Let us note that the radiative correction displayed on Fig. 1(b) preserves the pure V-A structure of the tree amplitude, and can accordingly be absorbed by the Fermi coupling. On top of it there are one-loop electroweak corrections to the tree-level process, which change its V-A structure. We refer to [9] for a more complete exposition of the electroweak W-box diagrams (that are power suppressed), and the Z-triangle diagrams (that are suppressed by the  $q^2/M_Z^2$  factor). On Fig. 2(a) we explicate only the one-loop (1L) radiative contribution that dominates in the set of electroweak diagrams considered in [9]. The pertinent amplitude

$$\mathcal{A}_{\text{rad}}^{1\text{L}} = \frac{G_F}{\sqrt{2}} \frac{e^2}{24\pi^2} \left[ \sum_{\alpha=\mu,\tau} \lambda_\alpha \ln \frac{m_\alpha^2}{m_e^2} \right] \bar{u}(p) \gamma^\mu (1 - \gamma_5) u(P) \times \bar{u}(k_-) \gamma_\mu v(k_+) , \quad (7)$$

contains purely vector electron current in comparison to the V-A one contained in (6). Thus, in the sum of (6) and (7)

$$\mathcal{A}_{\text{tree}} + \mathcal{A}_{\text{rad}}^{1\text{L}} = \frac{G_F}{\sqrt{2}} \bar{u}(p) \gamma^\mu (1 - \gamma_5) u(P) \times \bar{u}(k_-) \gamma_\mu (f_V - f_A \gamma_5) v(k_+) , \quad (8)$$

this one-loop radiative correction modifies only the *vector* form factor

$$f_V = \sum_{\alpha=\mu,\tau} \lambda_\alpha (1 + f_\alpha^{1\text{L}}) , \quad (9)$$

leaving  $f_A = 1$  intact. The correction term in (9) acquires a simple leading logarithmic form,

$$f_\alpha^{1\text{L}} = \frac{\alpha}{3\pi} \ln \frac{m_\alpha}{m_e} . \quad (10)$$

In what follows we focus to the next order radiative correction shown on Fig. 2(b) which will modify (in complementary way) the *axial-vector* form factor  $f_A$  in (8). This contribution corresponds to the two-loop electroweak diagrams considered by us [13] in the context of the flavour-changing  $s\bar{d} \rightarrow \mu^+ \mu^-$  transitions. In the neutrino nondiagonal transition at hand, we employ the one-particle-irreducible diagrams in 't Hooft-Feynman gauge, displayed on Fig. 3. These diagrams replace the shaded blob on Fig. 2(b).

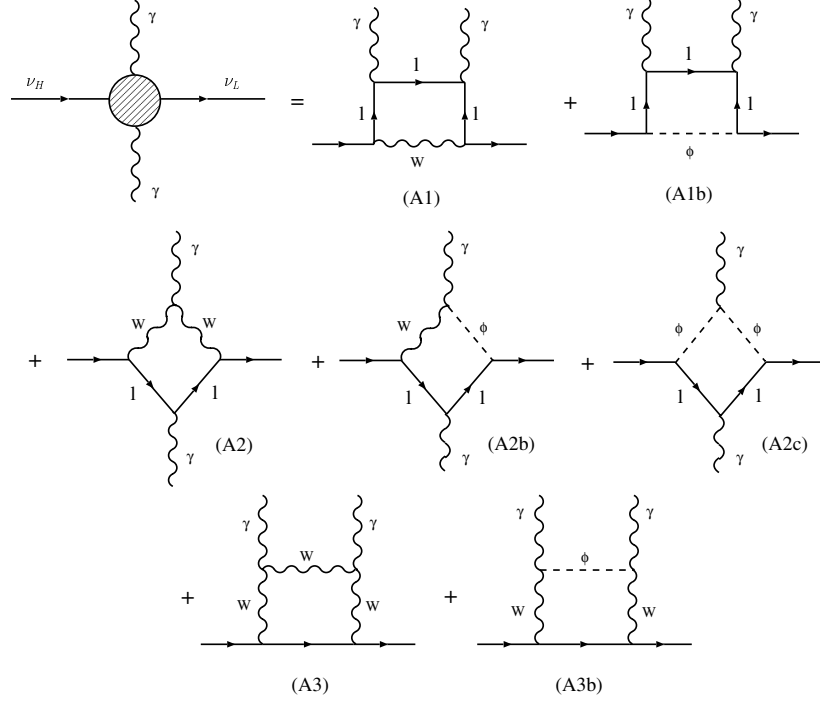


**Fig. 3.** Electroweak one-loop Feynman diagrams contributing to  $\nu_H \rightarrow \nu_L \gamma \gamma$  in the 't Hooft-Feynman gauge

In [13] we exposed in detail the dominant diagrams having a leading log form. Table 1 displays the contributions denoted by the respective insertions of the diagrams from Fig. 3. They build up the two-loop radiative amplitude

$$\mathcal{A}_{\text{rad}}^{2L} = \frac{G_F}{4\sqrt{2}} \frac{9}{4} \frac{\alpha^2}{\pi^2} \sum_{\alpha=\mu,\tau} \lambda_\alpha A_{(\alpha,e)} \bar{u}(p) \gamma^\mu (1 - \gamma_5) u(P) \times \bar{u}(k_-) \gamma_\mu \gamma_5 v(k_+) , \quad (11)$$

which modifies the axial-vector form factor  $f_A$ . The net result

$$f_A = \sum_{\alpha=\mu,\tau} \lambda_\alpha \left( 1 + \frac{9\alpha^2}{16\pi^2} A_{(\alpha,e)} \right) , \quad (12)$$

is expressed in terms of GIM-like combinations  $A_{(\mu,e)}$  and  $A_{(\tau,e)}$ , displayed in Table 1.

Since the dominant contribution comes from the first diagram in Fig. 3, one can rely on the simple analytical form of these functions ( $A_{(\alpha,e)} \propto f_\alpha^{2L}$ ) deduced previously [14,13]. In close analogy to the one-loop radiative correction in (9) and (10), our two-loop radiative correction reads

$$f_A = \sum_{\alpha=\mu,\tau} \lambda_\alpha (1 + f_\alpha^{2L}) , \quad (13)$$

**Table 1.** Contributions  $A1, \dots, A3b$  from Fig. 3 leading to the pertinent GIM-like loop-diagram factors  $A_{(\tau,e)}$  and  $A_{(\mu,e)}$ 

Diagram	$A_{(\tau,e)}$	$A_{(\mu,e)}$
A1	21.4	14.0
A1b	-0.002	$\sim 0$
A2	0.0007	$\sim 0$
A2b	0.12	0.0007
A2c	0.009	$\sim 0$
A3	0.4	0.0001
A3b	0.03	$\sim 0$
Total	21.6	14.0

$$f_{\alpha}^{2L} = \frac{3}{4} \frac{\alpha^2}{\pi^2} \ln \frac{m_{\alpha}^2}{m_e^2} . \quad (14)$$

The dominant  $\tau$ -loop ( $\alpha = \tau$ ) corrections to the referent tree-loop amplitude, given by expressions (10) and (14), are numerically

$$f_{\tau}^{1L} \simeq 6.3 \cdot 10^{-3} , \quad f_{\tau}^{2L} \simeq 6.6 \cdot 10^{-5} . \quad (15)$$

In order to estimate  $f_V$  and  $f_A$ , one has to include also the MNS-matrix prefactors, for which we now have the first strong experimental hints.

### 3 Conclusions

In the present account we provide the interaction (5) where the form-factors are given by (9)–(10) and (12)–(14). These form-factors have a simple leading-log behaviour and describe the nondiagonal neutrino transition in SM, as probed by photons. In this sense, our interaction (5) provides a starting point for some future considerations of the neutrino electromagnetic properties beyond the SM.

Actually, recent consideration of the  $\nu_H \rightarrow \nu_L$  neutrino conversion in hot media [15] resides on the variant of our interaction (5) with  $f_V = f_A = 1$ . Although we calculate only small departures from this purely V-A interaction, it is conceivable [16] that their effects might be considerably amplified (the MSW resonant oscillations [17,18] being a well known example). Thus, our study may be of relevance for some astrophysical and cosmological considerations.

### Acknowledgement

I.P. thanks E. Akhmedov, J.O. Eeg and M. Fukugita for enlightening discussions.

### References

1. Super-Kamiokande, Y. Fukuda *et al.*, Phys. Rev. Lett. **81**, 1562 (1998), hep-ex/9807003



2. SNO, Q. R. Ahmad *et al.*, Phys. Rev. Lett. **87**, 071301 (2001), nucl-ex/0106015
3. Z. Maki, M. Nakagawa, and S. Sakata, Prog. Theor. Phys. **28**, 870 (1962)
4. CHOOZ, M. Apollonio *et al.*, Phys. Lett. **B466**, 415 (1999), hep-ex/9907037
5. F. Boehm *et al.*, Phys. Rev. **D64**, 112001 (2001), hep-ex/0107009
6. M. Fukugita and M. Tanimoto, Phys. Lett. **B515**, 30 (2001), hep-ph/0107082
7. H. Murayama, (2002), hep-ph/0201022
8. R. E. Shrock, Phys. Rev. **D24**, 1275 (1981)
9. Q. Ho-Kim, B. Machet, and X. Y. Pham, Eur. Phys. J. **C13**, 117 (2000), hep-ph/9902442
10. C. Hagner *et al.*, Phys. Rev. **D52**, 1343 (1995)
11. J. O. Eeg, K. Kumericki, and I. Picek, Eur. Phys. J. **C17**, 163 (2000), hep-ph/9605337
12. J. O. Eeg, K. Kumericki, and I. Picek, Fizika **B10**, (2002)
13. J. O. Eeg, K. Kumericki, and I. Picek, Eur. Phys. J. **C1**, 531 (1998), hep-ph/9605337
14. M. B. Voloshin and E. P. Shabalin, Pisma Zh. Eksp. Teor. Fiz. **23**, 123 (1976)
15. N. Asida, A. Niegawa, H. Ozaki, and M. Kubota, (2001), hep-ph/0109227
16. D. Grasso and V. Semikoz, Phys. Rev. **D60**, 053010 (1999), hep-ph/9808390
17. L. Wolfenstein, Phys. Rev. **D17**, 2369 (1978)
18. S. P. Mikheev and A. Y. Smirnov, Nuovo Cim. **C9**, 17 (1986)

# Pion and Vacuum Properties in the Nonlocal NJL Model\*

Michał Praszalowicz and Andrzej Rostworowski

M. Smoluchowski Institute of Physics, Jagellonian University, ul. Reymonta 4, 30-59  
Kraków, Poland

**Abstract.** We formulate the nonlocal NJL model with a momentum dependent constituent quark mass and calculate pion light cone wave functions of twist 2 and 3. The leading twist wave function is not asymptotic and agrees well with the new CLEO data. Normalization conditions for the twist 3 wave functions are used to calculate the quark condensate. A prescription to calculate the gluon condensate is proposed. The numerical value of the gluon condensate nicely agrees with the phenomenological value, whereas the quark condensate is larger than the phenomenological value of  $-(250 \text{ MeV})^3$ . The relation between the  $k_T^2$  moments and mixed condensates are used to estimate the mixed quark-gluon condensate of dimension 5.

## 1 Introduction

In this short note we shall describe a simple and tractable model for the pion light cone wave functions which is based on the instanton model of the QCD vacuum. Hadron light cone wave functions were theoretically introduced more than 20 years ago [1]-[5]. Recently the analysis of [6] based on the latest CLEO measurements [7] put some limits on the expansion coefficients of the axial-vector (AV) pion wave function in terms of the Gegenbauer polynomials. This analysis indicates that the pion wave function measured at  $Q^2 = 1.5 - 9.2 \text{ GeV}^2$  is neither asymptotic  $\phi_{\text{as}}^{AV}(u) = 6 u(1-u)$  (with  $u$  being the fraction of the pion momentum carried by the quark) nor of the form proposed by Chernyak and Zhitnitsky in 1977 [8]:  $\phi_{\text{CZ}}^{AV}(u) = 30 u(1-u)(1-2u)^2$ . These two wave functions together with a typical prediction of the present model are shown in Fig. 1a. In Fig. 1b we show the 95% and 68% confidence level contour plots in the  $a_2 - a_4$  parameter space from the analysis of Schmedding and Yakovlev (Fig. 6 in [6]) together with the values of  $a_2$  and  $a_4$  for  $\phi_{\text{as}}^{AV}$ ,  $\phi_{\text{CZ}}^{AV}$  and various parameters of the present model.

The instanton model, after integrating out gluons and performing the bosonization, reduces to a simple Nambu-Jona-Lasinio type model where the quarks interact *nonlocally* with an external meson field  $U$  [9,10]:

$$S_I = \int \frac{d^4k d^4l}{(2\pi)^8} \bar{\psi}(k) \sqrt{M(k)} U^{\gamma_5}(k-l) \sqrt{M(l)} \psi(l) \quad (1)$$

---

\* Talk given by M. Praszalowicz

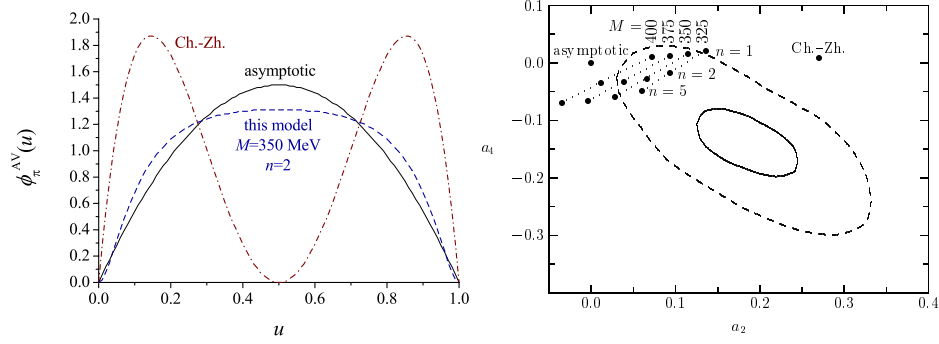


**Fig. 1.** Left: Asymptotic and Chernyak-Zhytnitsky leading twist pion wave functions together with a typical wave function from the present model. Right: The parameter space  $(a_2, a_4)$  of [6]. Black dots represent different model predictions, solid contour corresponds to 68% confidence level, whereas the dashed one to 95%

and  $U^{\gamma_5}$  can be expanded in terms of the pion fields:

$$U^{\gamma_5} = 1 + \frac{i}{F_\pi} \gamma^5 \tau^A \pi^A - \frac{1}{2F_\pi^2} \pi^A \pi^A + \dots \quad (2)$$

Here  $F_\pi = 93$  MeV and  $M(k) = MF^2(k)$  is a momentum dependent constituent quark mass which also plays a role of the pion-quark coupling. Let us note that in the instanton model both quark and gluon condensation occur at the same scale  $\mu_0$  which is associated with the average instanton size  $1/\bar{\rho} = 600$  MeV.

In principle  $F(k)$  has been calculated in the instanton model in the Euclidean space time. Here, following Refs.[11,12], we will perform calculations directly in the Minkowski space. To this end we shall choose a simple pole formula [12]

$$F(k) = \left( -\frac{\Lambda^2}{k^2 - \Lambda^2 + i\epsilon} \right)^n \quad (3)$$

which for  $n \sim 2 - 3$  and for  $k^2 < 0$  reproduces the  $k$  dependence obtained from the instantons reasonably well [12] (see Fig. 2a). Here  $M = M(0)$  is a model parameter which we choose to be of the order of 350 MeV.

As we shall see, the model is technically very simple and allows to calculate pion wave functions (not only the axial-vector, but also the pseudo-scalar (PS) and the pseudo-tensor (PT) ones) analytically up to a numerical solution of a certain algebraical equation of the order  $4n + 1$ . Given this simplicity it is of importance to perform various tests in order to gain confidence in the model as well as to find its limitations. In this paper we provide 4 kinds of tests.

First we calculate the leading twist pion wave function and compare with the existing data. Next we calculate the non-leading twist wave functions, which are normalized to the quark condensate. This allows us to calculate  $\langle \bar{q}q \rangle$ .

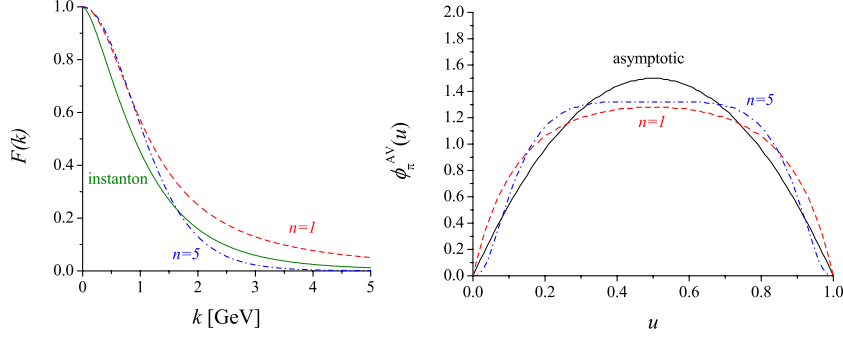


**Fig. 2.** Left:  $F(k)$  for Euclidean momentum  $k^2 < 0$ , for  $n = 1$  (dashed), 5 (dashed-dotted) and for the instanton model (solid). Right: Axial-vector pion wave function for  $M = 350$  MeV and for  $n = 1$  (dashed) and 5 (dashed-dotted) together with the asymptotic one (solid)

It is important to note that in our approach we calculate not only the  $u$  dependence but also the dependence on the transverse momentum  $k_T$ :

$$\phi_\pi(u) = \int_0^\infty dk_T^2 \psi_\pi(u, k_T^2), \quad \tilde{\phi}_\pi(k_T^2) = \int_0^1 du \psi_\pi(u, k_T^2). \quad (4)$$

By calculating  $k_T^2$  moments we get the mixed condensate of dimension 5.

Another advantage of our method is that the analytical expression for the quark condensate is given in terms of a Minkowskian integral which in a limit of a constant  $M(k)$  and  $k^2 \rightarrow -k_E^2$  reduces to the well known Euclidean form. By comparing the two expressions one can by inspection guess a continuation prescription which allows to rewrite certain Euclidean integrals as the Minkowskian ones. We use this in some respect *ad hoc* prescription to calculate the gluon condensate  $\langle \alpha/\pi GG \rangle$ , which provides another test of our approach.

## 2 Pion Wave Functions in the Nonlocal Quark Model

We shall be dealing with the leading twist axial-vector (AV), twist 3 pseudo-scalar (PS) and pseudo-tensor (PT) wave functions defined as follows [13,14]:

$$\begin{aligned} \phi_\pi^{AV}(u) &= \frac{1}{i\sqrt{2}F_\pi} \int_{-\infty}^{\infty} \frac{d\tau}{\pi} e^{-i\tau(2u-1)(nP)} \langle 0 | \bar{\psi}(n\tau) \not{n} \gamma_5 \psi(-n\tau) | \pi^+(P) \rangle, \\ \phi_\pi^{PS}(u) &= -(nP) \frac{F_\pi}{\sqrt{2}\langle \bar{q}q \rangle} \int_{-\infty}^{\infty} \frac{d\tau}{\pi} e^{-i\tau(2u-1)(nP)} \langle 0 | \bar{\psi}(n\tau) i\gamma_5 \psi(-n\tau) | \pi^+(P) \rangle, \\ \phi_\pi^{PT}(u) &= \frac{-6F_\pi}{\sqrt{2}\langle \bar{q}q \rangle} \int_0^u dw \int_{-\infty}^{\infty} \frac{d\tau}{\pi} e^{-i\tau(2w-1)(nP)} n^\alpha P^\beta \langle 0 | \bar{\psi}(n\tau) \sigma_{\alpha\beta} \gamma_5 \psi(-n\tau) | \pi^+(P) \rangle. \end{aligned} \quad (5)$$

where we have chosen  $n = (1, 0, 0, -1)$  as a light-cone vector parallel to  $z_\mu = \tau n_\mu$  and  $\tilde{n} = (1, 0, 0, 1)$  parallel to  $P_\mu$ . All three wave functions are normalized to 1. The normalization condition for  $\phi_\pi^{PS}$  and yield  $\phi_\pi^{PS}$  therefore the expression for  $\langle \bar{q}q \rangle$ , whereas normalization of  $\phi_\pi^{AV}$  is used to fix the model parameter  $\Lambda$  for given  $M$  and  $n$ .

Technically speaking all three wave functions (6) are given in terms of a loop integral with a momentum dependent quark mass  $M(k)$ , which also acts as a quark-pion coupling. In order to calculate the loop integral we have to find zeros of the propagators which are generically of the form

$$k^2 - M^2 \left[ \frac{\Lambda^2}{k^2 - \Lambda^2 + i\epsilon} \right]^{4n} + i\epsilon = 0. \quad (6)$$

Equation (6) can be conveniently rewritten as:

$$z^{4n+1} + z^{4n} - \mu^2 = 0 \quad (7)$$

where  $z = k^2/\Lambda^2 - 1 + i\epsilon$  and  $\mu^2 = M^2/\Lambda^2$ . In the light cone parametrization  $d^4k = 1/2 dk^+ dk^- d^2\mathbf{k}_T$  where  $k^\mu = k^+ \tilde{n}^\mu/2 + k^- n^\mu/2 + k_T^\mu$ . Since  $k^+ = uP^+$  is fixed, (6) should be understood as an equation for  $k^-$ . Generally, equation (7) has  $4n + 1$  complex solutions which in the following will be denoted as  $z_i$ . These solutions depend on the specific value of  $\mu^2$  and have to be calculated numerically.

Here one faces immediately the problem how to choose the integration contour in the complex  $k^-$  plane. The prescription is very simple and has been at length discussed in [12]. As a result the  $dk^-$  integrals yield real wave functions which vanish for  $u$  outside the region  $0 < u < 1$ . Moreover for  $\Lambda \rightarrow \infty$ , i.e. for a constant  $M(k)$ , this prescription reduces in a continuous way to the standard one of Feynman.

With this prescription the calculations are rather straightforward and we obtain:

$$\psi_\pi^{AV}(u, k_T^2) = \frac{N_c}{(2\pi)^2} \frac{M^2}{\Lambda^2 F_\pi^2} \sum_{i,k=1}^{4n+1} f_i f_k \frac{u z_i^n z_k^{3n} + (1-u) z_i^{3n} z_k^n}{t + 1 + u z_i + (1-u) z_k}, \quad (8)$$

$$\psi_\pi^{PS}(u, k_T^2) = \frac{N_c}{(2\pi)^2} \frac{M}{\langle \bar{q}q \rangle} \sum_{i,k=1}^{4n+1} f_i f_k \frac{z_i^{3n} z_k^{3n} (1 + \frac{z_i + z_k}{2}) - \mu^2 z_i^n z_k^n}{t + 1 + u z_i + (1-u) z_k}, \quad (9)$$

$$\psi_\pi^{PT}(u, k_T^2) = \frac{3N_c}{(2\pi)^2} \frac{M\Lambda^2}{\langle \bar{q}q \rangle} \sum_{i,k=1}^{4n+1} f_i f_k z_i^{3n} z_k^{3n} \ln(1 + t + u z_i + (1-u) z_k). \quad (10)$$

(where  $t = k_T^2/\Lambda^2$ ). Factors  $f_i$  obey the following properties:

$$f_i = \prod_{\substack{k=1 \\ k \neq i}}^{4n+1} \frac{1}{z_i - z_k}, \quad \sum_{i=1}^{4n+1} z_i^m f_i = \begin{cases} 0 & \text{for } m < 4n \\ 1 & \text{for } m = 4n \end{cases} \quad (11)$$

which are crucial for the convergence of the  $dt$  integrals.

It is now straightforward to perform either the  $dt$  integration in order to get  $\phi_\pi$ , or the  $du$  integration to get the  $k_T$ -dependent functions  $\tilde{\phi}_\pi$ .

### 3 Properties of the Pion Wave Functions

In order to study the model dependence on the choice of  $M$  and  $n$  we have calculated pion wave functions for  $M = 325 - 400$  MeV and  $n = 1 - 5$ . The cutoff parameter  $\Lambda$  was adjusted by imposing the normalization condition on  $\phi_\pi^{AV}$ . In fact, as discussed in [12], the leading twist pion wave function  $\phi_\pi^{AV}(u)$  does not change any more if we increase  $n$  above 5. On the other hand for  $n > 5$  the cutoff function (3), if continued to the Euclidean metric, starts to deviate significantly from the one obtained in the instanton model. Therefore we have chosen to work with  $n_{\max} = 5$ . In Figs. 2b and 3 we have plotted  $\phi_\pi^{AV}$ ,  $\phi_\pi^{PS}$  and  $\phi_\pi^{PT}$  for  $M = 350$  MeV and  $n = 1, 5$ .

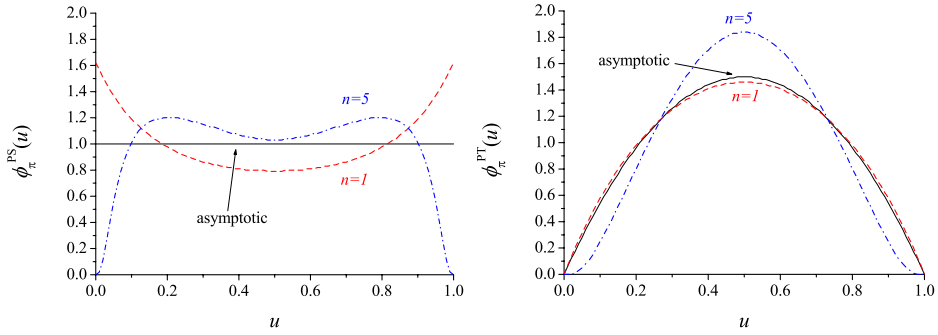


**Fig. 3.** Pseudo scalar (left panel) and pseudo-tensor (right panel) pion wave function for  $M = 350$  MeV and for  $n = 1$  (dashed) and 5 (dashed-dotted) together with the asymptotic one (solid)

Let us shortly summarize our findings. The axial-vector wave function,  $\phi_\pi^{AV}$ , vanishes at the end points as  $u^n$  (or  $(1-u)^n$ ) and shows a plateau around  $u = 0.5$  with a small dip for  $n = 5$ . It differs from the asymptotic wave function  $\phi_{\text{as}}^{AV}$  and, as seen from Fig. 1b, the best agreement with the recent analysis of the CLEO data is obtained for  $M = 325$  MeV and  $n = 2 - 5$  or  $M = 350$  MeV and  $n = 2$ . The fact that the true pion distribution amplitude may be broader than the asymptotic one has been already pointed out in [15]. Such a behavior was found then in [16] where not only the nonlocality (within the sum rules approach) but also the radiative corrections have been taken into account.

The pseudo-scalar pion wave function,  $\phi_\pi^{PS}$ , was calculated within the QCD sum rules in Refs.[13,14]. It had a  $u$ - shape and did not vanish at the end points.

In our case  $\phi_\pi^{PS}$  vanishes at the end points for  $n > 1$ . Indeed

$$\phi_\pi^{PS}(1) \sim \sum_i f_i \ln(1 + uz_i) \sum_k f_k \left[ z_i^{3n} z_k^{3n} + \frac{1}{2} z_i^{3n+1} z_k^{3n} + \frac{1}{2} z_i^{3n} z_k^{3n+1} - \mu^2 z_i^n z_k^n \right] \quad (12)$$

(and similarly for  $u = 0$ ) which is equal to 0 due to the property (11) except for  $n = 1$  where  $3n + 1 = 4n$ . Interestingly, the vanishing of  $\phi_\pi^{PS}$  for  $u = 0, 1$  is correlated with the nonconvexity of  $\phi_\pi^{AV}$  at the end points, which, as stated above, behaves like  $u^n$  (or  $(1 - u)^n$ ) for  $u \rightarrow 0$  (or 1). In any case  $\phi_\pi^{PS}$  differs from its asymptotic form  $\phi_{as}^{PS} \equiv 1$ .

Both pseudo-scalar and pseudo-tensor wave functions show stronger  $n$  dependence than  $\phi_\pi^{AV}$ . For  $n = 1$   $\phi_\pi^{PT}$  coincides with the asymptotic expression  $\phi_{as}^{PT} = \phi_{as}^{AV}$ , while for  $n = 5$  its is depleted at the end points and peaked in the center.

## 4 Condensates

Since the model parameters are fixed by the normalization of the axial-vector wave function we could use the normalization condition for  $\phi_\pi^{PS}$  or  $\phi_\pi^{PT}$  to calculate the quark condensate. The results are presented in Table 1. We see that the quark condensates obtained from the two normalization conditions do not coincide. In fact, for almost all model parameters considered, we find

$$\sqrt[3]{\langle \bar{q}q \rangle_{PS} / \langle \bar{q}q \rangle_{PT}} \simeq 0.9. \quad (13)$$

In absolute values the quark condensate calculated within our model overshoots the phenomenological value of  $-(250 \text{ MeV})^3$ . This is mostly due to the rather poor convergence of the  $dk_T^2$  integrals (4). Indeed for large  $k_T^2$ :

$$\tilde{\phi}_\pi^{AV}(k_T^2) \sim \left( \frac{1}{k_T^2} \right)^{4n+1}, \quad \tilde{\phi}_\pi^{PS}(k_T^2) \sim \left( \frac{1}{k_T^2} \right)^{2n}, \quad \tilde{\phi}_\pi^{PT}(k_T^2) \sim \left( \frac{1}{k_T^2} \right)^{2n}. \quad (14)$$

This is also the reason of rather strong  $n$  dependence of  $\phi_\pi^{PS}$  and  $\phi_\pi^{PT}$ .

The Euclidean formula for the gluon condensate in the instanton model of the QCD vacuum reads [9]:

$$\left\langle \frac{\alpha}{\pi} GG \right\rangle = 32N_c \int \frac{d^4 k_E}{(2\pi)^4} \frac{M^2(k_E)}{k_E^2 + M^2(k_E)}. \quad (15)$$

**Table 1.** Condensates for  $M = 350 \text{ MeV}$

$n$	$A$	$\left\langle \frac{\alpha}{\pi} GG \right\rangle$	$\langle \bar{q}q \rangle_{PS}$	$\langle \bar{q}q \rangle_{PT}$	$\langle ig \bar{q} \sigma \cdot G q \rangle_{AV}$
1	1156 MeV	$(399 \text{ MeV})^4$	$-(318 \text{ MeV})^3$	$-(357 \text{ MeV})^3$	$-(553 \text{ MeV})^5$
5	2819 MeV	$(389 \text{ MeV})^4$	$-(271 \text{ MeV})^3$	$-(301 \text{ MeV})^3$	$-(475 \text{ MeV})^5$

Apart from the numerical factor in front it differs from  $\langle \bar{q}q \rangle$  by an additional power of  $M(k_E)$  in the numerator. In [12] we have suggested the continuation prescription of (15) to the Minkowski metric with the result

$$\left\langle \frac{\alpha}{\pi} GG \right\rangle = -\frac{8N_c M^2 \Lambda^2}{(2\pi)^2} \int du dt \sum_{i,k} f_i f_k \frac{z_i^{2n} z_k^{2n} (1 + \frac{z_i + z_k}{2}) - \mu^2}{t + 1 + u z_i + (1 - u) z_k}. \quad (16)$$

Numerical result (Table 1) depends very weakly on  $n$  and is compatible with the phenomenological value [17]:  $\langle \alpha/\pi GG \rangle = (393_{-38}^{+29} \text{ MeV})^4$ .

Soft pion theorems provide link between dynamical objects like the light cone wave functions [1–4] and static properties of the physical vacuum [5,18]. It has been shown in Refs.[5,18] that moments of  $\tilde{\phi}_\pi(k_T^2)$  are given in terms of the mixed quark-gluon condensates

$$\langle k_T^2 \rangle_{AV} = \frac{5}{36} \frac{\langle ig \bar{q} \sigma \cdot G q \rangle}{\langle \bar{q}q \rangle}, \quad \langle k_T^2 \rangle_{PS} = \frac{1}{4} \frac{\langle ig \bar{q} \sigma \cdot G q \rangle}{\langle \bar{q}q \rangle}. \quad (17)$$

Here  $G_{\mu\nu}^a$  is a gluon field strength and  $\sigma \cdot G = \sigma_{\mu\nu} G^{\mu\nu}$ ,  $G_{\mu\nu} = \lambda^a/2 G_{\mu\nu}^a$ .

Unfortunately the ratio  $\langle k_T^2 \rangle_{AV} / \langle k_T^2 \rangle_{PS} \sim 5/9$  which follow from (17) is not reproduced within our approach<sup>1</sup> due to the slow convergence of the  $dk_T^2$  integration in the case of  $\langle k_T^2 \rangle_{PS}$ . In order to estimate the value of the mixed condensate of dimension 5,  $\langle ig \bar{q} \sigma \cdot G q \rangle$ , we choose therefore the first equation of (17). Interestingly, for the parameters which are closest to the original instanton model,  $M = 350 \text{ MeV}$  and  $n = 2$ , we get  $-(493 \text{ MeV})^5$  in perfect agreement with the direct calculation of  $\langle ig \bar{q} \sigma \cdot G q \rangle$  in the instanton model [19] which gives  $-(490 \text{ MeV})^5$ .

## 5 Summary and Outlook

The nonlocal NJL model with the momentum dependent constituent quark mass has been applied to calculate pion light cone wave functions [12]. It gives a satisfactory description of the leading twist  $AV$  wave function, whereas for the twist 3 wave functions we find a somewhat larger sensitivity to the model parameters.

Present prescription can be easily extended to describe kaon wave functions with an explicit symmetry breaking due to the non zero current strange quark mass. Also two meson generalized parton distributions both for pions and kaons can be easily calculated. By crossing symmetry one can also apply our method to calculate the skewed distributions and structure functions [22,23].

On the theoretical side one has to investigate more closely the PCAC relation within the present approach. It is known that the properly defined currents should include additional terms with respect to those considered here [20,21]. Although these new terms are not unique and suppressed by the instanton packing fraction, their influence on our results should be investigated.

<sup>1</sup> It is of the order of 0.2 instead of 0.54



M.P. thanks the organizers for the warm hospitality at this very stimulating meeting. This work was partially supported by the Polish KBN Grant PB 2 P03B 019 17. M.P. is grateful to W.Broniowski, K.Goeke, H.-Ch. Kim, D. Müller, M.V.Polyakov and N.G.Stefanis for discussions and interesting suggestions.

## References

1. V.L. Chernyak and A.R. Zhitnitsky, Sov. J. of Exp. and Theor. Phys. Lett. **26** (1977) 359.
2. S. Brodsky and G.P. Lepage, Phys. Lett. **B87** (1979) 594; Phys. Rev **D22** (1980) 2157.
3. G. Farrar and D. Jackson, Phys. Rev. Lett. **43** (1979) 246.
4. A.V. Efremov and A.V. Radyushkin, Theor. Mat. Phys. **42** (1980) 97; Phys. Lett. **B94** (1980) 245.
5. V.L. Chernyak, A.R. Zhitnitsky and I.R. Zhitnitsky Sov. J. of Nucl. Phys. **38** (1983) 645 [Yad. Fiz. **38** (1983) 1074].
6. A. Schmedding and O. Yakovlev, Phys. Rev **D62** (2000) 116002, [arXiv:hep-ph/9905392].
7. J. Gronberg (CLEO Collaboration), Phys. Rev **D57** (1998) 33, [arXiv:hep-ex/9707031].
8. V.L. Chernyak and A.R. Zhitnitsky, Phys. Rep. **112** (1984) 173.
9. D.I. Diakonov and V.Yu. Petrov, hep-ph/0009006 and references therein.
10. D.I. Diakonov and V.Yu. Petrov, Nucl. Phys. **B245** (1984) 259; **B272** (1986) 457.
11. V.Yu. Petrov and P.V. Pobylitsa, hep-ph/9712203, V.Yu. Petrov, M.V. Polyakov, R. Ruskov, C. Weiss and K. Goeke, Phys. Rev. **D59** (1999) 114018, [arXiv:hep-ph/9807229].
12. M. Praszalowicz and A. Rostworowski, Phys. Rev. D **64** (2001) 074003, [arXiv:hep-ph/0105188] and hep-ph/0111196.
13. V.M. Braun and I.E. Filyanov, Z. Physik. **C48** (1990) 239.
14. P. Ball, JHEP **9901** (1999) 010, [arXiv:hep-ph/9812375].
15. N. G. Stefanis, W. Schroers and H.-Ch. Kim, Eur. Phys. J. **C18** (2000) 137, [arXiv:hep-ph/0005218].
16. A.P. Bakulev, S.V. Mikhailov and N.G. Stefanis, Phys.Lett. **B508** (2001), [arXiv:hep-ph/0103119]; hep-ph/0104290.
17. S. Narison, Phys. Lett. **B361** (1995) 121, [arXiv:hep-ph/9504334]; Phys. Lett. **B387** (1996) 162, [arXiv:hep-ph/9512348].
18. A.R. Zhitnitsky, Phys. Lett. **B329** (1994) 493, [arXiv: hep-ph/9401278]; A.R. Zhitnitsky, Talk given at 10th Summer School and Symposium on Nuclear Physics: QCD, Light cone Physics and Hadron Phenomenology (NuSS 97), Seoul, Korea, 23-28 June 1997, hep-ph/9801228 and references therein.
19. M. V. Polyakov and C. Weiss, Phys. Lett. B **387** (1996) 841, [arXiv:hep-ph/9607244].
20. B. Golli, W. Broniowski and G. Ripka, Phys. Lett. **B 437** (1998) 24, [arXiv:hep-ph/9807261]; hep-ph/0107139.
21. R. S. Plant, M. C. Birse, Nucl. Phys. **A628** (1998) 607, R.D. Bowler, M. C. Birse, Nucl. Phys. **A582** (1995) 655, W. Broniowski, talk presented at the Miniworkshop on Hadrons as Solitons, Bled, Slovenia, 6-17 Jul 1999, hep-ph/9909438.

- 22. R.M. Davidson, E. Ruiz Arriola, hep-ph/0110291; Phys. Lett. **B348** (1995) 163; H. Weigel, E. Ruiz Arriola, L.P. Gamberg, Nucl. Phys.**B560** (1999) 383, [arXiv: hep-ph/9905329].
- 23. T. Shigetani, K. Suzuki, H. Toki, Phys. Lett. **B308** (1993) 383 [arXiv:hep-ph/9402286]; Nucl. Phys. **A579** (1994) 413 [arXiv:hep-ph/9402277].

# Black Hole Entropy from Horizon CFT in Gauss-Bonnet Gravity

Maro Cvitan, Silvio Pallua, and Predrag Prester

Department of Theoretical Physics, Faculty for Natural Sciences and Mathematics,  
University of Zagreb, Bijenička c. 32, pp. 331, 10001 Zagreb, Croatia

**Abstract.** We obtain correct expression for the entropy of spherically symmetric black holes in general  $D$ -dimensional Gauss-Bonnet gravity from the asymptotic CFT near the horizon.

## 1 Introduction

From the early seventies it is known that to preserve the laws of thermodynamics when gravity is included one should add to the total entropy a term  $S_h$ , which in Einstein gravity is given by Bekenstein-Hawking (BH) formula [1]

$$S_{bh} = S_{BH} = \frac{A_h}{4\hbar G} \quad (1)$$

where  $A$  is the total proper area of all event horizons (not just those connected to black holes, black strings and all types of black branes, but also cosmological horizons).<sup>1</sup>

Formula (1) has a number of puzzling properties. It gives enormous entropy (comparing to the entropy of the star which could collapse to the given black hole). Also, the entropy is not proportional to the bulk volume, which would be normally expected, but to the surface area. And last but not least, it suggests that black hole (a microscopic state in classical gravity) is in fact intrinsically a macroscopic state (a “thermal” state with temperature measured from infinity given by Hawking formula  $T_H = \hbar\kappa/2\pi$ , where  $\kappa$  is the surface gravity). Now one can ask what are the corresponding microscopic degrees of freedom. Obviously, the classical gravity alone could hardly provide satisfactory explanation because of the no-hair theorem (not to mention explicit dependence on  $\hbar$ ). So, it appears that one needs quantum theory to explain (1), and we mention here three most popular frameworks for explaining/deriving it:

- *Quantum fluctuations of matter fields near horizon* [2]. Doing standard *QFT* calculation, but in classical black hole background, one obtains  $S_{bh} \propto A$ , but with formally divergent coefficient (“natural” Planck length cutoff gives correct order of magnitude). But, one also obtains  $S_{bh} \propto$  number of matter fields, which means that this explanation works only in some “induced gravity” theory.

---

<sup>1</sup> We are using units in which the speed of light and Boltzman’s constant are set to one, but keeping  $\hbar$  and Newton’s constant  $G$  explicit. In this units Planck length is  $l_P = (G\hbar)^{1/2}$ .

- *Loop quantum gravity* [3]. Gives (1), although there are some open questions about the coefficient.
- *String theory* [4]. Gives (1) for large class of extremal and near extremal black holes (SUSY is crucial).

It should be emphasized that in loop gravity and string theory a calculation of the entropy is fully microscopic and it uses mathematical machinery which is apparently completely different in two frameworks, but with the same result. A natural explanation would be that BH entropy formula does not depend on detail how the gravity is quantized, but only on some (semi)classical properties. Indeed, this reasoning, combined with the results for (2+1)-dimensional black holes [5], inspired Carlip [6,7] to derive (1) from classical asymptotic diffeomorphism symmetries near the horizon. The crucial property was that for some class of boundary conditions on the horizon (which is treated as a sort of boundary) the corresponding symmetry algebra contains Virasoro algebra with nonvanishing classical central charge. The number of microstates could be obtained using Cardy formula [8], and the logarithm gave BH formula (1).

One way of testing the above idea is to see does it work for black holes in more general gravity theories. It was shown [9] that in general diffeomorphism invariant theories black hole entropy formula is not given by BH area law (1) but it contains additional terms. Here we concentrate on one class of such generalized theories called Gauss-Bonnet (GB) gravity (also known as Lovelock gravity [10]). Using Solodukhin's method (originally used for Einstein gravity in [11]) we obtain correct entropy formula for spherically symmetric black holes in general  $D$ -dimensional GB gravity from asymptotic CFT near the horizon [12].

## 2 Gauss-Bonnet Gravity

It is generally believed today that Einstein's general relativity (i.e., theory of gravity described by Einstein action) is just low energy limit of some yet unknown more fundamental theory, where the most prominent candidate looks to be string theory. Such a view predicts that as we probe higher energies new interactions become important and one should add additional terms in effective action. If the general covariance is still satisfied new terms are constructed as products of Riemann tensor and its covariant derivatives. Also, as in string theory, it is possible that in the process new dimensions would open, so we are led to consider actions in  $D \geq 4$  dimensions.

It was realised long time ago [10] that among all the possible terms there is a class of them called extended Gauss-Bonnet (GB) terms with some very special properties. They are defined with Lagrangian<sup>2</sup>

$$\mathcal{L}_m(g) = \frac{(-1)^m}{2^m} \delta^{\rho_1 \sigma_1 \dots \rho_m \sigma_m}_{\mu_1 \nu_1 \dots \mu_m \nu_m} R^{\mu_1 \nu_1}_{\rho_1 \sigma_1} \dots R^{\mu_m \nu_m}_{\rho_m \sigma_m} \quad (2)$$

<sup>2</sup> We use conventions from Weinberg's book [13] except that our  $g = \det(g_{\mu\nu})$ .

where  $R_{\mu\nu\rho\sigma}$  is Riemann tensor for metric  $g_{\mu\nu}$  and  $\delta_{\alpha_1\ldots\alpha_k}^{\beta_1\ldots\beta_k}$  is totally antisymmetric product of  $k$  Kronecker deltas, normalized to take values 0 and  $\pm 1$ . By definition, we take  $\mathcal{L}_0 = 1$  (cosmological constant term). Notice also that  $\mathcal{L}_1 = -R$ , i.e. ordinary Einstein action. General GB action (also known as Lovelock gravity [10]) is now given as

$$I_{\text{GB}} = - \sum_{m=0}^{[D/2]} \lambda_m \int d^D x \sqrt{-g} \mathcal{L}_m(g) \quad (3)$$

where  $g = \det(g_{\mu\nu})$  and  $[z]$  denotes integer part of  $z$ . Notice that coupling constant  $\lambda_1$  is related to more familiar  $D$ -dimensional Newton gravitational constant  $G_D$  through  $\lambda_1 = (16\pi G_D)^{-1}$ .

This action has many interesting properties:

- In  $D$ -dimensional space all terms for which  $m > D/2$  are identically equal to zero. Term  $m = D/2$  is a topological term (Euler character). So, only terms for which  $m < D/2$  are contributing to equations of motion. It means that in  $D = 4$  GB action is (neglecting topological effects) just the Einstein action.
- *Only* GB terms have the property that resulting equations of motion contain no more than second derivative of metric [10]. They are also free of ghosts when expanded not only about flat space [14] but also about some Randall-Sundrum brane solutions in  $5D$  [15].
- It has a good boundary value problem [16], in the sense that we can add surface terms such that the action can be extremized on space  $M$  while keeping only the metric fixed on the boundary  $\partial M$  (if non-GB terms are present in the action we have to also fix derivatives of components of the metric tensor on  $\partial M$ ).
- Analysis of spherically symmetric classical solutions in empty space is almost as simple as for pure Einstein case. But, unlike the Einstein case where there was unique solution (Schwarzschild), for general GB action there are black hole solutions having more complicated global topologies with multiple horizons and/or naked singularities [17].
- The entropy of GB black holes can be written (at least in stationary cases) as a sum of *intrinsic* curvature invariants integrated over a cross section of the horizon. As far as is known only GB actions have this property. Explicit expression for the entropy of general stationary black hole in GB theory is [18]

$$S_{\text{GB}} = \frac{4\pi}{\hbar} \sum_{m=1}^{[D/2]} m \lambda_m \oint d^{D-2} x \sqrt{\tilde{g}} \mathcal{L}_{m-1}(\tilde{g}_{ij}) \quad (4)$$

where the integration can be made on any  $(D-2)$ -dimensional spacelike slice of the Killing horizon and  $\tilde{g}_{ij}$  is the induced metric on it. Interesting property that the entropy has the same form as the action (3) can be described as dimensional continuation of the Gauss-Bonnet theorem.

- The entropy of GB black holes is negative for some region of parameter space. It is speculated that this is connected with the existence of a new type instability [19].
- It can be supersymmetrised.
- It is nonrenormalisable.

These properties suggest that GB action could be considered as a natural generalisation of Einstein action.

### 3 Effective CFT near the Horizon

Now we turn our attention to particular microscopic derivation of “macroscopic” expression (4) for entropy of spherically symmetric black holes in general  $D$ -dimensional GB gravity [12]. Following [11] we neglect matter and restrict ourselves to spherically symmetric perturbations (S-wave sector), which means that the metric takes the form

$$ds^2 = \gamma_{ab}(x)dx^a dx^b + r(x)^2 d\Omega_{D-2} \quad (5)$$

where  $d\Omega_{D-2}$  is metric on  $(D-2)$ -dimensional sphere of unit radius,  $x = \{x^a, a = 0, 1\} = (t, r)$  are coordinates on “ $t$ - $r$  plane” and  $\gamma_{ab}(x)$  is corresponding effective two-dimensional metric. Using (5) it is easy to show that Lagrangian (3) can be written in the form of an effective two-dimensional “higher-order Liouville theory” given with

$$\begin{aligned} I_{\text{GB}} = & \Omega_{D-2} \sum_{m=0}^{[D/2]} \lambda_m \frac{(D-2)!}{(D-2m)!} \int d^2x \sqrt{-\gamma} r^{D-2m-2} [1 - (\nabla r)^2]^{m-2} \\ & \times \left\{ 2m(m-1)r^2 [(\nabla_a \nabla_b r)^2 - (\nabla^2 r)^2] \right. \\ & + 2m(D-2m)r \nabla^2 r [1 - (\nabla r)^2] + m\mathcal{R}r^2 [1 - (\nabla r)^2] \\ & \left. - (D-2m)(D-2m-1) [1 - (\nabla r)^2]^2 \right\} \end{aligned} \quad (6)$$

where  $\mathcal{R}$  is two-dimensional Ricci scalar.

We now suppose that black hole with horizon *is existing* and we are interested in fluctuations (or better quantum states) near it. In the spherical geometry apparent horizon  $\mathcal{H}$  (a line in  $x$ -plane) can be defined by the condition

$$(\nabla r)^2|_{\mathcal{H}} \equiv \gamma^{ab} \partial_a r \partial_b r|_{\mathcal{H}} = 0. \quad (7)$$

Notice that (7) is invariant under (regular) conformal rescalings of the effective two-dimensional metric  $\gamma_{ab}$ . Near the horizon (7) is approximately satisfied.

After partial integration and implementation of horizon condition  $(\nabla r)^2 \approx 0$ , action (6) becomes near the horizon approximately

$$I_{\text{GB}} = -\Omega_{D-2} \sum_{m=0}^{[D/2]} \lambda_m \frac{(D-2)!}{(D-2m-2)!} \int d^2x \sqrt{-\gamma} r^{D-2m-2}$$

$$\times \left\{ m(\nabla r)^2 - \frac{m}{(D-2m)(D-2m-1)} \mathcal{R}r^2 + 1 \right\} \quad (8)$$

If we make reparametrizations

$$\phi \equiv \frac{2\Phi^2}{q\Phi_h}, \quad \bar{\gamma}_{ab} \equiv \frac{d\phi}{dr} e^{-\frac{2\phi}{q\Phi_h}} \gamma_{ab} \quad (9)$$

where

$$\Phi^2 \equiv 2\Omega_{D-2} \sum_{m=1}^{[D/2]} m\lambda_m \frac{(D-2)!}{(D-2m)!} r^{D-2m} \quad (10)$$

the action (8) becomes

$$I_{\text{GB}} = - \int d^2x \sqrt{-\bar{\gamma}} \left[ \frac{1}{2} (\bar{\nabla} \phi)^2 - \frac{1}{4} q\Phi_h \phi \bar{\mathcal{R}} + U(\phi) \right] \quad (11)$$

which is similar to the Liouville action. The difference is that potential  $U(\phi)$  is not purely exponential but its exact form will turn out to be irrelevant for our purpose.

Action (11) is of the same form as that obtained from pure Einstein action. In [11] it was shown that if one imposes condition that the metric  $\bar{\gamma}_{ab}$  is *non-dynamical* then the action (11) describes CFT *near the horizon*<sup>3</sup>. We therefore fix  $\bar{\gamma}_{ab}$  near the horizon and take it to be metric of static spherically symmetric black hole:

$$d\bar{s}_{(2)}^2 \equiv \bar{\gamma}_{ab} dx^a dx^b = -f(w) dt^2 + \frac{dw^2}{f(w)} \quad (12)$$

where near the horizon  $f(w_h) = 0$  we have

$$f(w) = \frac{2}{\beta} (w - w_h) + O((w - w_h)^2) \quad (13)$$

We now make coordinate reparametrization  $w \rightarrow z$

$$z = \int^w \frac{dw}{f(w)} = \frac{\beta}{2} \ln \frac{w - w_h}{f_0} + O(w - w_h) \quad (14)$$

in which 2-dim metric has a simple form

$$d\bar{s}_{(2)}^2 = f(z) (-dt^2 + dz^2) \quad (15)$$

and the function  $f$  behaves near the horizon ( $z_h = -\infty$ ) as

$$f(z) \approx f_0 e^{2z/\beta} \quad (16)$$

i.e., it *exponentially* vanishes. It is easy to show that equation of motion for  $\phi$  which follows from (11,15,16) is

$$(-\partial_t^2 + \partial_z^2) \phi = \frac{1}{4} q\Phi_h \bar{\mathcal{R}} f + f U'(\phi) \approx O(e^{2z/\beta}) \quad (17)$$

<sup>3</sup> Carlip showed that above condition is indeed consistent boundary condition [20].

and that the “flat” trace of the energy-momentum tensor is

$$-T_{00} + T_{zz} = \frac{1}{4}q\Phi_h(-\partial_t^2 + \partial_z^2)\phi - fU(\phi) \approx O(e^{2z/\beta}) \quad (18)$$

which is exponentially vanishing near the horizon. From (17) and (18) follows that the theory of the scalar field  $\phi$  exponentially approaches CFT near the horizon.

Now, one can construct corresponding Virasoro algebra using standard procedure. Using light-cone coordinates  $z_{\pm} = t \pm z$  right-moving component of energy-momentum tensor near the horizon is approximately

$$T_{++} = (\partial_+\phi)^2 - \frac{1}{2}q\Phi_h\partial_+^2\phi + \frac{q\Phi_h}{2\beta}\partial_+\phi \quad (19)$$

It is important to notice that horizon condition (7) implies that  $r$  and  $\phi$  are (approximately) functions only of one light-cone coordinate (we take it to be  $x_+$ ), which means that only one set of modes (left *or* right) is contributing.

Virasoro generators are coefficients in the Fourier expansion of  $T_{++}$ :

$$T_n = \frac{\ell}{2\pi} \int_{-\ell/2}^{\ell/2} dz e^{i2\pi n z/\ell} T_{++} \quad (20)$$

where we compactified  $z$ -coordinate on a circle of circumference  $\ell$ . Using canonical commutation relations it is easy to show that Poisson brackets of  $T_n$ 's are given with

$$i\{T_n, T_m\}_{PB} = (n-m)T_{n+m} + \frac{\pi}{4}q^2\Phi_h^2 \left( n^3 + n \left( \frac{\ell}{2\pi\beta} \right)^2 \right) \delta_{n+m,0} . \quad (21)$$

To obtain the algebra in quantum theory (at least in semiclassical approximation) one replaces Poisson brackets with commutators using  $[\cdot, \cdot] = i\hbar\{\cdot, \cdot\}_{PB}$ , and divide generators by  $\hbar$ . From (21) it follows that “shifted” generators

$$L_n = \frac{T_n}{\hbar} + \frac{c}{24} \left( \left( \frac{\ell}{2\pi\beta} \right)^2 + 1 \right) \delta_{n,0} , \quad (22)$$

where

$$c = 3\pi q^2 \frac{\Phi_h^2}{\hbar} , \quad (23)$$

satisfy Virasoro algebra

$$[L_n, L_m] = (n-m)L_{n+m} + \frac{c}{12} (n^3 - n) \delta_{n+m,0} \quad (24)$$

with central charge  $c$  given in (23).

Outstanding (and unique, as far as is known) property of the Virasoro algebra is that in its representations a logarithm of the number of states (i.e., entropy)



with the eigenvalue of  $L_0$  equal to  $\Delta$  is asymptotically given with Cardy formula [8]

$$S_C = 2\pi \sqrt{\left(\frac{c}{6} - 4\Delta_g\right) \left(\Delta - \frac{c}{24}\right)} \quad (25)$$

where  $\Delta$  is the eigenvalue of Virasoro generator  $L_0$  for the state we calculate the entropy and  $\Delta_g$  is the smallest eigenvalue. If we assume that in our case  $\Delta_g = 0$  in semiclassical approximation (more precisely  $\Delta_g \ll c/24$ ), one can see that number of microstates (purely quantum quantity) is in leading approximation completely determined by (semi)classical values of  $c$  and  $L_0$ . Now it only remains to determine  $\Delta$ . In a classical black hole solution we have

$$r = w = w_h + (w - w_h) \approx r_h + f_0 e^{2z/\beta} \quad (26)$$

so from (9) and (10) follows that near the horizon  $\phi \approx \phi_h$ . Using this configuration in (20) one obtains  $T_0 = 0$ , which plugged in (22) gives

$$\Delta = \frac{c}{24} \left( \left( \frac{\ell}{2\pi\beta} \right)^2 + 1 \right) \quad (27)$$

Finally, using (23) and (27) in Cardy formula (25) one obtains

$$S_C = \frac{c}{12} \frac{\ell}{\beta} = \frac{\pi}{4} q^2 \frac{\ell}{\beta} \frac{\Phi_h^2}{\hbar} \quad (28)$$

Let us now compare (28) with classical formula (4). For spherically symmetric metric (5) where horizon is a  $(D-2)$ -dimensional sphere with radius  $r_h$  one can show that (4) can be written as

$$S_{GB} = \frac{4\pi}{\hbar} \Omega_{D-2} \sum_{m=1}^{[D/2]} m \lambda_m \frac{(D-2)!}{(D-2m)!} r^{D-2m} = 2\pi \frac{\Phi_h^2}{\hbar} \quad (29)$$

Using this our expression (28) can be written as

$$S_C = \frac{q^2}{8} \frac{\ell}{\beta} S_{GB} \quad (30)$$

so it gives correct result apart from dimensionless coefficient, which can be determined in the same way as in pure Einstein case [20]. First, it is natural to set the compactification period  $\ell$  equal to period of Euclidean-rotated black hole, i.e.,

$$\ell = 2\pi\beta \quad (31)$$

The relation between eigenvalue  $\Delta$  of  $L_0$  and  $c$  then becomes

$$\Delta = \frac{c}{12} \quad (32)$$

One could be tempted to expect this to be valid for larger class of black holes and interactions then those treated so far.

To determine  $q$ , one may consider  $\lambda_m = 0$ ,  $m \geq 2$  case and compare expression for central charge (23) with that obtained in [7], which is

$$c = \frac{3A_h}{2\pi\hbar G_D} \quad (33)$$

where  $A_h = \Omega_{D-2} r_h^{D-2}$  is the area of horizon. One obtains that

$$q^2 = \frac{4}{\pi} \quad (34)$$

One could also perform boundary analysis of Ref. [7] for GB gravity [21]. This procedure confirms relation (34).

Using (31) and (34) one finally obtains desired result

$$S_C = S_{GB} \quad (35)$$

## References

1. J. D. Bekenstein: Lett. Nuovo. Cim. **4**, 737 (1972) Phys. Rev. D **7**, 2333 (1973) Phys. Rev. D **9**, 3292 (1974) S. W. Hawking: Nature **248**, 30 (1974) Commun. Math. Phys. **43**, 199 (1975)
2. K. S. Thorne, W. H. Zurek: Phys. Rev. Lett. **54**, 2171 (1985) G. 't Hooft: Nucl. Phys. **B256**, 727 (1985)
3. A. Ashtekar, J. Baez, A. Corichi, K. Krasnov: Phys. Rev. Lett. **80**, 904 (1998)
4. A. Strominger, C. Vafa: Phys. Lett. **B379**, 99 (1996) J. R. David, G. Mandal, S. R. Wadia: hep-th/0203048
5. J. D. Brown, M. Henneaux: Commun. Math. Phys. **104**, 207 (1986) M. Banados, C. Teitelboim, J. Zanelli: Phys. Rev. Lett. **69**, 1849 (1992) A. Strominger: JHEP **9802**, 009 (1998)
6. S. Carlip: Phys. Rev. Lett. **82**, 2828 (1999)
7. S. Carlip: Class. Quant. Grav. **16**, 3327 (1999)
8. J. A. Cardy: Nucl. Phys. **B270**, 186 (1986) H. W. J. Blöte, J. A. Cardy, M. P. Nightingale: Phys. Rev. Lett. **56**, 742 (1986)
9. R. M. Wald: Phys. Rev. D **48**, 3427 (1993) V. Iyer, R. M. Wald: Phys. Rev. D **50**, 846 (1994) T. Jacobson, G. Kang, R. C. Myers: Phys. Rev. D **49**, 6587 (1994)
10. D. Lovelock: J. Math. Phys. **12**, 498 (1971) J. Math. Phys. **13**, 874 (1972)
11. S. N. Solodukhin: Phys. Lett. **B454**, 213 (1999)
12. M. Cvitan, S. Pallua, P. Prester: ZTF-02-03, hep-th/0207265
13. S. Weinberg: *Gravitation and Cosmology* (John Wiley & Sons, New York 1972)
14. B. Zwiebach: Phys. Lett. **B156**, 315 (1985) B. Zumino: Phys. Rept. **137**, 109 (1986)
15. Y.M. Cho, I. P. Neupane, P.S. Wesson: Nucl. Phys. **B621**, 388 (2002)
16. R. C. Myers: Phys. Rev. D **36**, 392 (1987)
17. R. C. Myers, J. Z. Simon: Phys. Rev. D **38**, 2434 (1988) R. G. Cai: Phys. Rev. D **65**, 084014 (2002) R. G. Cai, K. S. Soh: Phys. Rev. D **59**, 044013 (1999)
18. T. Jacobson, R. C. Myers: Phys. Rev. Lett. **70**, 3684 (1993)
19. M. Cvetič, S. Nojiri, S. D. Odintsov: Nucl. Phys. **B628**, 295 (2002)
20. S. Carlip: Phys. Lett. **B508**, 168 (2001)
21. M. Cvitan, S. Pallua, P. Prester: in preparation

# An Overview of the Sources for Electroweak Baryogenesis

Tomislav Prokopec

Institut für Theoretische Physik, Universität Heidelberg, Philosophenweg 16, D-69120  
Heidelberg, Germany

**Abstract.** After a short review of electroweak scale baryogenesis, we consider the dynamics of chiral fermions coupled to a complex scalar field through the standard Yukawa interaction term at a strongly first order electroweak phase transition. By performing a systematic gradient expansion we can use this simple model to study electroweak scale baryogenesis. We show that the dominant sources for electroweak baryogenesis appear at linear order in the Planck constant  $\hbar$ . We provide explicit expressions for the sources both in the flow term and in the collision term of the relevant kinetic Boltzmann equation. Finally, we indicate how the kinetic equation sources appear in the fluid transport equations used for baryogenesis calculations.

## 1 Introduction

The necessary requirements on dynamical baryogenesis at an epoch of the early Universe are provided by the following Sakharov conditions:

- baryon number (B) violation
- *charge* (C) and *charge-parity* (CP) violation
- departure from thermal and kinetic equilibrium

The Sakharov conditions may be realised at the electroweak transition [1], provided the transition is strongly first order. Namely, C and CP violation are realised in the standard model (SM) for example through the Cabibbo-Kobayashi-Maskawa (CKM) matrix of quarks. B violation is mediated through the Adler-Bell-Jackiw (ABJ) anomaly. At high temperatures the ABJ anomaly is manifest via the unsuppressed sphaleron transitions, and may be responsible for the observed baryon asymmetry today, which is usually expressed as the baryon-to-entropy ratio:

$$\frac{n_B}{s} = 3 - 7 \times 10^{-11}. \quad (1)$$

This is obtained both as a nucleosynthesis constraint and from recent cosmic microwave background observations.

The standard model (SM) of elementary particles and interactions cannot alone be responsible for the observed matter-antimatter asymmetry (1), primarily because the LEP bound on the Higgs mass  $m_H \gtrsim 112$  GeV is inconsistent with the requirement that the transition be strongly first order. A strongly first order transition is namely required in order for the baryons produced in the symmetric phase not be washed-out by the sphaleron transitions in the Higgs

(‘broken’) phase. And this is so provided the transition is strong enough. This is usually expressed as the requirement  $\Delta\phi \gtrsim 1.1T$  on the jump in the Higgs expectation value  $\phi$  of the phase transition [2].

Supersymmetric extensions of the Standard Model on the other hand may result in a strongly first order transition. For example, in the Minimal supersymmetric standard model the sphaleron bound can be satisfied provided the stop and the lightest Higgs particles are not too heavy,  $m_{\tilde{t}} \sim 120$  GeV and  $m_H \lesssim 120$  GeV [3].

An efficient mechanism for baryon production at the electroweak phase transition is the *charge transport mechanism* [4], which works as follows. At a first order transition, when the Universe supercools, the bubbles of the Higgs phase nucleate and grow. In presence of a CP-violating condensate at the bubble interface, as a consequence of collisions of chiral fermions with scalar particles in presence of a scalar field condensate, CP-violating currents are created and transported into the symmetric phase, where they bias baryon number production. The baryons thus produced are transported back into the Higgs phase where they are frozen-in. The main unsolved problem of electroweak baryogenesis is systematic computation of the relevant CP-violating currents generated at the bubble interface. Here we shall reformulate this problem in terms of calculating CP-violating sources in the kinetic Boltzmann equations for fermions.

The techniques we report here are relevant for calculation of sources in the limit of thick phase boundaries and a weak coupling to the Higgs condensate. In this case one can show that, to linear order in the Planck constant  $\hbar$ , the quasiparticle picture for fermions survives [5,6]. In presence of a CP-violating condensate there are two types of sources: the semiclassical force in the flow term of the kinetic Boltzmann equation, and the collisional sources. The semiclassical force was originally introduced for baryogenesis in two-Higgs doublet models in [7], and subsequently adapted to the chargino baryogenesis in the Minimal Supersymmetric Standard Model (MSSM) in [8]. The semiclassical force corresponds to tree level interactions with the condensate shown in Fig. 1 and it is universal in that its form is independent on interactions. The collisional sources on the other hand arise when fermions in the loop diagrams interact with scalar condensates. In Fig. 2 we show typical CP-violating one-loop contributions to the collisional source. This source arises from one-loop diagrams in which fermions interact with a CP-violating scalar condensate. When viewed in the kinetic Boltzmann equation, these processes correspond to tree-level inter-

$$tree = \overline{\text{---} \text{S} \text{---}} + \overline{\text{---}} \text{---} \overline{\text{---}} + \overline{\text{---}} \text{---} \overline{\text{---}} + \dots$$

x CP violating condensate

**Fig. 1.** The tree level interactions of fermions with the scalar field condensate which, when expanded in gradients, lead to the CP-violating semiclassical force in the kinetic Boltzmann equation.

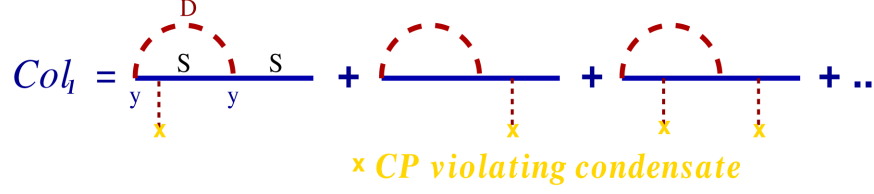


**Fig. 2.** The one-loop fermion-scalar diagrams, where interactions of fermions with the scalar field condensate are explicitly shown. The condensate interactions, when expanded in gradients, result in a CP-violating collisional source in the kinetic Boltzmann equation. Upon projecting (or ‘cutting’) the loop propagators on-shell one obtains the CP-violating scalar particle absorption and emission processes.

actions in which fermions absorb or emit scalar particles, whilst interacting in a CP-violating manner with the scalar condensate. The precise form of the collisional source depends on the form of the interaction. In the following sections we discuss how one can study the CP-violating collisional sources induced by a typical Yukawa interaction term.

## 2 Kinetic Equations

Here we work in the simple model of chiral fermions coupled to a complex scalar field *via* the Yukawa interaction with the Lagrangian of the form [5,6]

$$\mathcal{L} = i\bar{\psi}\not{\partial}\psi - \bar{\psi}_L m \psi_R - \bar{\psi}_R m^* \psi_L + \mathcal{L}_{\text{Yu}}, \quad (2)$$

where  $\mathcal{L}_{\text{Yu}}$  denotes the Yukawa interaction term

$$\mathcal{L}_{\text{Yu}} = -y\phi\bar{\psi}_L\psi_R - y\phi^*\bar{\psi}_R\psi_L, \quad (3)$$

and  $m$  is a complex, spatially varying mass term

$$m(u) \equiv y'\Phi_0 = m_R(u) + im_I(u) = |m(u)|e^{i\theta(u)}. \quad (4)$$

Such a mass term arises naturally from an interaction with a scalar field condensate  $\Phi_0 = \langle\hat{\Phi}(u)\rangle$ . This situation is realised for example by the Higgs field condensate of a first order electroweak phase transition in supersymmetric models. When  $\phi$  in (3) is the Higgs field the coupling constants  $y$  and  $y'$  coincide. Our considerations are however not limited to this case.

The dynamics of quantum fields can be studied by considering the equations of motion arising from the two-particle irreducible (2PI) effective action [9] in the Schwinger-Keldysh closed-time-path formalism [10,11]. This formalism is suitable for studying the dynamics of the non-equilibrium fermionic and bosonic two-point functions

$$iS_{\alpha\beta}(u, v) = \langle\Omega|T_C[\psi_\alpha(u)\bar{\psi}_\beta(v)]|\Omega\rangle \quad (5)$$

$$i\Delta(u, v) = \langle\Omega|T_C[\phi(u)\phi^\dagger(v)]|\Omega\rangle, \quad (6)$$

where  $|\Omega\rangle$  is the physical state, and the time ordering  $T_C$  is along the Schwinger contour shown in Fig. 3. For our purposes it suffices to consider the limit when  $t_0 \rightarrow -\infty$ . The complex path time ordering can be conveniently represented in the Keldysh component formalism. For example, for nonequilibrium dynamics of quantum fields the following Wightman propagator is relevant

$$iS^<(u, v) = -\langle \Omega | \bar{\psi}(v) \psi(u) | \Omega \rangle. \quad (7)$$

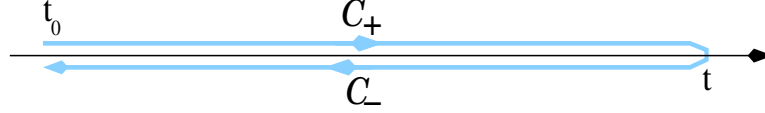


**Fig. 3.** The complex time contour for the Schwinger-Keldysh nonequilibrium formalism.

For thick walls, that is for the plasma excitations whose de Broglie wavelength  $\ell_{\text{dB}}$  is small in comparison to the phase interface thickness  $L_w$ , it is suitable to work in the Wigner representation for the propagators, which corresponds to the Fourier transform with respect to the relative coordinate  $r = u - v$ , and expand in the gradients of average coordinate  $x = (u + v)/2$ . This then represents an expansion in powers of  $\ell_{\text{dB}}/L_w$ . When written in this Wigner representation, the kinetic equations for fermions become [12]

$$\mathcal{D}S^< \equiv \left( \frac{i}{2} \not{\partial} + \not{k} - (mP_R - m^*P_L) e^{-\frac{i}{2} \overleftarrow{\partial} \cdot \partial_k} \right) S^< = \mathcal{C}_\psi, \quad (8)$$

where for simplicity we neglected the contributions from self-energy corrections to the mass and the collisional broadening term [12]. When the collision term  $\mathcal{C}_\psi$  is approximated at one loop, equation (8) corresponds to the nonequilibrium fermionic Schwinger-Dyson equation shown in Fig. 4. Since the scalar equation (also shown in Fig. 4) does not yield CP-violating sources at first order in gradients [5,14], we shall not discuss it here.

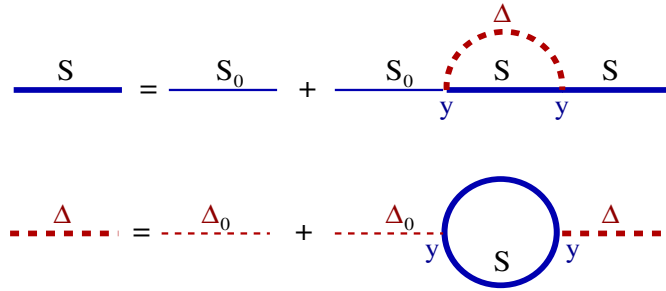


**Fig. 4.** The one-loop Schwinger-Dyson equations for the out-of-equilibrium fermionic ( $S$ ) and scalar ( $\Delta$ ) propagators. When projected on-shell and expanded in gradients, these equations reduce to the kinetic Boltzmann equations.

As the bubbles grow large, they tend to become more and more planar. Hence, it suffices to consider the limit of a planar phase interface, in which the mass condensate in the wall frame becomes a function of one coordinate only,  $m = m(z)$ . Further, we keep only the terms that contribute at order  $\hbar$  to (8), which implies that we need to keep second order gradients of the mass term

$$me^{-\frac{i}{2}\overleftarrow{\partial} \cdot \partial_k} = m + \frac{i}{2}m'\partial_{k_z} - \frac{1}{8}m''\partial_{k_z}^2 + o(\partial_z^3), \quad (9)$$

where  $m = m(z)$ ,  $m' \equiv \partial_z m$  and  $m'' \equiv \partial_z^2 m$ . On the other hand, in the collision term  $\mathcal{C}_\psi$  we need to consider terms only up to linear order in derivatives

$$\begin{aligned} \mathcal{C}_\psi &= \mathcal{C}_{\psi 0} + \mathcal{C}_{\psi 1} + \dots \\ \mathcal{C}_{\psi 0} &= -\frac{1}{2}(\Sigma^> S^< - \Sigma^< S^>) \\ \mathcal{C}_{\psi 1} &= -\frac{i}{4}(\partial_z^{(1)} \partial_{k_z}^{(2)} - \partial_{k_z}^{(1)} \partial_z^{(2)})(\Sigma^> S^< - \Sigma^< S^>), \end{aligned} \quad (10)$$

where  $\Sigma^<$  and  $\Sigma^>$  represent the fermionic self-energies, and the derivatives  $\partial_z^{(1)}$ ,  $\partial_{k_z}^{(1)}$  ( $\partial_z^{(2)}$ ,  $\partial_{k_z}^{(2)}$ ) act on the first (second) factor in the parentheses.

An important observation is that, when  $G = G(k_\mu, t - \mathbf{x}_\parallel \cdot \mathbf{k}_\parallel, z)$ , the spin in the  $z$ -direction (of the interface motion)

$$S_z \equiv L^{-1}(\Lambda) \tilde{S}_z L(\Lambda) = \gamma_\parallel (\tilde{S}_z - i(\mathbf{v}_\parallel \times \boldsymbol{\alpha})_z) \quad (11)$$

is conserved

$$[\mathcal{D}, S_z] S^< = 0, \quad (12)$$

where  $\mathcal{D}$  is the differential operator in (8),  $\boldsymbol{\alpha} = \gamma^0 \boldsymbol{\gamma}$ ,  $\tilde{S}_z = \gamma^0 \gamma^3 \gamma^5$ , and  $\gamma_\parallel = 1/(1 - \mathbf{v}_\parallel^2)^{1/2}$ . This then implies that, without a loss of generality, the fermionic Wigner function can be written in the following block-diagonal form

$$\begin{aligned} S^< &= \sum_{s=\pm} S_s^< \\ S^< &= L(\Lambda)^{-1} \tilde{S}^< L(\Lambda) \\ -i\gamma^0 \tilde{S}_s^< &= \frac{1}{4}(\mathbf{1} + s\sigma^3) \otimes \rho^a \tilde{g}_a^s, \end{aligned} \quad (13)$$

where  $\sigma^3$  and  $\rho^i$  ( $i = 1, 2, 3$ ) are the Pauli matrices and  $\rho^0 = \mathbf{1}$  is the  $2 \times 2$  unity matrix and  $L(\Lambda)$  is the following Lorentz boost operator

$$L(\Lambda) = \frac{k_0 + \tilde{k}_0 - \gamma^0 \boldsymbol{\gamma} \cdot \mathbf{k}_\parallel}{\sqrt{2\tilde{k}_0(k_0 + \tilde{k}_0)}}, \quad (14)$$

with  $\tilde{k}_0 = \text{sign}(k_0)(k_0^2 - \mathbf{k}_\parallel^2)^{1/2}$ . The boost  $\Lambda$  corresponds to a Lorentz transformation that transforms away  $\mathbf{k}_\parallel$ .

With the decomposition (13) the trace of the antihermitean part of (8) can be written as the following *algebraic* constraint equation [6]

$$\left(k^2 - |m|^2 + \frac{s}{\tilde{k}_0}(|m|^2\theta')\right)g_{00}^s = 0, \quad (15)$$

where  $g_{00}^s = \gamma_{\parallel}\tilde{g}_0^{s<}$  denotes the particle density on phase space  $\{k_{\mu}, x_{\nu}\}$ . Equation (15) has a spectral solution

$$g_{00}^s \equiv \sum_{\pm} \frac{2\pi}{Z_{s\pm}} n_s \delta(k_0 \mp \omega_{s\pm}), \quad (16)$$

where  $\omega_{s\pm}$  denotes the dispersion relation

$$\omega_{s\pm} = \omega_0 \mp s \frac{|m|^2\theta'}{2\omega_0\tilde{\omega}_0}, \quad \omega_0 = \sqrt{\mathbf{k}^2 + |m|^2}, \quad \tilde{\omega}_0 = \sqrt{\omega_0^2 - \mathbf{k}_{\parallel}^2} \quad (17)$$

and  $Z_{s\pm} = 1 \mp s|m|^2\theta'/2\tilde{\omega}_0^3$ . The delta functions in (16) project  $n_s(k_{\mu}, t - \mathbf{x}_{\parallel} \cdot \mathbf{k}_{\parallel}, z)$  on-shell, thus yielding the distribution functions  $f_{s+}$  and  $f_{s-}$  for particles and antiparticles with spin  $s$ , respectively, defined by

$$\begin{aligned} f_{s+} &\equiv n_s(\omega_{s+}, k_z, t - \mathbf{x}_{\parallel} \cdot \mathbf{k}_{\parallel}, z) \\ f_{s-} &\equiv 1 - n_s(-\omega_{s-}, -k_z, t + \mathbf{x}_{\parallel} \cdot \mathbf{k}_{\parallel}, z). \end{aligned} \quad (18)$$

This on-shell projection proves the implicit assumption underlying the semiclassical WKB-methods, that the plasma can be described as a collection of single-particle excitations with a nontrivial space-dependent dispersion relation. In fact, the decomposition (13), (15) and the subsequent discussion imply that the physical states that correspond to the quasiparticle plasma excitations are the eigenstates of the spin operator (11).

Taking the trace of the Hermitean part of (8), integrating over the positive and negative frequencies and taking account of (16) and (18), one obtains the following on-shell kinetic equations [6]

$$\partial_t f_{s\pm} + \mathbf{v}_{\parallel} \cdot \nabla_{\parallel} f_{s\pm} + v_{s\pm} \partial_z f_{s\pm} + F_{s\pm} \partial_{k_z} f_{s\pm} = \mathcal{C}_{\psi s\pm}[f_{s\pm}], \quad (19)$$

where  $f_{s\pm} = f_{s\pm}(k_{\mu}, z, t - \mathbf{v}_{\parallel} \cdot \mathbf{x}_{\parallel})$ ,  $\mathcal{C}_{s\pm}[f_{s\pm}]$  is the collision term obtained by integrating (10) over the positive and negative frequencies, respectively, the quasiparticle *group velocity*  $v_{s\pm} \equiv k_z/\omega_{s\pm}$  is expressed in terms of the kinetic momentum  $k_z$  and the quasiparticle energy  $\omega_{s\pm}$  (17), and the *semiclassical force*

$$F_{s\pm} = -\frac{|m|^2\theta'}{2\omega_{s\pm}} \pm \frac{s(|m|^2\theta')'}{2\omega_0\tilde{\omega}_0}. \quad (20)$$

In the stationary limit in the wall frame the distribution function simplifies to  $f_{s\pm} = f_{s\pm}(k_{\mu}, z)$ . When compared with the 1+1 dimensional case studied in [5] the sole, but significant, difference in the force (20) is that the CP-violating  $\theta'$ -term is enhanced by the boost-factor  $\gamma_{\parallel} = \omega_0/\tilde{\omega}_0$ ,  $\tilde{\omega}_0 = (\omega_0^2 - \mathbf{k}_{\parallel}^2)^{1/2}$ , which, when integrated over the momenta, leads to an enhancement by about a factor *two* in the CP-violating source from the semiclassical force.



### 3 Sources for Baryogenesis in the Fluid Equations

Fluid transport equations are usually obtained by taking first two moments of the Boltzmann transport equation (19). That is, integrating (19) over the spatial momenta results in the continuity equation for the vector current, while multiplying by the velocity and integrating over the momenta yields the Euler equation. The physical content of these equations can be summarized as the particle number and fluid momentum density conservation laws for fluids, respectively. This procedure is necessarily approximate simply because the fluid equations describe only very roughly the rich momentum dependence described by the distribution functions of the Boltzmann equation (20). The fluid equations can be easily reduced to the diffusion equation which has so far being used almost exclusively for electroweak baryogenesis calculations at a first order electroweak phase transition. A useful intermediate step in derivation of the fluid equations is rewriting (19) for the CP-violating departure from equilibrium  $\delta f_{si} = \delta f_{si+} - \delta f_{si-}$  as follows

$$\begin{aligned} & \left( \partial_t + \frac{k_z}{\omega_{0i}} \partial_z - \frac{|m_i|^{2'}}{2\omega_{0i}} \partial_{k_z} \right) \delta f_{si} + v_w \delta F_{si} (\partial_\omega f_\omega)_{\omega_{0i}} \\ & + v_w F_{0i} \delta \omega_{si} \left[ \left( \frac{\partial_\omega f_\omega}{\omega} \right)_{\omega_{0i}} - (\partial_\omega^2 f_\omega)_{\omega_{0i}} \right] = \mathcal{C}_{\psi si}, \end{aligned} \quad (21)$$

where  $i$  is the species (flavour) index,  $f_\omega = 1/(e^{\beta\omega} + 1)$ , and

$$\begin{aligned} F_{0i} &= -\frac{|m_i|^{2'}}{2\omega_{0i}} \\ \delta \omega_{si} &= s \frac{(|m_i|^{2'} \theta_i)'}{\omega_{0i} \tilde{\omega}_{0i}} \\ \delta F_{si} &\equiv F_{si+} - F_{si-} = s \frac{(|m_i|^{2'} \theta_i')'}{\omega_{0i} \tilde{\omega}_{0i}} \\ \mathcal{C}_{\psi si} &\equiv \mathcal{C}_{\psi si+} - \mathcal{C}_{\psi si-}. \end{aligned} \quad (22)$$

When integrating (21) over the momenta, the flow term yields two sources in the continuity equation for the vector current. The former comes from the CP-violating spin dependent semiclassical force, and has the form

$$\begin{aligned} \mathcal{S}_{si}^a &= v_w \int \frac{d^3 k}{(2\pi)^3} \delta F_{si} (\partial_\omega f_\omega)_{\omega=\omega_{0i}} \\ &= -s v_w \frac{(|m_i|^{2'} \theta_i')'}{4\pi^2} \mathcal{J}_a(x_i) \end{aligned} \quad (23)$$

with  $x_i = |m_i|/T$ , while the latter comes from the CP-violating shift in the quasiparticle energy, and can be written as

$$\begin{aligned} \mathcal{S}_{si}^b &= v_w \int \frac{d^3 k}{(2\pi)^3} F_{0i} \delta \omega_{si} \left[ (\partial_\omega f_\omega / \omega)_{\omega_{0i}} - (\partial_\omega^2 f_\omega)_{\omega_{0i}} \right] \\ &= s v_w \frac{(|m_i|^{2'} \theta_i')}{2\pi^2 T} |m_i|' \mathcal{J}_b(x_i). \end{aligned} \quad (24)$$

The total source is simply the sum of the two,  $\mathcal{S}_{si} = \mathcal{S}_{si}^a + \mathcal{S}_{si}^b$ . To get a more quantitative understanding of these sources, in Fig. 5 we plot the integrals  $\mathcal{J}_a$  and  $\mathcal{J}_b$  in equations (23) and (24). A closer inspection of the sources  $\mathcal{S}_{si}^a$  and  $\mathcal{S}_{si}^b$  indicates that the total source  $\mathcal{S}_{si}$  can be also rewritten as the sum of two sources: the source  $\propto |m_i|^{2'}\Theta'_i$ , characterized by  $x_i^2\mathcal{J}_a + x_i^3\mathcal{J}_b$ , and the source  $\propto |m_i|^2\Theta''_i$ , characterized by  $x_i^2\mathcal{J}_a$ . We note that in the spin state quasiparticle basis the flow term sources appear in the continuity equation for the vector current, while in the helicity basis, which is usually used in literature [7,8], the flow term sources appear in the Euler equation. In Fig. 6 we show recent results of baryogenesis calculations of [8] based on the CP-violating contribution to the semiclassical force in the chargino sector of the Minimal Supersymmetric Standard Model (MSSM). This calculation is based on the quasiparticle picture based on helicity states. The analysis suggests that one can dynamically obtain

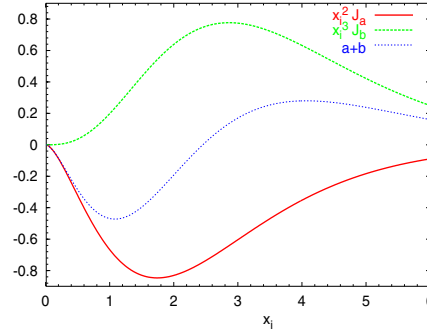


**Fig. 5.** The flow term sources (23)-(24) characterised by the integrals  $x_i^2\mathcal{J}_a(x_i)$  (red solid) and  $x_i^3\mathcal{J}_b(x_i)$  (green dashed) as a function of the rescaled mass  $x_i = |m_i|/T$ . The sum of the two sources (thin blue line) is also shown.

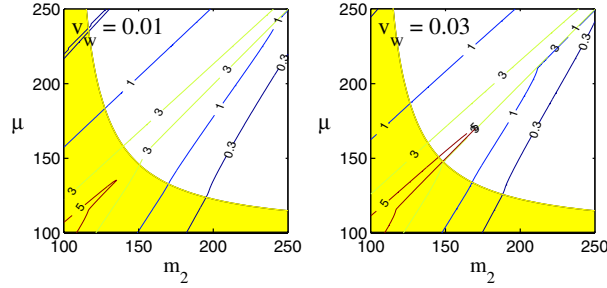


**Fig. 6.** The semiclassical force baryogenesis mediated by charginos of the MSSM calculated in the helicity basis. The figures show contours for the baryon-to-entropy ratio in the units of  $10^{-11}$  for two wall velocities  $v_w = 0.01$  and  $v_w = 0.03$  as a function of the soft susy breaking parameters  $\mu$  and  $m_2$ . A maximal CP violation in the chargino sector is assumed. The shaded (yellow) regions are ruled out by the LEP measurements. The observed baryon asymmetry is in these units 3 – 7. (The figure is taken from the latter reference in [8].)

baryon production marginally consistent with the observed value (1), provided  $m_2 \sim \mu \sim 150$  GeV and  $v_w \sim 0.03c$ .

We now turn to discussion of the collision term sources in (19) and (21). We assume that the self-energies  $\Sigma^{>,<}$  are approximated by the one-loop expressions (*cf.* Fig. 4)

$$\begin{aligned} \Sigma^{<,>}(k, x) = iy^2 \int \frac{d^4 k' d^4 k''}{(2\pi)^8} & [(2\pi)^4 \delta(k - k' + k'') P_L S^{<,>}(k', x) P_R \Delta^{>,<}(k'', x) \\ & + (2\pi)^4 \delta(k - k' - k'') P_R S^{<,>}(k', x) P_L \Delta^{<,>}(k'', x)], \end{aligned} \quad (25)$$

where  $\Delta^{<}$  and  $\Delta^{>}$  denote the bosonic Wigner functions. This expression contains both the CP-violating sources and relaxation towards equilibrium. The CP-violating sources can be evaluated by approximating the Wigner functions  $S^{>,<}$  and  $\Delta^{>,<}$  by the equilibrium expressions accurate to first order in derivatives. The result of the investigation is as follows. There is no source contributing to the continuity equation, while the source arising in the Euler equation is of the form [12]

$$2 \int_{\pm} \frac{d^4 k}{(2\pi)^4} \frac{k_z}{\omega_0} \mathcal{C}_{\psi si} = v_w y^2 \frac{s|m|^2 \theta'}{32\pi^3 T} \mathcal{I}_f(|m|, m_\phi), \quad (26)$$

where the function  $\mathcal{I}_f(|m|, m_\phi)$  is plotted in Fig. 7. It is encouraging that the source vanishes for small values of the mass parameters, which suggests that the expansion in gradients we used here may yield the dominant sources. Note that the source is nonvanishing only in the kinematically allowed region,  $m_\phi \geq 2|m|$ . When the masses are large,  $|m|, m_\phi \gg T$ , the source is as expected Boltzmann suppressed. It would be of interest to make a detailed comparison between the sources in the flow term and those in the collision term. This is a subject of an upcoming publication.

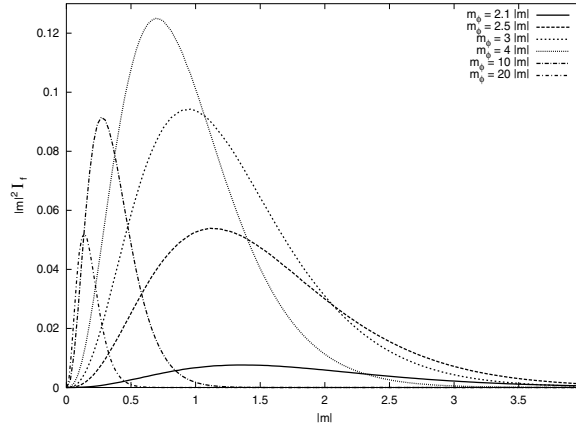


**Fig. 7.** The collisional source contributing to the fermionic kinetic equation at one loop for the mass ratios  $m_\phi/|m| = 2.1, 2.5, 3, 4, 10$  and  $20$ , respectively. The source peaks for  $|m| \approx 0.7T$  and  $m_\phi \approx 4|m|$ .

## References

1. Kuzmin V. A., Rubakov V. A., Shaposhnikov M. E. (1985): On The Anomalous Electroweak Baryon Number Nonconservation In The Early Universe. *Phys. Lett. B* **155**, 36.
2. Shaposhnikov M. E. (1987): Baryon Asymmetry Of The Universe In Standard Electroweak Theory. *Nucl. Phys. B* **287**, 757.
3. Quiros M., Seco M. (2000): Electroweak baryogenesis in the MSSM. *Nucl. Phys. Proc. Suppl.* **81**, 63 [arXiv:hep-ph/9903274].
4. Cohen A. G., Kaplan D. B., Nelson A. E. (1990): Weak Scale Baryogenesis. *Phys. Lett. B* **245**, 561; Cohen A. G., Kaplan D. B., Nelson A. E. (1991): Baryogenesis At The Weak Phase Transition. *Nucl. Phys. B* **349**, 727.
5. Kainulainen K., Prokopec T., Schmidt M. G., Weinstock S. (2001): First principle derivation of semiclassical force for electroweak baryogenesis. *JHEP* **0106**, 031 [arXiv:hep-ph/0105295].
6. Kainulainen K., Prokopec T., Schmidt M. G., Weinstock S. (2002): Semiclassical force for electroweak baryogenesis: Three-dimensional derivation. arXiv:hep-ph/0202177.
7. Joyce M., Prokopec T., Turok N. (1996): Nonlocal electroweak baryogenesis. Part 2: The Classical regime. *Phys. Rev. D* **53**, 2958 [arXiv:hep-ph/9410282]; Joyce M., Prokopec T., Turok N. (1995): Electroweak baryogenesis from a classical force. *Phys. Rev. Lett.* **75**, 1695 [Erratum-ibid. **75** (1995) 3375] [arXiv:hep-ph/9408339].
8. Cline J. M., Kainulainen K. (2000): A new source for electroweak baryogenesis in the MSSM. *Phys. Rev. Lett.* **85**, 5519 [hep-ph/0002272]; Cline J. M., Joyce M., Kainulainen K. (2000): Supersymmetric electroweak baryogenesis. *JHEP* **0007**, 018 [arXiv:hep-ph/0006119]; *ibid.* hep-ph/0110031.
9. Cornwall J. M., Jackiw R., Tomboulis E. (1974): Effective Action For Composite Operators. *Phys. Rev. D* **10**, 2428.
10. Schwinger J. (1961): *J. Math. Phys.* **2**, 407; Keldysh L. V. (1964): *Zh. Eksp. Teor. Fiz.* **47**, 1515 [*Sov. Phys. JETP* **20** (1965) 235].
11. Chou K., Su Z., Hao B., Yu L. (1985): Equilibrium And Nonequilibrium Formalisms Made Unified. *Phys. Rept.* **118** 1; Calzetta E., Hu B. L. (1988): Nonequilibrium Quantum Fields: Closed Time Path Effective Action, Wigner Function And Boltzmann Equation. *Phys. Rev. D* **37**, 2878.
12. Kainulainen K., Prokopec T., Schmidt M. G., Weinstock S. (2002): Some aspects of collisional sources for electroweak baryogenesis. arXiv:hep-ph/0201245.
13. Kainulainen K., Prokopec T., Schmidt M. G., Weinstock S. (2002): Quantum Boltzmann equations for electroweak baryogenesis including gauge fields. arXiv:hep-ph/0201293.
14. Kainulainen K., Prokopec T., Schmidt M. G., Weinstock S. (2002): in preparation.

# Quantum Corrections for BTZ Black Hole via 2D Reduced Model

Maja Burić, Marija Dimitrijević, and Voja Radovanović

Faculty of Physics, University of Belgrade, P. O. Box 368, 11001 Belgrade, Yugoslavia

**Abstract.** The one-loop quantum corrections for BTZ black hole are considered using the dimensionally reduced 2D model. In 3D minimal case Unruh vacuum states is defined and the corresponding semiclassical corrections of the geometry are found.

For a long time it was believed that black hole solutions do not exist in three dimensions, and therefore the discovery of Banados, Teitelboim and Zanelli [1] came as a surprise. This solution has many properties which the familiar black hole solutions in four dimensions (4D) do not possess. BTZ black hole can be obtained by identifications of points in 3D anti-de Sitter (AdS) space [2], the space of constant negative curvature. BTZ black hole is locally anti-de Sitter space, and therefore its singularity is not a curvature singularity.

One of the most interesting questions in the analysis of black holes is the Hawking radiation. A considerable work has been done in the last couple of years in an effort to find 2D effective models which can describe the properties of 4D black holes and radiated field. The main idea of this approach is to consider the effective action obtained by functional integration of scalar field as semiclassical correction to the gravitational action. There are a couple of different variants of 2D effective action but usually it describes the effects of s-modes of scalar field to the one-loop order. A similar analysis has been recently extended [3] to the reduction of BTZ black hole from three to two dimensions in the case of minimal 3D coupling with scalar matter.

Our goal is to define the Unruh vacuum by means of dimensionally reduced model. The definition of the Unruh vacuum seems still to be an open question for BTZ black hole.

We start with the three dimensional gravitational action with negative cosmological constant ( $-2\Lambda = -2l^{-2} < 0$ ) coupled to the scalar field  $f$ :

$$I_0^{(3)} = \frac{1}{16\pi G} \int d^3x \sqrt{-g^{(3)}} \left( R^{(3)} + \frac{2}{l^2} \right) - \frac{1}{16\pi G} \int d^3x \sqrt{-g^{(3)}} (\nabla f)^2. \quad (1)$$

We consider the BTZ black hole solution which is locally  $\text{AdS}_3$  space:

$$ds_{(3)}^2 = - \left( \frac{r^2}{l^2} - lM \right) dt^2 + J l dt d\theta + r^2 d\theta^2 + \left( \frac{r^2}{l^2} - lM + \frac{J^2 l^2}{4r^2} \right)^{-1} dr^2. \quad (2)$$

If we construct the metric reduced from (2) to two-dimensional  $t, r$  hypersurface by the standard procedure, we obtain

$$ds^2 = -g_{cl} dt^2 + \frac{1}{g_{cl}} dr^2, \quad (3)$$

where the metric function  $g_{cl}(r)$  is given by

$$g_{cl} = \frac{r^2}{l^2} - lM + \frac{J^2 l^2}{4r^2} = \frac{(r^2 - r_+^2)(r^2 - r_-^2)}{r^2 l^2} . \quad (4)$$

As showed in [2], quantities  $M$  and  $J$  have the meaning of mass and angular momentum. The last equality holds when  $Ml \geq J$ ; the case  $Ml = J$  is the extremal BTZ black hole. Let us assume the axially symmetric metric ansatz in three dimensions:

$$ds_{(3)}^2 = g_{\mu\nu} dx^\mu dx^\nu + l^2 \Phi^2 (\alpha d\theta + A_\mu dx^\mu)^2 , \quad (5)$$

where  $g_{\mu\nu}, \Phi, A_\mu$  are two-dimensional metric, dilaton and U(1) gauge field. All quantities do not depend on  $\theta$ . The constant  $\alpha$  will be fixed later.

Introducing the reduction formula (5) into the action (1) and integrating over the angular variable  $\theta$ , we obtain 2D action

$$\Gamma = \frac{l\alpha}{8G} \int d^2x \sqrt{-g} \Phi \left( R - \frac{l^2 \Phi^2}{4} F^2 + \frac{2}{l^2} - (\nabla f)^2 \right) , \quad (6)$$

In the following, we will choose  $\alpha$  such that  $\frac{l\alpha}{8G} = 1$ . Also, instead of the dilaton field  $\Phi$ , we will use its logarithm  $\varphi = \log \Phi$ .

In order to analyze the vacuum fluctuations of the scalar field  $f$ , one has to integrate it functionally to the first order in  $\hbar$ . Our approximation consists of the fact that we do the functional integration of  $f$  in 2D action and not in the full 3D action. We use the methods developed in [4,5]. The result which we obtained for the one-loop effective action is

$$\Gamma_1 = -\frac{1}{96\pi} \int d^2x \sqrt{-g} R \frac{1}{\nabla^2} R + \frac{1}{8\pi} \int d^2x \sqrt{-g} \left( \frac{1}{4} R \frac{1}{\nabla^2} (\nabla \varphi)^2 + \frac{1}{2} R \varphi \right) . \quad (7)$$

It is easier to use the local form of the action (6); it can be obtained by a suitable introduction of auxiliary fields [6]. The local form is given by

$$\Gamma_1 = -\frac{1}{96\pi} \int d^2x \sqrt{-g} \left( 2R(\psi - \frac{3}{2}\chi) + (\nabla \psi)^2 - 3(\nabla \psi)(\nabla \chi) - 3(\nabla \varphi)^2 \psi - 6R\varphi \right) , \quad (8)$$

where the auxiliary fields  $\psi$  and  $\chi$  satisfy equations

$$\nabla^2 \psi = R , \quad (9)$$

$$\nabla^2 \chi = (\nabla \varphi)^2 . \quad (10)$$

The equations of motion are

$$\nabla_\mu (e^{3\varphi} F^{\mu\nu}) = 0 , \quad (11)$$

$$R + \frac{2}{l^2} - \frac{3l^2}{4} e^{2\varphi} F^2 = 6\kappa e^{-\varphi} (-R + \nabla_\mu (\psi \nabla^\mu \varphi)) , \quad (12)$$

$$\begin{aligned}
& g_{\alpha\beta} \nabla^2 \Phi - \nabla_\alpha \nabla_\beta \Phi - \Phi g_{\alpha\beta} \left( \frac{1}{l^2} - \frac{l^2}{8} \Phi^2 F_{\mu\nu} F^{\mu\nu} \right) - \frac{l^2}{2} \Phi^3 F_{\beta\mu} F_\alpha^\mu \\
& = T_{\alpha\beta}/2 \\
& = \kappa \left( \nabla_\alpha \psi \nabla_\beta \psi - \frac{3}{2} \nabla_\alpha \psi \nabla_\beta \chi - \frac{3}{2} \nabla_\alpha \chi \nabla_\beta \psi \right. \\
& \quad - 3\psi \nabla_\alpha \varphi \nabla_\beta \varphi - 2\nabla_\beta \nabla_\alpha (\psi - 3\varphi - \frac{3}{2}\chi) \\
& \quad \left. - \frac{1}{2} g_{\alpha\beta} ((\nabla\psi)^2 - 3\nabla\psi\nabla\chi - 3\psi(\nabla\varphi)^2) + 2g_{\alpha\beta} \nabla^2 (\psi - 3\varphi - \frac{3}{2}\chi) \right),
\end{aligned} \tag{13}$$

where  $\kappa = 1/96\pi$ .  $T_{\alpha\beta}$  is the energy-momentum tensor of the radiated matter.

The Unruh vacuum can be defined as the state of matter whose energy-momentum tensor is regular on the future event horizon. From this demand we find expression for  $T_{\mu\nu}$ .

Now we will find the corrected geometry. The one-loop ansatz for the metric is

$$ds^2 = -ge^{2\kappa\omega} dv^2 + 2e^{\kappa\omega} dv dr, \tag{14}$$

where  $g = g_{cl} - \kappa lm$ . Solving the equations of motion we obtain the one-loop correction for the metric:

$$\begin{aligned}
m = & -v \frac{r_+^2 - r_-^2}{l^4 r_+ r_-^3} (-3r^4 + 8r_+ r^3 - 3(r_+^2 + r_-^2)r^2 + r_+^2 r_-^2) \\
& + \frac{4r^2 - 6(r_+^2 + r_-^2)}{l^2 r} + 16 \frac{r_-}{l^2} \log \frac{r + r_-}{r - r_-} \\
& + \frac{3r^4 + 3(r_+^2 + r_-^2)r^2 - r_+^2 r_-^2}{l^2 r^3} \left( \log \frac{(r + r_+)^2 (r^2 - r_-^2)}{r^2 l^2} - \frac{r_-}{r_+} \log \frac{r + r_-}{r - r_-} \right), \\
\omega = & \frac{l(3r_- - r_+)(r_+ + r_-)}{r_+(r + r_-)(r_- - r_+)} - \frac{l(r_- - r_+)(r_+ + 3r_-)}{r_+(r - r_-)(r_- + r_+)} - \frac{2l(3r_+^2 + r_-^2)}{(r + r_+)(r_+^2 - r_-^2)} \\
& + \frac{8lr_-}{(r_+^2 - r_-^2)^2} \left( (r_+^2 + r_-^2) \log \frac{r - r_-}{r + r_-} + 2r_+ r_- \log \frac{(r + r_+)^2}{r^2 - r_-^2} \right) \\
& - \frac{3l}{r} \left( \log \frac{(r + r_+)^2 (r^2 - r_-^2)}{r^2 l^2} - \frac{r_-}{r_+} \log \frac{r + r_-}{r - r_-} \right) + \frac{l}{r} - 3v \frac{r_+^2 - r_-^2}{l r_+ r}.
\end{aligned} \tag{15}$$

The value for the apparent horizon in this case is

$$\begin{aligned}
r_{AH} = & r_+ + \kappa \frac{l}{r_+(r_+^2 - r_-^2)} \left( r_+(3r_+^2 + r_-^2) \log \frac{4(r_+^2 - r_-^2)}{l^2} \right. \\
& \left. - r_-(r_-^2 - 5r_+^2) \log \frac{r_+ + r_-}{r_+ - r_-} - r_+(r_+^2 + 3r_-^2) - \frac{v}{l^2} (r_+^2 - r_-^2)^2 \right).
\end{aligned} \tag{17}$$

In this paper we treated the one-loop corrections of dimensionally reduced BTZ black hole. The main result is the analysis of the Unruh vacuum for reduced BTZ model. This state is defined demanding that EMT is regular on the future horizon. It has peculiar properties.

We would like to mention that the one-loop geometry for conformal case is found in [7] and it is in a relatively good agreement with Neumann boundary conditions for the scalar field.

Note that the energy density in the asymptotic region does not obey Stefan-Boltzman law. This is not surprising if we keep in mind that the Hawking radiation is not a free boson gas in this region. The one-loop correction of entropy are logarithmic as it is often the case.

## References

1. M. Bañados, C. Teitelboim and J. Zanelli, Phys. Rev. Lett. **69**, 1849 (1992).
2. M. Bañados, C. Teitelboim and J. Zanelli, Phys. Rev. Lett. **69**, 1849 (1992).
3. A. J. M. Medved and G. Kunstatter, Phys. Rev. D **63**, 104005 (2001).
4. A. Miković and V. Radovanović, Class. Quant. Grav. **15**, 827 (1998).
5. A. Miković and V. Radovanović, Nucl. Phys. B **504**, 511 (1997).
6. M. Burić, V. Radovanović and A. Miković, Phys. Rev. D **59**, 084002 (1999).
7. M. Burić, M. Dimitrijević and V. Radovanović, “Quantum corrections for BTZ black hole via 2D reduced model”, preprint hep-th/0108.



# Squarks and Gluino Searches with CMS at LHC

Gabriele Segneri

Università degli studi di Pisa and INFN

**Abstract.** In this paper the studies about squarks and gluino searches with the CMS detector are reviewed. Inclusive squarks and gluino searches are described and the 5 sigma discovery contours are shown. The scalar bottom quark (*sbottom* or  $\tilde{b}$ ) and gluino ( $\tilde{g}$ ) reconstructions using the process  $\tilde{g} \rightarrow \tilde{b}b$  are discussed and the resolutions on sbottom and gluino masses are presented. The scalar top quark (*stop* or  $\tilde{t}$ ) search is also described and it is shown how the stop signal can be separated from the  $t\bar{t}$  background and the background due to the overall supersymmetric production.

## 1 Introduction

One of the main goals of the experiments at the Large Hadron Collider (LHC) [1] will be to find out new physics beyond the Standard Model. The Supersymmetry (SUSY) [2] and in particular the Minimal Supersymmetric Standard Model (MSSM) are possible extensions of this theory. Thanks to the centre of mass energy of 14 TeV which will be available at the LHC, it will be possible to extend the searches of the particles predicted by SUSY up to masses of 2.5 TeV.

The paper is dedicated to the searches with the CMS detector [3] of the new strongly interacting SUSY particles, the squarks and the gluino. The first part of the paper provides some general remarks about the MSSM-mSUGRA model which is assumed in the analyses. The inclusive squarks and gluino searches are described and for each of them the reach of the CMS experiment is provided. The reconstruction of the decay  $\tilde{g} \rightarrow \tilde{b}b$  and the stop search are also discussed and some preliminary results are shown.

## 2 General Remarks

These studies are performed in the framework of the Minimal Supergravity (mSUGRA) model, a constrained version of the MSSM model. In this model Supersymmetry breaking occurs through the mediation of the universal gravitational interaction. At the Grand Unification (GUT) scale ( $m_{GUT} \sim 2 \cdot 10^{16}$  GeV) gauginos and scalars have common masses and couplings. Masses and couplings at the Electroweak scale are derived from those at GUT scale through Renormalisation Group Equations. The independent parameters of the model are: the common scalar mass  $m_0$ , the common gaugino mass  $m_{1/2}$ , the common trilinear coupling among the scalars  $A_0$ , the ratio between the vacuum expectation values of the two Higgs doublets  $\tan \beta$  and the sign of the higgsino mixing parameter  $\mu$ .

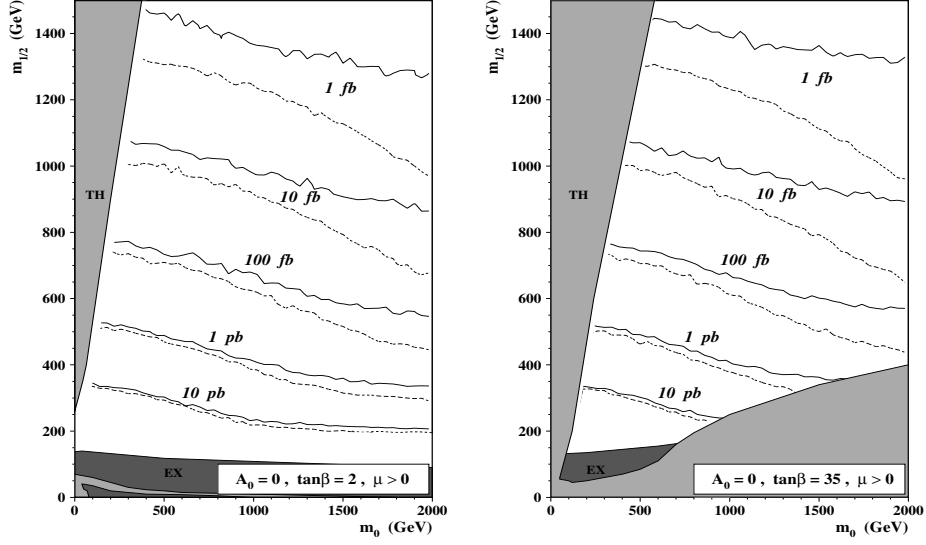


**Fig. 1.** Total mSUGRA cross-section contours as function of  $m_0$  and  $m_{1/2}$  for  $A_0 = 0$ ,  $\mu > 0$  and  $\tan \beta = 2$  (left figure) and  $\tan \beta = 35$  (right figure) [5]

An additional requirement is the R-parity conservation: as a consequence of this assumption, the SUSY particles can only be produced in even numbers at accelerator experiments. Moreover, the lightest SUSY particle (LSP) should be stable and each SUSY particle would decay into Standard Model particles and one LSP. The LSP in this model is the lightest neutralino  $\tilde{\chi}_1^0$ .

Contours corresponding to constant cross sections obtained with ISAJET 7.32 [4] are shown in Fig. 1 for  $A_0 = 0$ ,  $\mu > 0$ , different values of  $m_0$  and  $m_{1/2}$  and  $\tan \beta = 2$  (left plot) and  $\tan \beta = 35$  (right plot) [5]. The  $\mu < 0$  case is very similar and it is omitted. The overall SUSY production cross section (continuous line) is compared with the total cross section for processes with at least one strongly interacting SUSY particle (dashed line). At low values of  $m_0$  and  $m_{1/2}$  the two lines are very close since squarks and gluino are relatively light and dominate the SUSY particles production. Contours separate at higher  $m_0$  and  $m_{1/2}$  as squarks and sleptons become more massive.

### 3 Inclusive Searches

The inclusive searches are based on peculiar features which are common to all the SUSY processes involving squarks and gluino. A very high tagging efficiency can be achieved since the identification of the specific processes is not required.

The most remarkable features of squarks and gluino decays are:

- a large number of leptons produced by  $Z^0 \rightarrow \ell^+ \ell^-$ ,  $W^\pm \rightarrow \ell \nu$ ,  $\tilde{\chi}_2^0 \rightarrow \ell \tilde{\ell}$ ,  $\tilde{\ell} \tilde{\ell}^*$ ,  $\tilde{\ell} \rightarrow \ell \tilde{\chi}_1^0$  decays

- high  $E_T$  hadron jets from squarks and gluino decays ( $\tilde{q} \rightarrow q\tilde{\chi}_i^0$ ,  $\tilde{q} \rightarrow q'\tilde{\chi}_i^\pm$ ,  $\tilde{g} \rightarrow q\tilde{q}$ )
- large missing transverse momentum due to LSPs which do not interact with the detector
- a large number of  $b$  quarks (from decays of  $\tilde{t}$ ,  $\tilde{b}$ ,  $h$ ,  $t$ ) and  $\tau$  leptons (specially at high  $\tan\beta$ ).

Several search strategies based on some of these peculiarities are investigated [5] and for each of them the region of sensitivity of the CMS experiment is calculated.

Signal events are generated for several  $m_0$  and  $m_{1/2}$  values,  $\tan\beta = 2$  and 35,  $A_0 = 0$  and both signs of  $\mu$ . The SUSY processes are simulated with ISAJET 7.32 and the backgrounds ( $t\bar{t}$ ,  $Z^0$  plus jets,  $W^\pm$  plus jets, QCD) with PYTHIA 5.7[6]. The detector response is reproduced with a fast detector simulation package (CMSJET[7]). For each of these points the SUSY selection cuts are optimised in order to achieve the best sensitivity. Sensitivity is defined as  $S/\sqrt{S+B}$  being  $S$  and  $B$  the expected SUSY signal and the Standard Model background.

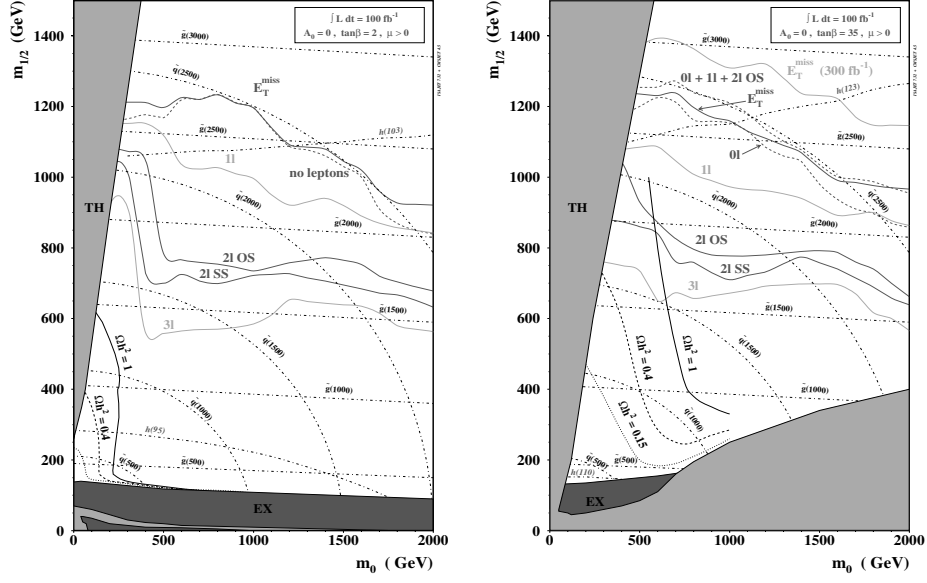
Five analyses, called 0l, 1l, 2lOS, 2lSS, 3l are based on the requirements of no leptons, at least one lepton, two leptons with opposite charge, two leptons with the same charge and three lepton respectively and one analysis is based only on missing transverse momentum ( $E_T^{miss}$ ). The basic requirements of  $E_T^{miss} > 200$  GeV and at least 2 jets with  $E_T^{jet} > 40$  GeV and  $|\eta^{jet}| < 3$  are common to all the analyses.

Figure 2 shows the five sigma discovery contours (corresponding to  $S/\sqrt{S+B} = 5$ ) for an integrated luminosity  $\int L dt = 100 \text{ fb}^{-1}$ ,  $A_0 = 0$ ,  $\mu > 0$ ,  $\tan\beta = 2$  (left plot) and 35 (right plot). The explorable regions lie below the contours. The  $\mu < 0$  case is very similar. The isomass contours of some SUSY particles and countours corresponding to  $\Omega h^2 = 1$  and 0.4 are also superimposed. The  $E_T^{miss}$  search, which has the best performance, allows to explore regions with  $m_{\tilde{q}} \sim 2.5 \text{ TeV}$ . The muon isolation, pile-up and uncertainty on cross-sections effects have been investigated as well and do not show a dramatic degradation in performance.

## 4 Scalar Bottom and Gluino Reconstructions

The gluino and the sbottom are the strongly interacting SUSY particles which are the simplest to reconstruct. The decay  $\tilde{g} \rightarrow b\tilde{b}$ , where  $\tilde{b} \rightarrow b\tilde{\chi}_2^0$ ,  $\tilde{\chi}_2^0 \rightarrow \tilde{\ell}\ell(\tilde{\ell}\ell) \rightarrow \tilde{\chi}_1^0\ell^+\ell^-$  would allow to reconstruct both particles simultaneously.

In this decay two  $b$ -jets, two same flavour and opposite charge leptons and large missing transverse momentum are produced and leptons have a peculiar  $\ell^+\ell^-$  invariant mass distribution with a sharp edge. If  $m_{\tilde{\chi}_2^0} < m_{\tilde{\ell}} + m_\ell$  the  $\tilde{\chi}_2^0$  decay would be a three body decay mediated by a virtual slepton and the edge would be placed at  $m_{\tilde{\chi}_2^0} - m_{\tilde{\chi}_1^0}$ . An example of lepton invariant mass distribution is shown in the left plot of Fig. 3. In the case  $m_{\tilde{\chi}_2^0} > m_{\tilde{\ell}} + m_\ell$  the neutralino



**Fig. 2.** Five sigma discovery contours for various final states in  $\int L dt = 100 \text{ fb}^{-1}$  for  $A_0 = 0$ ,  $\mu > 0$  and  $\tan \beta = 2$  (left figure) and  $\tan \beta = 35$  (right figure) [5]

decay is a two body decay and the edge would be placed at:

$$m_{\ell^+\ell^-} = \frac{\sqrt{(m_{\tilde{\chi}_2^0}^2 - m_l^2)(m_l^2 - m_{\tilde{\chi}_1^0}^2)}}{m_{\tilde{l}}}. \quad (1)$$

The point corresponding to the values of the mSUGRA parameters  $m_0 = 200$  GeV,  $m_{1/2} = 100$  GeV,  $\tan \beta = 2$ ,  $A_0 = 0$  and  $\mu < 0$  is examined. The signal events as well as the main background events are generated with PYTHIA 6.136 and detector simulation is performed with CMSJET. The statistics corresponds to an integrated luminosity of  $3 \text{ fb}^{-1}$ .

The  $\tilde{b}$  reconstruction is performed in two steps. Opposite charge leptons with an invariant mass distribution close to the edge are selected. This requirement allows to select a kinematical condition in which the leptons are emitted back to back in the  $\tilde{\chi}_2^0$  reference frame. In this condition and under the assumption  $m_{\tilde{\chi}_2^0} \sim 2m_{\tilde{\chi}_1^0}$ , which is usually valid, the  $\tilde{\chi}_2^0$  momentum is reconstructed through the formula:

$$\vec{P}_{\tilde{\chi}_2^0} = \left(1 + \frac{m_{\tilde{\chi}_1^0}}{m_{\ell^+\ell^-}}\right) \vec{P}_{\ell^+\ell^-}. \quad (2)$$

The  $\tilde{\chi}_2^0$  momentum is then summed with the momentum of the highest  $E_T$   $b$ -tagged jet and the  $\tilde{b}$  can be reconstructed. The gluino is reconstructed from the sbottom momentum and that of the closest  $b$ -tagged jet.

The mass distributions for these mSUGRA parameters values are shown in the right plot of Fig. 3. The resolutions on the  $\tilde{b}$  and  $\tilde{g}$  masses are 32 GeV and

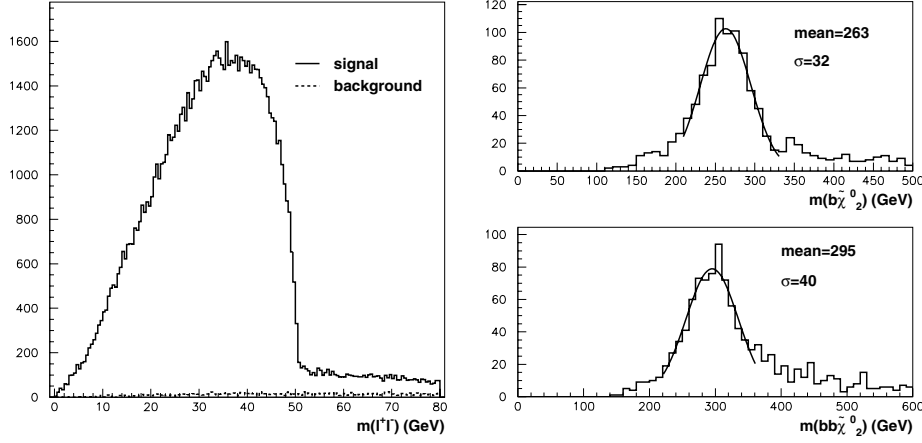


**Fig. 3.**  $m_{\ell+\ell-}$  distribution for leptons coming from  $\tilde{\chi}_2^0$  decay (left side) and invariant  $\tilde{b}$  and  $\tilde{g}$  mass distributions (right side) at  $m_0 = 200$  GeV,  $m_{1/2} = 100$  GeV,  $\tan\beta = 2$ ,  $A_0 = 0$  and  $\mu < 0$

40 GeV respectively. The measured values of  $m_{\tilde{b}}$  and  $m_{\tilde{g}}$  are 263 GeV and 295 GeV which are not far from the corresponding Monte Carlo input values 275 GeV and 299 GeV.

## 5 Scalar Top Quark Search

The stop eigenstate with the lowest mass would be the lightest scalar quark for a large set of values of the mSUGRA parameters. It can be abundantly produced at LHC and has special decay topologies. The possibility to observe a stop signal over the Standard Model and SUSY backgrounds is here discussed[9].

The main production processes would be the  $t\bar{t}$  pair production and the production from the gluino decay  $\tilde{g} \rightarrow t\bar{t}$  ( $t\bar{t}$ ). The study is concentrated on the  $t\bar{t}$  process since it would be the simplest one: despite its lower cross section it would provide a simpler event topology.

The dependence of the  $\tilde{t}$  mass with respect to  $m_0$  is shown in the left plot of Fig. 4 for different values of  $m_{1/2}$  at  $\tan\beta = 10$ ,  $\mu > 0$  and  $A_0=0$ : no remarkable dependence is foreseen on  $\tan\beta$  and the sign of  $\mu$ .

The  $t\bar{t}$  production cross-section is shown in the right plot of Fig. 4 as a function of the  $\tilde{t}$  mass. It rapidly decreases with  $m_{\tilde{t}}$  and depends on other parameters only through higher order corrections[8].

The  $\tilde{t} \rightarrow t\tilde{\chi}_1^0$  (with  $t \rightarrow bW^\pm$ ) and  $\tilde{t} \rightarrow b\tilde{\chi}_1^\pm$  ( $\tilde{\chi}_1^\pm \rightarrow W^\pm\tilde{\chi}_1^0$ ) decay modes are considered in the analysis since they would dominate in most of the parameter space points examined. Both channels provide one  $b$ -jet, one  $W^\pm$  and one  $\tilde{\chi}_1^0$ . The analysis is concentrated on  $t\bar{t}$  events where one of the two  $W^\pm$  (from  $t$  or  $\tilde{\chi}_1^\pm$ ) decays leptonically to provide lepton trigger and the other one decays hadronically to achieve high statistics.

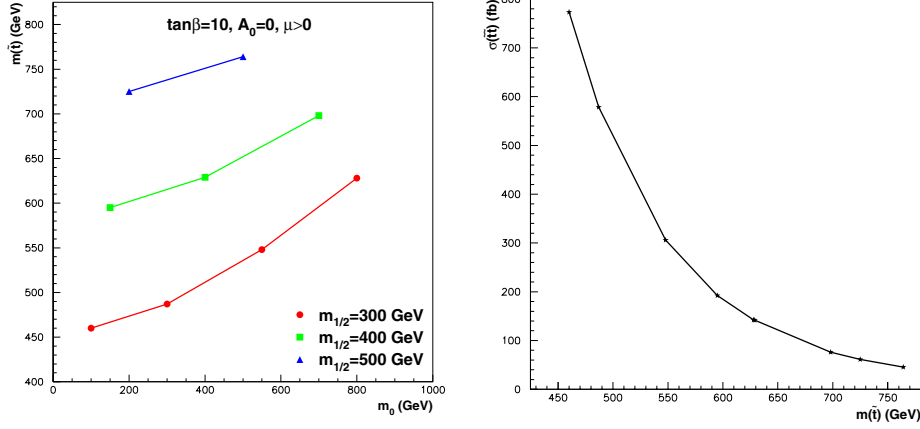


**Fig. 4.**  $\tilde{t}$  mass with respect to  $m_0$  for different values of  $m_{1/2}$  (left) and  $t\bar{t}$  production cross section as a function of  $m_{\tilde{t}}$  (right)[9]

This study is performed with PYTHIA 6.152 and detector simulation is performed with CMSJET. The analysis is split in two parts: in the first part the possibility to discriminate this signal from the known Standard Model backgrounds is investigated, while in the second part the backgrounds due to the other SUSY processes are also included.

The main Standard Model background is  $t\bar{t}$  since it has the same final state particles of the signal.  $W^\pm$  plus jets,  $Z^0$  plus jets,  $W^\pm W^\mp$ ,  $W^\pm Z^0$  backgrounds are also considered. The variables which are used to perform the Standard Model backgrounds rejection are  $E_T^{miss}$ , the total transverse mass ( $m_T^{tot}$ ) and the transverse mass of the highest  $p_T$  lepton- $E_T^{miss}$  system ( $m_T^{\ell\nu}$ ). The distributions of  $E_T^{miss}$  and  $m_T^{\ell\nu}$  are shown in Fig. 5 for the  $\tilde{t}\bar{\tilde{t}}$  signal and  $t\bar{t}$  background: the distributions are broader for signal events. The Standard Model backgrounds rejection is accomplished by lower cuts on these variables.

The largest contribution to SUSY backgrounds would come from  $\tilde{q}\tilde{q}$  and  $\tilde{g}\tilde{g}$  production. A large number of these events is expected to pass the  $\tilde{t}\bar{\tilde{t}}$  selection because squarks and gluino would produce a large number of hadron jets, leptons and  $E_T^{miss}$  in their decays. These backgrounds can be rejected only using the general features of the event because the number of decay topologies is very large.

Since squarks and gluino are heavier than  $\tilde{t}$  for almost all points in the parameter space considered, the  $E_T^{miss}$  and  $m_T^{tot}$  distributions for the SUSY backgrounds are concentrated at higher values with respect to the signal. SUSY backgrounds are reduced by upper cuts on these variables. An additional  $E_T$  cut on the hardest jet in the event is also applied because very high  $E_T$  jets are produced in the  $\tilde{q} \rightarrow q\tilde{\chi}_i^0$  and  $\tilde{q} \rightarrow q'\tilde{\chi}_i^\pm$  decays. The existence of a  $\tilde{t}$ -like particle can thus be indicated by an excess of events in the intermediate mass range.

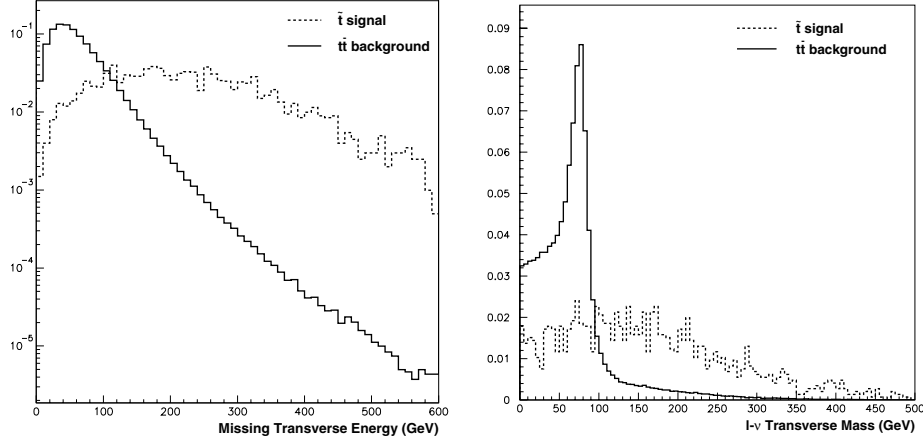


**Fig. 5.**  $E_T^{miss}$  (left side) and  $m_T^{\ell\nu}$  (right side) distributions for the  $t\bar{t}$  signal and the  $t\bar{t}$  background at  $m_0=400$  GeV,  $m_{1/2}=400$  GeV,  $A_0 = 0$ ,  $\tan\beta = 10$  and  $\mu > 0$  [9]

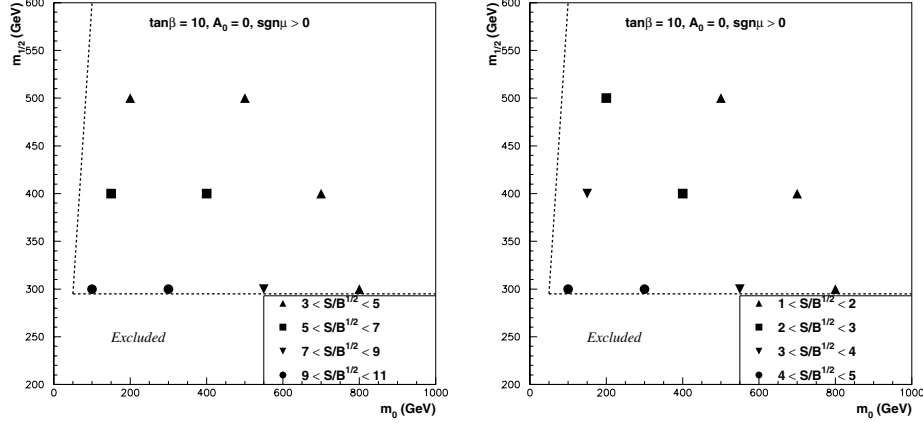


**Fig. 6.**  $S/\sqrt{B}$  as a function of  $m_0$  and  $m_{1/2}$  for only Standard Model backgrounds (left) and Standard Model plus SUSY backgrounds (right) [9]

For each point examined cuts are tuned in order to maximise the signal significance defined by  $S/\sqrt{B}$ , being  $S$  and  $B$  the expected signal and background respectively. The signal significance is calculated with the Standard Model backgrounds and the Standard Model backgrounds together with the SUSY ones separately. Figure 6 shows the highest signal significance which can be obtained with this analysis for the low luminosity period ( $\int L dt = 30 \text{ fb}^{-1}$ ) as a function of  $m_0$  and  $m_{1/2}$  in the Standard Model background case (left) and in the Standard Model plus SUSY backgrounds case (right). The region excluded by theory and the LEP Higgs mass bound is also displayed.

The signal is visible over the Standard Model backgrounds with a significance higher than 5 for  $m_{1/2} < 450$  GeV and  $m_0 < 700$  GeV. At higher  $m_0$  values

the signal significance decreases because the  $\tilde{t} \rightarrow \tilde{\chi}_2^0 b$  branching ratio becomes higher than that of the signal processes considered. At higher  $m_{1/2}$  the low value of the significance is due to a lower cross section.

The effect of  $\tan\beta$  on the expected signal is negligible since the  $\tilde{t}$  mass is almost independent on it. The only difference would be observed at low  $m_{1/2}$  values where the  $\tilde{\chi}_1^\pm \rightarrow \tilde{\tau}\nu_\tau$  decay mode is enhanced. A different search is required in this case.

In the presence of SUSY backgrounds, the  $\tilde{t}$  discovery with a signal significance of 5 would not be possible in the low luminosity period for most of the parameter space points examined. However, assuming a comparable detector performance at high luminosity, the 5-sigma discovery would be possible with an integrated luminosity of  $500 \text{ fb}^{-1}$  in most of the points. At a large  $A_0$ , the  $\tilde{t}$  would be lighter and the  $\tilde{t}\tilde{t}$  cross section would be high enough to allow the 5-sigma observability even in the low luminosity period[9].

## 6 Conclusions

The CMS detector will allow the discovery of Supersymmetry in a very large range of mSUGRA parameters up to masses of 2.5 TeV. The squarks and gluino decays offer many special signatures to discriminate the SUSY processes from the Standard Model ones. Although studies are still preliminary, it will be possible in many cases to separate some signals from the overall SUSY production and perform measurements. In particular the decay  $\tilde{g} \rightarrow \tilde{b}b$  would allow to reconstruct both sbottom and gluino masses. An excess of stop-like events can be observed over the Standard Model backgrounds and in some cases also over the SUSY backgrounds.

## References

1. The LHC Study Group, CERN/AC/95-05
2. H.P. Nilles, Phys. Rep. **110**, 1 (1984)
3. The CMS Collaboration, CERN/LHCC 94-038
4. H. Baer, F. Paige, S. Protopopescu and X. Tata, hep-ph/9305342
5. S. Abdullin and F. Charles, Nucl. Phys. B **547**, 60 (1999)
6. T. Sjöstrand, Comp. Phys. Comm. **82**, 74 (1994)
7. S. Abdullin, A. Khanov and N. Stepanov, CMS-TN 94-180
8. W. Beenakker, M. Krämer, T. Plehn, M. Spira, P.M. Zerwas, Nucl. Phys. B **515** (1998), 3
9. G. Segneri: Scalar Top Quark Search at LHC with the CMS Detector, Ph.D. Thesis, Università di Pisa (2002)



# Target Mass Effects and the Jost-Lehmann-Dyson Representation for Structure Functions

Igor L. Solovtsov

<sup>1</sup> Bogoliubov Laboratory of Theoretical Physics, JINR, Dubna, 141980, Russia

<sup>2</sup> Gomel State Technical University, Gomel, Belarus

**Abstract.** A method of studying target mass effects in inelastic lepton-hadron scattering is suggested. The Jost-Lehmann-Dyson integral representation for structure functions which accumulates general principles of local quantum field theory is used. It is shown that a new expression obtained for the structure function that depends on the target mass has a correct spectral property.

## 1 Introduction

The inclusive cross section for inelastic lepton-hadron scattering is expressed as the Fourier transform of the expectation value of the current product  $J(z)J(0)$  in the target state. The operator product expansion (OPE) is a powerful tool to study inelastic scattering processes. This method has been applied to define the contribution of target mass terms to the structure functions in paper [1]. The scheme that has been elaborated is the following. The first step is to organize the OPE by using the operators with definite twist and to take the leading twist contribution to get the free-field OPE. The second step is to collect the terms in the OPE of the form  $(q \cdot P)^n$  and relate corresponding coefficients to the moments of the structure function. Then, one can restore physical structure functions by inverting the moments through the Mellin transformation. These functions are parameterized by the quark distribution function  $F(x)$  that appears with the argument

$$\xi = \frac{2x}{1 + \sqrt{1 + 4x^2\epsilon}}, \quad (1)$$

where  $x$  is the Bjorken scaling variable  $x = Q^2/2\nu = Q^2/2(q \cdot P)$ , and  $\epsilon$  is expressed through the target mass  $M$  and the transfer momentum  $Q$  as  $\epsilon = M^2/Q^2$ . The scaling variable (1) is usually called the Nachtmann variable [2]. The trouble with the  $\xi$  scaling has widely been discussed in the literature (see, for example, [3–6]). For example, the structure function  $W_2(x, Q^2)$  within this method reads [5]

$$W_2(x, Q^2) = x^2 \frac{\partial^2}{\partial x^2} \left[ \frac{xG(\xi)}{\xi(1 + \xi^2 4M^2/Q^2)} \right], \quad G(x) = \int_x^1 dy (y - x) F(y),$$

where  $F(x)$  is the quark distribution function. The defect of this equation is that there is a clear mismatch at  $x = 1$ . The physical structure function  $W_2(Q^2, x)$  in the left hand side vanishes at  $x = 1$ , whereas in the right hand side does not.

The fact that an approximation can conflict with general principles of a theory is not rare event in quantum physics. For example, it is well known that when the renormalization group equation for the running coupling is solved directly, there arise unphysical singularities, for example, the ghost pole in the one-loop approximation, and they subsequently appear in physical quantities. This trouble can be resolved within the analytic approach proposed in [7,8] and elaborated in [9–15,17,16,18]. This method combines the renormalization invariance and the  $Q^2$ -analyticity of the Källén–Lehmann type has revealed new important properties of the analytic coupling [7,8,15]. The invariant analytic formulation essentially modifies the behavior of the analytic running coupling in the infrared region by making it stable with respect to higher-loop corrections. This is radically different from the situation encountered in the standard renormalization-group perturbation theory, which is characterized by strong instability with respect to the next-loop corrections in the domain of small energy scale. The analytic perturbation theory leads to new non-power-series expansions with new nonsingular functions [16]. Applying this algorithm to analyze the amplitudes of processes like the  $e^+e^-$ -annihilation into hadrons [13], the inclusive  $\tau$ -decay [11,17,18], and the sum rules for the inelastic lepton-hadron scattering [14], it has been demonstrated that, in addition to loop stability, the analytic perturbation theory results are much less sensitive to the choice of the renormalization scheme than those in the standard approach. The three-loop level practically insures both the loop saturation and the scheme invariance of the relevant physical quantities in the entire energy or momentum range. An investigation of hadronic form-factors by using the analytic running coupling has been performed in [19].

In this paper, following [20], we will apply the Jost–Lehmann–Dyson (JLD) integral representation for the structure function accumulating general principles of the theory. We argue that in this case it is possible to get an expression for the structure function in terms of the quark distribution incorporating the target mass effects and having the correct spectral property.

The method that will be considered is a generalization of the idea used in the analytic approach to quantum chromodynamics [7,8]. We base our consideration on the JLD representation for structure functions of the inelastic lepton-hadron process that has been suggested in [21,22]. The structure functions depend on two arguments, and the corresponding representation that accumulates the fundamental properties of the theory (such as relativistic invariance, spectrality, and causality) have a more complicated form in our analysis than in the representation of the Källén–Lehmann type for functions of one variable. We use the 4-dimensional integral representation proposed by Jost and Lehmann [21] for the so-called symmetric case. A more general case has been considered by Dyson [22], and similar representation are therefore often called the Jost–Lehmann–Dyson representation. Applications of this representation to automodel asymptotic structure functions were considered by Bogoliubov, Vladimirov, and Tavkhelidze [23]; some of these results and notation will be used in what follows.

## 2 The Jost-Lehmann-Dyson Representation

The proof of the JLD representation is based on the most general properties of the theory, such as covariance, Hermiticity, spectrality, and causality [24]. For the function  $W(\nu, Q^2)$  satisfying all these conditions, there exists a real moderately growing distribution  $\psi(\mathbf{u}, \lambda^2)$  such that the JLD integral representation holds; in the nucleon rest frame, this can be written as [23]

$$W(\nu, Q^2) = \varepsilon(q_0) \int d\mathbf{u} d\lambda^2 \delta[q_0^2 - (M\mathbf{u} - \mathbf{q})^2 - \lambda^2] \psi(\mathbf{u}, \lambda^2) \quad (2)$$

where the function  $\psi(\mathbf{u}, \lambda^2)$  has a support for

$$\rho = |\mathbf{u}| \leq 1, \quad \lambda^2 \geq \lambda_{\min}^2 = M^2(1 - \sqrt{1 - \rho^2})^2.$$

For the process under consideration, the physical values of  $\nu$  and  $Q^2$  are positive. We, thus, can neglect the factor  $\varepsilon(q_0) = \varepsilon(\nu)$  and keep the same notation for  $W(\nu, Q^2)$ . Taking into account that the weight function  $\psi(\mathbf{u}, \lambda^2) = \psi(\rho, \lambda^2)$  is radial-symmetric, as follows from covariance, we write down the JLD representation for  $W$  in the covariant form,

$$\begin{aligned} W(\nu, Q^2) &= \int_0^1 d\rho \rho^2 \int_{\lambda_{\min}^2}^{\infty} d\lambda^2 \int_{-1}^1 dz \\ &\times \delta(Q^2 + M^2\rho^2 + \lambda^2 - 2z\rho\sqrt{\nu^2 + M^2Q^2}) \psi(\rho, \lambda^2). \end{aligned} \quad (3)$$

As follows from representation (3), a natural scaling variable is given by

$$s = x \sqrt{\frac{1 + 4\epsilon}{1 + 4x^2\epsilon}}, \quad (4)$$

which accumulates the root structure determined by the  $\delta$ -function argument. At the same time, in the physical region of the process, the  $s$  variable changes in the same way as the Bjorken variable  $x$  does, i.e., from zero to one (cf. [25]). The variable  $s$  depends on the mass of the target (the nucleon) and is different from both the Bjorken variable and the Nachtmann variable. However, only the  $s$  variable leads to the moments that have the analytic properties in  $Q^2$  that we need.

Defining the modified  $s$ -moments of the structure functions [15],  $\mathcal{M}_n(Q^2)$ , and introducing the weight function

$$U_n(\sigma) = \frac{1}{n} \int_0^1 d\rho \rho^{n+1} \theta(\sigma - \sigma_{\min}) \psi(\rho, \sigma - M^2\rho^2),$$

we obtain the representation

$$\mathcal{M}_n(Q^2) = (Q^2)^{n-1} \int_0^\infty d\sigma \frac{U_n(\sigma)}{(\sigma + Q^2)^n}, \quad (5)$$

which implies the analyticity of  $\mathcal{M}_n(Q^2)$  in the complex  $Q^2$  plane cut along the negative semi-axis, i.e., the Källén–Lehmann type analyticity. Note here that in [26], the Deser–Gilbert–Sudarshan integral representation [27] was used to arrive at a similar statement regarding the analyticity of the Källén–Lehmann type for  $x$ -moments. However, the status of this representation in quantum field theory is less clear, since it cannot be obtained starting only with the fundamental principles of the theory (see the discussion in [28]). The relation between analytic moments and the  $x$ -moments can be found in [15]. In this paper a dispersion relation with respect to the  $s$ -variable has been obtained, and a relation with the OPE has been established.

The JLD representation (3) can be rewritten in the form [20]

$$W(\nu, Q^2) = \int_0^1 d\beta \int_0^\infty d\sigma \times \delta \left[ \sigma + Q^2 + 2M^2 \left( 1 - \sqrt{1 - \beta^2} \right) - \frac{\beta}{s} Q^2 \sqrt{1 + 4\epsilon} \right] H(\beta, \sigma) \quad (6)$$

convenient for our further consideration, where we introduced the new weight function  $H(\beta, \sigma)$  connected with the initial weight function  $\psi(\rho, \lambda^2)$  via an integral expression and supported in:  $\{0 < \beta < 1; \sigma > 0\}$ .

Introducing the function  $\mathcal{F}(x, Q^2)$  that corresponds to the structure function  $W(\nu, Q^2)$ , when the target mass  $M$  is neglected, one finds the representation

$$\mathcal{F}(x, Q^2) = \int_x^1 dy H \left[ y, \left( \frac{y}{x} - 1 \right) Q^2 \right]. \quad (7)$$

Define a parton distribution function  $F(x)$  as the limit of  $\mathcal{F}(x, Q^2)$  as  $Q^2 \rightarrow \infty$ . The limit of the weight function  $H(x, \sigma)$ , when the second argument goes to infinity, is determined by  $H(x)$ . From (7) we find the simple relation

$$F(x) = \int_x^1 dy H(y), \quad (8)$$

and, therefore, the weight function  $H(x)$  connects with the parton distribution  $F(x)$  as follows  $H(x) = -dF(x)/dx$ . Thus, in the Bjorken limit, the weight function  $H$  in the JLD representation is associated with the derivative of the parton distribution.

### 3 $\xi$ -Scaling

Now we consider the method of incorporating the target mass corrections. To make our explanation more transparent and not to obscure an essence of the approach with details of technical character we here consider the case of scalar currents. Following the approach suggested in [1], consider the twist-two symmetrical local operators  $\bar{\psi} \partial^{\mu_1} \dots \partial^{\mu_{2N}} \psi$ . For massless quarks  $\langle P | O^{\mu_1 \dots \mu_{2N}} | P \rangle = O_{2N} \{ P^{\mu_1} \dots P^{\mu_{2N}} \}$ , where  $\{ P^{\mu_1} \dots P^{\mu_{2N}} \}$  is a traceless combination of the

products of vectors  $P^{\mu_i}$ . By using the expression for the scalar combination of  $\{P^{\mu_1} \dots P^{\mu_{2N}}\}$  with the tensor  $q_{\mu_1} \dots q_{\mu_{2N}}$  and relating the parameters  $O_k$  according to [1] to the moments of the quark distribution function  $F(x)$  of the parton language

$$O_k = \int_0^1 dx x^{k-2} F(x), \quad (9)$$

for the moments of the ‘physical’ structure function  $W(x, Q^2)$ , we find

$$M_n(Q^2) = \int_0^1 dx x^{n-2} W(x, Q^2) = \frac{1}{n!} \sum_{m=0}^{\infty} \frac{(n+m)!}{m!} \epsilon^m O_{n+2m}. \quad (10)$$

The formal Mellin transformation of (10) gives

$$W(x, Q^2) = \frac{x}{\xi} \frac{F(\xi)}{1 + \epsilon \xi^2}. \quad (11)$$

This relation has obvious an trouble with the spectrality at  $x = 1$  that has been mentioned above.

#### 4 The JLD Representation and Target Mass Dependence

The difficulty with the spectrality condition which is appear in the  $\xi$ -scaling approach can be overcome by applying the JLD representation in a manner as the momentum analyticity is used for resolving the ghost pole problem.

The analytic moments can be written as follows

$$\mathcal{M}_n(Q^2) = \int_0^1 dx \frac{x^{n-2}}{(1 + \epsilon x^2)^{n+1}} F(x).$$

The first step of our procedure is to find the weight function  $U_n(\sigma)$  in the representation (5) for the analytic moments. As a result, we have

$$U_n(\sigma) = U_n(\infty) + \frac{\sigma^2}{n} \Phi'_n(\sigma) - 2\sigma \frac{n-1}{n} \Phi_n(\sigma) - (n-1) \int_{\sigma}^{\infty} ds \Phi_n(s). \quad (12)$$

Here  $U_n(\infty)$  is defined by the relation  $\mathcal{M}_n(\infty) = U_n(\infty)/(n-1)$  and  $\Phi_n(\sigma) = (\sigma/M^2)^{(n-3)/2} F(\sqrt{\sigma/M^2})$ .

The weight functions  $H(\beta, \sigma)$  in (6) and  $U_n(\sigma)$  in the integral representation for the analytic moments (5) are related as follows

$$U_n(\sigma) = \int_0^1 d\beta \beta^{n-1} \tilde{H}(\beta, \sigma), \quad (13)$$

where  $\tilde{H}(\beta, \sigma) = H(\beta, \sigma - 2M^2(1 - \sqrt{1 - \beta^2}))$ . Thus, the functions  $U_n(\sigma)$  are the moments of the weight function  $H(\beta, \sigma)$  and, therefore,  $U_n(\sigma)$  can be restored by the Mellin transformation.

Then, we represent the function  $H(\beta, \sigma)$  in the form

$$H(\beta, \sigma) = H_0(\beta) + h(\beta, \sigma),$$

where the function  $H_0$  is connected with the parton distribution function, and define the function  $\tilde{h}(\beta, \sigma) = h(\beta, \sigma - 2M^2(1 - \sqrt{1 - \beta^2}))$ , for which one can write

$$\tilde{h}(\beta, \sigma) = \frac{1}{2\pi i} \int_{\gamma-i\infty}^{\gamma+i\infty} dn \beta^{-n} [U_n(\sigma) - U_n(\infty)],$$

where the difference  $U_n(\sigma) - U_n(\infty)$  is expressed via the parton distribution function as follows

$$\begin{aligned} U_n(\sigma) - U_n(\infty) = & \frac{1}{2M^2} \frac{\sigma^2}{n} \frac{\partial}{\partial \sigma} \left[ \left( \frac{\sigma}{M^2} \right)^{(n-3)/2} F \left( \sqrt{\frac{\sigma}{M^2}} \right) \right] \\ & - \frac{\sigma}{M^2} \frac{n-1}{n} \left[ \left( \frac{\sigma}{M^2} \right)^{(n-3)/2} F \left( \sqrt{\frac{\sigma}{M^2}} \right) \right] \\ & - \frac{n-1}{2M^2} \int_{\sigma}^{\infty} ds \left[ \left( \frac{s}{M^2} \right)^{(n-3)/2} F \left( \sqrt{\frac{s}{M^2}} \right) \right]. \end{aligned} \quad (14)$$

Next, we represent the structure function as

$$W(x, Q^2) = W_0(x, Q^2) + w(x, Q^2),$$

where  $W_0(x, Q^2)$  corresponds to the weight function  $H_0(\beta)$ ; and  $w(x, Q^2)$ , to  $h(\beta, \sigma)$ , and express  $W_0(x, Q^2)$  in the form

$$\begin{aligned} W_0(x, Q^2) &= \int_0^1 d\beta \theta[f(\beta; x, \epsilon)] H_0(\beta), \\ f(\beta; x, \epsilon) &= \frac{\beta}{s} \sqrt{1 + 4\epsilon} - 1 - 2\epsilon(1 - \sqrt{1 - \beta^2}). \end{aligned} \quad (15)$$

The variables  $\beta_-$  and  $\beta_+$ , if  $x > \tilde{x} \equiv 1/\sqrt{1 + 4\epsilon^2}$ ,

$$\beta_{\pm} = \frac{x\sqrt{1 + 4\epsilon x^2}}{1 + 4\epsilon x^2 + 4\epsilon^2 x^2} \left[ 1 + 2\epsilon \pm 2\epsilon \sqrt{\frac{1 - x^2}{1 + 4\epsilon x^2}} \right], \quad (16)$$

are the roots of the equation  $f(\beta; x, \epsilon) = 0$ . Thus, we have

$$W_0(x, Q^2) = \begin{cases} F(\beta_-) - F(1), & 0 \leq x < \tilde{x}, \\ F(\beta_-) - F(\beta_+), & \tilde{x} \leq x \leq 1. \end{cases} \quad (17)$$

The spectral property of  $W_0(x, Q^2)$ , its vanishing at  $x = 1$ , comes from the relation  $\beta_-(x = 1) = \beta_+(x = 1)$ . The function  $W_0(x, Q^2)$  is a continuous function at  $x = \tilde{x}$  because  $\beta_+(\tilde{x}) = 1$ .

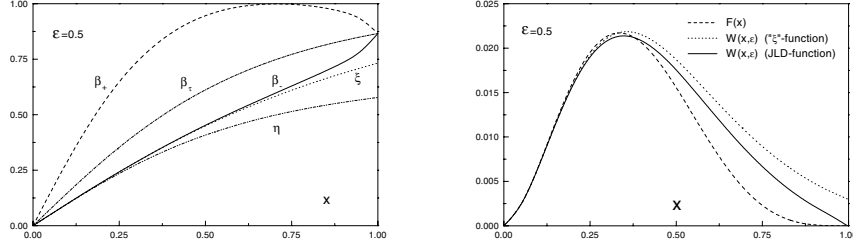


**Fig. 1.** Behavior of functions  $\beta_{\pm}$ ,  $\beta_{\tau}$ ,  $\xi$ , and  $\eta$  as function of  $x$  for  $\epsilon = 0.5$ . **Fig. 2.** Behavior of structure functions for  $\epsilon = 0.5$ .

For the function  $w(x, Q^2)$ , one finds

$$w(x, Q^2) = \int_0^1 d\beta \theta[f(\beta; x, \epsilon)] \theta[g(\beta; x, \epsilon)] \phi(\beta; x, \epsilon), \quad (18)$$

where  $f(\beta; x, \epsilon)$  is defined by (15) and

$$g(\beta; x, \epsilon) = [(\beta/s)\sqrt{1+4\epsilon} - 1] / \epsilon - \beta^2, \quad (19)$$

$$\phi(\beta; x, \epsilon) = \frac{1}{4\sqrt{\tau}} \theta(\tau) \theta(1-\tau) \frac{\partial}{\partial(\sqrt{\tau})} [\sqrt{\tau} F(\sqrt{\tau})], \quad (20)$$

with  $\tau \equiv \tau(\beta; x, \epsilon) = [(\beta/s)\sqrt{1+4\epsilon} - 1] / \epsilon$ . The equation  $\tau(\beta; x, \epsilon) = 1$  has the root  $\beta_{\tau} = (1+\epsilon)s/\sqrt{1+4\epsilon}$ . The solutions of the equation  $g(\beta; \eta, \epsilon) = 0$  are connected with the  $\xi$ -variable ( $\xi_{-} = \xi$ ) and are of the form  $\xi_{\pm} = (\sqrt{1+4\epsilon x^2 \pm 1})/2\epsilon x$ .

The relative behavior of the functions  $\beta_{\pm}$ ,  $\beta_{\tau}$ ,  $\xi$ , and  $\eta = s/\sqrt{1+4\epsilon}$  as a function of  $x$  for  $\epsilon = 0.5$  is shown in Fig. 1. This figure demonstrates that the  $\xi$  does not appear in the expression for the structure function, because the range of integration in (18) includes the interval from  $\beta_{-}$  to  $\beta_{\tau}$ .

In Fig. 2, we plot the structure functions as functions of  $x$  for  $\epsilon = 0.5$ . The parton distribution is taken in the form  $F(x) = x^2(1-x)^4$  (dashed curve). The physical structure functions,  $W(x, \epsilon)$ , that depend on the target mass are obtained in two ways: the dotted curve was constructed by the "ξ"-scaling expression (11), and the solid line was constructed by using the JLD representation. This figure demonstrates the difference between these methods. The structure function obtained by the JLD representation has the correct spectral behavior at  $x = 1$  as compared with the "ξ"-scaling prediction.

## 5 Conclusions

The JLD representation reflecting the general principles of the local quantum field theory (covariance, Hermiticity, spectrality, and causality) has been ap-

plied for studying the inelastic lepton-hadron process. Here we have concentrated on the well-known trouble that is a characteristic feature of the so-called “ $\zeta$ ”-scaling approach. We have argued that the approach proposed here gives the self-consistent method of incorporating the target mass dependence into the structure function and does not lead to the conflict with the spectral condition.

### Acknowledgments

The author would like to express sincere thanks to L. Gamberg, S.V. Mikhailov, K.A. Milton, D.V. Shirkov, A.N. Sissakian, N.G. Stefanis, and O.P. Solovtsova for interest in the work and helpful discussions. Partial support of the work by the RFBR, grants 99-01-00091, 99-02-17727, 00-15-96691 is gratefully acknowledged.

### References

1. H. Georgi, H.D. Politzer: Phys. Rev. D **14**, 1829 (1976)
2. O. Nachtmann: Nucl. Phys. B **63**, 237 (1973)
3. D.J. Gross, S.B. Treiman, F.A. Wilczek: Phys. Rev. D **15**, 2486 (1977)
4. A. De Rújula, H. Georgi, H.D. Politzer: Phys. Rev. D **15**, 2495 (1977)
5. J.L. Miramontes, J.S. Guillén: Z. Phys. C **41**, 247 (1988)
6. R.G. Roberts: *The Structure of the Proton. Deep Inelastic Scattering* (Cambridge University Press, 1990)
7. D.V. Shirkov, I.L. Solovtsov: JINR Rapid Comm. **76**, 5 (1996), hep-ph/9604363
8. D.V. Shirkov, I.L. Solovtsov: Phys. Rev. Lett. **79**, 1209 (1997)
9. K.A. Milton, I.L. Solovtsov: Phys. Rev. D **55**, 5295 (1997); Phys. Rev. D **59**, 107701 (1999)
10. D.V. Shirkov: Nucl. Phys. B (Proc. Suppl.) **64**, 106 (1998)
11. K.A. Milton, I.L. Solovtsov, O.P. Solovtsova: Phys. Lett. B **415**, 104 (1997); *Proceedings the XXIX Int. Conference on High Energy Physics*, Vancouver, B.C., Canada, July 23-29, 1998, v.II, p.1608
12. K.A. Milton, O.P. Solovtsova: Phys. Rev. D **57**, 5402 (1998)
13. I.L. Solovtsov, D.V. Shirkov: Phys. Lett. B **442**, 344 (1998)
14. K.A. Milton, I.L. Solovtsov, O.P. Solovtsova: Phys. Lett. B **439**, 421 (1998); Phys. Rev. D **60**, 016001 (1999)
15. I.L. Solovtsov, D.V. Shirkov: Theor. Math. Phys. **120**, 1220 (1999)
16. D.V. Shirkov: Lett. Math. Phys. **48**, 135 (1999); Eur. Phys. J. C **22**, 331 (2001)
17. K.A. Milton, I.L. Solovtsov, O.P. Solovtsova, V.I. Yasnov: Eur. Phys. J. C **14**, 495 (2000)
18. K.A. Milton, I.L. Solovtsov, O.P. Solovtsova: Phys. Rev. D **64**, 016005 (2001)
19. N.G. Stefanis, W. Schroers, Hyun-Chul Kim: Eur. Phys. J. C **18**, 137 (2000); A.P. Bakulev, A.V. Radyushkin, N.G. Stefanis: Phys. Rev. D **62**, 113001 (2000); A.I. Karanikas, N.G. Stefanis: Phys. Lett. B **504**, 225 (2001)
20. I.L. Solovtsov: Part. Nucl. Lett. **101**, 10 (2000)
21. R. Jost, H. Lehmann: Nuovo Cim. **5**, 1598 (1957)
22. F.J. Dyson: Phys. Rev. **110**, 1460 (1958)
23. N.N. Bogoliubov, V.S. Vladimirov, A.N. Tavkhelidze: Theor. Math. Phys. **12**, 305 (1972)



24. N.N. Bogoliubov, D.V. Shirkov: *Introduction to the Theory of Quantum Fields*, (Wiley, New York, 1980)
25. B. Geyer, D. Robaschik, E. Wieczorek: Fortschr. Phys. **27**, 75 (1979)
26. W. Wetzel: Nucl. Phys. B **139**, 170 (1978)
27. S. Deser, W. Gilbert, E.C.S. Sudarshan: Phys. Rev. **117**, 266 (1960)
28. B.V. Geshkenbein, A.I. Komech: Sov. J. Nucl. Phys. **26**, 446 (1977)

# Family Replicated Calculation of Baryogenesis

Holger B. Nielsen and Yasutaka Takanishi

<sup>1</sup> Deutsches Elektronen-Synchrotron DESY, Notkestraße 85, D-22603 Hamburg, Germany

<sup>2</sup> The Niels Bohr Institute, Blegdamsvej 17, DK-2100 Copenhagen Ø, Denmark

**Abstract.** In our model with a Standard Model gauge group extended with a baryon number minus lepton number charge *for each family of quarks and leptons*, we calculate the baryon number relative to entropy produced in early Big Bang by the Fukugita-Yanagida mechanism. With the parameters, *i.e.*, the Higgs VEVs already fitted in a very successful way to quark and lepton masses and mixing angles we obtain the *order of magnitude* pure prediction  $Y_B = 2.59^{+17.0}_{-2.25} \times 10^{-11}$  which according to a theoretical estimate should mean in this case an uncertainty of the order of a factor 7 up or down (to be compared to  $Y_B = (1.7 - 8.1) \times 10^{-11}$ ) using a relatively crude approximation for the dilution factor, while using another estimate based on Buchmüller and Plümacher a factor 500 less, but this should rather be considered a lower limit. With a realistic uncertainty due to wash-out of a factor 100 up or down we even with the low estimate only deviate by  $1.5\sigma$ .

## 1 Introduction

Using the model for mass matrices presented by us in an other contribution [1] at this conference we want to compute the amount of baryons produced in the early universe. This model works by having the mass matrix elements being suppressed by approximately conserved quantum numbers from a gauge group repeated for each family of quarks and leptons and also having a  $(B - L)$  charge for each family.

The baryon number density relative to entropy density,  $Y_B$ , is one of the rather few quantities that can give us information about the laws of nature beyond the Standard Model and luckily we have from the understanding of the production of light isotopes at the minute scale in Big Bang fits to this quantity [2]. The “experimental” data of the ratio of baryon number density to the entropy density is

$$Y_B \Big|_{\text{exp}} = (1.7 - 8.1) \times 10^{-11} . \quad (1)$$

We already had a good fit of all the masses and mixings [3,4] for both quarks and leptons measured so far and agreeing with all the bounds such as neutrinoless beta decay and proton decay not being seen and matching on the borderline but consistent with the accuracy of our model and of the experiment of CHOOZ the electron to heaviest left-handed neutrino mixing, and that in a version of our model in which the dominant matrix element in the right-handed neutrino mass matrix is the diagonal one for the “third” (*i.e.* with same  $(B - L)_i$  as the third

family) family  $\nu_{R3}$  right-handed neutrino. This version of our model which fits otherwise very well does not give sufficient  $(B - L)$  excess, that survives, but the by now the best model in our series should have the right-handed mass matrix dominated by the off-diagonal elements  $(2, 3)$  and  $(3, 2)$ , so that there appears two almost mass degenerate see-saw neutrinos, in addition to the third one (first family) which is much lighter.

## 2 Mass Matrices and Results for Masses and Mixing Angles

Our model produces mass matrix elements – or effective Yukawa couplings – which are suppressed from being of the order of the top-mass because they are forbidden by the conservation of the gauge charges of our model and can only become different from zero using the 6 Higgs fields [4,5] which we have in addition to the field replacing the Weinberg-Salam one. In the neutrino sector according to the see-saw mechanism [6] we have to calculate Dirac- and Majorana-mass matrices,  $M_{\text{eff}} \approx M_\nu^D M_R^{-1} (M_\nu^D)^T$ , to obtain the effective mass matrix  $M_{\text{eff}}$  for the left handed neutrinos we in practice can “see”. Here we present all mass matrices as they follow from our choice of quantum numbers for the 7 Higgs fields in our model and for the quarks and leptons (as they can be found in the other contribution). Only the quantum numbers for the field called  $\phi_{B-L}$  is – in order to get degenerate see-saw neutrinos – changed into having the  $B - L$  quantum numbers of family 2 and 3 equal to 1, *i.e.*,  $(B - L)_2 = (B - L)_3 = 1$ , while the other family quantum numbers are just zero:

the up-type quarks:

$$M_U \simeq \frac{\langle (\phi_{\text{ws}})^\dagger \rangle}{\sqrt{2}} \begin{pmatrix} (\omega^\dagger)^3 W^\dagger T^2 & \omega \rho^\dagger W^\dagger T^2 & \omega \rho^\dagger (W^\dagger)^2 T \\ (\omega^\dagger)^4 \rho W^\dagger T^2 & W^\dagger T^2 & (W^\dagger)^2 T \\ (\omega^\dagger)^4 \rho & 1 & W^\dagger T^\dagger \end{pmatrix} \quad (2)$$

the down-type quarks:

$$M_D \simeq \frac{\langle \phi_{\text{ws}} \rangle}{\sqrt{2}} \begin{pmatrix} \omega^3 W (T^\dagger)^2 & \omega \rho^\dagger W (T^\dagger)^2 & \omega \rho^\dagger T^3 \\ \omega^2 \rho W (T^\dagger)^2 & W (T^\dagger)^2 & T^3 \\ \omega^2 \rho W^2 (T^\dagger)^4 & W^2 (T^\dagger)^4 & WT \end{pmatrix} \quad (3)$$

the charged leptons:

$$M_E \simeq \frac{\langle \phi_{\text{ws}} \rangle}{\sqrt{2}} \begin{pmatrix} \omega^3 W (T^\dagger)^2 & (\omega^\dagger)^3 \rho^3 W (T^\dagger)^2 & (\omega^\dagger)^3 \rho^3 WT^4 \chi \\ \omega^6 (\rho^\dagger)^3 W (T^\dagger)^2 & W (T^\dagger)^2 & WT^4 \chi \\ \omega^6 (\rho^\dagger)^3 (W^\dagger)^2 T^4 & (W^\dagger)^2 T^4 & WT \end{pmatrix} \quad (4)$$

the Dirac neutrinos:

$$M_\nu^D \simeq \frac{\langle (\phi_{\text{ws}})^\dagger \rangle}{\sqrt{2}} \begin{pmatrix} (\omega^\dagger)^3 W^\dagger T^2 & (\omega^\dagger)^3 \rho^3 W^\dagger T^2 & (\omega^\dagger)^3 \rho^3 W^\dagger T^2 \chi \\ (\rho^\dagger)^3 W^\dagger T^2 & W^\dagger T^2 & W^\dagger T^2 \chi \\ (\rho^\dagger)^3 W^\dagger T^\dagger \chi^\dagger & W^\dagger T^\dagger \chi^\dagger & W^\dagger T^\dagger \end{pmatrix} \quad (5)$$

and the Majorana (right-handed) neutrinos:

$$M_R \simeq \langle \phi_{B-L} \rangle \begin{pmatrix} (\rho^\dagger)^6 \chi^\dagger & (\rho^\dagger)^3 \chi^\dagger / 2 & (\rho^\dagger)^3 / 2 \\ (\rho^\dagger)^3 \chi^\dagger / 2 & \chi^\dagger & 1 \\ (\rho^\dagger)^3 / 2 & 1 & \chi \end{pmatrix} \quad (6)$$

We shall remember that it is here understood that all the matrix elements are to be provided with order of unity factors which we do not know and in practice have treated by inserting random order of unity factors over which we then average at the end (in a logarithmic way).

### 3 Renormalisation Group Equations

The model for the Yukawa couplings we use gives, in principle, these couplings at the fundamental scale, taken to be the Planck scale, at first, and we then use the renormalisation group to run them down to the scales where they are to be confronted with experiment. From the Planck scale down to the see-saw scale or rather from where our gauge group is broken down to  $SMG \times U(1)_{B-L}$  we use the one-loop renormalisation group running of the Yukawa coupling constant matrices and the gauge couplings [3] in GUT notation including the running of Dirac neutrino Yukawa coupling:

$$\begin{aligned} 16\pi^2 \frac{dg_1}{dt} &= \frac{41}{10} g_1^3, & 16\pi^2 \frac{dg_2}{dt} &= -\frac{19}{16} g_2^3, & 16\pi^2 \frac{dg_3}{dt} &= -7 g_3^3, \\ 16\pi^2 \frac{dY_U}{dt} &= \frac{3}{2} (Y_U(Y_U)^\dagger - Y_D(Y_D)^\dagger) Y_U + \left\{ Y_S - \left( \frac{17}{20} g_1^2 + \frac{9}{4} g_2^2 + 8g_3^2 \right) \right\} Y_U, \\ 16\pi^2 \frac{dY_D}{dt} &= \frac{3}{2} (Y_D(Y_D)^\dagger - Y_U(Y_U)^\dagger) Y_D + \left\{ Y_S - \left( \frac{1}{4} g_1^2 + \frac{9}{4} g_2^2 + 8g_3^2 \right) \right\} Y_D, \\ 16\pi^2 \frac{dY_E}{dt} &= \frac{3}{2} (Y_E(Y_E)^\dagger - Y_\nu(Y_\nu)^\dagger) Y_E + \left\{ Y_S - \left( \frac{9}{4} g_1^2 + \frac{9}{4} g_2^2 \right) \right\} Y_E, \\ 16\pi^2 \frac{dY_\nu}{dt} &= \frac{3}{2} (Y_\nu(Y_\nu)^\dagger - Y_E(Y_E)^\dagger) Y_\nu + \left\{ Y_S - \left( \frac{9}{20} g_1^2 + \frac{9}{4} g_2^2 \right) \right\} Y_\nu, \\ Y_S &= \text{Tr} (3 Y_U^\dagger Y_U + 3 Y_D^\dagger Y_D + Y_E^\dagger Y_E + Y_\nu^\dagger Y_\nu), \end{aligned}$$

where  $t = \ln \mu$  and  $\mu$  is the renormalisation point.

In order to run the renormalisation group equations down to 1 GeV, we use the following initial values:

$$U(1): \quad g_1(M_Z) = 0.462, \quad g_1(M_{\text{Planck}}) = 0.614, \quad (7)$$

$$SU(2): \quad g_2(M_Z) = 0.651, \quad g_2(M_{\text{Planck}}) = 0.504, \quad (8)$$

$$SU(3): \quad g_3(M_Z) = 1.22, \quad g_3(M_{\text{Planck}}) = 0.491. \quad (9)$$

We varied the 6 free parameters and found the best fit, corresponding to the lowest value for the quantity  $\text{g.o.f.} \equiv \sum \left[ \ln \left( \frac{\langle m \rangle_{\text{pred}}}{m_{\text{exp}}} \right) \right]^2 = 3.38$ , with the following

**Table 1.** Best fit to conventional experimental data. All masses are running masses at 1 GeV except the top quark mass which is the pole mass. Note that we use the square roots of the neutrino data in this Table, as the fitted neutrino mass and mixing parameters  $\langle m \rangle$ , in our goodness of fit (g.o.f.) definition.

	Fitted	Experimental		Fitted	Experimental
$m_u$	5.2 MeV	4 MeV	$m_d$	5.0 MeV	9 MeV
$m_c$	0.70 GeV	1.4 GeV	$m_s$	340 MeV	200 MeV
$M_t$	208 GeV	180 GeV	$m_b$	7.4 GeV	6.3 GeV
$m_e$	1.1 MeV	0.5 MeV	$V_{us}$	0.10	0.22
$m_\mu$	81 MeV	105 MeV	$V_{cb}$	0.024	0.041
$m_\tau$	1.11 GeV	1.78 GeV	$V_{ub}$	0.0025	0.0035
$\Delta m_\odot^2$	$9.0 \times 10^{-5} \text{ eV}^2$	$4.5 \times 10^{-5} \text{ eV}^2$	$\Delta m_{\text{atm}}^2$	$1.8 \times 10^{-3} \text{ eV}^2$	$3.0 \times 10^{-3} \text{ eV}^2$
$\tan^2 \theta_\odot$	0.23	0.35	$\tan^2 \theta_{\text{atm}}$	0.83	1.0
$\tan^2 \theta_{\text{chooz}}$	$3.3 \times 10^{-2}$	$\lesssim 2.6 \times 10^{-2}$	g.o.f.	3.38	—

values for the VEVs:

$$\begin{aligned} \langle \phi_{WS} \rangle &= 246 \text{ GeV} , \quad \langle \phi_{B-L} \rangle = 1.23 \times 10^{10} \text{ GeV} , \quad \langle \omega \rangle = 0.245 , \\ \langle \rho \rangle &= 0.256 , \quad \langle W \rangle = 0.143 , \quad \langle T \rangle = 0.0742 , \quad \langle \chi \rangle = 0.0408 , \end{aligned} \quad (10)$$

where, except for the Weinberg-Salam Higgs field and  $\langle \phi_{B-L} \rangle$ , the VEVs are expressed in Planck units. Hereby we have considered that the Weinberg-Salam Higgs field VEV is already fixed by the Fermi constant. The results of the best fit, with the VEVs in eq. (10), are shown in Table 1.

## 4 Quantities to Use for Baryogenesis Calculation

Since the baryogenesis in the Fukugita-Yanagida scheme [7] arises from a negative excess of lepton number being converted by Sphalerons to a positive baryon number excess partly and this negative excess comes from the  $CP$  violating decay of the see-saw neutrinos we shall introduce the parameters  $\epsilon_i$  giving the measure of the relative asymmetry under  $C$  or  $CP$  in the decay of neutrino number  $i$ : Defining the measure  $\epsilon_i$  for the  $CP$  violation

$$\epsilon_i \equiv \frac{\sum_{\alpha,\beta} \Gamma(N_{Ri} \rightarrow \ell^\alpha \phi_{WS}^\beta) - \sum_{\alpha,\beta} \Gamma(N_{Ri} \rightarrow \bar{\ell}^\alpha \phi_{WS}^{\beta\dagger})}{\sum_{\alpha,\beta} \Gamma(N_{Ri} \rightarrow \ell^\alpha \phi_{WS}^\beta) + \sum_{\alpha,\beta} \Gamma(N_{Ri} \rightarrow \bar{\ell}^\alpha \phi_{WS}^{\beta\dagger})} , \quad (11)$$

where  $\Gamma$  are  $N_{Ri}$  decay rates (in the  $N_{Ri}$  rest frame), summed over the neutral and charged leptons (and Weinberg-Salam Higgs fields) which appear as final states in the  $N_{Ri}$  decays one sees that the excess of leptons over anti-leptons produced in the decay of one  $N_{Ri}$  is just  $\epsilon_i$ . The total decay rate at the tree level is given by

$$\Gamma_{N_i} = \Gamma_{N_i \ell} + \Gamma_{N_i \bar{\ell}} = \frac{((\widetilde{M}_\nu^D)^\dagger \widetilde{M}_\nu^D)_{ii}}{4\pi \langle \phi_{WS} \rangle^2} M_i , \quad (12)$$

where  $\widetilde{M}_\nu^D$  can be expressed through the unitary matrix diagonalising the right-handed neutrino mass matrix  $V_R$ :

$$\widetilde{M}_\nu^D \equiv M_\nu^D V_R , \quad (13)$$

$$V_R^\dagger M_R M_R^\dagger V_R = \text{diag} (M_1^2, M_2^2, M_3^2) . \quad (14)$$

The  $CP$  violation rate is computed according to [8,9]

$$\epsilon_i = \frac{\sum_{j \neq i} \text{Im}[(\widetilde{M}_\nu^D)^\dagger \widetilde{M}_\nu^D]_{ji} \left[ f\left(\frac{M_j^2}{M_i^2}\right) + g\left(\frac{M_j^2}{M_i^2}\right) \right]}{4\pi \langle \phi_{ws} \rangle^2 ((\widetilde{M}_\nu^D)^\dagger \widetilde{M}_\nu^D)_{ii}} \quad (15)$$

where the function,  $f(x)$ , comes from the one-loop vertex contribution and the other function,  $g(x)$ , comes from the self-energy contribution. These  $\epsilon$ 's can be calculated in perturbation theory only for differences between Majorana neutrino masses which are sufficiently large compare to their decay widths, *i.e.*, the mass splittings satisfy the condition,  $|M_i - M_j| \gg |\Gamma_i - \Gamma_j|$ :

$$f(x) = \sqrt{x} \left[ 1 - (1+x) \ln \frac{1+x}{x} \right] , \quad g(x) = \frac{\sqrt{x}}{1-x} . \quad (16)$$

We as usual [2] introduce the decay rate relative to

$$K_i \equiv \frac{\Gamma_i}{2H} \Big|_{T=M_i} = \frac{M_{\text{Planck}}}{1.66 \langle \phi_{ws} \rangle^2 8\pi g_{*i}^{1/2}} \frac{((\widetilde{M}_\nu^D)^\dagger \widetilde{M}_\nu^D)_{ii}}{M_i} \quad (i = 1, 2, 3) , \quad (17)$$

where  $\Gamma_i$  is the width of the flavour  $i$  Majorana neutrino,  $M_i$  is its mass and  $g_{*i}$  is the number of degrees of freedom at the temperature  $M_i$  (in our model  $\sim 100$ ).

In order to estimate the effective  $K$  factors we first introduce some normalized state vectors for the decay products:

$$|i\rangle \equiv \left( \sum_{k=1}^3 \left| \left[ \widetilde{M}_\nu^D(M_i) \right]_{ki} \right|^2 \right)^{-\frac{1}{2}} \left( \left[ \widetilde{M}_\nu^D(M_i) \right]_{1i} , \left[ \widetilde{M}_\nu^D(M_i) \right]_{2i} , \left[ \widetilde{M}_\nu^D(M_i) \right]_{3i} \right) , \quad (18)$$

Then we may take an approximation for the effective  $K$  factors:

$$K_{\text{eff}1} = K_1(M_1) , \quad (19)$$

$$K_{\text{eff}2} = K_2(M_2) + |\langle 2|3 \rangle|^2 K_3(M_3) + |\langle 2|1 \rangle|^2 K_1(M_1) , \quad (20)$$

$$K_{\text{eff}3} = K_3(M_3) + |\langle 3|2 \rangle|^2 K_2(M_2) + |\langle 3|1 \rangle|^2 K_1(M_1) . \quad (21)$$

## 5 Result for Baryogenesis

Using the Yukawa couplings – as coming from the VEVs of our seven different Higgs fields – the numerical calculation of baryogenesis were performed using

our random order unity factor method. In order to get baryogenesis in Fukugita-Yanagida scheme, we calculated the see-saw neutrino masses,  $K_{\text{eff } i}$  factors and  $CP$  violation parameters using  $N = 10,000$  random number combinations and logarithmic average method:

$$\begin{aligned} M_1 &= 2.1 \times 10^5 \text{ GeV} , K_{\text{eff } 1} = 31.6 , |\epsilon_1| = 4.62 \times 10^{-12} \\ M_2 &= 8.8 \times 10^9 \text{ GeV} , K_{\text{eff } 2} = 116.2 , |\epsilon_2| = 4.00 \times 10^{-6} \\ M_3 &= 9.9 \times 10^9 \text{ GeV} , K_{\text{eff } 3} = 114.7 , |\epsilon_3| = 3.27 \times 10^{-6} \end{aligned}$$

The sign of  $\epsilon_i$  is unpredictable due to the complex random number coefficients in mass matrices, therefore we are not in the position to say the sign of  $\epsilon$ 's. Using the complex order unity random numbers being given by a Gaussian distribution we get after logarithmic averaging using the dilution factors as presented by [2,3]

$$Y_B = 2.59^{+17.0}_{-2.25} \times 10^{-11} , \quad (22)$$

where we have estimated the uncertainty in the natural exponent according [10] to be  $64 \% \cdot \sqrt{10} \approx 200 \%$ .

The understanding of how this baryon to entropy prediction  $Y_B$  comes about in the model may be seen from the following (analytical) estimate

$$Y_B \approx \frac{1}{3} \cdot \frac{\chi}{\sqrt{g_*} T^2} \cdot \frac{M_3}{M_{\text{Planck}}} \approx \frac{1}{3} \cdot 10^{-9} \quad (23)$$

where we left out for simplicity the  $\ln K$  factor in the denominator of the dilution factor  $\kappa$  and where  $M_3$  is the mass of one of the heavy right-handed neutrinos in our model  $M_3 \approx \langle \phi_{B-L} \rangle$ . Since the atmospheric mass square difference square root  $\sqrt{\Delta m_{\text{atm}}^2} \approx 0.05 \text{ eV} \approx \langle \phi_{WS} \rangle^2 (WT)^2 / M_3$  we see that keeping it leaves us with the dependence

$$Y_B \approx \frac{\langle \phi_{WS} \rangle^2 \chi}{3 \sqrt{0.05 \text{ eV} \cdot g_* M_{\text{Planck}} W^2 T^4}} \approx \frac{1}{5} \times 10^{-4} \cdot \frac{\chi}{\sqrt{g_*} W^2 T^4} \quad (24)$$

## 6 Problem with Wash-Out Effects?

To make a better estimate of the wash-out effect we may make use of the calculations by [11] by putting effective values for the see-saw neutrino mass  $M$  and  $\tilde{m}$ . The most important wash-out is due to “on-shell” formation of right-handed neutrinos and only depends on  $K$  or the thereto proportional  $\tilde{m}$ , but next there are wash-out effects going rather than by  $K$  or  $\tilde{m}$  as  $M\tilde{m}^2$ . In the presentation of the results by [11] fixed ratios between right-handed neutrino masses were assumed. However, in reality a very important wash-out comes from the off-shell inverse decay and that goes as

$$M_1 \sum_j \frac{M_j^2}{M_1^2} \tilde{m}_j^2 \quad \text{with} \quad \tilde{m}_j \equiv \frac{[(\widetilde{M}_\nu^D)^\dagger \widetilde{M}_\nu^D]_{jj}}{M_j} \quad (25)$$

Here we use the notation with  $\tilde{m}_j$  from [11]:  $\tilde{m}_j \approx K_j \cdot 2.2 \cdot 10^{-3} \text{eV}$ .

Using such a term (see eq. 25) with the ansatz ratios used in [11],  $M_3^2 = 10^6 M_1^2$  and  $M_2^2 = 10^3 M_1^2$  one gets for eq. (25)  $\approx 10^6 M_1 \tilde{m}_3^2$ , while we would with our mass ratios (eq. 22)  $M_3^2 \approx 1/4 \cdot 10^{10} M_1^2$  and  $M_2^2 \approx 1/4 \cdot 10^{10} M_1^2$  obtain correspondingly  $2 \cdot 10^5 \text{ GeV} \cdot 1/4 \cdot 10^{10} \tilde{m}_3^2 \approx 1/2 \cdot 10^{15} \text{ GeV} \tilde{m}_3^2$ , which then being identified with  $10^6 M_{1 \text{ use}} \tilde{m}_3^2$  would lead to that we should effectively use for simulating our model the mass of the right handed neutrino – which is a parameter in the presentation of the dilution effects in [11] –  $M_{1 \text{ use}} = 1/2 \cdot 10^{15} \text{ GeV}/10^6 = 1/2 \cdot 10^9 \text{ GeV}$ . Inserting this  $M_{1 \text{ use}}$  value for our estimate  $\tilde{m}_2 \approx \tilde{m}_3 \approx 0.1 \text{ eV}$  gives a dilution factor  $\kappa \approx 10^{-4}$ , *i.e.*, a factor 500 less than what we used with our estimate using the  $K_{\text{eff}}$ 's. (Our  $\tilde{m}_3 = \tilde{m}_2$  are surprisingly large compared to the  $\sqrt{\Delta m_{\text{atm}}^2}$  because of renormalization running.) Using the better calculation of [11] which has a very steep dependence – a fourth power say – as function of  $\tilde{m}$  our uncertainty should also be corrected to a factor 100 up or down. So then we have one and a half standard deviations of getting too little baryon number.

## 7 Conclusion

We calculated the baryon density relative to the entropy density – baryogenesis – from our model order of magnitudewise. This model already fits to quark and lepton masses and mixing angles using *only six parameters*, vacuum expectation values. We got a result for the baryon number predicting about a factor only three less than the fitting to microwave background fluctuations obtained by Buchmüller *et al.* [12], when we used our crude  $K_{\text{eff}}$ 's approximation. However, using the estimate extracted from the calculations of [11] we got three orders of magnitude too low prediction of the baryon number. This estimate must though be considered a possibly too low estimate because there is one scattering effect that is strongly suppressed with our masses but which were included in that calculation. But even the latter estimate should because of the steep dependence of the result on the parameters be considered more uncertain and considering the deviation of our prediction only  $1.56\sigma$  is not unreasonable.

Since we used the Fukugita-Yanagida mechanism of obtaining first a lepton number excess being converted (successively by Sphalerons) into the baryon number, our success in this prediction should be considered not only a victory for our model for mass matrices but also for this mechanism. Since our model would be hard to combine with supersymmetry – it would loose much of its predictive power by having to double the Higgs fields – we should consider it in a non SUSY scenario and thus we can without problems take the energy scale to inflation/reheating to be so high that the plasma had already had time to go roughly to thermal equilibrium before the right-handed neutrinos go out-of-equilibrium due to their masses. We namely simply have no problem with getting too many gravitinos because gravitinos do not exist at all in our scheme.

Another “unusual” feature of our model is that the dominant contribution to the baryogenesis comes from the heavier right-handed neutrinos. In our model it



could be arranged without any troubles that the two heaviest right-handed neutrinos have masses only deviating by 10% namely given by our VEV parameters  $\chi$ . This leads to significant enhancement of the  $\epsilon_2$  and  $\epsilon_3$  which is crucial for the success of our prediction. There is namely a significant wash-out taking place, by a factor of the order of  $\kappa = 10^{-3}$  to  $10^{-6}$ . It is remarkable that we have here worked with a model that order of magnitudewise has with only six adjustable parameters been able to fit all the masses and mixings angles for quarks and leptons measured so far, including the Jarlskog  $CP$  violation area and most importantly and interestingly the baryogenesis in the early Universe. To confirm further our model we are in strong need for further data – which is not already predicted by the Standard Model, or we would have to improve it to give in principle accurate results rather than only orders of magnitudes. The latter would, however, be against the hall mark of our model, which precisely makes use of that we can guess that the huge amount of unknown coupling constants in our scheme with lots of particles can be counted as being *of order unity*.

### Acknowledgments

We wish to thank W. Buchmüller, P. Di Bari and M. Hirsch for useful discussions. We thank the Alexander von Humboldt-Stiftung and DESY for financial support.

### References

1. H. B. Nielsen and Y. Takanishi, these proceedings; hep-ph/0203147.
2. E. W. Kolb and M. S. Turner, *The Early Universe*, Addison-Wesley, Redwood City, USA, 1990.
3. H. B. Nielsen and Y. Takanishi, hep-ph/0204027.
4. C. D. Froggatt, H. B. Nielsen and Y. Takanishi, hep-ph/0201152.
5. H. B. Nielsen and Y. Takanishi, Nucl. Phys. B **588** (2000) 281; Nucl. Phys. B **604** (2001) 405; Phys. Lett. B **507** (2001) 241.
6. T. Yanagida, in Proceedings of the Workshop on Unified Theories and Baryon Number in the Universe, Tsukuba, Japan (1979), eds. O. Sawada and A. Sugamoto, KEK Report No. 79-18; M. Gell-Mann, P. Ramond and R. Slansky in Supergravity, Proceedings of the Workshop at Stony Brook, NY (1979), eds. P. van Nieuwenhuizen and D. Freedman (North-Holland, Amsterdam, 1979).
7. M. Fukugita and T. Yanagida, Phys. Lett. **B174** (1986) 45.
8. L. Covi, E. Roulet and F. Vissani, Phys. Lett. **B384** (1996) 169.
9. W. Buchmüller and M. Plümacher, Phys. Lett. **B431** (1998) 354.
10. C. D. Froggatt, H. B. Nielsen and D. J. Smith, hep-ph/0108262.
11. W. Buchmüller and M. Plümacher, Int. J. Mod. Phys. A **15** (2000) 5047.
12. W. Buchmüller and P. Di Bari, private communication.

# Measurement of $\sin(2\beta)$ with BaBar

Gloria Vuagnin (for the BaBar Collaboration)

Dipartimento di Fisica and INFN, Trieste, Italy

**Abstract.** The measurement of  $\sin(2\beta)$  presented here establishes CP violation in the  $B^0$  meson system at the  $4.1\sigma$  level. The probability of obtaining this value of  $\sin(2\beta)$  or higher in the absence of CP violation is consistent with the range implied by measurement and theoretical estimates of the magnitudes of CKM matrix elements.

## 1 Introduction

CP violation was observed for the first time in 1964 in the decay of  $K_L^0$  mesons [1] and since its discovery it has been the subject of many experiments and the motivation of many theoretical developments in particle physics. In Standard Model CP violation arises from the existence of a complex irremovable phase in the three-generation CKM quark mixing matrix [2]. The unitarity of this matrix can be expressed in geometric form by six triangles of equal area in the complex plane. A non-zero area of the triangles directly implies CP violation.

The most experimentally accessible unitarity relation, involving the smallest elements of the CKM matrix,  $V_{ub}$  and  $V_{td}$ , is known as Unitarity Triangle. The primary goal of the BaBar experiment is to overconstrain the Unitarity Triangle through CP violation measurements of its angles  $\alpha$ ,  $\beta$  and  $\gamma$  and the determination of its sides  $|V_{ub}|$ ,  $|V_{cb}|$  in semileptonic  $B$  decays and  $|V_{td}|$  in  $B^0\bar{B}^0$  mixing.

We present here the measurement of time-dependent CP-asymmetry in a sample of fully reconstructed  $B$  meson decays to CP eigenstates containing charmonium:  $b \rightarrow c\bar{c}s$ . This measurement is used to probe the angle  $\beta = \arg[-V_{cd}V_{cb}^*/V_{td}V_{tb}^*]$  [3].

The data for this study were recorded by the BaBar detector at the PEP-II  $B$  factory at SLAC, that consists of two storage rings producing asymmetric  $e^+e^-$  collisions, at a centre-of-mass energy corresponding to the mass of the  $\Upsilon(4S)$  resonance (10.58 GeV). The  $\Upsilon(4S)$  decays almost exclusively to  $B^+B^-$  or to coherent  $B^0\bar{B}^0$  pairs.

The two neutral  $B$  mesons oscillate coherently between  $B^0\bar{B}^0$  and  $\bar{B}^0B^0$ . If one of them,  $B_{tag}$ , decays at a time  $t = t_{tag}$  into a state that identifies its flavour, the flavour of the other  $B$  meson,  $B_{rec}$ , is also known at that time.  $B_{rec}$  then oscillates until it also decays at a time  $t = t_{rec}$  into a CP ( $B_{CP}$ ) or flavour ( $B_{flav}$ ) eigenstate which are fully reconstructed.

The coherent  $B^0\bar{B}^0$  state is in a p-wave state, so that its time evolution [4] is governed by the expression

$$f_{\pm}(\Delta t) = \frac{e^{-|\Delta t|/\tau_{B^0}}}{4\tau_{B^0}} [1 \pm S \sin(\Delta m_d \Delta t) \mp C \cos(\Delta m_d \Delta t)], \quad (1)$$

where  $\Delta t = t_{rec} - t_{tag}$  is the signed difference between the two  $B$  decay times,  $\tau$  is the  $B^0$  lifetime [6] and  $\Delta m_d$  is the  $B^0\bar{B}^0$  mixing frequency [6].

The sine term in 1 is due to the interference between direct decay and the decay after mixing. The cosine term is due to direct  $CP$  violation.

The  $CP$  violating parameters  $S$  and  $C$  can be defined in terms of the complex parameter  $\lambda$  that depends on both  $B^0\bar{B}^0$  mixing and on the amplitudes  $A_f$  or  $\bar{A}_{\bar{f}}$  describing  $B^0$  and  $\bar{B}^0$  decays to a final state  $f$ :

$$S = \frac{2 \operatorname{Im} \lambda}{1 + |\lambda|^2} \quad \text{and} \quad C = \frac{1 - |\lambda|^2}{1 + |\lambda|^2}. \quad (2)$$

For  $B_{rec}$  decaying into a flavour eigenstate, either  $A_f$  or  $\bar{A}_{\bar{f}}$  are null, so that  $\operatorname{Im} \lambda = 0$  and  $\lambda = 0$  and expression (1) gives in this case  $\tau_{B^0}$  from the exponential term and  $\Delta m_d$  from the oscillating term.

For  $B_{rec}$  decaying into a  $CP$  eigenstate, a difference between  $B^0$  and  $\bar{B}^0$   $\Delta t$  distributions or an asymmetry between negative and positive  $\Delta t$  for either flavor tag is evidence of  $CP$  violation. In the Standard Model  $\lambda = \eta_f e^{-i\beta}$  for charmonium-containing  $b \rightarrow c\bar{c}s$  decays, where  $\eta_f$  is the  $CP$  eigenvalue of the final state  $f$  and  $\beta$  is the angle of the Unitarity Triangle of the three-generation CKM matrix [2].

The time-dependent  $CP$  asymmetry is:

$$A_{CP}(\Delta t) = \frac{f_+(\Delta t) - f_-(\Delta t)}{f_+(\Delta t) + f_-(\Delta t)} = -\eta_f \sin 2\beta \sin(\Delta m_d \Delta t). \quad (3)$$

## 2 The BaBar Detector

A detailed description of the BaBar detector can be found in [5]. Charged particles are detected and their momenta measured by a combination of silicon vertex tracker (SVT) consisting of five layers of double side silicon microstrip detectors and a drift chamber (DCH) placed inside a 1.5 T superconducting solenoid. The average vertex resolution in the  $z$  direction is  $70\mu\text{m}$  for a fully reconstructed  $B$  meson. Leptons and hadrons are identified with measurements from all detector systems, including the energy loss ( $dE/dx$ ) in the DCH and SVT. The identification of electrons and photons is done by a CsI crystal electromagnetic calorimeter (EMC). Muons are identified in the instrumented flux return (IFR) consisting of layers of iron alternate with resistive plate counters. A Cherenkov ring imaging detector (DIRC) covering the central region, together with  $dE/dx$  information, provides  $K/\pi$  separation of at least three standard deviations for  $B$  decay products with momentum greater than 250 MeV/ $c$  in the laboratory.

### 3 B Reconstruction

The  $B_{flav}$  sample of fully reconstructed decays of  $B^0$  and  $B^+$  mesons to flavour eigenstates, contains approximately 23 million  $B\bar{B}$  pairs<sup>1</sup>.

The reconstructed modes are  $B^0 \rightarrow D^{(*)-}\pi^+$ ,  $D^{(*)-}\rho^+$ ,  $D^{(*)-}a_1^+$ ,  $J/\psi K^{*0}$  and  $B^+ \rightarrow D^{(*)0}\pi^+$ ,  $J/\psi K^+$ ,  $\Psi(2S)K^+$ . Charged and neutral  $D^*$  candidates are reconstructed in the decay channels  $K^+\pi^-$ ,  $K^+\pi^-\pi^0$ ,  $K^+\pi^+\pi^-\pi^-$  and  $K_S^0\pi^+\pi^-$  and  $D^-$  candidates in the decay channels  $K^+\pi^-\pi^-$  and  $K_S^0\pi^-$ . We reconstruct  $J/\psi$  and  $\Psi(2S)$  in the decays to  $e^+e^-$  and  $\mu^+\mu^-$  and the  $\Psi(2S)$  decay to  $J/\psi\pi^+\pi^-$ .

We extract  $\sin(2\beta)$  from a sample of fully reconstructed  $B^0$  decays into final states with  $\eta_f = -1$  ( $J/\psi K_S^0$ ,  $\Psi(2S)K_S^0$ ,  $\chi_{c1}K_S^0$ ),  $\eta_f = +1$  ( $J/\psi K_L^0$ ) and  $\eta_f(effective) = +0.65 \pm 0.07$  ( $J/\psi K^{*0}$  with  $K^{*0} \rightarrow K_S^0\pi^0$ ).

$B$  candidates are identified by the difference  $\Delta E$  between the reconstructed  $B$  energy and the beam energy  $\sqrt{s}/2$  in the  $\Upsilon(4S)$  frame, and by the beam-energy substituted mass  $m_{ES}$  calculated from  $\sqrt{s}/2$  and the reconstructed  $B$  momentum. We require  $m_{ES} > 5.27 \text{ GeV}/c^2$  and  $|\Delta E| < 3\sigma_{\Delta E}$ . The  $|\Delta E|$  resolution is mode dependent and ranges from 10 to 40 MeV.

### 4 Flavor Tagging

Each event is assigned to one of four hierarchical, mutually exclusive tagging categories or excluded from the analysis. The **Lepton** and **Kaon** categories contain events with high momentum leptons ( $p_{CM} > 1.0$  and  $1.1 \text{ GeV}/c$  for electrons and muons respectively) from semileptonic  $B$  decays or with kaons, whose charge is correlated with the flavour of the decaying  $b$  quark. The NT1 and NT2 categories are based on a neural network algorithm that exploits the information carried by non-identified leptons and kaons and by soft pions from  $D^*$  decays. The yields, efficiencies, purities and mistag rates  $w$  for each tagging category are listed in Table 1.

**Table 1.** Tagging Performances

Category	Fraction of tagged events $\epsilon(\%)$	Wrong tag fraction $w(\%)$	$Q=\epsilon(1-2w)^2(\%)$
<b>Lepton</b>	$10.9 \pm 0.3$	$8.9 \pm 1.3$	$7.4 \pm 0.5$
<b>Kaon</b>	$35.8 \pm 0.5$	$17.6 \pm 1.0$	$15.0 \pm 0.9$
<b>NT1</b>	$7.8 \pm 0.3$	$22.0 \pm 2.1$	$2.5 \pm 0.4$
<b>NT2</b>	$13.8 \pm 0.3$	$35.1 \pm 1.9$	$1.2 \pm 0.3$

<sup>1</sup> Charge-conjugation is implied throughout this document unless otherwise noted.

## 5 $\Delta t$ Measurement and Resolution

The measured distance between the two  $B$  decay vertices along the detector axis,  $\Delta z \sim \beta\gamma c\Delta t$ , provides a good estimate of  $\Delta t$ .

The  $B_{rec}$  vertex is reconstructed from the charged  $B_{rec}$  daughters, with a resolution  $\sigma_z = 70\mu m$  (the core of the distribution, describing 80% of the events has a width,  $\sigma_z = 45\mu m$ ).

The  $B_{tag}$  vertex is determined from the charged tracks not belonging to  $B_{rec}$ . An additional constraint is provided by the calculated  $B_{tag}$  production vertex and three-momentum. These quantities are determined by the measured three-momentum of the  $B_{rec}$  candidate, its decay vertex and the average position of the interaction point and the  $\Upsilon(4S)$  boost. Reconstructed  $\Lambda$  and  $K_S$  candidates are used as input to the fit instead of their daughters, to reduce the bias due to long-lived particles.

The overall  $\Delta z$  reconstruction efficiency is 97%. The  $\Delta z$  resolution, dominated by the  $z$  resolution of the  $B_{tag}$  vertex, is  $\sigma_{\Delta z} = 190\mu m$  (65% of the events have  $\sigma_{\Delta z} = 110\mu m$ ).

The  $\Delta t$  resolution function for signal events is represented as a sum of three Gaussian distributions. All offsets are modeled to be proportional to the event-by-event error,  $\sigma_{\Delta t}$ , which is correlated with the weight that the daughters of long-lived charm particles have in the tag vertex reconstruction. The “core” and “tail” Gaussian distributions have widths scaled by the event-by-event measurement error derived from the vertex fits. A separate offset for the core distribution is allowed for each tagging category to account for small shifts caused by inclusion of residual charm decay products in the tag vertex. The third Gaussian has a fixed width of 8 ps and accounts for fewer than 1% of events with incorrectly reconstructed vertices. Identical resolution function parameters are used for all modes, since the  $\Delta t$  resolution is dominated by the  $B_{tag}$  vertex precision. Separate resolution function parameters have been used for data collected in 1999-2000 and 2001, due to the significant improvement in the SVT alignment.

## 6 $CP$ Analysis and $\sin(2\beta)$

The measurement is made with a simultaneous unbinned likelihood fit to the  $\Delta t$  distribution of the flavour and the  $CP$  tagged events. The oscillation amplitudes on both  $CP$  and  $B_{flav}^0$  samples are reduced by the same  $(1 - 2w)$  factor due to wrong tags. Both distributions are also convoluted with the same resolution function described in the previous section. Background terms are included in the likelihood, each with its own time distribution and resolution function. Events are assigned signal and background probabilities based on the  $\Delta E$  ( $J/\Psi K_L^0$ ) or  $m_{ES}$  (all other modes) distributions shown in Fig. 1.

Including  $\sin(2\beta)$ , a total of 45 parameters are floated in the fit: the average signal mistag fractions  $w$  and differences  $\Delta w$  (8 parameters), the signal  $\Delta t$  resolution parameters (16) and all the background parameters: time dependence(9),  $\Delta t$  resolution (3) and mistag fractions(8). The determination of the signal mistag

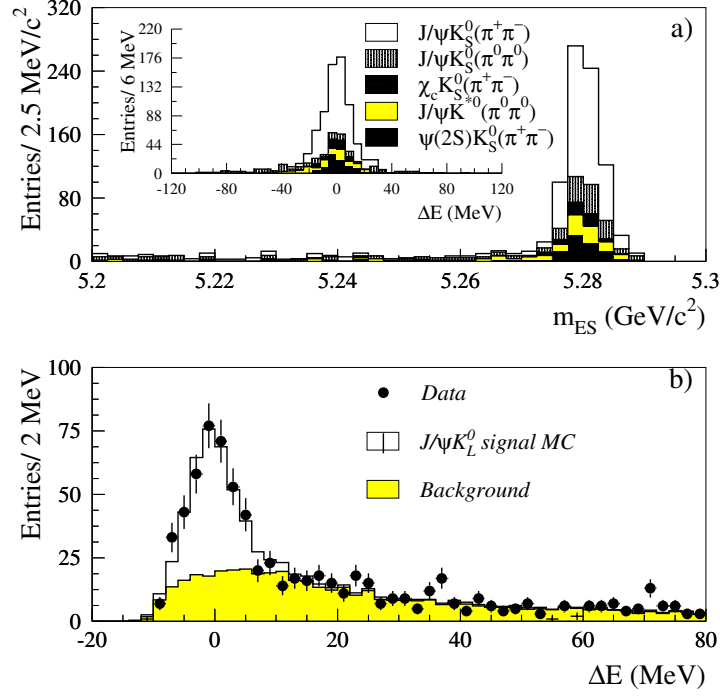


**Fig. 1.** a) Distribution of  $m_{ES}$  for  $B_{CP}$  candidates having a  $K_S^0$  in the final state; b) distribution of  $\Delta E$  for  $J/\psi K_L^0$  candidates.

fractions and resolution parameters are dominated by the large  $B_{flav}$  sample; the background parameters by the events with  $m_{ES} < 5.27 \text{ GeV}/c^2$ . As a result, the largest correlation between  $\sin(2\beta)$  and any linear combination of all the other free parameters is only 0.13. We fix  $\tau_B = 1.548 \text{ ps}$  and  $\Delta m_d = 0.472 \text{ ps}^{-1}$  [6].

Figure 2 shows the  $\Delta t$  distributions of the events overlaid with the fit results for the  $\eta_f = -1$  and  $\eta_f = +1$  samples. In a sample of 32 million  $B\bar{B}$  pairs, the simultaneous fit to all  $CP$  modes and flavour decays yields:

$$\sin(2\beta) = 0.59 \pm 0.14(stat) \pm 0.05(syst). \quad (4)$$

The probability to obtain a lower likelihood value than the one from the fit is 27%.

The main contributions to the systematic error are the parameterization of the  $\Delta t$  resolution function (0.03), due in part to residual uncertainties in the alignment, possible differences in the mistag fractions between the  $B_{CP}$  and  $B_{flav}$  samples (0.03) and uncertainties in the level, composition and  $CP$  asymmetry of the background in the selected  $CP$  events (0.02).

The results split into categories and classes are shown in Fig. 3.

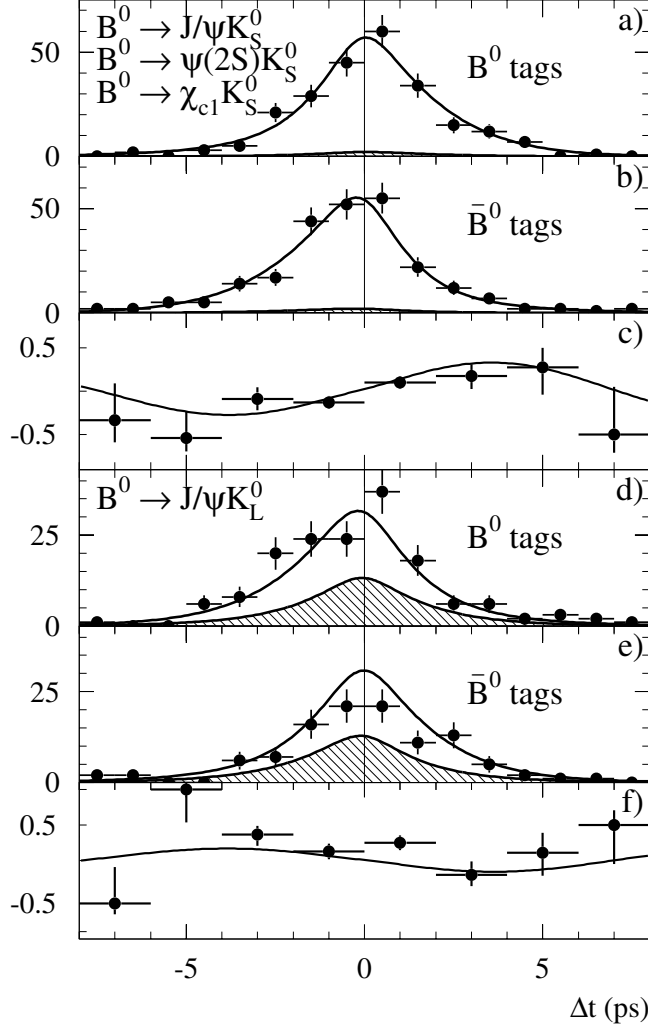


**Fig. 2.** Number of  $\eta_f = -1$  candidates in the signal region a) with a  $B^0$  tag,  $N_{B^0}$  and b) with a  $\bar{B}^0$  tag,  $N_{\bar{B}^0}$  and c) the asymmetry  $(N_{B^0} - N_{\bar{B}^0}) / (N_{B^0} + N_{\bar{B}^0})$  as a function of  $\Delta t$ . The solid curves represent the result of the combined fit to all selected  $CP$  events and the shaded regions represent the background contributions. Figures d)-f) contain the corresponding information for the  $\eta_f = +1$  candidates.

## 7 Conclusions and Outlook

The measurement of  $\sin(2\beta)$  presented here establishes CP violation in the  $B^0$  meson system at the  $4.1\sigma$  level, 37 years after its discovery in the Kaon system. The probability of obtaining this value of  $\sin(2\beta)$  or higher in the absence of CP violation is  $3 \times 10^{-5}$ . This direct measurement is consistent with the range implied by measurements and theoretical estimates of the magnitudes of CKM

Sample	$N_{\text{tag}}$	Purity (%)	$\sin 2\beta$
$J/\psi K_S^0, \psi(2S)K_S^0, \chi_{c1}K_S^0$	480	96	$0.56 \pm 0.15$
$J/\psi K_L^0 (\eta_f = +1)$	273	51	$0.70 \pm 0.34$
$J/\psi K^{*0}, K^{*0} \rightarrow K_S^0 \pi^0$	50	74	$0.82 \pm 1.00$
Full $CP$ sample	803	80	$0.59 \pm 0.14$
<hr/>			
$J/\psi K_S^0, \psi(2S)K_S^0, \chi_{c1}K_S^0$ only ( $\eta_f = -1$ )			
$J/\psi K_S^0 (K_S^0 \rightarrow \pi^+ \pi^-)$	316	98	$0.45 \pm 0.18$
$J/\psi K_S^0 (K_S^0 \rightarrow \pi^0 \pi^0)$	64	94	$0.70 \pm 0.50$
$\psi(2S)K_S^0 (K_S^0 \rightarrow \pi^+ \pi^-)$	67	98	$0.47 \pm 0.42$
$\chi_{c1}K_S^0 (K_S^0 \rightarrow \pi^+ \pi^-)$	33	97	$2.59 \pm \begin{smallmatrix} 0.55 \\ 0.67 \end{smallmatrix}$
Lepton tags	74	100	$0.54 \pm 0.29$
Kaon tags	271	98	$0.59 \pm 0.20$
NT1 tags	46	97	$0.67 \pm 0.45$
NT2 tags	89	95	$0.10 \pm 0.74$
$B^0$ tags	234	98	$0.50 \pm 0.22$
$\bar{B}^0$ tags	246	97	$0.61 \pm 0.22$
$B_{\text{flav}}$ non- $CP$ sample	7591	86	$0.02 \pm 0.04$
Charged $B$ non- $CP$ sample	6814	86	$0.03 \pm 0.04$

**Fig. 3.** Number of tagged events, signal purity and result of fitting for CP asymmetries in the full CP sample and in various subsamples, as well as in the Bflav and charged B control samples. Errors are statistical only.

matrix elements. By the summer of 2002, with a data sample of more than 100 million BB pairs a measurement of  $\sin(2\beta)$  with a precision of less than 0.1 will be possible.

## References

1. J.H. Christenson *et al.*: Phys. Rev. Lett. **13**, 138 (1964);
2. N. Cabibbo: Phys. Rev. Lett. **10**, 5311 (1963); M. Kobayashi and T. Maskawa : Prog. Th. Phys. **49**, 652 (1973)
3. A.B. Carter and A.I. Sanda: Phys. Rev. **D23**, 1567 (1981); I.I. Bigi and A.I. Sanda: Nucl. Phys. **B193**, 85 (1981)
4. Y. Nir and H. Quinn: Ann. Rev. Nucl. Part. Sci. **42**, 211 (1992).
5. B. Aubert *et al.* [BaBar Collaboration]: SLAC-PUB-8569, HEP-EX/0105044, to appear in Nucl. Instr. and Methods.
6. Particle Data Group, D.E. Groom *et al.*: Eur. Phys. J. **C15**, 1 (2000)



# Rare Decay $D^0 \rightarrow \gamma\gamma^*$

Svjetlana Fajfer<sup>1,2</sup>, Paul Singer<sup>3</sup>, and Jure Zupan<sup>1</sup>

<sup>1</sup> J. Stefan Institute, Jamova 39, P. O. Box 3000, 1001 Ljubljana, Slovenia

<sup>2</sup> Department of Physics, University of Ljubljana, Jadranska 19, 1000 Ljubljana, Slovenia

<sup>3</sup> Department of Physics, Technion - Israel Institute of Technology, Haifa 32000, Israel

**Abstract.** We present main results of the investigation of the rare decay mode  $D^0 \rightarrow \gamma\gamma$ , in which the long distance contributions are expected to be dominant. Using the Heavy Quark Chiral Lagrangian we have considered the anomaly contribution which relates to the annihilation part of the weak Lagrangian and the one - loop  $\pi$ ,  $K$  diagrams. The loop contributions which are proportional to  $g$  and contain the  $a_1$  Wilson coefficient are found to dominate the decay amplitude. The branching ratio is then calculated to be  $(1.0 \pm 0.5) \times 10^{-8}$ . Observation of an order of magnitude larger branching ratio could signal new physics.

In the past years the rare decays of B mesons came under the spotlights as *the* source of possible signals of new physics. In the meanwhile studies of rare D decays have received much less attention. Partially this is because theoretical investigations of D weak decays are rather difficult, also due to the presence of many resonances close to this energy region. The penguin effects on the other hand, which are very important in B and also in K decays, are usually suppressed in the case of charm mesons due to the presence of  $d$ ,  $s$ ,  $b$  quarks in the loop with the respective values of CKM elements.

Nevertheless, D meson physics has produced some interesting results in the past year. Experimental results on time dependent decay rates of  $D^0 \rightarrow K^+\pi^-$  by CLEO [1] and  $D^0 \rightarrow K^+K^-$  and  $D^0 \rightarrow K^-\pi^+$  by FOCUS [2] have stimulated several studies on the  $D^0 - \bar{D}^0$  oscillations [3]. The recently measured  $D^*$  decay width by CLEO [4] has provided the long expected information on the value of  $D^*D\pi$  coupling. Among the rare D decays, the decays  $D \rightarrow V\gamma$  and  $D \rightarrow V(P)l^+l^-$  are subjects of CLEO and FERMILAB searches [5]. On the theoretical side, these rare decays of charm mesons into light vector meson and photon or lepton pair have been considered lately by several authors (see, e.g., [6]-[11], for radiative leptonic D meson decay see [12]). The investigations of  $D \rightarrow V\gamma$  showed that certain branching ratios can be as large as  $10^{-5}$ , like for  $D^0 \rightarrow \bar{K}^{*0}\gamma$ ,  $D_s^+ \rightarrow \rho^+\gamma$  [6,11]. However, the decays which are of some relevance to the  $D^0 \rightarrow 2\gamma$  mode studied here, like  $D^0 \rightarrow \rho^0\gamma$ ,  $D^0 \rightarrow \omega\gamma$ , are expected with branching ratios in the  $10^{-6}$  range [13]. Thus, it is hard to believe that the branching ratio of the  $D^0 \rightarrow 2\gamma$  decay mode can be as high as  $10^{-5}$  in the Standard Model (SM), as found by [14]. Apart from this estimation, there has

---

\* Talk given by J. Zupan

been no other detailed work on  $D^0 \rightarrow 2\gamma$  prior to our analysis [15]. In addition to these theoretical studies there are experimental attempts to observe this decay rate done by CLEO and FOCUS [16].

Motivated by the experimental efforts to observe rare D meson decays [16], and noticing that  $B_s \rightarrow \gamma\gamma$  offers possibility to observe physics beyond the SM, we undertook an investigation of the  $D^0 \rightarrow \gamma\gamma$  decay [15]. Here we present only the main results of our analyses, while the details of our work are presented in [15].

The short distance contribution is expected to be rather small, as already encountered in the one photon decays [6,7], hence the main contribution would come from long distance interactions. In order to treat the long distance contributions, we use the heavy quark effective theory combined with chiral perturbation theory (HQ $\chi$ PT) [17]. This approach was used before for treating  $D^*$  strong and electromagnetic decays [18]-[20]. The leptonic and semileptonic decays of D meson were also treated within the same framework (see [18] and references therein).

The approach of HQ $\chi$ PT introduces several coupling constants that have to be determined from experiment. The recent measurement of the  $D^*$  decay width [4] has determined the  $D^*D\pi$  coupling, which is related to  $g$ , the basic strong coupling of the Lagrangian. There is more ambiguity, however, concerning the value of the anomalous electromagnetic coupling, which is responsible for the  $D^*D\gamma$  decays [19,20] (for further discussion on this point see [15]).

Let us address now some issues concerning the theoretical framework used in our treatment. For the weak vertex we used the factorization of weak currents with nonfactorizable contributions coming from chiral loops. The typical energy of intermediate pseudoscalar mesons is of order  $m_D/2$ , so that the chiral expansion  $p/\Lambda_\chi$  (for  $\Lambda_\chi \simeq 1$  GeV) is rather close to unity. Thus, for the decay under study we extend the possible range of applicability of the chiral expansion of HQ $\chi$ PT, compared to previous treatments like  $D^* \rightarrow D\pi$ ,  $D^* \rightarrow D\gamma$  [19] or  $D^* \rightarrow D\gamma\gamma$  [20], in which a heavy meson appears in the final state, making the use of chiral perturbation theory rather natural. The suitability of our undertaking here must be confronted with experiment, and possibly other theoretical approaches.

At this point we also remark that the contribution of the order  $\mathcal{O}(p)$  does not exist in the  $D^0 \rightarrow \gamma\gamma$  decay, and the amplitude starts with contribution of the order  $\mathcal{O}(p^3)$ . At this order the amplitude receives an annihilation type contribution proportional to the  $a_2$  Wilson coefficient, with the Wess-Zumino anomalous term coupling light pseudoscalars to two photons. However, the total amplitude is dominated by terms proportional to  $a_1$  that contribute only through loops with Goldstone bosons. Loop contributions proportional to  $a_2$  vanish at this order. We point out that any other model which does not involve intermediate charged states cannot give this kind of contribution. Therefore, the chiral loops naturally include effects of intermediate meson exchange.

The chiral loops of order  $\mathcal{O}(p^3)$  are finite, as they are in the similar case of  $K \rightarrow \gamma\gamma$  decays [21]-[22]. The next to leading terms might be almost of the

same order of magnitude compared to the leading  $\mathcal{O}(p^3)$  term, the expected suppression being approximately  $p^2/\Lambda_\chi^2$ . The inclusion of next order terms in the chiral expansion is not straightforward in the present approach. We include, however, terms which contain the anomalous electromagnetic coupling, and appear as next to leading order terms in the chiral expansion, in view of their potentially large contribution (as in  $B^*(D^*) \rightarrow B(D)\gamma\gamma$  decays considered in [20]). As it turns out, these terms are suppressed compared to the leading loop effects, which at least partially justifies the use of HQ $\chi$ PT for the decay under consideration. Contributions of the same order could arise from light resonances like  $\rho$ ,  $K^*$ ,  $a_0(980)$ ,  $f_0(975)$ . Such resonances are sometimes treated with hidden gauge symmetry (see, e.g., [18]), which is not compatible with chiral perturbation symmetry. Therefore, a consistent calculation of these terms is beyond our scheme and we disregard their possible effect.

The invariant amplitude for  $D^0 \rightarrow \gamma\gamma$  decay can be written using gauge and Lorentz invariance in the following form:

$$M = \left[ iM^{(-)}(g^{\mu\nu} - \frac{k_2^\mu k_1^\nu}{k_1 k_2}) + M^{(+)}\epsilon^{\mu\nu\alpha\beta}k_{1\alpha}k_{2\beta} \right] \epsilon_{1\mu}\epsilon_{2\nu}, \quad (1)$$

where  $M^{(-)}$  is a parity violating and  $M^{(+)}$  a parity conserving part of the amplitude, while  $k_{1(2)}$ ,  $\epsilon_{1(2)}$  are respectively the four momenta and the polarization vectors of the outgoing photons.

In the discussion of weak radiative decays  $q' \rightarrow q\gamma\gamma$  or  $q' \rightarrow q\gamma$  decays, usually the short (SD) and long distance (LD) contribution are separated. The SD contribution in these transitions is a result of the penguin-like transition, while the long distance contribution arises in particular pseudoscalar meson decay as a result of the nonleptonic four quark weak Lagrangian, when the photon is emitted from the quark legs. Here we follow this classification. In the case of  $b \rightarrow s\gamma\gamma$  decay [23] it was noticed that without QCD corrections the rate  $\Gamma(b \rightarrow s\gamma\gamma)/\Gamma(b \rightarrow s\gamma)$  is about  $10^{-3}$ . One expects that a similar effect will show up in the case of  $c \rightarrow u\gamma\gamma$  decays. Namely, according to the result of [23] the largest contribution to  $c \rightarrow u\gamma\gamma$  amplitude would arise from the photon emitted either from  $c$  or  $u$  quark legs in the case of the penguin-like transition  $c \rightarrow u\gamma$ . Without QCD corrections the branching ratio for  $c \rightarrow u\gamma$  is rather suppressed, being of the order  $10^{-17}$  [7,8]. The QCD corrections [24] enhance it up to order of  $10^{-8}$ .

In our approach we include the  $c \rightarrow u\gamma$  short distance contribution by using the Lagrangian

$$\mathcal{L} = -\frac{G_f}{\sqrt{2}}V_{us}V_{cs}^*C_{7\gamma}^{eff}\frac{e}{4\pi^2}F_{\mu\nu}m_c(\bar{u}\sigma^{\mu\nu}\frac{1}{2}(1+\gamma_5)c), \quad (2)$$

where  $m_c$  is a charm quark mass. In our analysis we follow [24,26] and we take  $C_{7\gamma}^{eff} = (-0.7 + 2i) \times 10^{-2}$ .

The main LD contribution will arise from the effective four quark nonleptonic  $\Delta C = 1$  weak Lagrangian given by

$$\mathcal{L} = -\frac{G_f}{\sqrt{2}} \sum_{q=d,s} V_{uq} V_{cq}^* [a_1 (\bar{q} \Gamma^\mu c) (\bar{u} \Gamma_\mu q) + a_2 (\bar{u} \Gamma^\mu c) (\bar{q} \Gamma_\mu q)], \quad (3)$$

where  $\Gamma^\mu = \gamma^\mu(1 - \gamma_5)$ ,  $a_i$  are effective Wilson coefficients [27], and  $V_{q_i q_j}$  are CKM matrix elements. At this point it is worth pointing out that long distance interactions will contribute only if the  $SU(3)$  flavor symmetry is broken, i.e. if  $m_s \neq m_d$ . Namely, due to  $V_{ud} V_{cd}^* \simeq -V_{us} V_{cs}^*$  and  $m_d = m_s$  the contribution arising from the weak Lagrangian (3) disappears in the case of exact  $SU(3)$  flavor symmetry.

Going from quark to meson level effective Lagrangian one uses heavy quark symmetry for c-quark and chiral symmetry of light quarks to construct HQ $\chi$ PT Lagrangian [15]. This is then used to calculate the  $D^0 \rightarrow \gamma\gamma$  decay width to one loop order. Leaving out the details of our calculation (see [15]), we discuss the final results.

The decay width for the  $D^0 \rightarrow \gamma\gamma$  decay can be obtained using the amplitude decomposition in (1)

$$\Gamma_{D^0 \rightarrow \gamma\gamma} = \frac{1}{16\pi m_D} (|M^{(-)}|^2 + \frac{1}{4} |M^{(+)}|^2 m_D^4). \quad (4)$$

The main contribution to the decay width arises from the diagrams presented on Figs. 1, 2. The calculated amplitudes depend on the number of input parameters, as mentioned in [15]. The coupling  $g$  is extracted from existing experimental

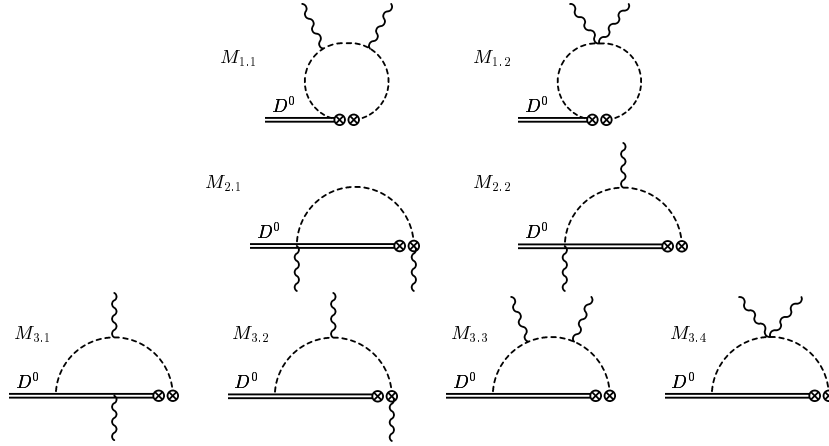


**Fig. 1.** One loop diagrams, not containing beta-like terms, that give nonvanishing contributions to the  $D^0 \rightarrow \gamma\gamma$  decay amplitude. Each sum of the amplitudes on diagrams in one row  $M_i = \sum_j M_{i,j}$  is gauge invariant and finite. Numerical values are listed in Table 1.

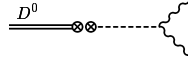


**Fig. 2.** Anomalous contributions to  $D^0 \rightarrow \gamma\gamma$  decay. The intermediate pseudoscalar mesons propagating from the weak vertex are  $\pi^0, \eta, \eta'$ .

data on  $D^* \rightarrow D\pi$ . Recently CLEO Collaboration has obtained the first measurement of  $D^{*+}$  decay width  $\Gamma(D^{*+}) = 96 \pm 4 \pm 22$  keV [4] by studying the  $D^{*+} \rightarrow D^0\pi^+$ . Using the value of decay width together with branching ratio  $Br(D^{*+} \rightarrow D^0\pi^+) = (67.7 \pm 0.5)\%$  one immediately finds at tree level that  $g = 0.59 \pm 0.08$ . The chiral corrections to this coupling were found to contribute about 10% [18,19]. In order to obtain the  $\alpha$  coupling, we use present experimental data on  $D_s$  leptonic decays ( $f_D \simeq f_{D_s} = \alpha/\sqrt{m_D}$ ). In our calculation we take  $\alpha = 0.31$  GeV<sup>3/2</sup> [15]. For the Wilson coefficients  $a_1$  we take 1.26 and  $a_2 = -0.47$  [27]. We give here the numerical results for the one-loop amplitudes in Table 1.

**Table 1.** Table of the nonvanishing finite amplitudes. The amplitudes coming from the anomalous and short distance ( $C_{7\gamma}^{eff}$ ) Lagrangians are presented. The finite and gauge invariant sums of one-loop amplitudes are listed in the next three lines ( $M_i^{(\pm)} = \sum_j M_{i,j}^{(\pm)}$ ). The numbers 1, 2, 3 denote the row of diagrams on the Fig. 1. In the last line the sum of all amplitudes is given.

	$M_i^{(-)} [\times 10^{-10} \text{ GeV}]$	$M_i^{(+)} [\times 10^{-10} \text{ GeV}^{-1}]$
Anom.	0	-0.53
SD	-0.27 -0.81 <i>i</i>	-0.16 -0.47 <i>i</i>
1	3.55 +9.36 <i>i</i>	0
2	1.67	0
3	-0.54 +2.84 <i>i</i>	0
$\sum_i M_i^{(\pm)}$	4.41 +11.39 <i>i</i>	-0.69 -0.47 <i>i</i>

In the determination of  $D^* \rightarrow D\gamma\gamma$  and  $B^* \rightarrow B\gamma\gamma$  a sizable contribution from  $\beta$ -like electromagnetic terms [15] has been found [20]. Therefore, we have to investigate their effect in the  $D^0 \rightarrow \gamma\gamma$  decay amplitude. The nonzero parity violating parts of the one loop diagrams containing  $\beta$  coupling are given on Fig. 3, while numerical results are presented in Table 2.

Using short distance contributions, the finite one loop diagrams and the anomaly parts of the amplitudes and with numerical values of the amplitudes as listed in Table 1, one obtains

$$Br(D^0 \rightarrow \gamma\gamma) = 1.0 \times 10^{-8}. \quad (5)$$

This result is slightly changed when one takes into account the terms dependent on  $\beta$ . The branching ratio obtained when we sum all contributions is

$$Br(D^0 \rightarrow \gamma\gamma) = 0.95 \times 10^{-8}. \quad (6)$$

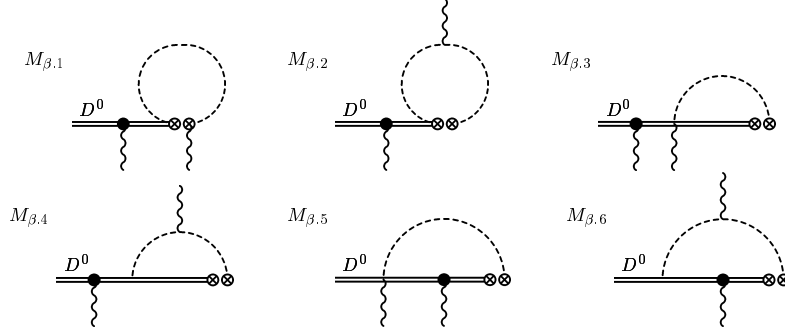


**Fig. 3.** The diagrams which give nonzero amplitudes with one  $\beta$ -like coupling (denoted by  $\bullet$ ).

**Table 2.** Table of nonzero contributions of the amplitudes coming from the diagrams with  $\beta$  coupling. In the last line the sums of the contributions are presented. We use  $\beta = 2.3 \text{ GeV}^{-1}$ ,  $m_c = 1.4 \text{ GeV}$ .

Diag.	$M_i^{(-)} [\times 10^{-10} \text{ GeV}]$	$M_i^{(+)} [\times 10^{-10} \text{ GeV}^{-1}]$
$\beta.1$	0	-2.69
$\beta.2$	0	2.69
$\beta.3$	0	2.11
$\beta.4$	0.88	-0.007
$\beta.5$	0	0.51
$\beta.6$	-2.88	-0.52
$\sum_i M_i^{(\pm)}$	-2.00	2.09

By varying  $\beta$  within  $1 \text{ GeV}^{-1} \leq \beta \leq 5 \text{ GeV}^{-1}$  and keeping  $g = 0.59 \pm 0.08$ , the branching ratio is changed by at most 10%. On the other hand, one has to keep in mind that the loop contributions involving  $\beta$  are not finite and have to be regulated. We have used  $\overline{\text{MS}}$  scheme, with the divergent parts being absorbed by counterterms. The size of these is not known, so they might influence the error in our prediction of the branching ratio. Note also that changing  $\alpha$  would affect the predicted branching ratio. For instance, if the chiral corrections do decrease the value of  $\alpha$  by 30% this would decrease the predicted branching ratio down to  $0.5 \times 10^{-8}$ .

It is interesting to estimate what sizes of new physics effects one can expect in this decay mode. In the following we use a rather simple estimate of possible SUSY contributions. In [25],[26] it has been found that  $c \rightarrow u\gamma$  short distance contribution (2) can get considerably enhanced, if one takes into consideration the MSSM spectrum. The leading contribution comes from the gluino exchange and can be at most as large as  $|C_7^{\text{MSSM}}| \lesssim 10|C_7^{\text{SM}}|$ . Comparing this with the Standard Model results listed in Table 1, it follows that in this most favorable case  $M_{\text{SD}}^{\text{MSSM}} \sim 10M_{\text{SD}}^{\text{SM}} \sim M_{\text{LD}}^{\text{SM}}$ . The MSSM contributions might thus increase the Standard Model prediction for the branching ratio by a factor of 4 or less.

In summary, we have presented the results of the detailed calculation of the decay amplitude  $D^0 \rightarrow \gamma\gamma$ , which includes short distance and long distance contributions, by making use of the theoretical tool of Heavy Quark Chiral Perturbation Theory Lagrangian. Within this framework, the leading contributions are found to arise from the charged  $\pi$  and  $K$  mesons running in the chiral loops, and are of order  $\mathcal{O}(p^3)$ . These terms are finite and contribute only to the parity violating part of the amplitude. The inclusion of terms of higher order in the chiral expansion is unfortunately plagued with the uncertainty caused by the lack of knowledge of the counterterms. As to the parity conserving part of the decay, it is given by terms coming from the short distance contribution, the anomaly and from loop terms containing the beta coupling, the latter giving most of the amplitude. The size of this part of the amplitude is approximately one order of magnitude smaller than the parity violating amplitude, thus contributing less than 10% to the decay rate. Therefore, our calculation predicts that the  $D \rightarrow 2\gamma$  decay is mostly a parity violating transition.

In addition to the uncertainties we have mentioned, there is the question of the suitability of the chiral expansion for the energy involved in this process; the size of the uncertainty related to this is difficult to estimate. Altogether, our estimate is that the total uncertainty is not larger than 50%. Accordingly, we conclude that the predicted branching ratio is

$$Br(D^0 \rightarrow \gamma\gamma) = (1.0 \pm 0.5) \times 10^{-8}. \quad (7)$$

The reasonability of this result can be deduced also from a comparison with the calculated decay rates for the  $D^0 \rightarrow \rho(\omega)\gamma$ , which are found to be expected with a branching ratio of approximately  $10^{-6}$  [6,7,13]. Recently another independent study of  $D^0 \rightarrow \gamma\gamma$  decay mode has been performed [28], where also vector meson contributions have been included. The use of vector meson dominance yields a factor of three larger result than what has been obtained by our analysis.

We look forward to experimental attempts of detecting this decay. Our result suggests that the observation of  $D \rightarrow 2\gamma$  at a rate which is an order of magnitude larger than (7), could be a signal for the type of “new physics”, which leads to sizable enhancement of the short-distance  $c \rightarrow u\gamma$  transition.

## References

1. R. Godang et al. (CLEO Collaboration), Phys. Rev. Lett. **84**, 5038 (2000).
2. J. M. Link et al. (FOCUS Collaboration), Phys. Lett. B **485**, 62 (2000).
3. S. Bergmann, Y. Grossman, Z. Ligeti, Y. Nir and A. A. Petrov, Phys. Lett. B **486**, 418 (2000); I. I. Bigi and N. G. Uraltsev, Nucl. Phys. B **592**, 92 (2001).
4. T. E. Coan et al. (CLEO Collaboration), hep-ex/0102007, M. Dubrovin (for CLEO Collaboration), hep-ex/0105030.
5. A. Freyberger et al. (CLEO Collaboration), Phys. Rev. Lett. **76**, 3065 (1996); D. M. Asner et al. (CLEO Collaboration), Phys. Rev. D **58**, 092001 (1998); E. M. Aitala et al. (E791 Collaboration), hep-ex/0011077; D. A. Sanders, Mod. Phys. Lett. A **15**, 1399 (2000); A. J. Schwartz, hep-ex/0101050; D. J. Summers, hep-ex/0011079.

6. S. Fajfer, S. Prelovšek, P. Singer, Eur. Phys. J. C **6**, 471, 751(E) (1999).
7. G. Burdman, E. Golowich, J. L. Hewett and S. Pakvasa, Phys. Rev. D **52**, 6383 (1995).
8. Q. Ho-Kim, X. Y. Pham, Phys. Rev. D **61**, 013008 (2000).
9. A. Khodjamirian, G. Stoll and D. Wyler, Phys. Lett. B **358**, 129 (1995).
10. S. Fajfer, S. Prelovšek and P. Singer, Phys. Rev. D **58**, 094038 (1998).
11. R. F. Lebed, Phys. Rev. D **61**, 033004 (2000).
12. C. Q. Geng, C. C. Lih, W-M. Zhang, Mod. Phys. Lett. A **15**, 2087 (2000).
13. S. Fajfer, S. Prelovšek, P. Singer and D. Wyler, Phys. Lett. B **487**, 81 (2000).
14. H. Routh, V. P. Gautam, Phys. Rev. D **54**, 1218 (1996); H. Routh, H. Roy, A. K. Maity and V. P. Gautam, Acta Phys. Pol. B **30**, 2687 (1999).
15. S. Fajfer, P. Singer, J. Zupan, Phys. Rev. D **64**, 074008 (2001).
16. M. Selen, Workshop on *Prospects for CLEO/CESR with  $3 < E_{cm} < 5$  GeV*, Cornell University, May 5-7, 2001; I. Bediaga, private communication.
17. M. B. Wise, Phys. Rev. D **45**, 2188 (1992); G. Burdman and J. Donoghue, Phys. Lett. B **280**, 287 (1992).
18. R. Casalbuoni, A. Deandrea, N. Di Bartolomeo, R. Gatto, F. Feruglio, and G. Nardulli, Phys. Rep. **281**, 145 (1997). This review provides many references on the use of HQCT in different processes.
19. I. W. Stewart, Nucl. Phys. B **529**, 62 (1998).
20. D. Guetta, P. Singer, Phys. Rev. D **61**, 054014 (2000).
21. M. K. Gaillard and B. W. Lee, Phys. Rev. D **10**, 897 (1974); E. Ma and A. Pramudita, Phys. Rev. D **24**, 2476 (1981);
22. J. Kambor and B. R. Holstein, Phys. Rev. D **49**, 2346 (1994).
23. S. Herrlich, J. Kalinowski, Nucl. Phys. B **381**, 502 (1992).
24. C. Greub, T. Hurth, M. Misiak and D. Wyler, Phys. Lett. B **382**, 415 (1996).
25. I. I. Bigi, F. Gabbiani, A. Masiero, Z. Phys. C **48**, 633 (1990).
26. S. Prelovšek, D. Wyler, Phys. Lett. B **500**, 304 (2001); S. Prelovšek, hep-ph/0010106.
27. A. J. Buras, Nucl. Phys. B **434**, 606 (1995).
28. G. Burdman, E. Golowich, J. Hewett and S. Pakvasa, hep-ph/0112235.